



OPTIMIZATION AND NONLINEAR MODEL PREDICTIVE CONTROL OF
SOME SIMULATED MOVING BED PROCESS VARIANTS

Reinaldo Calderón Supelano

Tese de Doutorado apresentada ao Programa de Pós-graduação em Engenharia Química, COPPE, da Universidade Federal do Rio de Janeiro, como parte dos requisitos necessários à obtenção do título de Doutor em Engenharia Química.

Orientadores: Argimiro Resende Secchi
Amaro Gomes Barreto Jr.

Rio de Janeiro
Setembro de 2021

OPTIMIZATION AND NONLINEAR MODEL PREDICTIVE CONTROL OF
SOME SIMULATED MOVING BED PROCESS VARIANTS

Reinaldo Calderón Supelano

TESE SUBMETIDA AO CORPO DOCENTE DO INSTITUTO ALBERTO
LUIZ COIMBRA DE PÓS-GRADUAÇÃO E PESQUISA DE ENGENHARIA
DA UNIVERSIDADE FEDERAL DO RIO DE JANEIRO COMO PARTE DOS
REQUISITOS NECESSÁRIOS PARA A OBTENÇÃO DO GRAU DE DOUTOR
EM CIÊNCIAS EM ENGENHARIA QUÍMICA.

Orientadores: Argimiro Resende Secchi
Amaro Gomes Barreto Jr.

Aprovada por: Prof. Argimiro Resende Secchi
Prof. Amaro Gomes Barreto Jr.
Prof. Alírio Egídio Rodrigues
Prof. Márcio André Fernandes Martins
Prof. Mauricio Bezerra de Souza Jr.

RIO DE JANEIRO, RJ – BRASIL
SETEMBRO DE 2021

Supelano, Reinaldo Calderón

Optimization and nonlinear model predictive control of some simulated moving bed process variants/Reinaldo Calderón Supelano. – Rio de Janeiro: UFRJ/COPPE, 2021.

XXIV, 161 p.: il.; 29, 7cm.

Orientadores: Argimiro Resende Secchi

Amaro Gomes Barreto Jr.

Tese (doutorado) – UFRJ/COPPE/Programa de Engenharia Química, 2021.

Referências Bibliográficas: p. 139 – 154.

1. Simulated Moving Bed. 2. ModiCon. 3. VariCol. 4. Optimization. 5. Control. 6. Enantioseparation. I. Secchi, Argimiro Resende *et al.* II. Universidade Federal do Rio de Janeiro, COPPE, Programa de Engenharia Química. III. Título.

Acknowledgments

I want to thank everyone who contributes to my academic accomplishment and the realization of this thesis. I have special gratitude for some people and institutions, as I will describe below.

I want to thank my family for their support and contributions in all my projects, endeavors, and accomplishments. My parents, Miguel and Cristina, have worked tirelessly to give me the best guidance, advice, and the possibility of accessing higher education. I would also thank my brothers Camilo and Leonel for their support and motivation all the time. My family had contributed the most to my achievements.

I want to thank my girlfriend Vero for all her love, her support, and for making my life colorful and happy. I also want to thank you for the design lesson and all the other contributions. I admire your creativity and your different skills. I am happy and proud of you.

I want to express my most sincere gratitude to my advisors, professor Argimiro Secchi and professor Amaro Barreto for all their teaching, discussion, patience, and support during this time. All their advice and teachings have contributed a lot to my academic and professional formation. A special thanks to professor Argimiro for believing in me and supporting me at various times, not only in the academics subjects.

I also like to thank my friends and colleagues, especially Nayher, Laura, Sergio, Jéssica, Leonardo, Johanna, Felipe, Douglas, Roymel, Mairely, and Julian, who have been significant support throughout this time. With you, it has been easier to be away from Colombia. Thanks for everything.

I want to thank the Chemical Engineering Program PEQ of COPPE/UFRJ and all teachers for academic formation.

I have gratitude to the G-130 laboratory and all the members for all the support and assistance.

I want to thank the Coordenação de Aperfeiçoamento de Pessoal de Nível Superior - Brasil (CAPES) and the Conselho Nacional de Desenvolvimento Científico e Tecnológico CNPq for the financial support.

I want to thank Brazil in general for receiving me and opening the doors to do my master's and doctorate degrees. I also thank all the Brazilian people who welcomed me and collaborated with me in everything I needed.

Resumo da Tese apresentada à COPPE/UFRJ como parte dos requisitos necessários para a obtenção do grau de Doutor em Ciências (D.Sc.)

OTIMIZAÇÃO E CONTROLE PREDITIVO NÃO LINEAR DE ALGUMAS VARIANTES DO LEITO MÓVEL SIMULADO

Reinaldo Calderón Supelano

Setembro/2021

Orientadores: Argimiro Resende Secchi
Amaro Gomes Barreto Jr.

Programa: Engenharia Química

O interesse na tecnologia de leito móvel simulado (SMB) tem se voltado para suas variantes devido ao maior desempenho na separação e purificação de diferentes compostos, como enantiômeros. Essas variantes estão relacionadas ao relaxamento de alguns parâmetros ou aos arranjos não convencionais do trem de colunas cromatográficas que compõem a tecnologia SMB. Duas das mais relevantes e populares são os processos ModiCon e VariCol, obtidos pelas modulações periódicas da concentração da alimentação e do comprimento dos arranjos de colunas, respectivamente. Os estudos de otimização e controle para cada uma dessas variantes são essenciais, pois ajudam a descobrir novos recursos e a criar diretrizes para selecioná-los e operá-los. Neste trabalho, ModiCon, VariCol, ModiCon + VariCol (operação híbrida) foram estudados em detalhes, e seus desempenhos ótimos foram comparados. A aplicação do controle preditivo não linear (NMPC) também foi avaliada para os processos ModiCon e VariCol. Diferentes exemplos de separações enantioméricas foram considerados nos estudos de otimização e controle. Como resultado, a complexidade do problema de otimização de projeto do processo VariCol foi reduzida de MINLP (programação não linear inteira mista) para NLP (programação não linear). O rendimento ideal dos processos ModiCon e ModiCon + VariCol foi quase o dobro do processo SMB convencional. O controlador respondeu satisfatoriamente a diferentes distúrbios. A pureza do refinado e do extrato e a máxima economia do processo foram atendidas em todos os casos estudados.

Abstract of Thesis presented to COPPE/UFRJ as a partial fulfillment of the requirements for the degree of Doctor of Science (D.Sc.)

OPTIMIZATION AND NONLINEAR MODEL PREDICTIVE CONTROL OF
SOME SIMULATED MOVING BED PROCESS VARIANTS

Reinaldo Calderón Supelano

September/2021

Advisors: Argimiro Resende Secchi
Amaro Gomes Barreto Jr.

Department: Chemical Engineering

The interest in the simulated moving bed (SMB) technology has turned towards its variants due to the higher performance in separating and purifying different compounds such as enantiomers. Those variants are related to the relaxation of some parameters or the non-conventional arrangements of the train of chromatography columns that make up the SMB technology. Some of the most relevant and popular are the ModiCon and the VariCol processes, obtained by the periodic modulations of feed concentration and the length of arrangements of columns. Optimization and control studies for each of these variants are essential as they help discover new features and create guidelines for selecting and operating them. In this work, ModiCon, VariCol, ModiCon+VariCol (hybrid operation) were studied in detail, and their optimal performances were compared. The application of nonlinear model predictive control (NMPC) was also evaluated for the ModiCon and the VariCol processes. Different examples of enantioseparations were considered in the optimization and control studies. As a result, the complexity of the design optimizing problem of the VariCol process was reduced from MINLP (mixed-integer nonlinear programming) to an NLP (nonlinear programming). The ModiCon and the ModiCon+VariCol processes' optimal throughput was almost doubled that of the conventional SMB process. The controller responded satisfactorily to different disturbances. In all cases, it fulfilled the purity of raffinate and extract and optimized the process's economics.

Contents

List of Figures	xii
List of Tables	xvii
List of Symbols	xx
List of Abbreviations	xxiii
1 Introduction	1
1.1 Relevance and Motivation	1
1.2 Objectives	4
1.2.1 Main Objective	4
1.2.2 Specific Objectives	4
1.3 Document arrangement	5
1.4 Publications	6
1.4.1 Publications in indexed journals	6
1.4.2 Conference papers	7
2 Bibliographic review	8
2.1 Chirality	8
2.2 Chromatographic separation	10
2.2.1 Chromatography	10

2.2.2	True Moving Bed	11
2.2.3	Simulated Moving Bed	12
2.2.4	Variants of the SMB Process	14
2.2.4.1	VariCol Process	14
2.2.4.2	ModiCon Process	16
2.2.4.3	PowerFeed Process	18
2.3	Modeling, optimization and control	18
2.3.1	Modeling	18
2.3.2	SMB Design	21
2.3.2.1	Triangle Theory	21
2.3.2.2	SMB Optimization	24
2.3.3	VariCol process optimization	29
2.3.4	Performance comparison of some variants of SMB process . . .	34
2.3.5	Control	38
2.3.6	Final Remarks	45
3	Proposed Method	48
3.1	Introduction	48
3.2	Operations modes of the SMB process	49
3.2.1	VariCol process	49
3.2.1.1	Calculation of the initial column configuration	53
3.2.2	ModiCon process	55
3.3	Mathematical model of SMB and its variants	56
3.3.1	Dimensionless mathematical model	60
3.4	Spatial discretization	61
3.4.1	Discretization using finite differences (FD)	61

3.4.2	Discretization using orthogonal collocation on fixed finite elements	62
3.5	Optimization strategy	65
3.6	Control strategy	70
4	Results and discussion	73
4.1	Simulation and model validation	73
4.1.1	Separation of praziquantel with SMB process	75
4.1.2	Separation of 1,1'-bi-2-naphthol with Varicol process	77
4.1.3	Explicit and implicit approaches	80
4.1.3.1	Explicit approach	80
4.1.3.2	Implicit approach	84
4.2	Optimization of VariCol process	85
4.2.1	Initial column configurations	85
4.2.1.1	Case 1	86
4.2.1.2	Case 2	87
4.2.1.3	Case 3	88
4.2.1.4	Shifting schemes	89
4.2.2	Optimization examples	91
4.2.2.1	Enantioseparation of 1,1'-bi-2-naphthol	92
4.2.2.2	Enantioseparation of aminoglutethimide	98
4.3	Performance comparison of some SMB process variants	102
4.3.1	ModiCon	103
4.3.2	Hybrid ModiCon+VariCol operation mode	108
4.3.3	Performance comparison of 5- and 6-columns operation modes	112
4.3.4	Performance comparison of 6-columns SMB with 3-columns ModiCon+VariCol processes at unequal product purities . . .	116

4.4	Control	119
4.4.1	Separation of 1,1'-bi-2-naphthol with the VariCol process . . .	119
4.4.1.1	Disturbance on the switching period	121
4.4.1.2	Disturbance on the switching time of extract and raffinate and ports	123
4.4.2	Separation of guaifenesin with the ModiCon process	125
4.4.2.1	Desorbent pump malfunction	126
4.4.2.2	Feeding pump malfunction	129
4.4.2.3	Solenoid valve malfunction	131
5	Conclusions and future works	134
5.1	Conclusions	134
5.2	Future works	137
	References	139
A	Chromatographic column simulator	155
A.1	Sensitivity analysis for the parameters of the transport dispersion model	156
A.2	Comparison between different models	157
A.3	Conclusion	160

List of Figures

2.1	Four-section True Moving Bed (TMB) process. The separation direction of species A and B of the binary mixture is indicated with arrows.	12
2.2	Scheme of 8-columns simulated moving bed unit with a closed loop. (a) Initial position of ports, (b) position after a switching period. . . .	14
2.3	Column configuration in zones in the SMB and the VariCol processes for two switching periods.	16
2.4	Schematic representation of the ModiCon process with a feed concentration modulation of two sub-intervals in a switching period (t_s). . .	17
2.5	Simulation approach for SMB process. Adapted from (RUTHVEN and CHING, 1989).	20
2.6	Projection of separation region for binary mixture on the (m_{II} , m_{III}) plane with (a) linear adsorption isotherm and (b) competitive binary Langmuir isotherm. It was adapted from (RODRIGUES, 2015; SCHMIDT-TRAUB <i>et al.</i> , 2012).	23
2.7	Approaches to reach the cyclic steady state in the optimization problem. (a) Sequential, (b) simultaneous.	26
3.1	Schematic representation of the VariCol operation policies within a switching time period (t_s). Modulation of length of zones in four sub-intervals.	50
3.2	Optimization methodologies for ASMB. (a) The methodology proposed by Yao <i>et al.</i> YAO <i>et al.</i> (2014, 2017) (Method 1). (b) The methodology proposed in this work (Method 2).	67
3.3	Scheme adopted for controlling the SMB unit using an NMPC approach.	71

4.1	Graphical interface of the new version of the SiMoBed tool	74
4.2	Instantaneous internal concentration profiles for components A and B in the separation of praziquantel, considering two spatial discretizations. (a) Finite differences for different internal points (IP) and (b) Polynomial approximation on finite elements for different internal points (IP) and finite elements (FE).	76
4.3	Approximation of internal concentration profiles at cyclic steady state, using Finite differences and Polynomial approximation.	77
4.4	Concentration profiles of the components A and B in the separation of 1,1'-bi-2-naphthol, considering two spatial discretization methods. (a) Finite differences for different internal points and (b) Polynomial approximation on finite elements for different internal points and finite elements.	78
4.5	Approximation of internal concentration profiles at cyclic steady state, using Finite differences and Polynomial approximation.	79
4.6	Sparse pattern of the Jacobian matrix for finite differences considering 21 IP. The points in the square correspond to the sparsity pattern of column 3. The points in the circle correspond to the coupling of column 3 with the previous column via boundary conditions.	81
4.7	Sparse pattern of the Jacobian matrix for polynomial approximation: (a) 1 FE and 21 IP, (b) 3 FE and 7 IP. The points in the square correspond to the sparsity pattern of column 3.	82
4.8	Sparse pattern of the Jacobian matrix for polynomial approximation without considering the coupling between columns and between elements. (a) 1 FE and 21 IP, (b) 3 FE and 7 IP.	83
4.9	Sparse pattern of the Jacobian matrix for polynomial approximation considering an implicit implementation of the DAEs (a) 1 FE and 21 IP, (b) 3 FE and 7 IP.	84
4.10	Possible shifting schemes with different initial column configurations for the average configuration of $\bar{\mathbf{N}} = [1.76, 2.09, 2.60, 1.55]$	90
4.11	Purity for the different shifting schemes in the (a) Extract and (b) Raffinate.	91

4.12 Recovery for the different shifting schemes in the (a) Extract and (b) Raffinate.	91
4.13 Comparison of instantaneous internal concentration profiles for (a) SMB1 with VariCol 2, (b) SMB 2 with VariCol 1 and VariCol 3.	95
4.14 Instantaneous internal concentration profiles for the less (A) and the more retained component (B) when (a) zone IV has zero columns and (b) zone I has zero columns.	100
4.15 Pareto optimal solutions of 5-columns VariCol process and 6-columns SMB for variation of (a) feed flow rate with purities and (b) productivity of raffinate with purities.	101
4.16 Comparison of instantaneous internal concentration profiles for SMB 1, VariCol 1 and ModiCon 2 at the cyclic steady state. The arrow mark shows the displacement to the left of the most retained component of ModiCon 2 compared with the SMB 1. The SMB 1 and ModiCon 2 were plotted at 50% of the first switching period of the 25th cycle. The VariCol 1 was plotted at an equivalent point that was at 50% of the last switching period of the 25th cycle.	105
4.17 Variation of the maximal concentration of the less retained component (A) during a switching period for a feed concentration modulation pattern of: $\mathbf{c}_{f,i} = [0, 10] [mg \cdot cm^{-3}]$ and $\delta\mathbf{t}_{sb} = [0.6, 1]$	107
4.18 Possibilities to incorporate the modulation pattern of ModiCon process formed by $\mathbf{c}_{f,i} = [0, 10] [mg \cdot cm^{-3}]$ and $\delta\mathbf{t}_{sb} = [0.6, 1]$ in the shifting schemes of VariCol process obtained from the average column lengths of $\bar{\mathbf{N}} = [1.40, 1.84, 1.86, 0.90]$. $t_{sb,1}$ and $t_{sb,2}$ could be positioned at the actual position presented in the figure or at the arrow signal for $t_{sb,1}$ and the switching period (t_s) for $t_{sb,2}$	109
4.19 Comparison of instantaneous internal concentration profiles of the ModiCon and ModiCon+VariCol processes for system with 6 and 5 columns. (a) ModiCon 4 and MC+VC 3, (b) ModiCon 6 and MC+VC 5. ModiCon 4 and ModiCon 6 were plotted at 50% of the first switching period of the 25th cycle. MC+VC3 and MC+VC5 were plotted at 50% of the last switching period of the same 25th cycle.	115

4.20	Maximal throughput and productivity concerning extract and raffinate purity values for 5- and 6-columns SMB, VariCol, ModiCon, and the hybrid ModiCon+VariCol processes. (a) throughput vs. purity. (b) Productivity vs. purity.	116
4.21	Internal concentration profiles for (a) MC+VC 6 and (b) MC+VC 7. The profiles were plotted at the 50% of first switching period of 25 th cycle.	118
4.22	Response of the VariCol process to a disturbance on the switching period. (a) Uncontrolled system for disturbances of +25% and -25%; (b) controlled system for disturbance of -25%.	121
4.23	Manipulated variables and internal flow rates for the disturbance of -25% on the on the flow rate of desorbent pump. (a) Disturbance and manipulated; (b) Internal flow rates.	122
4.24	Difference between the sampling time and the computational effort required to solve the control optimization problem.	122
4.25	Response of the VariCol process to a disturbance on the switching time of extract and raffinate ports. (a) Uncontrolled system for disturbances of -25% and +25%; (b) controlled system for disturbance of -25% in t_e	124
4.26	Manipulated variables and internal flow rates for the disturbance of -25% on the extract port's switching time. (a) Manipulated variables; (b) Internal flow rates.	124
4.27	Difference between the sampling time and the computational effort required to solve the control optimization problem.	125
4.28	Response of the ModiCon process to a disturbance on the flow rate of desorbent pump. (a) Uncontrolled system for disturbances of -25% and +25%; (b) controlled system for disturbance of -25%.	127
4.29	Manipulated variables and internal flow rates for the disturbance of -25% on the on the flow rate of desorbent pump. (a) Disturbance and manipulated variables; (b) Internal flow rates.	128
4.30	Difference between the sampling time and the computational effort required to solve the control optimization problem.	128

4.31	Response of the ModiCon process to a disturbance on the flow rate of feed pump. (a) Uncontrolled system for disturbances of +25% and -25%; (b) controlled system for disturbance of +25%.	129
4.32	Manipulated variables and internal flow rates for the disturbance of +25% on the on the flow rate of feed pump. (a) Disturbance and manipulated variables; (b) Internal flow rates.	130
4.33	Difference between the sampling time and the computational effort required to solve the control optimization problem.	131
4.34	Response of the ModiCon process to a disturbance on the times of subintervals (δt_{sb}). (a) Uncontrolled system for disturbances of -25% and +25% concerning the first subinterval; (b) Controlled system for disturbance of -25%.	132
4.35	Manipulated variables and internal flow rates for the disturbance of -25% on the $t_{sb,1}$. (a) manipulated variables; (b) Internal flow rates. .	133
4.36	Difference between the sampling time and the computational effort required to solve the control optimization problem.	133
A.1	Graphical interface of the SimCol tool, a package to simulate and estimate parameters in individuals columns.	155
A.2	Sensitivity analysis for critical parameters of the transport dispersion model. (a) Positive variations; (b) Negative variations	157
A.3	Comparison of two dispersion models for simulating (a) the elution curves, (b) and the internal concentration profiles of the enantioseparation of ModiCon+VariCol with 3 columns at the 50% of first switching period of 25th cycle.	159
A.4	Comparison of TD model and ED model for (a) the elution curves, (b) the internal concentration profiles of the enantioseparation of ModiCon+VariCol with 3 columns at the 50% of first switching period of 25th cycle.	160

List of Tables

2.1	Comparison of different approaches used in the control of the SMB process.	45
4.1	Parameters for the separation of a racemic mixture of praziquantel. Index A refers to the less retained enantiomer, and B to one more retained.	75
4.2	Parameters for the enantioseparation of 1,1'-bi-2-naphthol. Index A refers to the less retained enantiomer and index B to the one most retained.	77
4.3	Computational effort of the two discretization methods using the sparse matrix.	79
4.4	Computational effort to solve the DAEs explicitly and implicitly using as integrator <i>ode15s</i> and <i>ode15i</i>	85
4.5	Combinations of lower and upper integer values of $\bar{\mathbf{N}} = [1.76, 2.09, 2.60, 1.55]$, whose sum is equal to 8	86
4.6	Relative switching times for the different possible initial column configurations at the average configuration of $\bar{\mathbf{N}} = [1.76, 2.09, 2.60, 1.55]$	86
4.7	Vector of normalized switching times for the initial configuration options	87
4.8	Options for initial column configuration from the average column length of $\bar{\mathbf{N}} = [1.83, 1.98, 2.67, 1.52]$	87
4.9	Vector of normalized switching times for the initial configuration options	88
4.10	Options for initial column configuration from the average column configuration of $\bar{\mathbf{N}} = [1.85, 2.15, 2.50, 1.50]$	88
4.11	Vector of normalized switching times for the initial configuration options	88

4.12	Parameters for the enantioseparation of 1,1'-bi-2-naphthol and aminoglutethimide. Index <i>A</i> refers to the less retained and <i>B</i> to the more retained enantiomers.	92
4.13	Optimal operation parameters that maximize the feed flow rate for the enantioseparation of 1,1'-bi-2-naphthol	93
4.14	Separation performance of the VariCol and SMB processes at the cyclic steady state	95
4.15	Initial options for Method 1 that are equivalent to the initial average column configuration $\bar{N} = [1.50, 2.62, 2.43, 1.45]$ for Method 2	96
4.16	Computational effort for the methodology proposed by Yao et al. YAO <i>et al.</i> (2014, 2017) – Method 1, and for the one proposed in this work – Method 2	97
4.17	Optimal operation parameters that maximize the feed flow rate for the enantioseparation of aminoglutethimide	99
4.18	Parameters for the enantioseparation of guaifenesin racemate. Index <i>A</i> refers to the less retained and <i>B</i> to the most retained enantiomers .	103
4.19	Optimal operation parameters for the ModiCon process with two modulations in the feed concentration	104
4.20	The new configuration in the modulation pattern of feed concentration after displacement, which keeps the feed port as the reference	110
4.21	Purity in the extract and the raffinate for the hybrid ModiCon+VariCol considering a displacement in the modulation pattern of feed concentration for the different CCSs	110
4.22	Optimal results for the hybrid ModiCon+VariCol that were obtained using different reference ports	111
4.23	Optimal operating parameters for the ModiCon process and the hybrid operation mode ModiCon+VariCol considering systems with 5 and 6 columns	113
4.24	Optimal operation parameters for the 6-columns SMB and the 3-columns ModiCon+VariCol processes at unequal purity in the products	117

4.25	Optimal operation parameters for the enantioseparation of 1,1'-bi-2-naphthol with a 8-columns VariCol process and a maximal pressure drop of 3 bar for each zone	120
4.26	Optimal operation parameters for the enantioseparation of guaifenesin with a 6-columns ModiCon process and a maximal pressure drop of 6 bar for each zone	126
A.1	Parameters for the the racemic mixture of guaifenesin used in the transport dispersion model in terms of bed porosity. Index <i>A</i> refers to the less retained and <i>B</i> to the most retained enantiomers	159

List of Symbols

A	Matrix with the first derivative of Lagrange interpolators, p. 60
B	Matrix with the second derivative of Lagrange interpolators, p. 60
D_L	Axial dispersion coefficient [$L^2 T^{-1}$], p. 52
D_{app}	Apparent dispersion coefficient for total porosity [$L^2 T^{-1}$], p. 53
D_p	Lumped pore and surface diffusion [$L^2 T^{-1}$], p. 52
H	Henry constant, p. 21
H_c	Control horizon, p. 66
H_p	Prediction horizon, p. 66
K	Adsorption constant [ML^{-3}], p. 54
L	Interpolating Lagrange polynomials, p. 59
M	Subscript that refer to the sections I, II, III and IV, p. 21
P_e	Péclet number, p. 56
Q	Internal flow rate [$L^3 T^{-1}$], p. 53
Q_M	Internal flow rate in sections M [$L^3 T^{-1}$], p. 21
Q_p	External flow rate of desorbent, extract, feed and raffinate [$L^3 T^{-1}$], p. 56
S	Cross-sectional column area [L^2], p. 53
S_t	Stanton number, p. 56
V	Total column volume [L^3], p. 21

c	Mass concentration in the fluid phase [$M L^{-3}$], p. 52
c^{in}	Concentration of each component at the inlet of each column [$M L^{-3}$], p. 55
c_p	Concentration in the inlet or outlet streams [$M L^{-3}$], p. 56
\bar{c}_p	Mean concentration in the pores [$M L^{-3}$], p. 52
d	Desorbent port, p. 56
e	Extract port, p. 56
f	Feed port, p. 56
i	Refers to the components of the system, p. 52
j	Discretization points, p. 57
k	Refers to the columns of system, p. 52
k_{eff}	Lumped rate coefficient or apparent mass coefficient for total porosity [T^{-1}], p. 53
k_{eff}^*	Lumped rate coefficient or apparent mass coefficient [T^{-1}], p. 52
l	Column length [L], p. 55
m_M	Dimensionless flowrate ratio in each zone, p. 20
n_s	Equally spaced elements or subdomains, p. 59
p	Subscript that refers to desorbent, extract, feed and raffinate, p. 56
q_e	Adsorbed concentration at equilibrium with fluid phase concentration [$M L^{-3}$], p. 53
q_m	Saturation concentration [$M L^{-3}$], p. 54
\bar{q}	Mean concentration in the solid skeleton [$M L^{-3}$], p. 52
\bar{q}^*	Mean overall adsorbent loading in the adsorbed phase [$M L^{-3}$], p. 52
r	Raffinate port, p. 56
r_p	Particle radius [L], p. 52

s	Superscript that refers to elements or subdomains, p. 59
t	Time $[T]$, p. 52
t_s	Switching period of ports, p. 21
u	Superficial velocity $[L T^{-1}]$, p. 53
v	Interstitial velocity $[L T^{-1}]$, p. 52
\bar{v}_f	Maximum superficial velocity of all zones $[L T^{-1}]$, p. 56
v_k^{hyp}	Hypothetical effective velocity $[L T^{-1}]$, p. 53
x	Dimensionless axial coordinate, p. 56
z	Axial coordinate $[L]$, p. 52
ε	Column overall bed void fraction, p. 21
ε_b	Bed void fraction, p. 21
ε_p	intraparticle void fraction, p. 21
ξ	Dimensionless interstitial velocity, p. 56
τ	Dimensionless time, p. 56
χ	Dimensionless axial coordinate for each elements or subdomains, p. 59

List of Abbreviations

ACL	Average Column Length in zones in the VariCol process, p. 52
ASMB	Asynchronous Simulates Moving Bed, p. 14
CCS	Column Configuration Sequence for VariCol process, p. 15
CQ	Chloroquine Phosphate, p. 2
DAEs	Differential-Algebraic Equations, p. 65
EMA	European Medicines Agency, p. 2
FDA	Food and Drug Administration, p. 2
FD	Finite Differences, p. 73
FE	Finite Elements, p. 76
GRM	General Rate Model, a rigorous model, p. 19
HCQ	Hydroxychloroquine Sulfate, p. 2
IP	Internals Points, p. 76
JM	Jacobian Matrix, p. 38
MINLP	Mixed-Integer Nonlinear Programming, p. 25
MPC	Model Predictive Control, p. 40
NLP	Nonlinear Programming, p. 25
NMPC	Nonlinear Model Predictive control, p. 44
ODE	Ordinary Differential Equation, p. 43
ODEs	Ordinary Differential Equations, p. 65
PA	Polynomial Approximation on fixed finite elements, p. 62

PID	Proportional Integral Derivative controller, p. 39
PZQ	Praziquantel, p. 2
P	Proportional controller, p. 39
SMB	Simulated Moving Bed, p. 12
SNLIV	Sum of the Nearest Lower Integer Values of an average column length of zones, p. 53
ST	Switching Time of the ports in the VariCol process, p. 50
TMB	True Moving Bed, p. 11
WHO	World Health Organization, p. 2

Chapter 1

Introduction

1.1 Relevance and Motivation

The demand for chiral ¹ compounds is growing in diverse industries such as pharmaceutical, fine chemistry, and biotechnology, due to their different properties and various applications, especially in living organisms (JENCK *et al.*, 2004; LIN *et al.*, 2011; LORENZ and SEIDEL-MORGENSTERN, 2014; MARKETWATCH, 2021). The increase of the chiral compounds market during 2021-2026 is estimated at USD 53.2 billion, where the compound annual growth rate is about 11% (MARKETWATCH, 2021). Under the COVID-19 outbreak comprehensively, there are forecasts that the chiral chemical market could increase further for new market and consumers trends and government policies and interventions on public health issues (MARKETWATCH, 2021; REPORTLINKER, 2021). Interest in chiral compounds is mainly related to pure (single enantiomers) or almost pure forms due to their different properties in specific environments such as the body of living organisms (LIN *et al.*, 2011). However, the production of pure enantiomers at low cost is a challenging task (LORENZ and SEIDEL-MORGENSTERN, 2014). Therefore one of the most crucial issues in developing, designing, and marketing new chiral products is synthesizing the desired pure enantiomer (LORENZ and SEIDEL-MORGENSTERN, 2014).

The chiral compounds represent an essential part of the synthetic drugs of the pharmaceutical industry. When the chiral compounds are in the form of racemic mixtures (mixture in equal proportion of two enantiomers), generally, only one of the enantiomers is therapeutically active, while the other represents impurities and, in

¹Compound with asymmetric center (chiral atom or chiral center), occurring in two non-superimposable mirror-image forms (enantiomers).

some cases, unwanted properties (LORENZ and SEIDEL-MORGENSTERN, 2014; MURAKAMI, 2006). A large number of drugs are found in the market as a racemic mixture. For example, among the 754 new drugs launched in the world between 1985 and 2004 (20 years), 313 (41.5%) were chiral (MURAKAMI, 2006). From those chiral drugs, 137 (43.8%) were racemic mixtures. One example is the praziquantel (PZQ), a chiral drug found in the market as a racemic mixture of (R)-PZQ and (S)-PZQ. Only the (R)-PZQ enantiomer is the active compound for the treatment of schistosomiasis (CIOLI and PICA-MATTOCCIA, 2003; LIU *et al.*, 1993, 2004). PZQ is listed as an essential drug of the world health organization (WHO) to treat schistosomiasis species (WORLD HEALTH ORGANIZATION, 2006). That disease is a global public health problem, and it is estimated that over 200 million people in the world are affected by schistosomiasis (CHITSULO *et al.*, 2000). The enantiomer (R)-PZQ should be used in a more pure form to treat schistosomiasis since the (S)-PZQ enantiomer in high doses may cause undesirable effects and is responsible for the bitter taste (BAGCHUS *et al.*, 2019; FENWICK *et al.*, 2003; ZWANG and OLLIARO, 2014). Since 2014, the [Pediatric Praziquantel Consortium](#) (the Brazilian Farmanginhos is participating), a nonprofit organization, has been developing a formula based only on (R)-PZQ (BAGCHUS *et al.*, 2019; ZWANG and OLLIARO, 2014).

Under the COVID-19 outbreak, two chiral drugs, chloroquine phosphate (CQ) and hydroxychloroquine sulfate (HCQ), have generated diverse political and economic debate due to their apparent efficacy in treating COVID-19 (D'ACQUARICA and AGRANAT, 2020; GASMI *et al.*, 2021; LENTINI *et al.*, 2020). Those drugs are used in the form of racemates to treat malaria, rheumatoid arthritis, lupus erythematosus, and other autoimmune diseases (D'ACQUARICA and AGRANAT, 2020). CQ and HCQ were considered initial candidates for treatment and therapy for shortening the COVID-19 due to the initial *in vitro* activity to inhibit this viral disease (LIU *et al.*, 2020). However, after different treatment evaluations of these drugs, the WHO reported that "they have little or no effect on overall mortality, initiation of ventilation, and duration of hospital stay in hospitalized patients" (WORLD HEALTH ORGANIZATION, 2020). Studies for the separation and purification of CQ and HCQ have also been recently reported (XIONG *et al.*, 2021), as the S-CQ and S-HCQ have shown lower side effects than R-CQ and R-HCQ (D'ACQUARICA and AGRANAT, 2020).

The regulatory agencies such as the Food and Drug Administration (FDA) or the European Medicines Agency (EMA) are demanding the use of racemic drugs only in the pure enantiomeric form (CALCATERRA and D'ACQUARICA, 2018; LORENZ and SEIDEL-MORGENSTERN, 2014; MURAKAMI, 2006). The separation of

racemic mixtures or the synthesis of the pure enantiomers turns a crucial stage in manufacturing chiral drugs. Different methods can be used to produce pure enantiomers. Those methods usually are classified as those based on asymmetric synthesis and those that use a resolution step from a racemic mixture (LORENZ and SEIDEL-MORGENSTERN, 2014; RAJENDRAN *et al.*, 2009). The last group is becoming most popular since they are cheaper and less complex than former one (LORENZ and SEIDEL-MORGENSTERN, 2014; RODRIGUES, 2015). In the last group, the separation can be reached with the kinetic resolution (enantioselective crystallization) and the preparative chromatography. The most important technique in the preparative chromatography is the Simulated Moving Bed (SMB), based on a train of multiple columns that operate continuously (CHANKVETADZE, 2001; LORENZ and SEIDEL-MORGENSTERN, 2014; RAJENDRAN *et al.*, 2009; RODRIGUES, 2015).

The SMB process was initially developed for petrochemical separation but was later applied in other industries, such as sugar, pharmaceutical, fine chemistry, and biotechnological industries (CHING *et al.*, 1993; FRANCOITTE, 2001; FRANCOITTE and RICHERT, 1997; NEGAWA and SHOJI, 1992; NICOUD *et al.*, 1993; SCHULTE and STRUBE, 2001). That wide application is due to its potential to operate continuously, at a large scale and reach high purity and productivity with low solvent consumption (BROUGHTON and GERHOLD, 1961; JUZA *et al.*, 2000). The synergism of the SMB can be further exploited with the new variants based on the modulation of some parameters. When more general objectives are pursued, SMB can also be combined with other processes such as crystallization and racemization (LORENZ and SEIDEL-MORGENSTERN, 2014).

Some of the most relevant and widespread variants of the SMB process are PowerFeed, ModiCon, and VariCol processes obtained by the periodic modulations of some parameters (LUDEMANN-HOMBOURGER *et al.*, 2000; SCHRAMM *et al.*, 2003a,b; ZANG and WANKAT, 2002; ZHANG *et al.*, 2003). These operation modes can also be combined to create new hybrid variants (YU *et al.*, 2015; ZHANG *et al.*, 2004a). Although the variants are more complex to operate and describe than the conventional SMB process, they give more flexibility to the system and increase the separation performance (LUDEMANN-HOMBOURGER *et al.*, 2000; SCHRAMM *et al.*, 2003a,b; TOUMI *et al.*, 2007; YANG *et al.*, 2019; YAO *et al.*, 2014, 2017; YU *et al.*, 2015; ZHANG *et al.*, 2003, 2004a). Evaluating the performance of those variants and finding their appropriate operation points is important to have guidelines in selecting one of them and taking advantage of their maximum potential. As the optimal points are generally tricky to operate since those systems are sensitive to any changes, advanced control strategies are necessary (KLATT *et al.*, 2002).

The development of tools to model, optimize, and control the SMB process and its variants are fundamental for the study and application of the SMB technology. In a work of our laboratory (NETO, 2015), two tools called SiMoBed and SiMoCon based on the MATLAB suite were developed to simulate and control the conventional SMB process. Those tools used the transport dispersion and equilibrium dispersion models coupled with classic and explicit adsorption isotherms to describe the dynamics in the chromatographic columns. The solution of these models was based on the discretization of the spatial variable using finite differences and the direct integration of the resulting differential-algebraic equations system. However, SiMoBed and SiMoCon should be updated to include some of the most popular SMB process variants. In addition, more robust discretization methods should be used, such as orthogonal collocation on finite elements.

SMB is a promising technology applied for difficult separations such as racemic mixtures and heat sensitive products, challenging to outperform with conventional techniques as distillation. This technology's advantage is the continuous operation and the high purity and productivity with low solvent consumption. As the SMB process represent high fixed and operating cost, the functioning at the maximum potential is necessary (RODRIGUES, 2015; RODRIGUES *et al.*, 2012). The cost can be lower when variants of the SMB process are used since they have a higher separation performance. An in-depth study of the variants and the performance comparison between them is essential for selecting the appropriate variant that reduces the separation cost of those enantiomers with high value, especially in pharmaceutical industries. In addition, different computational tools must be available for the study and application of SMB technology.

1.2 Objectives

1.2.1 Main Objective

Compare the performance and evaluate the operating conditions at optimal points for some SMB process variants using optimization and nonlinear model predictive control.

1.2.2 Specific Objectives

- Compare and evaluate different models of chromatographic columns, such as the transport dispersion and the equilibrium dispersion.

- Implement and evaluate the convergence and convenience of orthogonal collocation on finite elements to discretize the transport dispersion and equilibrium dispersion models.
- Evaluate the performance to solve the mathematical models in an implicit or explicit form based on the sparse Jacobian matrix.
- Include and evaluate the performance of the following SMB process variants: VariCol, ModiCon, PowerFeed and the combinations of some of them.
- Study the VariCol process deeply and propose a new strategy that reduces the complexity of the optimization problem.
- Proof the use of nonlinear model predictive control in the digital twin for some SMB process variants.

1.3 Document arrangement

This thesis is structured in five chapters, as follows:

- Chapter 1: In this part, a brief contextualization of the research is given. Initially, the relevance and motivation that include a brief description of the need to take advantage of SMB technology to separate racemic mixtures are described. After, the principal and specific objectives of this work are presented. Finally, the structure of this document to facilitate its reading is given.
- Chapter 2: In this chapter, an extensive bibliographic review about the methods to simulate, optimize and control the SMB technology is presented. Initially, a contextualization about the need to separate chiral chemicals is presented. After a detailed description of SMB technology and the different variants is given. Finally, an in-depth bibliography review about simulation, optimization and control of the SMB process is introduced.
- Chapter 3: The mathematical approach to simulate, optimize and control the conventional SMB process and its variants is presented. Initially, the mathematical model of the SMB process and the methods to discretize and solving it are presented. After, the optimization strategies used to evaluate and compare the different SMB process variants are given. Finally, the control strategy to keep some of these processes operating at an optimal point based on an economic function is presented.

- Chapter 4: The results of the current research are shown in this chapter. In the beginning, a comparison between two methods for discretizing the partial differential equations of the system and analyses of explicit and implicit approaches for the models are presented. Then, an optimization strategy that reduces the original MINLP (mixed-integer nonlinear programming) formulation of the VariCol process to a single NLP (nonlinear programming) formulation is presented (CALDERÓN SUPELANO *et al.*, 2020). Later, a study of the ModiCon process with the performance comparison with other SMB process variants, including the hybrid VariCol+ ModicCon is presented (CALDERÓN SUPELANO *et al.*, 2021). Finally, some studies of nonlinear model predictive control over some operation modes are presented.
- Chapter 5: In this chapter, conclusions are summarized, and the proposals for future works are presented.
- Appendix A: In this appendix, a package to simulate individual chromatographic columns is initially presented. After, the study and comparison of some models of chromatographic columns, such as the transport dispersion and the equilibrium dispersion, are shown.

1.4 Publications

1.4.1 Publications in indexed journals

- CALDERÓN SUPELANO, R., BARRETO JR, A. G., ANDRADE NETO, A. S., et al., 2020, "One-step optimization strategy in the simulated moving bed process with asynchronous movement of ports: A VariCol case study", Journal of Chromatography A, v. 1634, pp. 461672. ISSN: 0021-9673. doi: <https://doi.org/10.1016/j.chroma.2020.461672>. Available in: <https://www.sciencedirect.com/science/article/pii/S0021967320309468>.
- CALDERÓN SUPELANO, R., BARRETO, A. G., SECCHI, A. R., 2021, "Optimal performance comparison of the simulated moving bed process variants based on the modulation of the length of zones and the feed concentration", Journal of Chromatography A, v. 1651, pp. 462280. ISSN: 0021-9673. doi:<https://doi.org/10.1016/j.chroma.2021.462280>. Available in: <https://www.sciencedirect.com/science/article/pii/S0021967321004040>.

1.4.2 Conference papers

- CALDERÓN SUPELANO, R., BARRETO JR, A. G., ANDRADE NETO, A. S., et al., 2018, "Nonlinear model predictive control of a simulated moving bed unit", XXII Congresso Brasileiro de Engenharia Química. doi: <https://doi.org/10.5151/cobeq2018-CO.143>.
- CALDERÓN SUPELANO, R., BARRETO, A. G., SECCHI, A. R., 2021, "Optimization and nonlinear model predictive control of simulated moving bed process with modulation in the feed concentration ", Paper submitted to the XXIII Congresso Brasileiro de Engenharia Química.

Chapter 2

Bibliographic review

2.1 Chirality

Chiral chemicals have the same molecular formula and sequence of bonded atoms but with an asymmetric spatial arrangement (stereoisomers). When two of these compounds are mirror images, not superimposable of each other as happens with the left and right hand of a person, they are called enantiomers (LIN *et al.*, 2011; LORENZ and SEIDEL-MORGENSTERN, 2014). A mixture of two enantiomers, called racemic mixture, will always be produced when the synthesis takes place without special conditions. The enantiomers in an achiral environment have the same physical and chemical properties, but they present different chemical properties in a chiral environment (LIN *et al.*, 2011). Many of the components associated with the living organism are chiral environments. As enantiomers are used in different industries for different purposes in living organisms, there is a higher necessity to produce them in the optically pure form or in specific proportions to avoid undesired effects (LORENZ and SEIDEL-MORGENSTERN, 2014). In particular, in the pharmaceutical industry, the enantiomers represent an essential part of synthetic drugs (MURAKAMI, 2006).

In chiral drugs, generally, one of the enantiomers is responsible for the desired pharmaceutical activity while the other is inactive or has different desirable or undesirable effects (LIN *et al.*, 2011). The enantiomers in the human body that is a chiral environment¹ present different chemical, pharmacological, toxicological, and pharmacokinetics (absorption, distribution, metabolism, and excretion) properties (LIN *et al.*, 2011; NGUYEN *et al.*, 2006). The US Food and Drug Administration

¹Chiral environment: a place where enantiomers can be distinguished by interacting differently with this environment.

and the European Medicines Agency regulators have imposed strict regulations in the purity constraints of the chiral drugs, being necessary in many cases to have one enantiomer more concentrated than the other or in the optically pure form (COLLINS *et al.*, 1997; LORENZ and SEIDEL-MORGENSTERN, 2014). The necessity to purify or produce pure enantiomers at low cost and reliable routes is evident since the demand for drugs based on pure or specific proportions of enantiomers has risen (LIN *et al.*, 2016; LORENZ and SEIDEL-MORGENSTERN, 2014; MAIER *et al.*, 2001).

Praziquantel is an example of a chiral drug where one of the enantiomers (R-praziquantel) is active for treating schistosomiasis, while the other (S-praziquantel) is inactive (BAGCHUS *et al.*, 2019; CIOLI and PICA-MATTOCCIA, 2003; FENWICK *et al.*, 2003; MEIER and BLASCHKE, 2001; ZWANG and OLLIARO, 2014). Besides, the inactive enantiomer in high doses may cause undesirable effects and is responsible for the bitter taste of the drug (FENWICK *et al.*, 2003). The pure production of R-praziquantel is desirable for reducing the doses and avoiding side effects (FENWICK *et al.*, 2003). Since 2014, the [Pediatric Praziquantel Consortium](#), a nonprofit organization, has been developing a formula based only on (R)-PZQ (BAGCHUS *et al.*, 2019; ZWANG and OLLIARO, 2014). Another example is Guaifenesin, an expectorant chiral drug used for cough remedy formulations (DICPINIGAITIS and GAYLE, 2003; GONG *et al.*, 2014a; KAGAN *et al.*, 2009). That drug is based on the racemic mixture since the different properties (chemical, pharmacological, and pharmacokinetics) of each enantiomer have not been well studied. However, only one is suspected of having the pharmacological properties (GONG *et al.*, 2014a; KAGAN *et al.*, 2009; YANG *et al.*, 2019).

Methods to produce pure enantiomers can be divided into two main groups: Asymmetric synthesis of one enantiomer or resolution from the racemic mixture (LORENZ and SEIDEL-MORGENSTERN, 2014; MAIER *et al.*, 2001). In the first case, an achiral raw material in a chiral environment is converted into a chiral product. However, the number of stages, the cost of all reagents, and the time to develop the route would increase the production costs (LIN *et al.*, 2011; LORENZ and SEIDEL-MORGENSTERN, 2014; MAIER *et al.*, 2001). The second group has been more applied in the last years since pure enantiomer can be obtained in a shorter period without developing a synthesis route. Additionally, in many cases, the production costs could be lower (JUZA *et al.*, 2000; LORENZ and SEIDEL-MORGENSTERN, 2014; MAIER *et al.*, 2001). There are different resolution methods, but the more flexible and productive ones are selective crystallization and chromatographic separation (LORENZ and SEIDEL-MORGENSTERN, 2014). Chromatography-based methods are considered the most powerful techniques to enantioseparation (LORENZ and

SEIDEL-MORGENSTERN, 2014; MAIER *et al.*, 2001).

2.2 Chromatographic separation

2.2.1 Chromatography

Chromatography is an adsorptive separation process in which a fluid phase of dissolved species (adsorbate) is transported to a stationary phase (adsorbent) where the molecules are deposited (BONILLA-PETRICIOLET *et al.*, 2017; RODRIGUES and TONDEUR, 1981; SCHMIDT-TRAUB *et al.*, 2012). The adsorbent binds the adsorbate molecules through physical (physisorption) and chemical forces (chemisorption). Only the physisorption is exploited in the chromatographic process since it requires the reversibility of the adsorption step (SCHMIDT-TRAUB *et al.*, 2012). Depending on the nature of the fluid phase (gas and liquid phases), the chromatographic systems can be divided into gas chromatography and liquid chromatography. In those types of chromatographic processes, the stationary phase can be solid and liquid. In the separation of chiral compounds, there is more interest in liquid chromatography with solid stationary phase (LORENZ and SEIDEL-MORGENSTERN, 2014). For chiral separations, naturally, the carrying agent in the fluid phase is achiral to be easily recuperated at the end. The stationary phase is a chiral environment to exploit the selective interactions (LORENZ and SEIDEL-MORGENSTERN, 2014).

In liquid chromatography, the adsorption process occurs when the fluid phase is forced through a column packed with the adsorbent particles. The difference of physical properties of adsorbed species with the solid phase leads to different adsorption times, resulting in different migration speeds of each component through a column, allowing the separation (SCHMIDT-TRAUB *et al.*, 2012). The liquid chromatography separation (preparative chromatography) is typically realized in a batch-wise manner on one column, but for large-scale separation, continuous processes are also used (LORENZ and SEIDEL-MORGENSTERN, 2014; RODRIGUES and TONDEUR, 1981; SCHMIDT-TRAUB *et al.*, 2012).

The mobile or fluid phase should be selected following the compound to be separated and the stationary phase (ANICETO and SILVA, 2015b; JUZA *et al.*, 2000). In the preparative chromatography, some complex and more selective mobile phases can be needed. However, in the simulated moving bed process, which will be described later, a common solvent can be used, such as water, ethanol, methanol, or mixtures thereof (ANICETO and SILVA, 2015b; SÁ GOMES and RODRIGUES,

2012).

The stationary phase used in liquid chromatography for enantioseparation needs to have different properties such as selectivity (chiral environment), loading capacity, chemical stability, mechanical stability, and a reasonable lifetime (JUZA *et al.*, 2000). Additionally, it needs to be relatively cheap, more than the desired enantiomer, to make the separation feasible. This phase is often derived from polysaccharide compounds such as cellulose and amylose immobilized in silica supports (FRANCOTTE, 2001; JUZA *et al.*, 2000). Although many stationary phases with chiral environment can be used for preparative enantioseparations, the bulk enantiomers can be resolved with not more than four polysaccharide (FRANCOTTE, 2001; RAJENDRAN *et al.*, 2009).

2.2.2 True Moving Bed

The True Moving Bed (TMB) process is a theoretical formulation of the chromatographic process to convert the batch operation into a continuous operation. The principle of the TMB is based on the counter-current movement between the solid and the fluid phase (continuous circulation of fluid and solid phases in opposite directions). The theory for the separation of binary mixtures with the TMB process is well detailed in the literature (BROUGHTON and GERHOLD, 1961; GUIOCHON *et al.*, 2006; JUZA *et al.*, 2000; RAJENDRAN *et al.*, 2009; RUTHVEN and CHING, 1989; SEIDEL-MORGENSTERN *et al.*, 2008). The TMB is represented by 4 sections or zones, separated by different input and output streams, as it is schematically depicted in Figure 2.1. The streams entering the process are the feed stream (located between sections two and three) containing a binary mixture to be separated and the desorbent or eluent stream (located in section one) that helps to regenerate the solid phase. Output streams are the raffinate stream (located between sections three and four) enriched with the less adsorbable component, and the extract stream (located between sections one and two) enriched with the more adsorbable component. The desorbent that exits from section four is recycled to section one, and similarly, the solid phase from section one is recycled to section four. Each zone or section has a specific function for the separation: zone I regenerates the solid phase, desorbing the more retained component; zone II enriches the solid phase with the more retained component that is collected in the extract port; zone III adsorbs the more retained component that has been moved with the fluid phase and zone IV regenerates the solvent, preventing contamination in the eluent that is recycled to zone I.

The counter-current movement of solid and liquid phases in the TMB process is

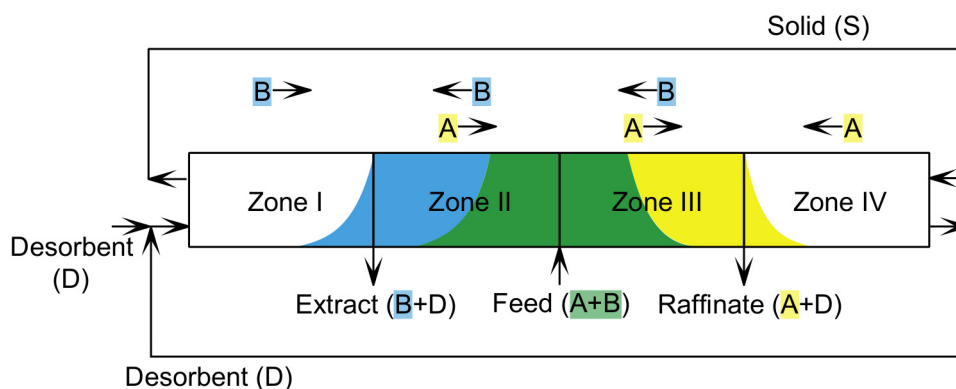


Figure 2.1: Four-section True Moving Bed (TMB) process. The separation direction of species A and B of the binary mixture is indicated with arrows.

advantageous because it enhances the transfer driving force, increases productivity, and reduces the use of solvent consumption. The TMB process also permits achieving high purity and productivity, even with low chromatographic resolution (reduced selectivity) and low efficiency of columns (MILLER *et al.*, 2003). Even though the counter-current movement of the TMB has significant advantages over traditional batch-wise preparative chromatography, it presents some technical problems related to the solid phase movement. Those problems are the mechanical erosion of the adsorbent, equipment abrasion, and difficulties maintaining the solid phase plug flow, among others (BROUGHTON and GERHOLD, 1961; RAJENDRAN *et al.*, 2009; RUTHVEN and CHING, 1989; SÁ GOMES and RODRIGUES, 2012). Those problems restrict a real implementation of the TMB and, nowadays, the TMB is only a theoretical concept (ANICETO and SILVA, 2015a).

The problems associated with the solid phase movement of the TMB process were surpassed with the simulated moving bed process (SMB), where there is not a real solid-phase movement but instead a simulated discrete movement of that solid phase. The SMB consists of a train of static columns with the same number of inputs and outputs ports as in the TMB. The simulated movement of the solid phase and the counter-current movement is reached with a synchronous switching of inlet and outlet ports in the fluid phase direction.

2.2.3 Simulated Moving Bed

The simulated moving bed process consists of multiple chromatographic separation columns connected in series in either an open- or closed-loop configuration, forming a train of chromatographic columns with two inputs and outputs ports. The SMB was developed and patented by Universal Oil Products in 1961 (BROUGHTON and

GERHOLD, 1961). However, in the 90s, this technology started growing significantly after being reported its potential for separation of pharmaceutical compounds and biomolecules (CHING *et al.*, 1993; FRANCOITTE, 2001; FRANCOITTE and RICHERT, 1997; NEGAWA and SHOJI, 1992; NICOUD *et al.*, 1993; SCHULTE and STRUBE, 2001). The SMB process has important operation advantages over other traditional chromatographic separation methods, such as continuous operation, capacity to produce high purity, and high productivity with low eluent consumption.

SMB can be considered a discretization in several fixed-bed columns of the TMB configuration. The solid phase movement is simulated with a discrete shifting of one column position for each input and output port in the same direction of the fluid phase. The shifting of inputs and output ports solves the limitations of the solid phase movement found in implementing a true moving bed concept (BROUGHTON and GERHOLD, 1961). To simulate the counter-current movement of the solid and fluid phases, the periodical switching of ports is carried out in a synchronized way and in the same direction as the fluid phase movement. When the ports return to the initial position after some periodical switchings, the process reaches a cycle. The cyclical SMB operation is closer to the TMB operation when the number of columns increases and the switching time decreases (ANICETO and SILVA, 2015b; BROUGHTON and GERHOLD, 1961; RUTHVEN and CHING, 1989). The complex dynamic of the SMB does not reach a real steady state as occurs in theoretical TMB process but instead achieves a cyclic steady state (CSS) (RAJENDRAN *et al.*, 2009). The schematic representation of the SMB process is depicted in Figure 2.2 for a system with 8 columns. The initial position of the SMB process is presented in Figure 2.2a, and the position after a switching period where all ports shift synchronously is presented in Figure 2.2b. In those figures a cycle is completed after 8 switching periods when all ports return to the same position of Figure 2.2a. The column length (l) divided by the switching period (t_s) represents the hypothetical solid velocity in the SMB.

Like the TMB, the SMB chromatographic column train is divided into 4 sections or zones, separated by the input and output ports, as shown in Figure 2.2. The roles of each zone in the separation of a mixture of two components are analogous to the TMB process: in zone I, the stationary phase is regenerated; in zone II, the less retained component is desorbed (component A in Figure 2.2); in zone III, the more retained component is adsorbed (component B in Figure 2.2); in zone 4 the solvent is regenerated. Zone II and zone III are called separation zones because that is where the separation occurs. The input and output ports that separate each zone are the feed port (between sections II and III), where the mixture to be separated enters; the refining port (sections III and IV), where the less retained component

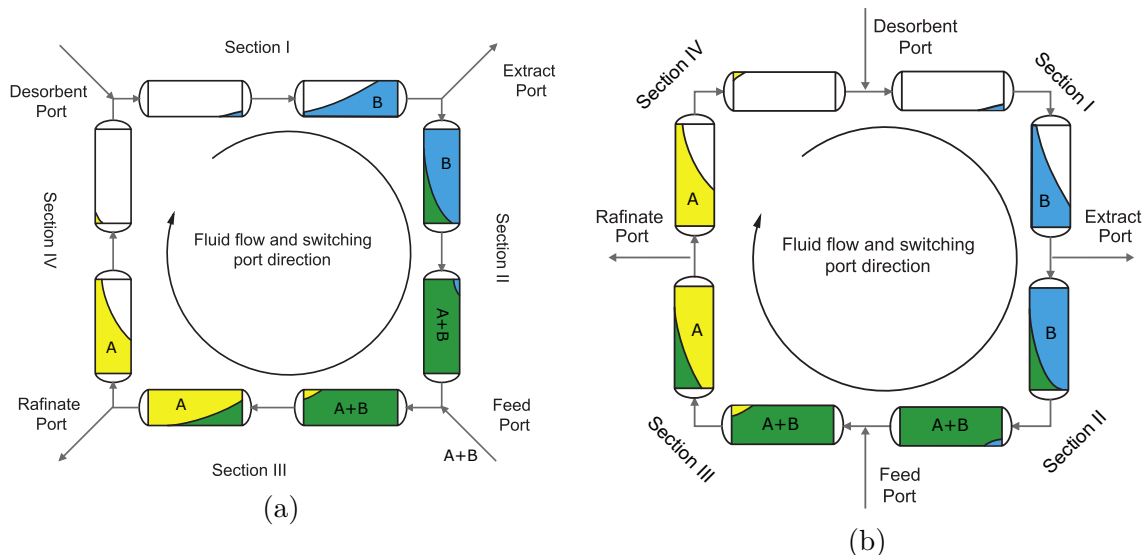


Figure 2.2: Scheme of 8-columns simulated moving bed unit with a closed loop. (a) Initial position of ports, (b) position after a switching period.

is collected; the desorbent port (sections IV and I), where the solvent is fed; the extract port (section I and II), where the more retained component is collected.

In general, the operation of the SMB process is defined by the following properties: four distinct sections or zones, a fixed number of columns per zone, constant operation parameters during a shift period, isocratic operation (constant elution strength), constant inlet and outlet flow rates, and synchronous operation. When some of these fixed operating parameters and characteristics are relaxed, many operation modes or variants, which are more efficient than the conventional SMB process, are produced, as described anywhere (ANICETO and SILVA, 2015a,b; RAJENDRAN *et al.*, 2009; SÁ GOMES and RODRIGUES, 2012). Some of the most relevant operation modes are PowerFeed, ModiCon, and VariCol processes obtained by the periodic modulations of feed flow rate, feed concentration, and the length of zones, respectively (LUDEMANN-HOMBOURGER *et al.*, 2000; SCHRAMM *et al.*, 2003a,b; ZANG and WANKAT, 2002; ZHANG *et al.*, 2003).

2.2.4 Variants of the SMB Process

2.2.4.1 VariCol Process

The VariCol process or asynchronous simulated moving bed (ASMB) process, introduced by LUDEMANN-HOMBOURGER *et al.* (2000), is based on the modulation of the lengths of zones in a switching period. The modulation is obtained with the asynchronous shifting of the inlet and outlet ports in the same direction of

the fluid phase flow (LUDEMANN-HOMBOURGER *et al.*, 2000; TOUMI *et al.*, 2002; YAO *et al.*, 2014). The characteristics of ASMB allow for a more flexible operation in column utilization and can also achieve higher separation performances (LUDEMANN-HOMBOURGER *et al.*, 2000; TOUMI *et al.*, 2002; YAO *et al.*, 2014). That is the case, for example, of several reports in the literature showing that a 5-columns ASMB process can achieve similar results and separation performance of a 6-columns SMB process (GONG *et al.*, 2014b; LIN *et al.*, 2016; LUDEMANN-HOMBOURGER *et al.*, 2000; TOUMI *et al.*, 2003, 2002; WONGSO *et al.*, 2005; YANG *et al.*, 2019; YAO *et al.*, 2014, 2017).

In the SMB, ports are moved together downstream by one column at the end of a switching period, while in the VariCol process, there could be different upstream and downstream sub-switches during the switching period. However, if a single-port is shifted one time upstream, it needs, in the same period, two downstream movements, one to return to the initial position and another to move forward in the cycle (SUBRAMANI *et al.*, 2003; TOUMI *et al.*, 2002; YAO *et al.*, 2014, 2017). Greater separation performance is reached when each port is shifted only one column downstream in a switching period, reducing the maximum number of movements of all ports to four (YAO *et al.*, 2014).

The asynchronous port movement in the VariCol process generates a variable number of columns per zone in a switching period. The variation in the number of columns is described as a column configuration sequence (CCS) in zones that depends on the sub-switching of each port. In Figure 2.3 through an example, the column configuration in zones in the VariCol process is compared with the conventional SMB process for two switching periods. In the SMB process, a column configuration of [1, 2, 3, 2] is used. That number of columns in the zones is invariant during the switching periods (see Figure 2.3). For the VariCol process, only downstream and independent movement of ports are considered, generating 4 movements and 4 column configurations. The column configuration sequence of [1, 2, 3, 2], [2, 1, 3, 2], [2 2 2 2], and [2 2 3 1] is used as an example. This CCS was obtained with the following shifting of ports order: extract port, feed port, raffinate port, and dissolvent port. The shifting of the dissolvent port was at the same time as the switching period (see Figure 2.3). That CCS is repeated in each switching period which is the same switching time of the SMB process (see Figure 2.3). At the end of switching period, the column configuration (number of column in zones) returns to the initial position. The shifting time of any port in the VariCol process causes an increase in the number of columns in the section on its left and a decrease in the section on its right, as verified in Figure 2.3. The unequal movement of ports in the ASMB is not limited to a specific time and port movement order. Sometimes

to reduce the complexity in the design, the shifting time of ports are set arbitrarily (PAIS and RODRIGUES, 2003; SUBRAMANI *et al.*, 2003; WONGSO *et al.*, 2005; ZHANG *et al.*, 2007, 2002, 2003). The concept of an average number of columns per zone, calculated with the column configuration sequence over a switching period and the sub-switching times leading to rational numbers, is adopted to count the number of columns per zone over a switching period (LUDEMANN-HOMBOURGER *et al.*, 2000; TOUMI *et al.*, 2002; YAO *et al.*, 2014). In case of Figure 2.3 the average number of columns per zone correspond to $\bar{\mathbf{N}} = [1.81, 1.98, 2.60, 1.61]$.

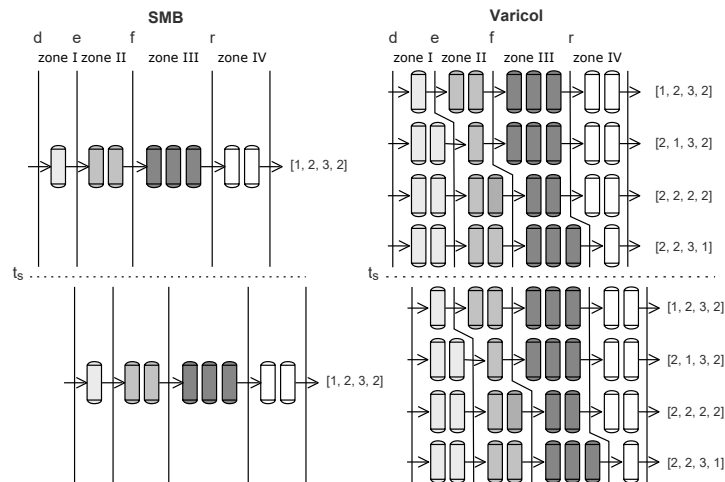


Figure 2.3: Column configuration in zones in the SMB and the VariCol processes for two switching periods.

When designing the asynchronous operation, the focus is on finding not only the proper operating parameters set in the usual SMB process but also the column configuration sequence and the switching times for ports during a switching period YAO *et al.* (2014, 2017). The switching period that is the design parameter of the SMB, which defines the hypothetically solid phase velocity, also continues to be a key design parameter in the VariCol process. The extra variables, intrinsic to the asynchronous operation, increase the degree of freedom and turn the design more difficult and challenging (TOUMI *et al.*, 2002; WONGSO *et al.*, 2005; YAO *et al.*, 2014, 2017; ZHANG *et al.*, 2002; ZÚÑIGA and WOUWER, 2014).

2.2.4.2 ModiCon Process

The ModiCon process is characterized by the modulation of feed concentration in a switching period (SCHRAMM *et al.*, 2002, 2003a,b). The periodic modulation pattern for ModiCon can be divided into different sub-intervals with distinct concentrations and durations (SCHRAMM *et al.*, 2003a,b; YANG *et al.*, 2019; YU *et al.*, 2015; ZHANG *et al.*, 2004a). Figure 2.4 presents a modulation with two sub-intervals,

where the first has a lower concentration -in this case, a zero concentration value- and a higher duration than the second. The average feed concentration in the ModiCon process can be used as a decision variable or as a reference point to compare with the SMB process or other variants. Figure 2.4 also presents the average feed concentration as equal to the SMB. The maximal value of feed concentration of a sub-interval has to be constrained by the mixture solubility limit to avoid precipitation phenomena in the columns (KASPEREIT *et al.*, 2002; SCHRAMM *et al.*, 2003a; YANG *et al.*, 2019; ZHANG *et al.*, 2004a).

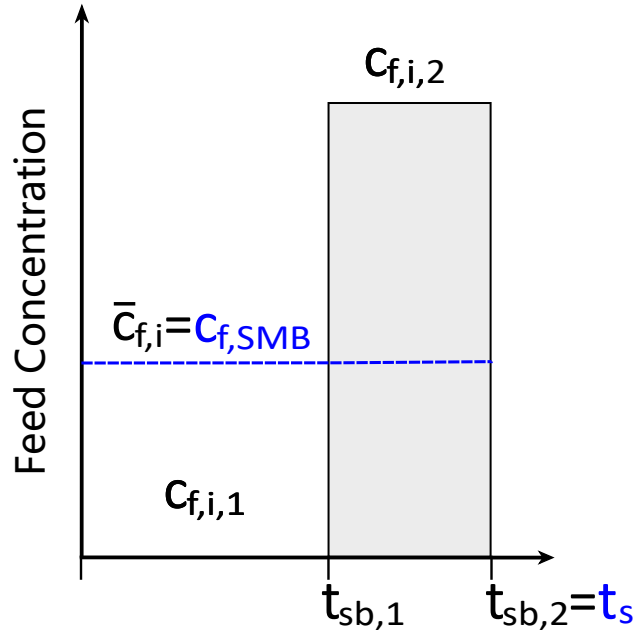


Figure 2.4: Schematic representation of the ModiCon process with a feed concentration modulation of two sub-intervals in a switching period (t_s).

The feed concentration modulation in the ModiCon process introduces changes in the migration velocities of the components in the zones where the separation takes place (zone II and zone III). That occurs if nonlinear adsorption isotherms of the components are used (SCHRAMM *et al.*, 2002, 2003a,b; SEIDEL-MORGENSTERN *et al.*, 2008). The variation in the velocity of the concentration fronts produces different effects on the purity in the extract and raffinate, leading to an increment in the performance compared with the conventional operation (SCHRAMM *et al.*, 2003a,b; YANG *et al.*, 2019; YU *et al.*, 2015; ZHANG *et al.*, 2004a). For modulation of two sub-intervals, different reports of literature have shown that it is more convenient to apply a low or zero concentration in the first sub-interval and a high in the second (SCHRAMM *et al.*, 2003a,b; YANG *et al.*, 2019; ZHANG *et al.*, 2004a). That modulation pattern increases further the purity in the raffinate for a fixed throughput (SCHRAMM *et al.*, 2003a,b; YANG *et al.*, 2019). The increment in the raffinate purity also gives space to improve productivity and reduce solvent consumption (SCHRAMM *et al.*, 2003a,b; SEIDEL-MORGENSTERN *et al.*, 2008;

YANG *et al.*, 2019). For the case of three sub-intervals, YU *et al.* (2015) reported that a higher concentration in the second sub-interval was the one that most improved the performance. In that work, the objective was to improve the raffinate purity and increase the most retained component recuperation.

Besides the benefits in modulating the feed concentrations, some essential aspects need to be taken into account. The ModiCon process benefits only apply to nonlinear isotherms that produce variable migration velocities of concentration fronts (SCHRAMM *et al.*, 2003a,b). The upper bound of feed concentration of each sub-interval should be below the solubility limits. For real plants, dead times and back-mixing effects can cause difficulties to keep the desired feed concentration profiles (SEIDEL-MORGENSTERN *et al.*, 2008).

2.2.4.3 PowerFeed Process

The PowerFeed, introduced by KLOPPENBURG and GILLES (1999b), relies on modulating the internal flow rates in a switching period. The modulations can also be expressed in terms of three external flow rates and one internal flow rate. Different works reported that the modulations in the flow rates improve the performance compared with the conventional SMB process (KLOPPENBURG and GILLES, 1999b; SCHRAMM *et al.*, 2003a; ZHANG *et al.*, 2003, 2004a). Some of the flow rates are also set constant as in the SMB process to reduce the complexity (YANG *et al.*, 2019; YU *et al.*, 2015; ZANG and WANKAT, 2002). For example, ZANG and WANKAT (2002) only modulated the internal flow rate in zone III. In that case, the external feed flow rate and the raffinate flow rate were varied. ZHANG *et al.* (2003) fixed the internal flow rate in section I (the highest internal flow rate) to avoid excess pressure drop and varied the other flow rates. SCHRAMM *et al.* (2003a) set constant the internal flow rates in section I and II, and the flow rates of products (extract and raffinate). Due to the complex nature of the PowerFeed, the design projects are more complicated because the degree of freedom increases with the variation of the flow rates (ZHANG *et al.*, 2003, 2004b).

2.3 Modeling, optimization and control

2.3.1 Modeling

A mathematical description of the physical phenomena and the dynamics involved in the SMB process operation is required, especially for process design, optimization,

and control. Two mathematical approaches are commonly used to describe the SMB operation: the first one employs the same mathematical model of TMB, while the second uses a mathematical model that directly considers the SMB process dynamics (GANETSOS and BARKER, 1992; PAIS *et al.*, 1998; RUTHVEN and CHING, 1989; XIE *et al.*, 2001). The first approach is based on the equivalence between SMB and TMB process, and it is justified in the case of units with a large number of columns. The first model also has less complexity, requires less computational effort, and the solution refers to steady state operation. The second model describes more closely the real operation of SMB, has a more physical meaning than the model based on TMB, but is more complex since it includes the dynamics of the switching time, and the solutions point out to cyclic steady state.

In both simulation approaches of the SMB process, the bed elements (chromatographic column or portion of chromatographic columns) are represented by either a continuous flow model (axial plug flow) or a mixing cell model, as is shown in Figure 2.5 (GANETSOS and BARKER, 1992; GUIOCHON *et al.*, 2006; PAIS *et al.*, 1998; RUTHVEN and CHING, 1989; XIE *et al.*, 2001). The continuous models are based on the balance of solute in a slice of a column and its kinetics of mass transfer. The balance produces a set of partial differential and algebraic equations that need to be solved to find the solution (GUIOCHON, 2002; GUIOCHON *et al.*, 2006). The mixing cell models are derived from plate theory, and they represent a continuous column in a discrete number of well-mixed cells. Those models are good approximations when processes such as advection and back-mixing are predominant (NICOUD, 2015). Additionally, when the number of cells is over 100, there are little differences between cell models and the continuous flow model (GUIOCHON *et al.*, 2006; NICOUD, 2015). The cell models are also convenient in terms of computational effort (RUTHVEN and CHING, 1989).

The continuous models can account for almost all contributions of mass transfer kinetics in the chromatographic columns or neglect some phenomena and lump others to reduce the complexity (GANETSOS and BARKER, 1992; GUIOCHON, 2002; GUIOCHON *et al.*, 2006; PAIS *et al.*, 1998; RUTHVEN and CHING, 1989; SCHMIDT-TRAUB *et al.*, 2012; XIE *et al.*, 2001). The most detailed model is the general rate model (GRM) that attempts to consider all mass transfer kinetics (GUIOCHON, 2002; GUIOCHON *et al.*, 2006; SCHMIDT-TRAUB *et al.*, 2012). This model is based on a mass balance in the bulk fluid phase and other in the stationary phase. The effects considered in those balances are advection, axial dispersion, pore diffusion, mass transfer resistance, and multiple-component adsorption/desorption kinetics. Simplifications of the GRM to reduce complexity are very common, especially in the SMB process (GONG *et al.*, 2014a; GUIOCHON, 2002; GUIOCHON

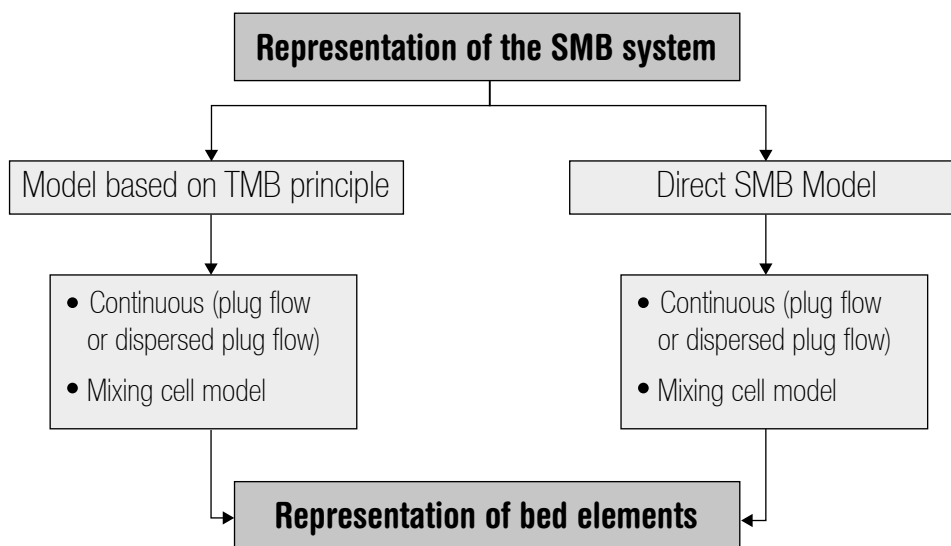


Figure 2.5: Simulation approach for SMB process. Adapted from (RUTHVEN and CHING, 1989).

et al., 2006; RODRIGUES, 2015; SCHMIDT-TRAUB *et al.*, 2012). Some of the most common simplifications are the lumped pore diffusion model, the transport dispersion model, the equilibrium dispersion model, and the ideal model. The lumped pore diffusion model considers the adsorbed concentration as a mean value in the mass balance of the stationary phase. The transport dispersion model summarizes the adsorbent particles' internal and external mass transfer in a unique coefficient. The mass balance in the stationary phase in that model is quantified with a linear driving force approach. The equilibrium dispersion model neglects the mass transfer resistance and considers that the fluid concentration is in equilibrium with the solid loading. In this model, the mass balance for the stationary phase is not included. The ideal model neglects the axial dispersion and assumes equilibrium theory (the mass transfer resistances are considered negligible). Hence, infinity column efficiency is assumed in this last model (RUTHVEN and CHING, 1989).

Some of the continuous models based on the TMB principle can be solved analytically. The transport dispersion and the equilibrium dispersion models can be solved analytically for the TMB process at the steady state when linear adsorption isotherms are considered (GUIOCHON *et al.*, 2006). The analytical solution of the ideal model applied to the TMB process produces an important result that allows deriving some principles for the design of the SMB (MAZZOTTI *et al.*, 1997; RAJENDRAN *et al.*, 2009). An approximated analytical solution for the ideal model applied directly to the SMB process can also be obtained (GUIOCHON *et al.*, 2006).

When a continuous flow model representing the SMB process is used, a system of coupled partial differential and algebraic equations is obtained (KAWAJIRI and BIEGLER, 2006; SWARTZ and KAWAJIRI, 2019; TOUMI *et al.*, 2007). Independently of the continuous flow model, two approaches are usually employed to solve that equation system, the spatial and full discretizations. In the first case, the spatial variables of fluid and stationary mass balances are discretized, leading to a differential-algebraic equation system. This system is solved by integrating it repeatedly until the process reaches a cyclic steady state (KAWAJIRI and BIEGLER, 2006; SWARTZ and KAWAJIRI, 2019; TOUMI *et al.*, 2007). In the second case, the spatial and temporal variables of the fluid and stationary mass balances are discretized, which generates a high dimension nonlinear algebraic equation system.

In the recent applications of the SMB, especially in the pharmaceutical area, it is more common to use systems with a low number of columns, mainly for economic reasons (6 or less) (KLATT *et al.*, 2002; ZHANG *et al.*, 2004a). In those cases, it is more convenient to use the model that describes the dynamics of SMB directly because the approximation of the SMB process with the TMB process is not accurate (KLATT *et al.*, 2002; TOUMI and ENGELL, 2004; ZHANG *et al.*, 2004a). Additionally, in the case of the SMB process variants that cannot be directly compared with the TMB process (LUDEMANN-HOMBOURGER *et al.*, 2000). Mathematical models that directly consider the dynamic of the SMB need to be used.

2.3.2 SMB Design

2.3.2.1 Triangle Theory

The SMB design requires selecting the proper operating parameters that lead to safe running conditions and influence in a positive way the economics of the process. The selection of the internal flow rates and the switching period in the SMB can be made through optimization or some analytical methods. The most known and important analytical method is the triangle theory. This method is based on the ideal model (continuous plug flow without axial dispersion and based on the local equilibrium) applied to the TMB process (GUIOCHON *et al.*, 2006; MAZZOTTI *et al.*, 1997; RAJENDRAN *et al.*, 2009; SCHMIDT-TRAUB *et al.*, 2012). The method name comes from the fact that the separation region for binary mixtures has a triangular form (GUIOCHON *et al.*, 2006; MAZZOTTI *et al.*, 1997; RAJENDRAN *et al.*, 2009; SCHMIDT-TRAUB *et al.*, 2012). The SMB process can be designed with the triangle theory when its dynamic is approximated with the TMB process. However, for linear isotherms, the same restriction of the triangle region is obtained when the

mathematical model based directly on the dynamics of the SMB is solved analytically (GUIOCHON *et al.*, 2006; RAJENDRAN *et al.*, 2009).

The design parameters in the triangle method are the dimensionless flowrate ratio (m_M) between the net fluid flow and the solid phase flow:

$$m_M = \frac{Q_M t_s - V\varepsilon}{V(1 - \varepsilon)} \quad (2.1)$$

where M is the SMB process sections ($M = I, II, III, IV$), Q_M is the volumetric flow rate in each section, t_s is the switching time, V is the total column volume, and ε the column overall bed void fraction. ε can be expressed in terms of bed void fraction (ε_b) and an intraparticle void fraction (ε_p) as follows:

$$\varepsilon = \varepsilon_b + \varepsilon_p(1 - \varepsilon_b) \quad (2.2)$$

In the case of a linear isotherm ($q_{ei} = H_i c_i, i = A, B$), to ensure complete separation, the following constraints need to be satisfied:

$$H_B < m_I < \infty \quad (2.3)$$

$$H_A < m_{II} < H_B \quad (2.4)$$

$$H_A < m_{III} < H_B \quad (2.5)$$

$$\frac{-\varepsilon_p}{1 - \varepsilon_p} < m_{IV} < H_A \quad (2.6)$$

where H is the Henry constant. Those constraints define the region in a four-dimension space enclosed by m_M , where complete separation is possible. The projection of that region on the $m_{II} - m_{III}$ and $m_I - m_{IV}$ planes is shown in Figure 2.6a. The $m_{II} - m_{III}$ plane is important because it is where the separation takes place in the SMB unit. The constraints of Equations 2.4 and 2.5 with $m_{III} > m_{II}$ (the feed flow rate needs to be positive) define a triangle-shaped region in the upper half of the $m_{II} - m_{III}$ plane, where it is possible to complete separation (GUIOCHON *et al.*, 2006; RAJENDRAN *et al.*, 2009). Other regions with different characteristics can also be identified in the m_{II}, m_{III} plane, as shown in Figure 2.6a. In these regions, only one of the components may or may not be obtained pure. The maximum theoretical productivity in the separation is reached in point \mathbf{w} (see Figure 2.6), where the difference between m_{II} and m_{III} is maximum. That point is not the most robust operation point. Instead, it is a sensitive point where any disturbance in the process can compromise the products' purities. On the other hand, the $m_I - m_{IV}$ plane gives information about the regeneration region. The constraints of Equations 2.3 and 2.6 define that regeneration region that corresponds to a rectangle. It can

also be seen in Figure 2.6a, on the right and bottom.

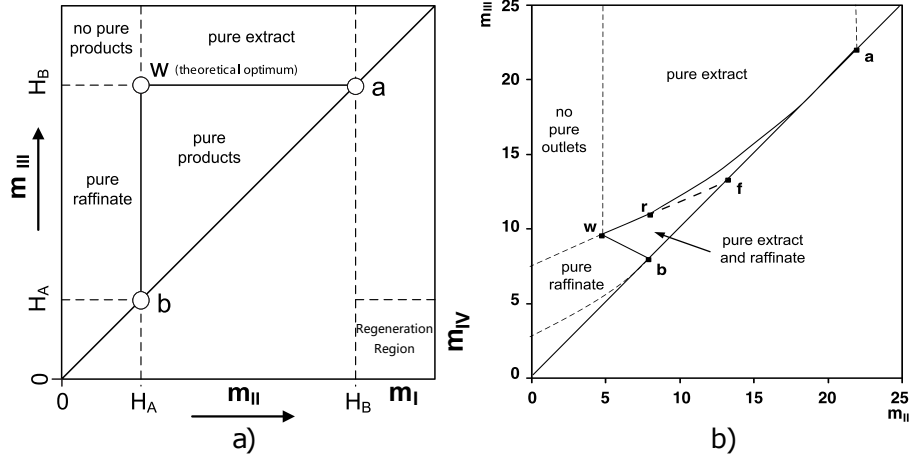


Figure 2.6: Projection of separation region for binary mixture on the (m_{II}, m_{III}) plane with (a) linear adsorption isotherm and (b) competitive binary Langmuir isotherm. It was adapted from (RODRIGUES, 2015; SCHMIDT-TRAUB *et al.*, 2012).

For the case of nonlinear isotherms, the region of complete separation changes depending on the type of isotherm. For instance, in the case of competitive binary Langmuir isotherm, $q_{ei} = \frac{H_i c_i}{1 + K_{ACA} + K_{BCB}}$, the constraints are:

$$H_B = m_{I,min} < m_I < \infty \quad (2.7)$$

$$m_{II,min} < m_{II} < m_{II,max} \quad (2.8)$$

$$m_{III,min} < m_{III} < m_{III,max} \quad (2.9)$$

$$\frac{-\varepsilon_p}{1 - \varepsilon_p} < m_{IV} < m_{IV,max} = H_A \quad (2.10)$$

where m_M bounds are functions that depend on m_{II} and m_{III} , the isotherms parameters, and the feed concentrations. Those m_M bounds for different isotherms can be found easily in the literature (GUIOCHON *et al.*, 2006; RAJENDRAN *et al.*, 2009). The projection of constraints m_{II} and m_{III} with $m_{III} > m_{II}$ on the two-dimensional plane, for competitive binary Langmuir isotherm, produces a distorted triangle, as shown in Figure 2.6b.

In addition to triangle theory, there are other extended methods to design the SMB process, such as the separation volume method and the standing wave analysis (AZEVEDO and RODRIGUES, 1999; MA and WANG, 1997; SILVA *et al.*, 2004; XIE *et al.*, 2000; ZHONG and GUIOCHON, 1996). The separation volume method is also based on the model of the TMB, but unlike triangle theory, it considers the resistance to mass transfer (AZEVEDO and RODRIGUES, 1999). In that method,

the entire separation region becomes smaller than triangle theory, when mass transfer limitations are considered, and bigger, when the purity requirements are not strict (AZEVEDO and RODRIGUES, 1999; RAJENDRAN *et al.*, 2009). The standing wave design method is based on the migration speed of mass fronts (concentration wave) (MA and WANG, 1997). That migration speed is related to the ports switching velocity (length of column/switching period). The separation will occur if the ports' switching velocity is higher than the most retained component migration speed and lower than the less retained component migration speed. From that concept, a set of boundaries that define a separation region can be defined (MA and WANG, 1997; XIE *et al.*, 2000).

Although the extended design methods can be more precise, the triangle theory is an excellent method to estimate the entire separation region (RAJENDRAN *et al.*, 2009). The triangle theory is frequently used in experimental studies to define the initials operations points (ANICETO *et al.*, 2016; AZEVEDO and RODRIGUES, 2001; MILLER *et al.*, 2003).

When the SMB operation design includes factors that the triangle theory or the other extended method do not consider, it is necessary to solve an optimization problem. Those new factors usually are associated with the economics of the process (JUPKE *et al.*, 2002). For example, these factors can be the increment of the recovery, the reduction of solvent consumption, the maximal productivity at desired purity, the column configuration. Triangle theory and extended methods also do not describe very well systems with axial dispersion and different characteristics such as no steady state of the process and non-linearity of isotherms (GUIOCHON *et al.*, 2006). In the variants of the SMB process, there are no analytical methods to design the additional parameters of those processes. In those cases, optimization problems are necessary to properly define the operation design (BORGES DA SILVA *et al.*, 2002; KAWAJIRI and BIEGLER, 2006; SWARTZ and KAWAJIRI, 2019; TOUMI *et al.*, 2007). A more detailed description of different optimization techniques applied to SMB unit and the SMB process variants is presented in the next sections.

2.3.2.2 SMB Optimization

In the SMB design, direct optimization techniques are necessary when different separation requirements and interests are desired (JUPKE *et al.*, 2002; MINCEVA and RODRIGUES, 2005; WONGSO *et al.*, 2005). Different optimization problems can be formulated and solved depending on the SMB operation mode (variants of the SMB process), the mathematical model of the process, and the type of

variables involved in the formulation (continuous or discrete) (HASAN *et al.*, 2017; TOUMI *et al.*, 2007; WONGSO *et al.*, 2005; ZÚÑIGA and WOUWER, 2014). Those formulations result mainly in a nonlinear programming (NLP) or mixed-integer nonlinear programming (MINLP) due to nonlinear models that describe the process and the use of integer variables to represent the columns configuration. Deterministic and non-deterministic algorithms were already used to solve those optimizations problem (GARCIA *et al.*, 2006; KAWAJIRI and BIEGLER, 2006; TOUMI *et al.*, 2007; ZHANG *et al.*, 2002)

The optimization of the SMB process requires high computational effort, particularly when models that directly describe the SMB process dynamics are used. That is mainly because the SMB process is nonlinear, intrinsically dynamic, and has a cyclic and periodic nature (KAWAJIRI and BIEGLER, 2006; SWARTZ and KAWAJIRI, 2019; TOUMI *et al.*, 2007). When the continuous plug flow model is used, the mathematical model corresponds to partial differential equations. The dynamic optimization problem, in this case, can be solved using different approaches according to the discretization strategy and the way that the cyclic steady state is reached. Partial or full discretization formulations of the dynamic optimization problem can be obtained depending on the discretization strategy (KAWAJIRI and BIEGLER, 2006; TOUMI *et al.*, 2003, 2007). In the partial method, when only the spatial variable is discretized, it results in the single-shooting approach. In the full strategy, both the spatial and temporal variables are discretized in the whole domain, resulting in a nonlinear programming problem with many variables and constraints. An intermediate formulation, the multiple-shooting approach, is obtained when the spatial variable is discretized and the time domain is partitioned in multiple intervals solved simultaneously. In this last method, continuity conditions between time intervals are needed to guarantee solution consistency. Additionally to discretization strategy, the dynamics to reach the cyclic steady state in the optimization problem can be handled with sequential or simultaneous approaches (KAWAJIRI and BIEGLER, 2006; SWARTZ and KAWAJIRI, 2019; TOUMI *et al.*, 2007). In the sequential process, the optimization is straightforward, and the cyclic steady state is reached independently in each optimization stage. In the simultaneous approach, the cyclic steady state is formulated as an additional constraint of the optimization problem. Those two approaches to reach the CSS are presented in Figure 2.7.

KAWAJIRI and BIEGLER (2006) solved the optimization problem by applying partial and full discretizations on the dynamic SMB model. The spatial variable was discretized by using finite center differences in both approaches. The temporal variable was discretized with the Radau collocation on finite elements method when applying the full discretization method. In the two cases, the cyclic steady state was

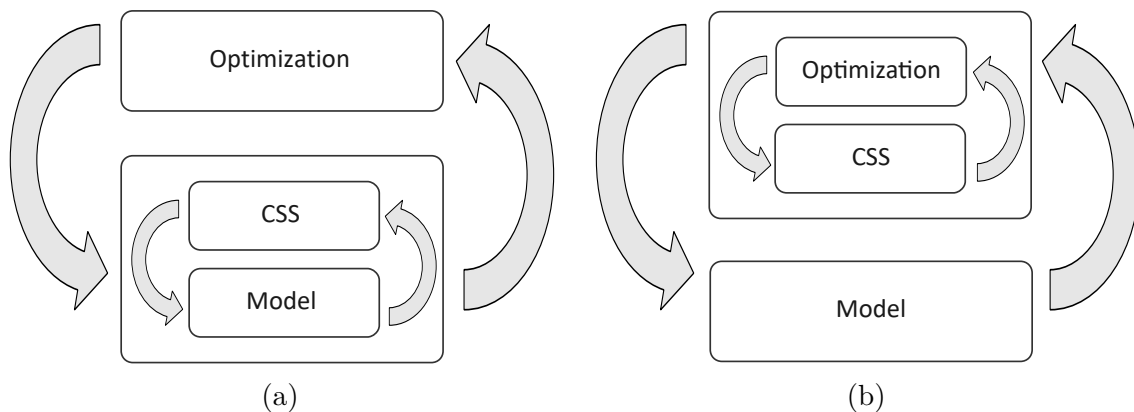


Figure 2.7: Approaches to reach the cyclic steady state in the optimization problem. (a) Sequential, (b) simultaneous.

reached simultaneously with the optimization problem. The partial discretization was implemented in the gPROMS program and solved with the SRQPD optimizer. The full discretization was implemented in the AMPL program and solved with the IPOPT optimizer. As an initial case study, they considered maximizing throughput for separating glucose and fructose with a linear isotherm. They found that the full discretization strategy was more efficient computationally than the partial discretization. They also applied the full discretization strategy in a more complex case study that was the enantioseparation of 1,1'-bi-2-naphthol described with the bi-Langmuir isotherm. The result was also promising for the second discretization approach. According to them, the full discretization method could be more appropriate for optimizing the SMB process. In other work KAWAJIRI and BIEGLER (2008) solved an optimization problem to find the best optimal zone configuration for standard (4 zones) and nonstandard (3 zones) SMB operations. They applied the same full discretization formulation as was presented in the former work (KAWAJIRI and BIEGLER, 2006). To represent all possible zone configurations, they built superstructures for standard and nonstandards SMB operations. The optimal configurations for standard and nonstandard operation led to solutions where discrete variables were not necessary, but multiple inlet and outlet flowrates were considered as decision variables, increasing considerably the size of the optimization problem. In those two works KAWAJIRI and BIEGLER (2006, 2008) used the plug flow model for the fluid phase and the linear driving force model for adsorbed phase. The axial dispersion and diffusion into adsorbent particles were lumped into the mass transfer coefficient.

TOUMI *et al.* (2007) implemented a numerical approach to solve the dynamic optimization problem of the SMB process based on the multiple-shooting method. They used the GRM (general rate model) to calculate the concentration profiles accurately. The system of coupled partial differential equations of the GRM was discretized spatially to get ordinary differential equations. Partial differential equations of the

bulk phase were discretized using a Galerkin finite element, while the solid phase equations were discretized with the orthogonal collocation method. They also applied the sequential and the simultaneous approaches to calculating the cyclic steady state in the optimization problem. In the simultaneous approach, they used two methods, an exact multiple-shooting method and an approximated multiple-shooting method. Those two methods differed in the way that stages of the optimal control problem were defined. In the exact multiple-shooting method, one stage was the SMB loop, while in the approximated multiple-shooting method, each column was a stage. When the exact multiple-shooting method was applied, the node conditions (mass balances in the inlet and outlet ports) were fulfilled internally, and the cyclic state was formulated as an additional equality constraint. On the other hand, when the approximated multiple-shooting method was applied, the cyclic steady state (the axial profile of a column at the end of the period is equal to that of the previous column at the start of the period) was fulfilled internally, and the node conditions was formulated as additional constraints. The inlet/outlet concentration profiles of columns were approximated with Legendre polynomials in this last method. They considered an enantioseparation described by a linear isotherm + Langmuir as a case study to compare the different optimization approaches. They reported that the approximated multiple-shooting method performed better reducing the computational time drastically compared with the other methods.

LEE *et al.* (2008) studied different factors which are often in conflict with each other in chiral separation through multiobjective optimization. For the optimization, they used the non-dominated sorting genetic algorithm, a non-deterministic optimization method. The standing wave design method equations were used to determine the objective functions, which are algebraic equations instead of ordinary differential equations (mixing cell model) or partial differential equations (plug flow model). In the optimization, seven system parameters (particle size, column length, the number of columns in each zone, and feed concentration) and five operation parameters (internal flow rates and the switching period) were considered. The objective functions were productivity, desorbent requirement, and yield, which are significant factors in separation. With those objective functions, they got general trends and conclusions since the cost functions for SMB equipment are not yet well established and the cost is case-dependent. Four optimizations based on two-objective optimization problems were formulated to find optimal system parameters and operation parameters. As a case study, they considered the enantioseparation of norephedrine or phenylpropanolamine, using a Langmuir isotherm. As a result, they found that large particles and short zones can increase productivity, but solvent consumption will increase with fixed purity and yield. When the pressure limits are

increased, smaller particles can increase productivity, or desorbent will decrease at fixed productivity. For the yield, it was showed that it is in opposite directions with productivity. They also demonstrated that short zones and high feed concentration favor high productivity, while long zones favor high yield and require low solvent consumption.

GIRI *et al.* (2013) applied multiobjective optimization to initially build meta-models (simplified models that describe the process) that were after used to evaluate some conflicting objectives in the SMB process. They build and compared meta-models using two techniques, genetic programming and evolutionary neural network. One of the main proposals of the work was to evaluate the meta-models obtained with the genetic programming. These meta-models were fitted with data obtained from the numerical solution of a rigorous partial differential equations system. The conflicting objectives in the model building were complexity and accuracy. For the SMB process, bi-objective optimizations studies based on the built meta-models were carried out for four objectives. The results were compared with the literature for optimizations based on rigorous models. They reported that the meta-models build with the genetic programming produce acceptable results, and the computational effort is low.

LI *et al.* (2014) studied the use of surrogate models (computational cheaper models containing the key characteristics of original models) to optimize the SMB process. They evaluated the potential of two different types of surrogate models in the SMB process optimization. The first surrogate model was built through a coarse spatial discretization of the first-principles equations of the process. The second was based on reducing the order of the original equations, employing orthogonal decomposition. To optimize the system, they applied the trust-region algorithm with a structure that could manage surrogate models. They also implemented a mechanism to update the surrogate model in the course of the optimization. The surrogate model's potential was evaluated by maximizing the feed throughput in separating a racemic mixture characterized by a nonlinear bi-Langmuir isotherm. The performance of surrogate models was compared with the full-order optimization problem. They showed the proposed method converged to the same optimum point achieved with the full order model with less computational time. They also found that the model correction steps are expensive and can restrict the exploitation of the surrogate model's full potential.

Optimization of conventional SMB operation is complex and requires high computational effort, especially when first-principle models, discrete variables, and multiple objective optimization problems are considered (GIRI *et al.*, 2013; KAWAJIRI and

BIEGLER, 2006; LEE *et al.*, 2008; LI *et al.*, 2014; TOUMI *et al.*, 2007). The SMB process variants are more complex because there are more degrees of freedom and the dynamics of these processes are more complex (GONG *et al.*, 2014b; LIN *et al.*, 2016; LUDEMANN-HOMBOURGER *et al.*, 2000; TOUMI *et al.*, 2003, 2002; WONGSO *et al.*, 2005; YANG *et al.*, 2019; YAO *et al.*, 2014, 2017). The VariCol process is the operation mode that is more challenging to optimize. Different integer variables need to be included to describe the column configurations obtained with the ports' asynchronous movement in a switching period.

2.3.3 VariCol process optimization

In the VariCol or ASMB process design, the interest is to find the proper operating parameters set in the usual SMB and those related to the modulation of the length of zones. Those new variables intrinsic of the ASMB can be expressed in terms of the shifting time of the ports and the CCS (column configuration sequence) in a switching period (YAO *et al.*, 2014, 2017). These variables, which are also referred to as shifting scheme, increase the degree of freedom and turn the optimization design problem more complex and challenging (TOUMI *et al.*, 2002; WONGSO *et al.*, 2005; YAO *et al.*, 2014, 2017; ZHANG *et al.*, 2002; ZÚÑIGA and WOUWER, 2014). The optimization complexity and variability in the ASMB process is commonly reduced by setting constant the values of the shifting times of the ports and using discrete variables to determine the CCS from possible column configuration (PAIS and RODRIGUES, 2003; SUBRAMANI *et al.*, 2003; WONGSO *et al.*, 2005; ZHANG *et al.*, 2007, 2002, 2003). For example ZHANG *et al.* (2002) and WONGSO *et al.* (2005) fixed the shifting times of ports in $1/4$, $1/2$, $3/4$, and 1 times the switching period and used a discrete variable to select the column configurations that define the CCS. A more robust strategy to explore the optimal solution in the VariCol process domain with all ports moving only one time downstream in a switching period process was proposed by YAO *et al.* (2014, 2017). That strategy consists of solving nonlinear programming (NLP) problems in subdomains that have the form of a dodecahedron.

ZHANG *et al.* (2002) were the first to perform a comprehensive multiobjective optimization study of the SMB and VariCol processes. Three optimization problems for the separation of the 1,2,3,4-tetrahydro-1-naphthol racemate were considered. In the first, a single-objective optimization was considered, and in the other two, multi-objective optimizations were considered. The single objective was the maximization of throughput. The conflicting factors in the multiobjective optimizations were the maximization of extract purity with simultaneous maximization of raffinate purity,

and the maximization of throughput with simultaneous minimization of the eluent consumption. In the first optimization, the problem was solved using the genetic algorithm. In the last two cases, the non-dominant sorting genetic algorithm was used. The mathematical model used was based on the mixing cells approach. The decision variables for the SMB process were two flow rates, the switching period, and one discrete variable to find an appropriate column configuration. As in the ASMB process, four sub-switchings were defined, the discrete variable was used to find the four-column configurations that make up the CCS. The sub-switchings that correspond to the shifting times of ports were set in 1/4, 1/2, 3/4, and 1 times the switching period. As a result of the multiobjective optimizations, they presented the Pareto optimal SMB and VariCol systems solutions. They reported a superior performance of the VariCol process than the SMB process in producing a better quality or increasing the throughput using less eluent consumption.

TOUMI *et al.* (2002) Optimized the VariCol process for different approaches in the number of design parameters and compared it with the SMB process. Two optimization proposals were considered for the VariCol process. One of them considers the same variables of the SMB process: the four flow rates and the switching period. The other includes the shifting time of the four ports as decision variables. The sequence and number of port movements in the ASMB were fixed in the two proposals. The mathematical model was the general rate model. Two study cases were considered: minimization of the desorbent consumption in the separation of tryptophan and phenylalanine, and the maximization of throughput in the separation of glucose and fructose. The two approaches of the VariCol process had a higher performance than the SMB process. In the VariCol process that includes the shifting times of the ports as decision variables, the performance was the highest in the two cases of study.

TOUMI *et al.* (2003) optimized the VariCol and the SMB processes, using the average length of three zones as the additional decision variables for the asynchronous process. The mathematical model used was the general rate model as the previous work (TOUMI *et al.*, 2002). Different optimizations changing the total number of columns were carried out for the case of the separation of the racemic mixture of propranolol. They showed that the VariCol process superiority is more marked for a small number of total columns. In general VariCol process needed one column less for some separation tasks. Some numerical optimization results were also tested experimentally, having some differences between simulated and experimental results. They suggested using a rigorous model-based optimization framework for the VariCol process because models based on equilibrium theory can fail to predict the region of complete separation accurately, as they showed. In this second work of TOUMI *et al.* (2003), it is worth highlighting that the number of decision variables in the

VariCol process (three average length of zones) was in discrepancy with the number used in the previous work (four shifting time of ports) (TOUMI *et al.*, 2002). The authors also point out that the shifting times and the initial column configuration of CCS are determined from the average length of the zone, but there is no strategy presented to make it.

SUBRAMANI *et al.* (2003) realized a comprehensive optimization study to evaluate the performance of the SMB and the VariCol processes in the separation of glucose and fructose. Optimizations based on two pairs of conflicting objectives were considered both for an existing system and for a design stage system. These conflicting objectives were the simultaneous maximization of the purity and productivity of fructose, and the simultaneous maximization of both glucose and fructose productivity. In the existing system, different optimization problems were considered only for the SMB process for distinct decision variables to improve the performance obtained in the experimental results for a system with 12 columns reported by AZEVEDO and RODRIGUES (2001). In the case of the system in the design stage, different optimization problems were solved for the SMB and the VariCol processes considering a lower number of columns that in this case was 8. In the VariCol process, different numbers of subintervals for the shifting of ports were considered. The switching period was divided into 3, 4, and 5 subintervals equally spaced. In these subintervals, different movements of ports in the forward and backward directions were allowed. The decision variables depended on the considered problem. These variables include the length of zones, column configuration, switching period, desorbent and raffinate flow rates. An adaptation of the non-dominated sorting genetic algorithm was used to obtain the Pareto optimal solutions. The mathematical model used was the transport dispersion model. As a result, the Pareto optimal solutions, which provide a set of equally good solutions, were presented. They reported that 8-column SMB and VariCol processes are competitive enough to produce fructose at very high purity and productivity as the 12-columns SMB process.

WONGSO *et al.* (2005) presented a comprehensive optimization study of the SMB configuration and VariCol process using, as an example, the separation of the 1,1'-bi-2-naphthol racemate. The mathematical model used is the transport dispersion model. The bi-Langmuir type adsorption equilibrium isotherms were used. The optimization algorithm was based on the non-deterministic technique, a non-dominated sorting genetic algorithm with jumping genes. Several optimizations were carried out for single and multiobjective functions. For the single objective, the optimizations were the maximization of throughput at fixed desorbent consumption and minimization of desorbent consumption at fixed throughput. In those two single objectives, the decision variables were two flow rates, the switching period, and a discrete variable for

determining the appropriate column configuration in the SMB process and the CCS in the VariCol process. For the multiobjective optimizations, different combinations of objectives that are conflicting with each other were considered. These objectives were the maximization of purity, maximization of productivity, maximization of throughput, minimization of desorbent, and minimization of column length. The decision variables in those cases were two flow rates, the switching period, the length of the column, and the discrete variable to determine the column configuration for the SMB process and the CCS for the ASMB process. The shifting times of the ASMB process ports were fixed in all cases in $1/4$, $1/2$, $3/4$, and 1 times the switching period to reduce the optimization variability and complexity. They showed the significant improvements that can be reached in the separation of 1,1'-bi-2-naphthol racemate using optimization. The VariCol process was superior to the SMB process for increase the throughput, reducing the desorbent consumption, reaching higher productivity, and achieving higher quality.

ZÚÑIGA and WOUWER (2014) expressed the optimization design problem of the VariCol process as an MINLP problem with a hybrid model that involves continuous and discrete dynamics. The continuous-time dynamic was represented by the transport dispersion model, while the discrete-time dynamic related to the shifting of the ports was described by the Moore machine. A Timed Transition Petri Net (TTPN) was used to set up the Moore machine in state equations. The optimization problem was formulated to find the design parameters of the VariCol process that are the flow rates, the switching period, and the fractional switching times of ports. The strategy of the solution was based on the same idea applied in the Branch & Bound method that consists of solving NLP subproblems in nodes of a tree. The authors' purpose was to build the coverability tree from a state equation defined with the TTPN. With that strategy, only CCSs that are possible are taken into account. Additionally, the candidates are classified based on the theoretical productivity achieved using the triangle theory-based optimal flow rate ratios. The NLP subproblems were solved for 25% of the best candidates. The objective of the optimization problem was to maximize productivity guaranteeing minimum purity values. The result showed that the optimization of the 6-columns VariCol process could improve the productivity over the 8-columns SMB process.

YAO *et al.* (2014) studied the asynchronous movement of the VariCol process ports in different directions (downstream and upstream) and optimized the VariCol process considering the relative shifting time of ports as decision variables. The mathematical model used was the transport dispersion model that uses the linear driving force approach for the stationary phase. The objective in the optimization was the minimization of desorbent consumption. The decision variables were two

flow rates, the switching period, and three relative shifting times of ports. As a case study, the enantioseparation of 1,1'-bi-2-naphthol was considered. As a result, they found that the best performance of the VariCol process is reached with only one downstream movement of each port. That was a significant result since the VariCol process complexity is reduced to 4 shiftings of ports in a switching period, which is the minimal moment. The CCS obtained with the shifting of ports is not unique for the same average column length of zones. There is a finite amount of them that produces the same results in the cyclic steady state. Each CCS is related to others by a parallel shifting. The determination of any of these CCS is based on the definition of an initial column configuration and the port shifting times. They also solved the discrepancy in the number of variables for the optimization problem found in the works of TOUMI *et al.* (2002) and TOUMI *et al.* (2003). It was showed that there are necessary to define three additional variables in the VariCol process and not four. In the optimization results, they showed that it was possible to reduce the desorbent consumption by 17% compared with the SMB process.

YAO *et al.* (2017) optimized the VariCol process using as additional decision variables the relative shifting time of ports proposed in the former work (YAO *et al.*, 2014). The mathematical model used was also the transport dispersion model. The optimization objective was the maximization of throughput for minimal requirements of purity in the products. The decision variables were two flow rates, the switching period and the relative shifting times. Two case studies for the 8-columns VariCol process were considered, the enantioseparation of 1,1'-bi-2-naphthol and the separation of glucose and fructose. They showed that port shifting strategy could be visualized in a dodecahedron with the origin in an initial column configuration that needs to be specified. Therefore for a different initial column configuration, a different dodecahedron can be constructed. In the optimization, the dodecahedron defines the search region. They proposed to solve a new optimization problem every time the solution was in the border of the dodecahedron since the best solution could be found in another one. The optimization results showed that in the enantioseparation of 1,1'-bi-2-naphthol, the throughput was increased by 87%, and in the separation of glucose and fructose, the throughput was increased by 15% compared with the SMB process.

The design of the operation parameter of the VariCol process related to the modulation of the length of zones is complex. It requires solving a mixed-integer nonlinear programming (MINLP) problem to consider all the variability. In some of the works where the VariCol and SMB processes performance is compared, the variability is reduced, fixing the shifting times (PAIS and RODRIGUES, 2003; SUBRAMANI *et al.*, 2003; WONGSO *et al.*, 2005; ZHANG *et al.*, 2002). The work

of TOUMI *et al.* (2002) was the first in considering the shifting times as decision variables. The same authors in other work (TOUMI *et al.*, 2003) considered the average length of zones as decision variables. However, those two last works have a discrepancy in the number of variables associated with the zones modulation length. Four shifting times were considered in that first work, while in the second, three average lengths were counted. That discrepancy was solved with the work of YAO *et al.* (2014) where it was shown that only three shifting times are necessary as decision variables and not four. That happens because one of the ports will always move at the same time as the switching period. Therefore if the switching period is used as a decision variable, only three additional shifting times of ports should be considered to describe the problem. Additionally, in the works of TOUMI *et al.* (2003, 2002) the strategy to determine the CCS was not clear. The most robust strategy to design the VariCol process operation considering all the variability was proposed by YAO *et al.* (2014, 2017). They proposed to use the relative shifting times as decision variables of the optimization problem and specify an initial column configuration for the CCS. That strategy limited the optimization problem to a subdomain described by a dodecahedron with origin in the initial column configuration. They proposed to solve a sequence of NLP problems until the solution is not in a dodecahedron border. Every time the solution falls on a dodecahedron border, a new NLP is solved with a different initial column configuration. Although that strategy allows exploring the VariCol process mode domain deeply, the problem continues to be an MINLP problem where the discrete variable is the initial column configuration of the CCS. The solution to this problem continues to be challenging, especially for real-time applications and when a hybrid operation mode that includes the modulations of the length of zones is used.

2.3.4 Performance comparison of some variants of SMB process

The modulation of parameters in the SMB process, such as the fluid flow rates, feed concentration, and column length, which correspond to the operation modes, PowerFeed, ModiCon, and VariCol, respectively, increases the degree of freedom and turns the design more complex. The complexity increases even more, when some of these single operation modes are combined to generate hybrid variants. The modulations in the single or hybrid variants can be divided into a different number of subintervals and take any forms (SCHRAMM *et al.*, 2003a,b; YANG *et al.*, 2019; YU *et al.*, 2015; ZHANG *et al.*, 2004a). However, the number of subintervals is usually set low to facilitate the design. Some parameters related to the modulation are also

defined arbitrarily to reduce the variability and complexity, as in the VariCol process where the shifting time of port is set to specific fractions of switching period, and in the PowerFeed where some flow rates are not modulated. The analytical design methods such as triangle theory and the standing wave design are not more applicable to the SMB process variants since the operation cannot be more compared with the TMB process (LUDEMANN-HOMBOURGER *et al.*, 2000; YU *et al.*, 2015). The design of the PowerFeed and the ModiCon process can be expressed as an optimal control problem, where the vector of control variables defines the values that would take the modulated parameters (GARCIA *et al.*, 2006; KAWAJIRI and BIEGLER, 2006; TOUMI *et al.*, 2007). The rigorous design of the VariCol process is one of the most challenging since the optimization problem requires the solution of an MINLP.

The performance comparison of the SMB process operation modes, including the hybrid ones, is essential for selecting an appropriate variant. Different comparisons are found in the literature based on simulations and optimizations (SCHRAMM *et al.*, 2003a; YANG *et al.*, 2019; YU *et al.*, 2015; ZHANG *et al.*, 2004a). For example, ZHANG *et al.* (2004a) was the first to compare the SMB process with different variants using multiobjective optimization. Other works also compared the performance based on simulations as the case of YANG *et al.* (2019); YU *et al.* (2015)

ZHANG *et al.* (2004a) compared the separation performance of the SMB process with some of its variants (VariCol, PowerFeed, ModiCon, and some hybrid operation modes) using multiobjective optimization. The hybrid operation modes corresponded to the combinations VariCol+PowerFeed, VariCol+ModiCon, and PowerFeed+ModiCon. The purity in the extract and the productivity were simultaneously maximized, keeping above 90% the raffinate purity. Case studies with 3-, 4-, and 5-columns were considered in the different operation modes. The non-dominate sorting genetic algorithm was used for the optimizations. In the PowerFeed process, a simplified operation is considered to reduce the complexity. That simplification consisted of only modulating the external feed and the raffinate flow rates, which correspond to modulating the internal flow rate of zone III. A pattern of modulation based on 3 subintervals was considered for the different variants. The decision variables, in general, were: 4 flow rates, the switching period, the feed concentration, and a discrete variable to determine the appropriate column configuration. In the case of each variant of the SMB process, the variable that is related to its correspondent modulation is a vector. The shifting times of ports in the VariCol process were fixed to 1/3, 2/3, and 1 times the switching period. The mathematical model used to describe each column was the mixing cells approach. As general results, the variants of the SMB process performed better than the same conventional process due to the

flexibility in the operation. The 5-column ModiCon process outperforms the other single operation modes, and for less number of columns, the PowerFeed presented better results. In the PowerFeed process with 4- and 5-columns, the optimal variation policy of feed flow rate was based on low values in the first and second subinterval and a high value in the third subinterval. In systems with 3-columns, the optimal variation policy of feed flow rate was based on high values in the second subinterval. In the ModiCon process with 3-, 4-, and 5-columns, the variation policy of feed concentration was based on a low value in the first and second subintervals and a high value in the last subinterval. Any of the hybrid operation modes VariCol+PowerFeed, VariCol+ModiCon, and PowerFeed+ModiCon perform better than the single operation modes. However, the improvements in the hybrid operation modes were insignificant. For 4- and 5-columns, the hybrid with the highest performance was the PowerFeed+ModiCon. For 3-columns, the best separation performance was obtained with the hybrid VariCol+PowerFeed.

YU *et al.* (2015) simulated and compared several SMB process variants and some of their combinations (VariCol, ModiCon, and PowerFeed, ModiCon+PowerFeed, and VariCol+ModiCon+PowerFeed) using Aspen Chromatography. Two case studies were considered, a binary chiral separation of Tröger's base enantiomers and a ternary separation of an amino acid mixture. The binary separation was accomplished in 4-zone systems and the ternary separation in 5-zone systems. Comparisons of the different operation modes were made in terms of purity, recovery, and productivity. The separation regions of the operation modes were also determined by simulating grid mesh points defined in the maximum throughput area determined with the triangle theory. The Pareto optimal solutions (maximal productivity for the purity of extract) for the different operation modes were also determined from these various simulations. The mathematical model was the transport dispersion model that uses the linear driving force approach for the stationary phases. Extra-column dead volume was included assuming effective dead volume with fixed pipe diameter and pipe length. In the VariCol process, the CCS and the average column length were determined with the relative shifting times of ports and an initial column configuration equal to that of the SMB process. In the PowerFeed, only the feed flow rate and the desorbent flow rate were modulated to reduce the complexity of the operation. Two and three modulation subintervals were considered in the PowerFeed, while three were analyzed the ModiCon process. As a result, the authors presented the separations regions for different values of purity and recovery of single and combined operation modes based on the various simulations. In general, all the operation modes increased the performance compared with the SMB process. The VariCol process improves the SMB process performance but was limited to

increase the purity of extract and raffinate simultaneously. The PowerFeed process gives only a tiny improvement over the base case in the 4-zone system but had a better performance in a 5-columns system. The policy of feed flow rate in the PowerFeed that improve the result the most was based on a low value in the first subinterval and a high in the second. Three subintervals had no benefit in the separation performance of PowerFeed. The ModiCon was the best single operation mode to improve the performance. The optimal feed concentration policy was based on a higher concentration in the second subinterval and lower values in the first and the third subintervals. The hybrid PowerFeed+ModiCon improves the performance compared with the single operations. The performance of hybrid formed by the three single operation modes VariCol+PowerFeed+ModiCon was slightly higher than one of the PowerFeed+ModiCon, but it was considered minimal based on the increment of complexity.

YANG *et al.* (2019) evaluated the variation of the performance of different SMB process variants (VariCol, PowerFeed, and ModiCon) concerning the conventional operation (SMB process). Simulations at the optimal point of triangle theory for the VariCol and the ModiCon processes were used to calculate different performance indices. The optimal point of PowerFed was calculated by evaluating different feed concentrations through simulations. The performance in the separation for both extract and raffinate was evaluated in terms of the following indices: purity, recovery, productivity, and solvent consumption. Similar operation parameters were used between each variant and the conventional operation mode to compare the separation performance. The mathematical model used to describe the different operation modes was the transport dispersion model. A 5-column system for the VariCol process and a 6-columns system for the other operation modes were studied to separate guaifenesin enantiomers. The complexity in the PowerFeed was reduced by modulating only the feed flow rate and the desorbent flow rate (the internal flow rates of zones III and IV also changed). The flow rates of extract and raffinate were set constant and equal to ones of the SMB process. A modulation pattern of two subintervals in both the feed flow rate and the feed concentration was used in the ModiCon and the PowerFeed processes. That modulation pattern was evaluated for the two possible forms of values in the subintervals: first high and last low, and first low and last high. The VariCol process based on 5-columns and an average column length in zones of [1, 1.5, 1.5, 1] was compared with the SMB process with 6-columns and a column configuration of [1, 2, 2, 1]. The average column length of the VariCol process corresponds to set the shifting times of port in 1/2 and 1 times the switching period. As a result, the authors reported that the effect on the performance of the SMB process variants is more significant for systems with a low number of columns.

The ModiCon process with a feed concentration policy based on a low value in the first subinterval and a high value in the second increased the productivity by 27.5% and decreased the desorbent consumption by 21.7%. PowerFeed increased the productivity by 10.6% and reduced the desorbent consumption by 8.7% with a modulation pattern of feed flow rate based on a high value in the first subinterval and a low value in the second. The VariCol process with 5-columns increased the productivity by 26% compared to the 6-columns SMB process due to the use of less chiral stationary phase.

From comparing the different variants of the SMB process described above, the ModiCon process was one of the most prominent operation modes. However, all its characteristics have not been fully explored. Additionally, in those comparisons, some of the VariCol process parameters were selected arbitrarily and without considering the maximal potential (YANG *et al.*, 2019; YU *et al.*, 2015; ZHANG *et al.*, 2004a). Comparing different SMB process variants based on rigorous mathematical models and using performance indices such as maximal throughput and specific purity requirements of products could be interesting. The maximal throughput is appropriate to compare the variants since it is possible to directly see the maximal mixture load that can accept each operation mode (YAO *et al.*, 2014, 2017). These comparisons are scarce in the literature because optimization problems are necessary. The optimizations could require higher computational effort when rigorous mathematical models are used. However, as the Jacobian matrix (JM) structure of the discretized mathematical model is sparse, computational effort can be reduced using sparse algebra and analytical Jacobian matrix. In those cases, optimizations with a rigorous model could be possible (ANDRADE NETO *et al.*, 2016).

2.3.5 Control

Operating the SMB process at an optimal economic point can be difficult because those points are generally sensitive to any disturbance or change in the operation conditions (KLATT *et al.*, 2002). For example, a minor disturbance in the feed concentration or changes in the isotherm parameter (variation of the packing material or temperature of the columns) could substantially affect the quality of the products (ABEL *et al.*, 2005; SONG *et al.*, 2006a). The operation in an optimal economic point could be guaranteed using a robust control technique. However, the control of the simulated moving bed process is challenging because of its dynamics (discrete and continuous process), the difficulty in measuring its states, and its long delays in responding to the effect of disturbances (ERDEM *et al.*, 2004a). Additionally, the measurement of the states is possible only in the outlet of separation columns.

Different control approaches have been used in the SMB process, although the most common has been the control concept based on optimization. In that approach, an optimization problem is solved to find the best actions that need to be taken to respond to any change in the plant. In those cases, the model predictive control and the repetitive model predictive control (model predictive control applied in the periodic process) have been the most used (ABEL *et al.*, 2005; ERDEM *et al.*, 2004a; GROSSMANN *et al.*, 2008; NOGUEIRA *et al.*, 2017; SONG *et al.*, 2006a). Classic control strategies have also been reported to control SMB processes, for example, proportional integral derivative (PID) and proportional (P) controllers have been applied (SUVAROV *et al.*, 2014; VALERY and MOREY, 2012). The controlled variables in the different control strategies have usually been the purity in the extract and raffinate or the axial concentration profiles at specific positions in the SMB unit train of columns (KLATT *et al.*, 2002; SUVAROV *et al.*, 2014). Some of the most relevant works in the control of the SMB process are presented as follows in a timeline. At the end, those different approaches are summarized in a table.

KLOPPENBURG and GILLES (1999a) were the first to present an approach for controlling an SMB process. They developed an automatic control with a state estimator, using as an example the separation of C_8 aromatics. A stationary extended Kalman filter was used as a state estimator, which requires less computational effort than when the filter matrix is time-dependent. The control algorithm was an exactly linearizing state feedback controller using asymptotically exact input/output linearization. The controller and the state estimator were based on the mathematical model of the TMB, which is more suited for design and control than the SMB model since it avoids the dynamics of the discrete ports switching. The mathematical model of the TMB was based on the transport dispersion model. As the TMB model can represent the SMB process in the middle of the switching period, the control design and the measurements sampling were based on that point. The control was connected to the virtual plant (SMB model with the discrete ports switching) with sample and hold units to take samples of the data, as it would be provided in the real process. As sampling units, four spectroscopic cells located in different positions of the columns train were considered. The purity and the yield in the extract where *p*-xylene is collected were the controlled variables, and the flow of the extract and raffinate were the manipulated variables. It was shown that the controller could be used to control the SMB process in the presence of different disturbances. It was also recommended to use PI controllers in combination with the feedback linearization to avoid the offsets of the controlled variables from their setpoints.

KLATT *et al.* (2002) proposed a two-layer architecture to optimize and control fructose and glucose separation in an 8-column SMB unit. The top-level layer has two

purposes: find offline and through optimization applied in a rigorous mathematical model the optimal operation trajectory, and estimate the model parameters based on online measurements. Every time the discrepancy between the actual model parameters used to calculate the optimal trajectory and the new ones estimated were high, a new offline optimization would be carried out. The mathematical model is based on the SMB approach and corresponds to the equilibrium dispersion model (the effects of axial dispersion and mass transfer are lumped in the dispersion coefficient). The bottom layer objective is to keep the process in the optimal trajectory calculated with the top layer, despite the presence of disturbances and plant model mismatch. The mathematical model used in the second layer is a simplified model identified from data of the rigorous mathematical model used in the first layer. As the dynamic of the identified model is approximately decoupled in the optimal trajectory vicinity, a simple decentralized control (internal model control) was used. The axial position fronts of the concentration profile, an indicator for the separation performance, were controlled by manipulating the normalized desorbent flow rate, extract flow rate, switching time, and recycling flow rate. An online concentration measurement was assumed at the end of each column to approximate the concentration profile. They showed the capabilities of the control structure to respond in different contexts. The second control layer rejected satisfactorily different types of disturbances both in a noise-free setting and noisy measurements.

ERDEM *et al.* (2004a) controlled the purity in the outlet streams of an SMB unit, in the separation of a mixture described by linear isotherm, using a control strategy based on repetitive model predictive control. This kind of control is an adaptation of the model predictive control (MPC) applied for periodic process. A simplified SMB model with key characteristics was used in the controller to avoid excessive computational time requirements. Online concentration measurements of the raffinate and extract and a periodic Kalman filter were used to reduce the effect of model errors. In the measurements, a zero-mean white noise with a standard deviation of 2% was added. As an SMB unit, they considered a virtual SMB plant with a closed-loop, four sections, and a configuration of two columns per section. That virtual plant was described by a rigorous model that directly considers the dynamics of the SMB process. That model was based on the equilibrium dispersion model. The purity of extract and raffinate was controlled, manipulating the four internal flow rates. The switching period of ports was set fixed due to the characteristics of the controller. As a result, they showed the control performance for some examples such as step disturbance, plant model mismatch, and system characteristics changes. In all examples, the control adapted to the operations conditions to fulfill the product requirements. In other work, ERDEM *et al.* (2004b) applied the same repetitive

model predictive control strategy based on linear isotherm, but this time to control systems characterized by a nonlinear competitive isotherm. They showed that the control based on a linear isotherm could find the right operating conditions to fulfill product specifications requirements in a system with nonlinear isotherms.

ABEL *et al.* (2005) were the first to implement the control concept in an SMB unit experimentally. They used repetitive model predictive control with a state estimator in an 8-column SMB unit. As an example, the separation of the nucleosides uridine-guanosine was considered. The control was based on online optimization with a simplified time-varying model of the SMB process to avoid excessive computation effort. The controlled variables were the purity in the extract and raffinate, and the manipulated variables were the internal flow rates. UV detectors were located in the outlet streams to measure the concentration of the products. A periodic time-varying Kalman filter with the outlet port concentration measures and the SMB model was used to estimate the other states. Two case studies, model mismatch and disturbance in the SMB operation, were considered to evaluate the control performance. In the two cases, the control fulfilled the required product specifications, despite those uncertainties and disturbances.

SONG *et al.* (2006a) proposed a predictive control strategy based on the subspace identification method. The realization of that control strategy was verified in the separation of the enantiomer 1-1'-bi-2-naphthol, a racemic mixture characterized by a bi-Langmuir isotherm, using a virtual SMB plant of eight columns. As controlled variables, they selected the average purities in the extract and raffinate and, as manipulated variables, the flow rates in sections II and III. A conventional quadratic programming method based on the quadratic objective function was used to determine the control actions. As a case study, the proposed control was applied to reject a disturbance and track a set-point variation. In all cases, they reported that the control showed excellent performance and reached the different goals. In other work, SONG *et al.* (2006b) designed a control based on subspace identification, but with an objective control function that includes an economic term. The average purities in the extract and raffinate, the reciprocal productivity, and solvent consumption were selected as controlled variables. As manipulated variables, the flow rates of extract, desorbent and solvent recycle, and the switching time were considered. The controller performance was evaluated with the same racemic mixture and virtual plant of the previous work. They reported an excellent performance of the controller in disturbance rejection and set-point tracking.

SONG *et al.* (2006c) implemented experimentally in an 8-column SMB unit a predictive control based on subspace identification. The separation of nucleosides

uridine and guanosine that are characterized by linear isotherm was considered as case study. The models of the controller were identified from experimental data instead of generated data from a rigorous model. The manipulated variables were three external and one internal flow rate, and the controlled variables, the productivity, solvent consumption, and average purities in the extract and raffinate. The concentration profile in the extract and raffinate was measured online with two ultraviolet detectors. The control performance was evaluated considering two options. In the first, the objective of the control was only to fulfill the purity requirements. In the second different economic objective controls were included, such as maximization of the productivity and a minimization of the solvent consumption. The two control options showed excellent results in different control scenarios, but the second option improved control performance in terms of profit.

GROSSMANN *et al.* (2008) implemented experimentally the repetitive model predictive control in an 8-column SMB unit. The separation of the nucleosides uridine and guanosine characterized by a linear isotherm was considered. A simplified SMB model was used in the controller to reduce computational efforts. The concentration in the output streams was measured with UV detectors. The non-measured states were estimated with a Kalman filter. The manipulated variables were the internal flow rates in the four sections and the controlled variables, the purities in the extract, and raffinate. The control objective was to fulfill the product's requirements and optimize the performance concerning the economic term. To evaluate the control performance, they considered different case studies, such as plant mismatch, feed pump malfunction, recycle pump malfunction, and change in the product requirements. They showed the controller's capability to fulfill the product's requirements and optimize the cost function in all the cases. They also evaluated the control performance considering a time delay in the measurements, but this time through simulations. In this case, they considered a case study with and without time delay. When they considered a time delay in the measurements, the control takes more time to achieve the specified purities.

VALERY and MOREY (2012) proposed a method for controlling the separation of mixture fractions in a chromatography device that can be the SMB process with some of its continuous or discontinuous variants. The continuous variants can be the same SMB process and the VariCol process, and in the intermittent operation, the CycloJet process. This last chromatographic device is based on only one column that re-inject product fractions in a determined order. The controller proposal is monitoring a variable related to the concentration, such as the UV detector signal in a node of the chromatographic device, and keeping a specific point of that variable in a target position at a specific time. One of the internal flow rates is modified in

case the point differs from the objective position. The control proposal is reached with four routines. The first routine positions the characteristic point; the second routine defines the target position; the third routine modifies the quantity of mixture injected; the fourth routine regulates the adsorption and desorption zones. Those routines use PID-type controllers that simultaneously act in the system or partly in parallel to maintain the variable history controlled at the desired value and reject any disturbance. Some case studies were presented for the different chromatographic devices where the proposed control methodology responded satisfactorily to different disturbances.

SUVAROV *et al.* (2014) applied an adaptive control to regulate the spatial location of the concentration fronts (adsorption and desorption concentration waves) related to the purity and productivity of the extract and raffinate. A proportional controller based on discrete-time and straightforward models of the concentration fronts movement was used. These models were derived from wave theory. The control strategy was applied on a virtual SMB unit based on the transport dispersion model that uses the linear driving force approximation. The mixtures fructo-oligosaccharides and cyclopentanone–cycloheptanone, characterized by a linear isotherm and competitive Langmuir isotherm, were considered case studies. The manipulated variables were the fluid flow rates and the switching time, and the controlled variables the internal concentration profiles position. They reported that the control responded satisfactorily to different disturbances and showed stability and robustness properties.

ANDRADE NETO *et al.* (2016) implemented an adaptive nonlinear model predictive control using as an example the enantioseparation of praziquantel with a to 8-columns SMB unit. As an internal model of the controller, a rigorous model based on the first principle of the SMB process was used. That mathematical model corresponds to the equilibrium dispersion model. The mathematical model was discretized spatially by finite differences, converting it into an ordinary differential equation system (ODE). The resulting ODE was solved with a numerical integration algorithm, taking advantage of the sparsity of the system. In the formulation of the optimization control problem, they considered an objective function that includes an economic term and the control term that tracks the error. The controlled variables were the purity in the extract and raffinate and the manipulated variables, the four internal flow rates. The controller performance was evaluated considering different case studies, such as pump and switching valve malfunction and mismatch problem. In the mismatch problem, a parameter estimation stage was included to update the parameters of the model. As a result, they reported that the controller responded satisfactorily in each scenario to maintain the purities of extract and raffinate in the desired values with a fast and smooth response. They also reported that the

computational effort was within the required limits that make the control viable.

NOGUEIRA *et al.* (2017) suggested controlling the purity and recovery in the extract and raffinate streams of TMB/SMB units using classical predictive control (MPC) based on transfer functions. The control was applied in an SMB unit, which is used for the separation of the enantiomer bi-naphthol. According to the authors in the optimal point of TMB, traditional MPC or PID controllers become infeasible when a unique transfer function is used. To overcome this problem, they presented a strategy to control TMB/SMB using a transfer function switching system. Two local transfer functions were identified, considering the TMB model and using step perturbations in the manipulated variables. One of them with an increase and the other with a decrease in the operation variables. The adequate transfer function used in the controller through the switching system is selected depending on the variation of the operating variables. The manipulated variables were selected according to a method based on successive orthogonalization of the system sensitivity. Different scenarios were studied, such as set-point changes and perturbations, to evaluate the controller performance. They showed that the MPC control responded satisfactorily to the different scenarios, keeping the controlled variables in the set-point.

NOGUEIRA *et al.* (2020) evaluated the use of infinite horizon model predictive control (IHMPC) in the SMB process. The advantage of this control approach is that it stabilizes and overcomes the limitations of the MPC. They evaluated and compared the performance, feasibility, and robustness of the IHMPC concerning the MPC, considering unmeasured disturbances and conflicting output tracking scenarios. As in the former work (NOGUEIRA *et al.*, 2017), they applied the controller in an SMB unit that separates the racemic mixture of bi-naphthol. The controller model was also the same as the work of NOGUEIRA *et al.* (2017), which is a transfer function switching system. They reported a superior performance of the IHMPC concerning the conventional MPC. Unlike the MPC that loses the process track, the IHMPC performed well in all scenarios.

The SMB process dynamic is complex and requires an appropriate control strategy to respond satisfactorily to disturbance scenarios. Although different approaches in the automatic control of an SMB unit are found in the literature (see Table 2.1), this topic continues to be a challenge. More research is necessary to improve the control schemes of the SMB process (ANDRADE NETO *et al.*, 2016; NOGUEIRA *et al.*, 2017). One of the most interesting approaches is the proposal of ANDRADE NETO *et al.* (2016) that is based on nonlinear model predictive control (NMPC) considering first principles equations. In this approach, it is not necessary to develop new sub-models for the controller's different operation points as it happens in the other

Table 2.1: Comparison of different approaches used in the control of the SMB process.

Author	Controlled Variables	Control strategy	Model of controller
KLOPPENBURG and GILLES (1999a)	Purity and yield in the extract.	Exactly linearizing state feedback controller	Asymptotically exact input/output linearization.
KLATT <i>et al.</i> (2002)	Axial positions of concentration profiles.	Two-layer architecture. (1) A optimal trajectory is determined. (2) The process is kept in that trajectory with an internal model control.	Model of bottom layer is identified from process.
ERDEM <i>et al.</i> (2004a,b)	Purity in the extract and raffinate.	Repetitive model predictive control.	Linear time-varying model.
ABEL <i>et al.</i> (2005)	Purity in the extract and raffinate.	Repetitive model predictive control.	Linear time-varying model.
SONG <i>et al.</i> (2006a,b,c)	Purity in the extract and raffinate.	Model predictive control.	Model determined through subspace identification.
GROSSMANN <i>et al.</i> (2008)	Purity in the extract and raffinate.	Repetitive model predictive control.	Linear time variant model.
VALERY and MOREY (2012)	Concentration in a certain position.	PID controllers.	
SUVAROV <i>et al.</i> (2014)	Concentration in a certain position.	Proportional control.	
ANDRADE NETO <i>et al.</i> (2016)	Purity in the extract and raffinate.	Adaptive nonlinear model predictive control.	Rigorous model based on the first principle of the SMB.
NOGUEIRA <i>et al.</i> (2017)	Purity and recoveries in the extract and raffinate.	Model predictive control.	Transfer function.
NOGUEIRA <i>et al.</i> (2020)	Purity and recoveries in the extract and raffinate.	Infinite horizon model predictive control.	Transfer function.

approaches. However, the higher computational effort could make the application infeasible in cases such as nonlinear equilibrium operation. The NMPC should be evaluated in more complex scenarios, such as different variants of the SMB process, and when the operating conditions lead to a nonlinear equilibrium between the species to be separated. Control studies applied to the SMB process variants are scarce. In the previous literature review, only the strategy used by VALERY and MOREY (2012) was studied in the VariCol and the CycloJet processes. Robust control structures that can be used in the SMB process variants need to be evaluated.

2.3.6 Final Remarks

Different approaches to modeling, optimizing, and controlling the SMB process are found in the literature. The strategies based on rigorous models can be more convenient when accurate results are desired. However, few works use those approaches,

especially for the optimization and control of SMB process variants. The following paragraphs describe some of the most important points of the bibliographic review on modeling, optimization, and control of some of the variants of the SMB process.

When modeling SMB process variants with a low column number (six or less), models that directly describe the ports' dynamics can be more appropriate, as the variants cannot be immediately compared with the TMB process (LUDEMANN-HOMBOURGER *et al.*, 2000; SCHRAMM *et al.*, 2003b). Continuous models instead of mixing cells models could be more convenient in terms of accuracy because they are based on first principles equations (GUIOCHON, 2002; GUIOCHON *et al.*, 2006).

In the optimization of SMB process with continuous models, different approaches can be used according to discretization strategy and the way the cyclic steady state is reached. Partial (single-shooting and multi-shooting) or full discretizations can be applied to the system of differential-algebraic equations. The cyclic steady state can be reached independently in each optimization stage or simultaneously with the optimization problem. The single-shooting method to reach the cyclic steady state in each optimization stage is a robust and straightforward way to solve the optimization problem, although the computational effort for the integration could be higher (KAWAJIRI and BIEGLER, 2006; TOUMI *et al.*, 2007). However, efficient integration strategies can be used to reduce the computational effort.

The optimization of the VariCol process is complex since it requires solving an MINLP problem. Its complexity is reduced on many works found in the literature by limiting the domain to specific switching times of ports and CCSs (PAIS and RODRIGUES, 2003; SUBRAMANI *et al.*, 2003; WONGSO *et al.*, 2005; ZHANG *et al.*, 2002). The most robust strategy to design the VariCol process was the one reported by YAO *et al.* (2014, 2017). They included all the variability of the VariCol process, solving a sequence of NLP problems for different subdomains described by a dodecahedron. Although that strategy allows exploring the entire VariCol process domain, the optimization continues to be an MINLP. A new proposal of optimization could be made, considering the symmetry properties when the average column length of zones is used as a reference to describe the VariCol process.

Few studies in the literature compare the performance of different SMB process variants (YANG *et al.*, 2019; YU *et al.*, 2015; ZHANG *et al.*, 2004a). In those studies, the ModiCon process has shown high performance in the separation. However, its characteristics have not been well explored. Additionally, the VariCol process has not been compared at its maximal performance. New studies comparing the performance of different SMB process variants in terms of maximal throughput could be interesting since it would be possible to directly evaluate the maximal mixture

load that can accept each one of them. In addition, new studies that evaluate in detail the characteristics of the ModiCon process are necessary. The synergy between the ModiCon and VariCol processes could also be exploited, considering the hybrid between these two variants.

Different approaches of automatic control are found in the literature to control the SMB process (ABEL *et al.*, 2005; ANDRADE NETO *et al.*, 2016; ERDEM *et al.*, 2004a; GROSSMANN *et al.*, 2008; KLATT *et al.*, 2002; KLOPPENBURG and GILLES, 1999a; NOGUEIRA *et al.*, 2017; SONG *et al.*, 2006a; VALERY and MOREY, 2012). However, the control of the SMB process variants has not been explored. Some of the proposed approaches could be used in the variants, but they need to be evaluated. One of the most promising control strategies is the one proposed by ANDRADE NETO *et al.* (2016), which is based on nonlinear model predictive control. In this approach, it is unnecessary to develop new sub-models for the controller. In addition, disturbances such as the switching period, which do not apply to RMPC strategies, could be considered. The high computational effort could be one of the limitations in the NMPC application. The characteristics of the NMPC in complex scenarios, such as operating in regions with nonlinear isotherms and using SMB process variants, need to be evaluated.

Chapter 3

Proposed Method

3.1 Introduction

The different strategies used to simulate, optimize, and control the SMB process and some of its variants based on modulations are presented in this chapter. The variants of the SMB process considered are the ModiCon and the VariCol processes based on modulation of feed concentration and column length of zones. Mathematical models that directly considers the ports' dynamics are used to model the SMB process and its variants. These models are the equilibrium dispersion and the transport dispersion, which corresponds to plug flow models. The first model considers local equilibrium between mobile and stationary phases. In contrast, the second considers mass transfer between mobile and stationary phase, which is quantified in a linear driving force approach. The mathematical models are discretized with two approaches methods, finite differences and orthogonal collocation on fixed finite elements. The finite difference approach was previously included in an SMB process virtual plant (NETO, 2015). That initial virtual plant was build for some adsorption isotherms. In this work, the virtual SMB plant is modified to include the orthogonal collocation on finite element method and to consider the SMB process variants' dynamics. Additionally, more complex adsorption isotherms are also included. For optimization of the SMB process and its different variants, the single-shooting method is used. The cyclic steady state is reached independently in each optimization stage. The control strategy, applied to some SMB process variants, is based on nonlinear model predictive control with a rigorous process model as an internal model.

3.2 Operations modes of the SMB process

In the design of VariCol and ModiCon processes, the parameters obtained by the periodic modulation of the length of zones and the feed concentration, respectively, must be specified (GARCIA *et al.*, 2006; KAWAJIRI and BIEGLER, 2006; SCHRAMM *et al.*, 2003a; TOUMI *et al.*, 2007). In the VariCol process, those parameters are the number of columns in each zone (column configuration) and the time where each sub-interval ends (when the ports move) (LUDEMANN-HOMBOURGER *et al.*, 2000; TOUMI *et al.*, 2002; YAO *et al.*, 2014). In the ModiCon process, those parameters are the feed concentration and the end time of each sub-interval generated with the modulations (SCHRAMM *et al.*, 2003a,b).

3.2.1 VariCol process

In the VariCol process, the modulation sub-intervals are defined by the asynchronous movement of the ports. The inlet and outlet ports can move upstream and downstream in a switching period. However, the most remarkable performance is reached when each port is shifted only one column downstream (YAO *et al.*, 2014), generating a maximum number of 4 sub-intervals. A schematic representation of the VariCol process with minimal movement of the ports (each port moves only one time downstream in a switching period) is presented in Figure 2.3 and Figure 3.1. The length of each zone changes with the ports' movement, starting from an initial column configuration and following a sequence of column configurations, also defined as a shifting scheme, repeated in each period. In the SMB, the length of zones is kept constant since all ports move at the same time of the switching period. Depending on the number of columns in the VariCol process, some zones' length can take a zero value in some sub-intervals (ZHANG *et al.*, 2004a), as can be seen in Figure 3.1 for zone IV in the last sub-interval. The modulation of the VariCol process can be described with the shifting times of ports (desorbent (d), extract (e), feed (f), and raffinate (r)) and the initial column configuration.

Three of the four ports' shifting times are independent because one of the ports will be moved at the same time of the switching period. The order of port movements depends on the values of the shifting times. The individual switching times of ports can be gathered in a vector and normalized by the switching period (t_s), as follows:

$$\delta\mathbf{t} = [t_d, t_e, t_f, t_r]/t_s = [\delta t_d, \delta t_e, \delta t_f, \delta t_r] \quad (3.1)$$

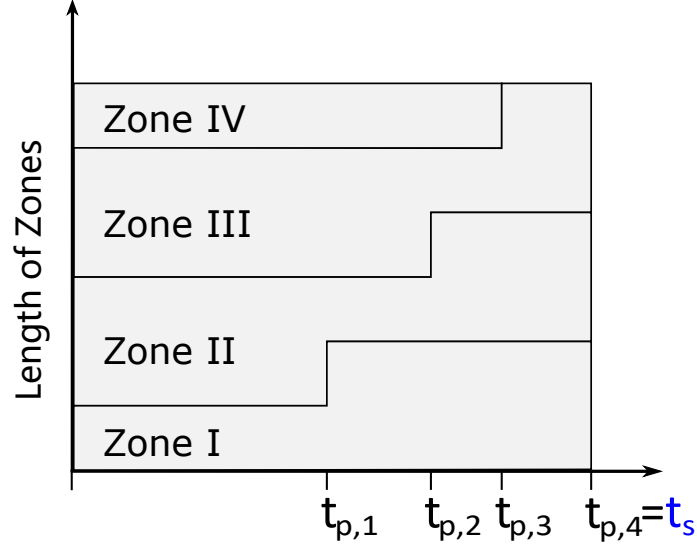


Figure 3.1: Schematic representation of the VariCol operation policies within a switching time period (t_s). Modulation of length of zones in four sub-intervals.

where δt_p is the normalized switching time (ST) of the port p $\{p = d, e, f, r\}$. The value of δt_p of at least one of the ports will always take the value of 1 since one of the ports has to move at the same time of the switching period. The values of δt_p of the other ports are bounded by the following constraint:

$$0 < \delta t_p \leq 1 \quad (3.2)$$

The constraint in Equation 3.2 was modified from previous reports in which the null value was included ($0 \leq \delta t_p \leq 1$) (TOUMI *et al.*, 2002; YAO *et al.*, 2014, 2017). This new definition excludes the scenario of ports moving at the same time at $\delta t_p = 0$ and $\delta t_p = 1$ as two different points because those points are equivalent due to the periodicity of the system. Additionally, in the VariCol process modeling, this also prevents the definition of column configurations between those equivalent points, which would not make physical sense.

A more convenient choice of the decision variables can be made to facilitate the switching scheme computation. Following some reports (YAO *et al.*, 2014; YU *et al.*, 2015), the difference between normalized switching times of two adjacent ports, expressed as follows, is better suited for that purpose:

$$\delta x = \delta t_e - \delta t_d \quad (3.3)$$

$$\delta y = \delta t_f - \delta t_e \quad (3.4)$$

$$\delta z = \delta t_r - \delta t_f \quad (3.5)$$

where δx , δy , and δz are the relative shifting time between the ports: extract and solvent, feed and extract, and raffinate and feed. As the ports could shift at any time and order within the interval given by Equation 3.2, the relative switching times must fulfill the following constraints:

$$-1 < \delta x \leq 1 \quad (3.6)$$

$$-1 < \delta y \leq 1 \quad (3.7)$$

$$-1 < \delta z \leq 1 \quad (3.8)$$

$$-1 < \delta x + \delta y \leq 1 \quad (3.9)$$

$$-1 < \delta y + \delta z \leq 1 \quad (3.10)$$

$$-1 < \delta x + \delta y + \delta z \leq 1 \quad (3.11)$$

The constraints in Equations 3.9 to 3.11 can be deduced by the combination of Equations 3.2 and 3.3 to 3.5. The ST vector in Equation 3.1 can also be expressed in terms of the relative shifting times by displacing each term of the ST vector with the switching time of the solvent port (δt_d), as follows:

$$\delta \mathbf{t}_0 = [\delta t_d, \delta t_e, \delta t_f, \delta t_r] - \delta t_d = [0, \delta x, \delta x + \delta y, \delta x + \delta y + \delta z] \quad (3.12)$$

Equation 3.12 shows that, to calculate the normalized ST vector ($\delta \mathbf{t}$), it is necessary to define only three relative switching times and specify a value of δt_d that makes the values of $\delta \mathbf{t}$ fall between 0 and 1. The selection of δt_d has to make that at least one port moves in a time equal to the switching period.

The other variable that needs to be defined to describe column length modulation in zones is the initial column configuration. That initial number of columns per zone in a switching period can be expressed as a vector, such as:

$$\mathbf{N}^0 = [N_I^0, N_{II}^0, N_{III}^0, N_{IV}^0] \quad (3.13)$$

where N_M^0 $\{M = I, II, III, IV\}$ is the number of initial columns in the zone M . That number of columns changes during each switching time, leading to a CCS repeated throughout each switching period. The other three column configurations ($\mathbf{N}^1, \mathbf{N}^2, \mathbf{N}^3$) of the CCS can be determined with the movement of the ports defined by the shifting times. The total number of column configurations in the CCS (\mathbf{N}^0 ,

$\mathbf{N}^1, \mathbf{N}^2, \mathbf{N}^3$) could be lower than four if some of the ports shift simultaneously. In the case of all ports moves synchronously, the VariCol process is reduced to the SMB process. From the CCS and the switching times of the ports, an average number of columns in each zone, which is constant in all periods, can be obtained. The average number of columns or average column length (ACL) in each zone ($\bar{\mathbf{N}}$) can be represented as follows:

$$\bar{\mathbf{N}} = [\bar{N}_I, \bar{N}_{II}, \bar{N}_{III}, \bar{N}_{IV}] \quad (3.14)$$

where \bar{N}_M is the average column length in zone M within a switching period. The \bar{N}_M of each zone can be calculated from the initial column configuration and the normalized shifting times of ports. For example the average column length of zone I (\bar{N}_I) can be calculated taken into account the initial number of columns in the zone I and the movement of the ports that affects the number of columns in that zone, which are the desorbent and the extract ports ($\delta t_d, \delta t_e$). Depending on the δt_d and δt_e values, there are two cases: when $\delta t_d < \delta t_e$ and when $\delta t_d \geq \delta t_e$. The average column length in the zone I for these two cases can be determined as follow:

$$\bar{N}_I = \delta t_d N_I^0 + (\delta t_e - \delta t_d)(N_I^0 - 1) + (1 - \delta t_e)N_I^0 = N_I^0 - \delta x \quad (3.15)$$

$$\bar{N}_I = \delta t_e N_I^0 + (\delta t_d - \delta t_e)(N_I^0 + 1) + (1 - \delta t_d)N_I^0 = N_I^0 - \delta x \quad (3.16)$$

Equations 3.15 and 3.16 show that the average column length of zone I can be calculated with the same equation independently when the desorbent and the extract ports move. Similar behavior can be found for the other average column length of zones. In general, the average column length for all zones can be related to the initial column configuration and the relative shifting times as follow:

$$\bar{N}_I = N_I^0 - \delta x \quad (3.17)$$

$$\bar{N}_{II} = N_{II}^0 - \delta y \quad (3.18)$$

$$\bar{N}_{III} = N_{III}^0 - \delta z \quad (3.19)$$

$$\bar{N}_{IV} = N_{IV}^0 + \delta x + \delta y + \delta z \quad (3.20)$$

From Equations 3.17 to 3.20, it is possible to see that with the definition of the initial column and the definition of either the relative shifting times or the ACL is possible to describe the modulation in the column length and to determine the CCS. In the case of using the ACL, only three of them are necessary since the other can be

determined with the total number of columns in the system. From the ACL, different CCSs that produce the same result in the cyclic steady state can be obtained (YAO *et al.*, 2014, 2017). These CCSs contain the same column configurations set, but each of them is displaced about the others. A second CCS would have the initial column configuration of \mathbf{N}^1 , followed by the subsequent column configurations of \mathbf{N}^2 , \mathbf{N}^3 , \mathbf{N}^0 . Each column configuration acts as an initial column configuration for the different CCSs. The CCSs can be determined by defining the ACL and finding the appropriate \mathbf{N}^P with $P = 0, 1, \dots, \leq 3$, as described in the next section.

3.2.1.1 Calculation of the initial column configuration

A method to determine the possible initial column configurations from an ACL was proposed. The options for the initial column configuration of a CCS can be deduced from the combinations of the nearest upper and lower integer values of an ACL with the constraint that the sum of columns for each option needs to result in the total number of columns (n) of the system.

In order to determine the options for initial column configurations, a procedure based on the solution of a combinatorial problem that depends on the difference between n and the sum of the nearest lower integer values (SNLIV) determined from the ACL was proposed. As different ACL for a system with the same number of columns can produce different results for $n - \text{SNLIV}$, the number of initial column configuration options that can be determined can also change. Possible initial column configuration can be determined from the combination of nearest upper and lower integer values of the ACL according to the result of $n - \text{SNLIV}$. The number of those combinations also depends on the number of zones with integer average column lengths. There are fewer combinations in systems with some zones with integer average column lengths than those with all zones with rational ACL. In the case of all zones with integer average column length, there is only one possible combination, and the VariCol process is reduced to the conventional SMB process. The number of column configuration options (ncc) in the VariCol process can be determined with the following combinatory equation expressed as a function of the zones with rational average values:

$$ncc = \frac{nz!}{nzc!(nz - nzc)!} \quad (3.21)$$

where nz is the number of zones of the VariCol process with rational average values, and nzc is the number of zones with either the nearest upper or the nearest lower

integer values of the ACL that have to be chosen from the set of nz zones to guarantee a sum of n . According to the difference between n and SNLIV, 3 scenarios are possible, as described below:

- When $n - \text{SNLIV} = 1$, the options for column configuration can be determined by choosing $nzc = nz - 1$ zones with lower integer values. The maximum number of combinations – that is, when all zones have rational average column number – is 4, meaning that, in this case, each option of column configuration has 3 lower integer values and 1 upper integer value of the ACL.
- When $n - \text{SNLIV} = 2$, the options for column configurations can be determined by choosing $nzc = nz - 2$ zones with lower integer values. The maximum number of possible combinations is 6, and, in this case, each option of column configuration has 2 lower integer values.
- When $n - \text{SNLIV} = 3$, the options for column configurations can be determined by choosing $nzc = nz - 1$ zones with the upper integer values. The maximum number of possible combinations is 4, and, in this case, each option of column configuration has 3 upper integer values.

Not all combinations can be used as the starting point of the CCS since some are related to switching times that cannot be applied in a VariCol unit. A methodology based on the evaluation of the normalized ST vector ($\delta\mathbf{t}$) of each option was proposed to determine which of them can be used as the starting point of the shifting scheme. In this methodology, the values of $\delta\mathbf{t}$ were evaluated to determine whether they could fall between the (0,1] range, as defined by the constraints of Equation 3.2. This methodology is described in more detail below:

- Initially, the relative switching times (δx , δy and δz) are calculated from the ACL and for all possible options of initial column configuration using Equations 3.17 to 3.19.
- From the relative switching times, vectors of displaced ST ($\delta\mathbf{t}_0$) are calculated from Equation 3.12.
- The $\delta\mathbf{t}$ can be calculated by displacing $\delta\mathbf{t}_0$, the value obtained from the difference between 1 and the maximum value of the $\delta\mathbf{t}_0$. In this case, all $\delta\mathbf{t}$ values should be between (0, 1] to originate a possible movement of the ports. The initial column configuration options that can be chosen are those that respond to these requirements.

The above procedure is interesting since from an ACL, column configurations' options that are the same initial column configurations of different CCSs can be determined. Any of the initial column configurations that can be determined can be used since the different CCSs that can be determined produce the same results in the cyclic steady state (YAO *et al.*, 2014, 2017). With the proposed approach, column length modulation in the VariCol process can be described only by defining the ACL, which will be very useful for optimization.

The proposed procedure that determines the options of column configuration was evaluated with three case studies of ACL. Additionally, for the first case, an analysis of the different CCSs was made and their performance in cyclic steady state was compared. The results of these case studies are included in Section 4.2.1.

3.2.2 ModiCon process

The periodic modulation pattern for ModiCon can have any number of sub-intervals and forms (SCHRAMM *et al.*, 2003a,b; YANG *et al.*, 2019; YU *et al.*, 2015; ZHANG *et al.*, 2004a). Figure 2.4 represents a modulation with two sub-intervals, where the first has zero concentration value and the second is larger. The average feed concentration of ModiCon process is usually defined as equal to the SMB (see in Figure 2.4) to compare the operations modes. The maximal value of feed concentration in the sub-intervals is constrained by the mixture solubility limit (KASPEREIT *et al.*, 2002; SCHRAMM *et al.*, 2003a; ZHANG *et al.*, 2004a). The number of specified feed concentrations and times is equal to the number of sub-intervals minus 1 ($nsb - 1$), since the average feed concentration and the switching period (t_s) are generally defined in the system, reducing the number of parameters specified in the sub-intervals. The times of the sub-intervals normalized with the switching period, and the feed concentrations can be gathered in vectors as follow:

$$\delta \mathbf{t}_{sb} = [t_{sb,1}, t_{sb,2}, \dots, t_{sb,nsb}] / t_s = [\delta t_{sb,1}, \delta t_{sb,2}, \dots, \delta t_{sb,nsb}] \quad (3.22)$$

$$\mathbf{c}_{f,i} = [c_{f,i,1}, c_{f,i,2}, \dots, c_{f,i,nsb}] \quad (3.23)$$

where $\delta t_{sb,s}$ is the normalized time in the sub-interval s and $c_{f,i,s}$ is the feed concentration of component i in the sub-interval s .

3.3 Mathematical model of SMB and its variants

The mathematical model used to describe the SMB process and its variants considers the ports' switching dynamics. Each of the chromatographic columns is described with a continuous model. The ports' dynamic is taken into account by changing the mathematical model's boundary conditions as ports shift. The mathematical models used in this work are the equilibrium dispersion and transport dispersion. These models are widely used in chiral separations, where good results have been reported (GONG *et al.*, 2014a; GUIOCHON, 2002; GUIOCHON *et al.*, 2006; RODRIGUES, 2015; SCHMIDT-TRAUB *et al.*, 2012).

The mass balance of the i -th component in the fluid phase of k -th column is given by:

$$\frac{\partial c_{i,k}}{\partial t} = -v_k \frac{\partial c_{i,k}}{\partial z} + D_{ax,i,k} \frac{\partial^2 c_{i,k}}{\partial z^2} - \left(\frac{1 - \varepsilon_{b,k}}{\varepsilon_{b,k}} \right) \frac{\partial \bar{q}_{i,k}^*}{\partial t} \quad (3.24)$$

where the subscript i corresponds to the components A or B , $k = 1, 2, \dots, N_c$ corresponds to the columns, $c [M L^{-3}]$ is the mass concentration in the fluid, $\bar{q}^* [M L^{-3}]$ is the mean overall adsorbent loading in the adsorbed phase, $t [T]$ is the time, $v [L T^{-1}]$ is the interstitial velocity, $z [L]$ is the axial coordinate, ε_b is the bed void fraction, $D_{ax} [L^2 T^{-1}]$ is the axial dispersion coefficient.

The mass balance of the i -th component in the adsorbed phase (pores and solid skeleton) of the k -th column can be expressed as follows:

$$\varepsilon_{p,k} \frac{\partial \bar{c}_{p,i,k}}{\partial t} + (1 - \varepsilon_{p,k}) \frac{\partial \bar{q}_{i,k}}{\partial t} = \frac{3}{r_p} \varepsilon_{p,k} D_{p,i,k} \frac{\partial c_{p,i,k}}{\partial r} \Big|_{r=r_p} \quad (3.25)$$

where $\bar{c}_p [M L^{-3}]$ is the mean concentration in the pores, $\bar{q} [M L^{-3}]$, is the mean phase loading related to the solid skeleton, $c_p [M L^{-3}]$ is the mass concentration in the pores, ε_p is the intraparticle void fraction, $r_p [L]$ is the particle radius, and $D_p [L^2 T^{-1}]$ is the lumped pore and surface diffusion (GUIOCHON *et al.*, 2006). The left side of Equation 3.25 corresponds to the mean overall adsorbent loading in the adsorbed phase and can be expressed as follows:

$$\varepsilon_{p,k} \frac{\partial \bar{c}_{p,i,k}}{\partial t} + (1 - \varepsilon_{p,k}) \frac{\partial \bar{q}_{i,k}}{\partial t} = \frac{\partial \bar{q}_{i,k}^*}{\partial t} \quad (3.26)$$

Different approaches can be used in the right side of Equation 3.25 to determine the mean overall adsorbent loading (GUIOCHON, 2002; GUIOCHON *et al.*, 2006; NICOU, 2015; SCHMIDT-TRAUB *et al.*, 2012). One of them is the transport

dispersion (TD) model. In this model, rate limitations in the mass transfer in the stationary phase are considered. Mass transport can be quantified by a linear driving force approach, where all external and internal mass transfer contributions are lumped in a transfer coefficient, $k_{eff}^* [T^{-1}]$. When the mass resistance in the adsorbed phase is considered the rate-limiting, the right side of Equation 3.25 can be approximated as follows:

$$\frac{\partial \bar{q}_{i,k}^*}{\partial t} = k_{eff,i,k}^* (q_{e,i,k}^* - \bar{q}_{i,k}^*) \quad (3.27)$$

where $q_{e,i,k}^* [ML^{-3}]$ is the adsorption isotherm, which represents the thermodynamic equilibrium between the mobile and stationary phases. In the TD model, the chromatography elution profiles can be described by solving Equations 3.24 and 3.27 (SCHMIDT-TRAUB *et al.*, 2012).

When the rate limitations in the mass transfer of the adsorbed phase is assumed only in the skeleton, the mean concentration in the pores of the adsorbent can be considered the same as the fluid phase, $\bar{c}_{p,i,k} = c_{i,k}$ (see Equations 3.25 and 3.26). In this case, the linear driving approach can be admitted only for the term $\bar{q}_{i,k}$ of Equation 3.25 or Equation 3.26. Considering total porosity (ε , see Equation 2.2) and approximating the mean phase loading of the solid skeleton with the linear driving force, Equations 3.24, 3.25, and 3.26 are transformed into:

$$\frac{\partial c_{i,k}}{\partial t} = -v_k^{hyp} \frac{\partial c_{i,k}}{\partial z} + D_{app,i,k} \frac{\partial^2 c_{i,k}}{\partial z^2} - \left(\frac{1 - \varepsilon_k}{\varepsilon_k} \right) \frac{\partial \bar{q}_{i,k}}{\partial t} \quad (3.28)$$

$$\frac{\partial \bar{q}_{i,k}}{\partial t} = k_{eff,i,k} (q_{e,i,k} - \bar{q}_{i,k}) \quad (3.29)$$

where $k_{eff} [T^{-1}]$ is the lumped rate coefficient. The apparent dispersion coefficient (D_{app}) and the hypothetical effective velocity (v_k^{hyp}) of Equation 3.28 are described as follow:

$$D_{app,i,k} = \frac{\varepsilon_{b,k} D_{ax,i,k}}{\varepsilon_k} \quad (3.30)$$

$$v_k^{hyp} = \frac{\varepsilon_{b,k} v_k}{\varepsilon_k} = \frac{u_k}{\varepsilon_k} = \frac{Q_k}{S_k \varepsilon_k} \quad (3.31)$$

where $u [LT^{-1}]$ is the superficial velocity, $Q [L^3 T^{-1}]$ is the internal flow rate, and $S [L^2]$ is the cross-sectional column area.

The value of the lumped rate coefficient (k_{eff}) and the adsorption isotherm ($q_{e,i,k}$) of Equation 3.29 are different from those of Equation 3.27.

Another approach used in Equations 3.25 and 3.26 is based on the equilibrium dispersion model (ED), where an instantaneous equilibrium between the mobile and stationary phase (mass transfer kinetics is very fast) is considered. In that case, the mean concentration in the particle is considered the same as the fluid phase ($\bar{c}_{p,i,k} = c_{i,k}$), and $\bar{q}_{i,k}$ is calculated using an adsorption isotherm directly ($(\bar{q}_{i,k} = q_{e,i,k})$). Therefore, the mathematical model in the ED approach is reduced to solve only Equation 3.28. The apparent dispersion for the ED (D_{app}) is not just the one that appears in Equation 3.28, but instead, a higher one that lumps different effects neglected.

In the above equations for ED and TD models, an adsorption isotherm model (q_e or q_e^*) that relates the thermodynamic equilibrium between the concentration of the adsorbed phase of each component with the concentration of the fluid phase needs to be defined. There are different types of isotherms with different degrees of complexity. However, explicit and simple isotherm models ($q_e = f(c_1, c_2, \dots)$) that facilitate the estimation of its parameters are preferable (GUIOCHON, 2002). The most common isotherms are the linear, Langmuir, competitive Langmuir, linear-Langmuir, and bi-Langmuir, which are expressed respectively as:

$$q_{e,i} = H_i c_i \quad (3.32)$$

$$q_{e,i} = \frac{q_m K_i c_i}{1 + K_i c_i} \quad (3.33)$$

$$q_{e,i} = \frac{q_m K_i c_i}{1 + K_1 c_1 + K_2 c_2} \quad (3.34)$$

$$q_{e,i} = H_i c_i + \frac{q_m K_i c_i}{1 + K_1 c_1 + K_2 c_2} \quad (3.35)$$

$$q_{e,i} = \frac{q_{m,1} K_{i,1} c_i}{1 + K_{1,1} c_1 + K_{2,1} c_2} + \frac{q_{m,2} K_{i,2} c_i}{1 + K_{1,2} c_1 + K_{2,2} c_2} \quad (3.36)$$

where H is the Henry constant, q_m [ML^{-3}] is the saturation concentration in the particle, and K [ML^{-3}] is the adsorption constant. Equation 3.32 assumes that at equilibrium, the concentration of the adsorbed component in the stationary phase is proportional to its concentration in the mobile phase. Equation 3.33 represents the adsorption of molecules in localized adsorption sites. Equation 3.34 considers competition between the components of a mixture to access the adsorption sites. Equation 3.35 combines the linear isotherm and competitive Langmuir isotherm. Equation 3.36 considers that the adsorbent surface is covered with two different types of sites, and the components compete for those sites.

The equation system for ED (Equation 3.28) and TD (Equations 3.24 and 3.27 or 3.28 and 3.29) models can be solved by providing appropriate initial and boundary conditions. The initial condition describes the values of state variables (concentration of each component in each column) at the beginning of the operation. The initial condition for the ED model is presented in Equation 3.37, and the initial conditions for the TD model in terms of bed porosity correspond to Equations 3.37 and 3.38. For the case of the TD model in terms of total porosity, the variable $\bar{q}_{i,k}^*$ needs to be changed by $\bar{q}_{i,k}$ in Equation 3.38.

$$c_{i,k}(0, z) = 0 \quad (3.37)$$

$$\bar{q}_{i,k}^*(0) = 0 \quad (3.38)$$

For the TD model in terms of bed porosity, the boundary conditions are given by Equations 3.39 and 3.40. For the TD model in terms of total porosity and the ED model, the boundary conditions are equivalent to Equations 3.39 and 3.40. However, the appropriate dispersion coefficients and velocity values need to be used.

$$D_{ax,i,k} \frac{\partial c_{i,k}}{\partial z}(t, 0) = v_k [c_{i,k}(t, 0) - c_{i,k}^{in}(t)] \quad (3.39)$$

$$\frac{\partial c_{i,k}(t, l)}{\partial z} = 0 \quad (3.40)$$

where $z = 0$ is the inlet of the column and $z = l$ is the outlet. The term $c_{i,k}^{in}(t)$ [$M L^{-3}$] of Equation 3.39 is the concentration of component i at the inlet of the k -th column, and the parameter l [L] of Equation 3.40 is the column length. The calculation of the inlet concentration for each column ($c_{i,k}^{in}(t)$) changes with the ports' movement in the SMB unit. In the nodes of the inlet and outlet ports, $c_{i,k}^{in}(t)$ is calculated with a mass balance. In the other nodes, the input concentration of a column is the same as the previous columns' output concentration. The mass balance at the nodes of the inlet and outlet ports can be expressed as follow:

$$\begin{aligned} Q_I &= Q_{IV} + Q_d && \text{(desorbent node)} && (3.41) \\ c_{i,I}^{in} Q_I &= c_{i,IV}^{out} Q_{IV} + c_{d,i} Q_d \end{aligned}$$

$$\begin{aligned} Q_{II} &= Q_I - Q_e && \text{(extract node)} && (3.42) \\ c_{i,II}^{in} &= c_{i,I}^{out} = c_{e,i} \end{aligned}$$

$$\begin{aligned} Q_{III} &= Q_{II} + Q_f && \text{(feed node)} && (3.43) \\ c_{i,III}^{in} Q_{III} &= c_{i,II}^{out} Q_{II} + c_{f,i} Q_f \end{aligned}$$

$$\begin{aligned}
Q_{IV} &= Q_{III} - Q_r & (\text{raffinate node}) & \quad (3.44) \\
c_{i,IV}^{in} &= c_{i,III}^{out} = c_{r,i}
\end{aligned}$$

where $c_{p,i}[ML^{-3}]$ is the concentration of the component i in the inlet/outlet ports $\{p = d, e, f, r\}$, $Q_p[L^3T^{-1}]$ is the external flow rate in the ports $\{p = d, e, f, r\}$, and $Q_M[L^3T^{-1}]$ is the internal flow rate in each zone of the column train $\{M = I, II, III, IV\}$. For other nodes, $c_{i,k}^{in}(t)$ correspond to the output concentration of the previous column $c_{i,k-1}^{out}(t)$.

3.3.1 Dimensionless mathematical model

The ED and TD models are more efficiently solved by expressing them in dimensionless forms (KACZMARSKI, 1996). As the dispersion coefficient and the velocity value depend on the approach used in the TD model, a dimensionless form is presented only for the TD model expressed using bed porosity. Dimensionless forms for the ED model and the other approach of the TD model are equivalent (not shown), but in those cases, the appropriate coefficient parameters have to be used.

Introducing the following dimensionless variables:

$$x = \frac{z}{l}; \quad \tau = \frac{t\bar{v}_f}{l}; \quad \xi = \frac{v}{\bar{v}_f}; \quad P_e = \frac{\bar{v}_f l}{D_{ax}}; \quad S_t = \frac{k_f l}{\bar{v}_f} \quad (3.45)$$

where $\bar{v}_f [LT^{-1}]$ is the highest superficial velocity in all zones, P_e is the Péclet number, and S_t the Stanton number.

Equations 3.24, and 3.27 can be rewritten using these dimensional variables as follows:

$$\frac{\partial c_{i,k}}{\partial \tau} = -\xi_k \frac{\partial c_{i,k}}{\partial x} + \frac{1}{P_{e i,k}} \frac{\partial^2 c_{i,k}}{\partial x^2} - \left(\frac{1 - \varepsilon_{bk}}{\varepsilon_{bk}} \right) \frac{\partial q_{i,k}}{\partial \tau} \quad (3.46)$$

$$\frac{\partial q_{i,k}^*}{\partial \tau} = St_{i,k} (q_{e i,k}^* - q_{i,k}^*) \quad (3.47)$$

The initial and boundary conditions (Equation 3.37, 3.38, 3.39, and 3.40) in dimensionless variables become:

$$c_{i,k}(0, x) = 0 \quad (3.48)$$

$$q_{i,k}^*(0) = 0 \quad (3.49)$$

$$\frac{1}{Pe_{i,k}} \frac{\partial c_{i,k}}{\partial x}(\tau, 0) = \xi_k [c_{i,k}(\tau, 0) - c_{i,k}^{in}(\tau)] \quad (3.50)$$

$$\frac{\partial c_{i,k}(\tau, 1)}{\partial x} = 0 \quad (3.51)$$

In Equation 3.50, axial dispersion (D_{ax}) and interstitial velocity (v) were considered. The form of Equation 3.46 is more appropriate to apply some discretization methods in the spatial variable, x . The new domain of x is between $0 \leq x \leq 1$. The methods of finite difference and orthogonal collocation on fixed finite elements are used.

3.4 Spatial discretization

Numerical methods are necessary to solve the ED and TD models since there are no analytical solutions that when using nonlinear isotherms and considering the dynamics of the ports of the SMB process and its variants (GUIOCHON *et al.*, 2006; RODRIGUES, 2015; SCHMIDT-TRAUB *et al.*, 2012). In this work, the single-shooting approach was employed, a strategy based on a spatial discretization with subsequent integration of the resulting system of differential-algebraic equations (DAE) or ordinary differential equations (ODE). The cyclic steady state was determined using the sequential procedure (see Figure 2.7a), which is based on finding that condition in each stage of the optimization.

A variety of numerical methods can be used to discretize the spatial variable. Some of the most used are the finite differences and the orthogonal collocation on fixed finite elements, which are employed in this work.

3.4.1 Discretization using finite differences (FD)

In this method, the continuous spatial variable is discretized at finite points, and the derivatives in those points are approximated with linear equations. In this work, the first-order spatial derivatives were approximated by finite upwind differences and the second-order partial derivatives were approximated by finite central differences, as shown in the following equations:

$$\frac{\partial c_{i,k}(\tau, x)}{\partial x} \simeq \frac{c_{i,j,k}(\tau, x_j) - c_{i,j-1,k}(\tau, x_{j-1})}{\Delta x} \quad (3.52)$$

$$\frac{\partial^2 c_{i,k}(\tau, x)}{\partial x^2} \cong \frac{c_{i,j+1,k}(\tau, x_{j+1}) - 2c_{i,j,k}(\tau, x_j) + c_{i,j-1,k}(\tau, x_{j-1})}{\Delta x^2} \quad (3.53)$$

where $j = 1, 2, \dots, n_m$ correspond to the discretization points. When Equations 3.52 and 3.53 are applied to the dimensionless balance equation of the fluid phase and the boundary conditions (Equations 3.46, 3.50 and 3.51), the resulting differential-algebraic equation system are obtained:

$$\begin{aligned} \frac{dc_{i,j,k}(\tau, x_j)}{d\tau} \cong & -\xi_k \frac{c_{i,j,k}(\tau, x_j) - c_{i,j-1,k}(\tau, x_{j-1})}{\Delta x} \\ & + \frac{1}{Pe_{i,k}} \frac{c_{i,j+1,k}(\tau, x_{j+1}) - 2c_{i,j,k}(\tau, x_j) + c_{i,j-1,k}(\tau, x_{j-1})}{\Delta x^2} \\ & - \left(\frac{1 - \varepsilon_{bk}}{\varepsilon_{bk}} \right) \frac{dq_{i,k}(\tau)}{d\tau}, \quad \text{for } j = 1, 2, 3, \dots, n_m \end{aligned} \quad (3.54)$$

$$c_{i,0,k} = \frac{c_{i,k}^{in}(\tau) + \frac{1}{Pe_{i,k}\xi_k\Delta x} c_{i,1,k}}{1 + \frac{1}{Pe_{i,k}\xi_k\Delta x}} \quad (3.55)$$

$$c_{i,n_m+1,k} = c_{i,n_m,k} \quad (3.56)$$

These differential-algebraic equations can be transformed into an ordinary differential equation system by direct substituting algebraic Equations 3.55 and 3.56 in Equation 3.54. The discretized ODE system and the additional equations for the stationary phase (see Equation 3.47), when the TD model is used, can be solved by applying a numerical integration algorithm.

The finite-differences discretization method is characterized not only by the simplicity but also because the Jacobian matrix has unique characteristics. The jacobian matrix is sparse, meaning that most of the Jacobian matrix elements are zero. That characteristic is favorable when sparse algebra is used in the integration (WANNER and HAIRER, 1996).

3.4.2 Discretization using orthogonal collocation on fixed finite elements

The other discretization method used to approximate the spatial variable was the orthogonal collocation on fixed finite elements, which is based on polynomial approximations. This method will also be referred as a polynomial approximation (PA). In this method, the domain of a spatial variable is divided into finite elements or sub-

domains. In each element, the concentration profiles are approximated spatially by n -th-degree polynomial functions and then piece together with the adjacent polynomials (GARDINI *et al.*, 1985; KACZMARSKI, 1996; VILLADSEN and MICHELSEN, 1978). This method has been found appropriate for use in systems that present steep gradients, such as the chromatographic columns (GUIOCHON *et al.*, 2006; KACZMARSKI *et al.*, 1997; MA and GUIOCHON, 1991; YU and WANG, 1989).

In this method, the normalized space coordinate (x) is divided into n_s equally spaced elements or subdomains to give n_{s+1} element boundaries or nodes:

$$0 = S^0 < S^1 < \dots < S^{n_s-1} < S^{n_s} = 1 \quad (3.57)$$

In each sub-domain, the space variable is also normalized to apply the orthogonal polynomial approximation properly. A new spatial variable in each subdomain is defined as follows:

$$\chi^s(x) = \frac{x - S^{s-1}}{\Delta S^s} \quad (3.58)$$

where $s = 1, 2, \dots, n_s$ correspond to the elements or subdomains, and $\Delta S^s = S^s - S^{s-1}$ is the width of the element S . The values of x for each new spatial variable needs to be within the appropriate subdomain ($x \in [S^{s-1}, S^s]$). The approximation of the spatial concentration profiles in each subdomain $c^s(\tau, \chi^s)$ can be expressed as follows:

$$c_{i,k}^s(\tau, \chi^s) \cong \sum_{j=0}^{w+1} L_j^s(\chi^s) c_{i,j,k}^s(\tau) \quad (3.59)$$

where $L_j^s(\chi^s)$ are the $w + 2$ interpolating Lagrange polynomials, which depend on the local variable χ^s . The discrete values of χ^s in each element (including the points 0 and 1) are used to build up a local polynomial approximation, where the internal points are chosen as the zeros (roots) of the Legendre polynomial of w degree. For each collocation point ($j = 0, 1, \dots, w + 1$), the interpolating Lagrange polynomials of degree $w + 1$ can be expressed as follows:

$$L_j^s(\chi^s) = \prod_{\substack{m=0 \\ m \neq j}}^{w+1} \frac{\chi^s - \chi_m^s}{\chi_j^s - \chi_m^s} \quad (3.60)$$

For the discrete values of χ_m^s , the interpolating Lagrange polynomial $L_j^s(\chi^s)$ fulfills the following property when $\chi^s = \chi_m^s$:

$$L_j^s(\chi_m^s) = \delta_{j,m} = \begin{cases} 0, & \text{se } j \neq m \\ 1, & \text{se } j = m \end{cases} \quad (3.61)$$

According to Equation 3.61, when $\chi^s = \chi_m^s$, the concentration profiles depend only on time, $c_{i,k}^s(\tau, \chi_j^s) = c_{i,j,k}^s(\tau)$. The first and second-order partial derivatives concerning the spatial variable are approximated as follow:

$$\frac{\partial c_{i,k}^s(\tau, \chi_j^s)}{\partial x} \cong \sum_{m=0}^{w+1} A_{j,m}^s c_{i,m,k}^s(\tau, \chi_m^s) \quad (3.62)$$

$$\frac{\partial^2 c_{i,k}^s(\tau, \chi_j^s)}{\partial x^2} \cong \sum_{m=0}^{w+1} B_{j,m}^s c_{i,m,k}^s(\tau, \chi_m^s) \quad (3.63)$$

where $A_{j,m}$ and $B_{j,m}$ are matrices with the first and second derivative of Lagrange interpolators, which are defined as follow:

$$A_{j,m}^s = \frac{1}{\Delta S^s} \left. \frac{dL_m^s(\chi^s)}{d\chi^s} \right|_{\chi_j^s} \quad (3.64)$$

$$B_{j,m}^s = \frac{1}{(\Delta S^s)^2} \left. \frac{d^2 L_m^s(\chi^s)}{d\chi^{s2}} \right|_{\chi_j^s} \quad (3.65)$$

By substituting Equations 3.62 and 3.63 in the mass balance of fluid phase and the boundary conditions (Equations 3.46, 3.50 and 3.51), the resulting system of differential-algebraic equations can be expressed as follows:

$$\begin{aligned} \frac{dc_{i,j,k}^s(\tau)}{d\tau} = & -\xi_k \sum_{m=0}^{w+1} A_{j,m}^s c_{i,m,k}^s(\tau) + \frac{1}{Pe_{i,k}} \sum_{m=0}^{w+1} B_{j,m}^s c_{i,m,k}^s(\tau) \\ & - \left(\frac{1 - \varepsilon_{bk}}{\varepsilon_{bk}} \right) \frac{dq_{i,k}(\tau)}{d\tau}, \quad \text{for } s = 1, 2, \dots, n_s \end{aligned} \quad (3.66)$$

$$\frac{1}{Pe} \sum_{m=0}^{w+1} A_{0,m}^1 c_{i,m,k}^1(\tau) = \xi_k [c_{i,0,k}^1(\tau) - c_{i,k}^{in}(\tau)] \quad (3.67)$$

$$\sum_{m=0}^{w+1} A_{w+1,m}^{n_s} c_{i,m,k}^{n_s}(\tau) = 0 \quad (3.68)$$

In order to piece together adjacent polynomials of the subdomains, it is necessary to satisfy the continuity of the function and the first-order spatial derivative in each node of the subdomain. These continuity conditions can be represented as follow,

for $s = 1, 2, \dots, n_s - 1$:

$$c_{i,w+1,k}^s(\tau) = c_{i,0,k}^{s+1}(\tau) \quad (3.69)$$

$$\sum_{m=0}^{w+1} A_{w+1,m}^s c_{i,m,k}^s(\tau) = \sum_{m=0}^{w+1} A_{0,m}^{s+1} c_{i,m,k}^{s+1}(\tau) \quad (3.70)$$

The discretized system of equations for the case of the TD approach in terms of bed porosity (Equations 3.66, 3.47, 3.67, 3.68, 3.69 and 3.70) can be solved implicitly as a differential-algebraic equations (DAEs) system or explicitly as ordinary differential equations (ODEs) system, as presented below:

$$\Psi(\chi, c, \frac{dc}{d\tau}) = 0 \quad (3.71)$$

$$\frac{dc}{d\tau} = \psi(\chi, c) \quad (3.72)$$

In the explicit approach (Equation 3.72), the boundary and the node (between subdomains) points (Equations 3.67, 3.68, 3.69, and 3.70) are solved individually for each column and not simultaneously for all columns. Those points were calculated starting from the first column of zone I to the last column of zone IV. However, as in the PA, all the boundary and node equations are coupled (see Equations 3.67 to 3.70), an additional approximation must be considered to decoupling some equations and solve the boundary conditions column by column. The approximation considered was to calculate the outlet concentration of zone IV required at the moment of calculating the inlet concentration of zone I, with Equation 3.56. Note that the outlet concentration of the last column of zone IV, in that case, depends only on the previous discretization point that is known by the values received in the integration function. With that approximation, it is possible to calculate the boundary and the node points of subdomains from the first column of zone I to the last column of zone IV. That approximation is reasonable since the concentration profile at the end of last column is flat and almost zero.

3.5 Optimization strategy

The operation regime of the SMB process and its variants is intrinsically dynamic because these processes do not reach a steady state condition, but instead, a cyclic steady state (SWARTZ and KAWAJIRI, 2019). According to these operation characteristics, the optimal design operation parameters can be determined by

solving a dynamic optimization problem. Different dynamic optimization problems can be formulated and solved in the SMB process and its variants. In this work, the single-shooting method was used to maximize the throughput. The CSS was reached with the sequential approach presented in Figure 2.7a.

The optimization problem for the SMB process and its variants can be expressed as follows:

$$\begin{aligned}
& \min_{\mathbf{Q}, t_s, [\bar{\mathbf{N}}, \mathbf{c}_f, \delta \mathbf{t}_m]} F(c_{i,j,k}, \mathbf{Q}, t_s, [\bar{\mathbf{N}}, \mathbf{c}_f, \delta \mathbf{t}_m]) \\
\text{subject to} & \quad \frac{dc_{i,j,k}}{dt} = f(c_{i,j,k}, \mathbf{Q}, t_s, [\bar{\mathbf{N}}, \mathbf{c}_f, \delta \mathbf{t}_m]) \\
& \quad g(c_{i,j,k}, \mathbf{Q}, t_s, [\bar{\mathbf{N}}, \mathbf{c}_f, \delta \mathbf{t}_m]) \leq 0 \\
& \quad h(c_{i,j,k}, \mathbf{Q}, t_s, [\bar{\mathbf{N}}, \mathbf{c}_f, \delta \mathbf{t}_m]) = 0 \\
& \quad c_{i,j,k}(0) = c_{0,i,j,k}
\end{aligned} \tag{3.73}$$

where F is the objective function that depends on the spatially discretized states ($c_{i,j,k}$, where j refers to the discretization points, using the notation of the FD method for clarity), \mathbf{Q} are the internals flow rates, t_s is the switching period, and $\bar{\mathbf{N}}, \mathbf{c}_f, \delta \mathbf{t}_m$ are some optional variables that are characteristic of the some variants of the SMB process. When the VariCol process is considered, average column lengths of zones are included ($\bar{\mathbf{N}}$); when the ModiCon process is taken into account, both the feed concentrations (\mathbf{c}_f) and the normalized times ($\delta \mathbf{t}_m$) are incorporated; whereas when the hybrid ModiCon+VariCol is considered, all these optional variables are included. The function f is the spatially discretized system of equations of the chromatographic columns. The function g corresponds to some inequality constraints that guarantee the following conditions: cyclic steady state, positive external flow rates (ANDRADE NETO *et al.*, 2016; BENTLEY and KAWAJIRI, 2013), and the upper and lower bounds of the decision variables. The function h corresponds to equality constraints, such as to guarantee the total number of columns in the system equals to n , the sum of the fraction length of subintervals equals to 1, and the average feed concentration equals to a specified value. The initial condition of the spatially discretized system of equations is given by $c_{0,i,j,k}$.

For optimizing the Varicol process, a new methodology that is more efficient than the one presented by YAO *et al.* (2014, 2017) was proposed. In the methodology of YAO *et al.* (2014, 2017), which will be referred to as Method 1, the relative shifting times of ports are used as decision variables. In that methodology, it is necessary to define an initial column configuration before the optimization problem. The initial column configuration bounds the search region of the optimization problem to a dodecahedron, and the CCS calculated in each optimization stage starts in

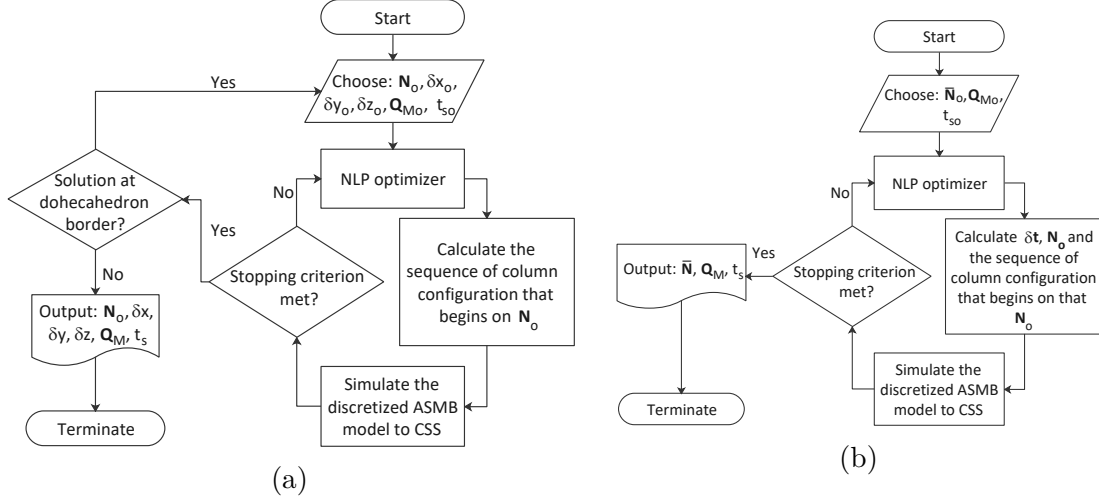


Figure 3.2: Optimization methodologies for ASMB. (a) The methodology proposed by Yao et al. YAO *et al.* (2014, 2017) (Method 1). (b) The methodology proposed in this work (Method 2).

that configuration. With Method 1, a new optimization problem must be solved every time that the optimal solution is on the border of the dodecahedron. In the methodology proposed in this work, referred to from now on as Method 2, the average column configuration of three zones is used as decision variables. That allows for deducing an appropriate initial column configuration from the combination of nearest lower and upper integer values of ACL and evaluating those combinations to define which can be used as the initial column configuration of a shifting scheme. The appropriate initial column configuration needs to be determined in each optimization stage since the average column configuration change in each iteration. With this approach, the optimization problem is reduced from an MINLP to an NLP. The flowcharts for both Method 1 (Yao et al.) and Method 2 (this work) are presented in Figure 3.2.

The performance evaluation of the SMB processes (SMB, VariCol, ModiCon, and hybrid ModiCon+VariCol) were done in terms of maximal throughput for specific values of purity in the extract and raffinate and a fixed value of desorbent consumption. The objective of the optimization-based formulation for the design of SMB processes (see Equation 3.73) is expressed as a function of feed throughput and two additional terms that ensure the desired values of purity in the extract and raffinate, as follows:

$$F = -Q_f + \lambda \left((P_{e,set} - \langle P_e \rangle)^2 + (P_{r,set} - \langle P_r \rangle)^2 \right) \quad (3.74)$$

where Q_f is the feed flow rate, $P_{p,set}$ is the desired purity at the outlet ports ($\{p = e, r\}$), $\langle P_p \rangle$ is the average purity in the outlet ports p , and λ is weighting

factor. The average concentration and the average purity in the extract and raffinate can be calculated as follow:

$$\langle c_{p,i} \rangle = \frac{1}{t_s} \int_{t_s}^{t_{s+1}} c_{p,i} dt \quad (3.75)$$

$$\langle P_p \rangle = \frac{\langle c_{p,i} \rangle}{\langle c_{p,A} \rangle + \langle c_{p,B} \rangle} \quad (3.76)$$

where p corresponds to the extract and raffinate ports ($p = e, r$). Additional performance parameters can also be used to evaluate the optimal results of the SMB process and its variants. Those parameters are productivity ($\langle Pr \rangle$), recovery ($\langle R_p \rangle$), and desorbent consumption ($\langle SC \rangle$), which are expressed as follow:

$$\langle Pr_p \rangle = \frac{Q_p \langle c_{p,i} \rangle}{(1 - \varepsilon) V_c n} \quad (3.77)$$

$$\langle R_p \rangle = \frac{Q_p \langle c_{p,i} \rangle}{t_s Q_f c_{f,i}} \quad (3.78)$$

$$\langle SC_p \rangle = \frac{Q_d}{Q_p \langle c_{p,i} \rangle} \quad (3.79)$$

where i correspond to the component A for the extract port and component B for the raffinate port, $V_c [L^3]$ is the volume of the column, and n is the number of columns.

The cyclic steady state criterion was defined based on the relative tolerances of products' average concentrations for consecutive switching periods. The relative tolerances need to be sufficiently small for the average concentration of both the most retained compound (B) in the extract and the less retained compound (A) in the raffinate. This criterion can be expressed as follows:

$$\left| \frac{\langle c_{e,B} \rangle(t_{s+1}) - \langle c_{e,B} \rangle(t_s)}{\langle c_{e,B} \rangle(t_s)} \right| \leq \epsilon_e \quad (3.80)$$

$$\left| \frac{\langle c_{r,A} \rangle(t_{s+1}) - \langle c_{r,A} \rangle(t_s)}{\langle c_{r,A} \rangle(t_s)} \right| \leq \epsilon_r \quad (3.81)$$

where ϵ_p is the tolerance for the extract and raffinate ports ($\{p = e, r\}$). Positive external flow rates for desorbent, extract, feed, and raffinate were guaranteed with the following inequality constraints:

$$Q_{IV} - Q_I \leq 0 \quad (3.82)$$

$$Q_{II} - Q_I \leq 0 \quad (3.83)$$

$$Q_{II} - Q_{III} \leq 0 \quad (3.84)$$

$$Q_{IV} - Q_{III} \leq 0 \quad (3.85)$$

Equality constraints as function of the decision variables (\bar{N} , \mathbf{c}_f , $\delta\mathbf{t}_m$) are required when the VariCol, the ModiCon or the hybrid combination of these two are included. Whereas equality constraints for the conventional SMB process were directly substituted in the model as happened with Equations 3.41 to 3.44 that determine the inlet concentration ($c_{i,k}^{in}(t)$). In the VariCol process, the sum of the average lengths of zones needs to be equal to the number of the system columns (n). In the ModiCon process, the sum of the fraction of length of the subintervals needs to be equal to 1, and the average feed concentration needs to be equal to the average concentration of the SMB process. These constraints can be expressed as follow:

$$\bar{N}_{c,I} + \bar{N}_{c,II} + \bar{N}_{c,III} + \bar{N}_{c,IV} = n \quad (3.86)$$

$$\delta t_{sb,1} + (\delta t_{sb,2} - \delta t_{sb,1}) + \dots + (\delta t_{sb,nsb} - \delta t_{sb,nsb-1}) = \delta t_{sb,nsb} = 1 \quad (3.87)$$

$$\delta t_{sb,1} c_{f,i,1} + (\delta t_{sb,2} - \delta t_{sb,1}) c_{f,i,2} + \dots + (\delta t_{sb,nsb} - \delta t_{sb,nsb-1}) c_{f,i,nsb} = \bar{c}_{f,i} \quad (3.88)$$

As all decision variables take real and positive values, the lower bounds were defined as zero. The upper bounds were adjusted for some decision variables by taking into account some specific criteria. In the case of internal flow rates, the upper bound was selected based on the Ergun equation (Equation 3.89) and considering a maximal pressure drop of 6 bar in each zone that corresponds to a typical low-pressure SMB system (SONG *et al.*, 2016).

$$\Delta P_M = 150 \frac{\mu v_M l}{d_p^2} \left(\frac{1 - \varepsilon_b}{\varepsilon_b} \right)^2 + \frac{7 \rho v_M^2 l}{4 d_p} \left(\frac{1 - \varepsilon_b}{\varepsilon_b} \right) \quad (3.89)$$

where ΔP_M is the pressure drop in each zone M $\{M = I, II, III, IV\}$, μ is the fluid viscosity, ρ is the fluid density, d_p is the size of the absorbent particle, v_M is the interstitial velocity in each zone M , ε_b is the bed void fraction, and l the column length. In the case of the feed concentration for each subinterval in the ModiCon process, the upper bound was selected based on the maximum available experimental concentration values for the adsorption isotherm or based on the limit of solubility of the solute in the solvent. The upper bound for the average column length of the VariCol process was n , and for the normalized times of the ModiCon process was 1.

In the optimization of the VariCol and the hybrid ModiCon+VariCol processes, the average column lengths of some zones could take values lower than 1, meaning that those zones would not have columns in intervals within the switching period. In those cases, the internal flow rates continue existing for these zones (zone formed by

tubes but without column), but the inlet concentrations of the columns (see Equation 3.39) that are located after these zones is calculated combining the equations of mass balance for the two previous nodes. For instance, if zone 4 had zero column, the inlet concentration of the first column of zone I ($c_{i,I}^{in}$) is calculated by joining Equations 3.41 and 3.44.

The dynamic optimization problem was solved with a sequential approach, which consists of determining the CSS in each optimization stage. The CSS is found integrating the DAEs or the ODEs systems until the relative tolerance for extract and raffinate were lower than $\epsilon_p = 10^{-6}$ (see Equations 3.80 and 3.81). The ode15s and ode15i of Matlab (SHAMPINE and REICHEL, 1997) were used as time integrators, with relative and absolute tolerances set to 1×10^{-6} . The analytical and sparse Jacobian matrix was also supplied to the integrators to reduce the computational effort. The ode15s and the ode15i include sparse algebra to reduce the computational effort in the solution based on a Newton method of the algebraic equation system generated in the backward differences formulae (SHAMPINE and REICHEL, 1997). The algorithm IPOPT linked to Matlab was used to solve the optimization problem. The IPOPT is a primal-dual interior-point algorithm with a filter line search for large-scale nonlinear programming (WÄCHTER and BIEGLER, 2006). The stopping criterion for IPOPT was 1×10^{-8} for termination tolerance. All optimization problems were solved with a computer equipped with an Intel Core i7-8550U 4GHz and 8GB of RAM running Windows 10.

3.6 Control strategy

The operation of the ModiCon process and its variants at optimal economic-based points require advanced control strategies (RODRIGUES, 2015; SCHMIDT-TRAUB *et al.*, 2012). Those optimal points are generally in regions that are very sensitive to process disturbances and uncertainties (KLATT *et al.*, 2002; SONG *et al.*, 2006c; TOUMI *et al.*, 2003). A nonlinear model predictive control is used in this work to evaluate the operation in optimal based economic points of the SMB process and some of its variants in the presence of some disturbances. This control strategy is based on first-principle models to determine the optimal control trajectory subject to system dynamics and constraints of the system. The main advantage of this approach over those based on linearized or identified models is that the same control model can be applied in any operation region (ANDRADE NETO *et al.*, 2016). However, the main concern can be the computational effort.

NMPC solves an optimal control problem at each sampling time in a horizon

fashion defined as a prediction horizon (H_p). The result of each optimal control problem is the sequence of inputs that should be implemented in a control horizon (H_c) to reach the desired performance objective. However, as disturbances and model plant mismatch can occur during that horizon control, the only first action is applied in the plant, and a new optimal sequence of control actions is calculated.

The control strategy adopted in this work is shown in Figure 3.3 and is based on the proposal of ANDRADE NETO *et al.* (2016). This architecture was used to control the purity in the extract and raffinate, manipulating the external flow rates and the switching time. The NMPC optimization problem follows the same structure presented in Section 3.5. The model used in the controller is the same as the model of the virtual plant.

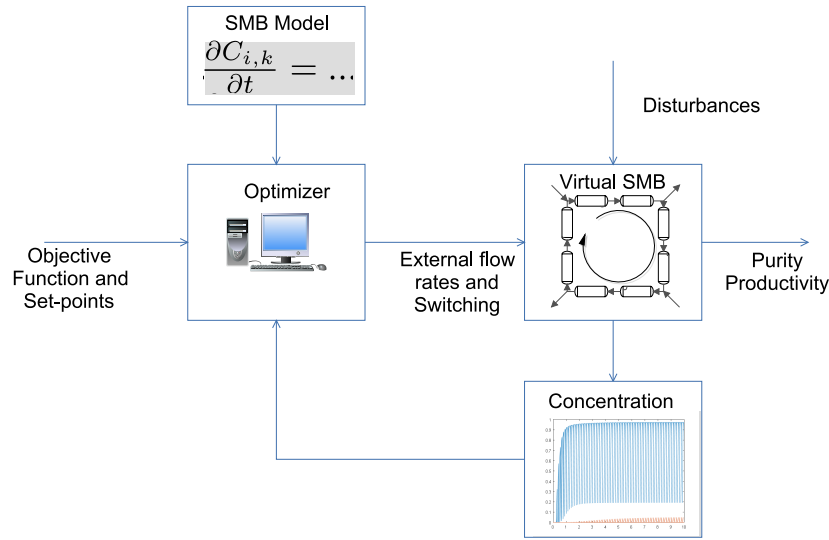


Figure 3.3: Scheme adopted for controlling the SMB unit using an NMPC approach.

The objective function of the controller is divided into two main terms, a setpoint term and an economic term. The setpoint term guarantees the desired purity in the extract and raffinate. The economic term maximizes the throughput and minimizes the solvent consumption. That objective function can be expressed as follows:

$$F = \underbrace{\lambda_1 \left[(p_{e, set} - \langle P_e \rangle)^2 + (p_{r, set} - \langle P_r \rangle)^2 \right]}_{Set-point} - \underbrace{[Q_f - \lambda_2 Q_d]}_{Economic term} \quad (3.90)$$

where λ_1 and λ_2 are weighting factors. The inequality constraints of the optimization control problem are the same as the optimization strategy of the previous section (see Equations 3.82-3.85). The optimal control problem uses external and internal flow rates and the switching period as decision variables. Depending on the disturbance, different decision variables can be selected. The manipulated variables are three

external flow rates (Q_d , Q_e and Q_f) and one internal flow rate (Q_{II}). When the flow rates used as decision variables are different from the manipulated variables, the missing ones are calculated with mass balance in the nodes (see Equations 3.41, 3.42, 3.43 and 3.44). The manipulated variables were defined based on the experimental unit in the laboratory (CUNHA *et al.*, 2019). The upper bound in internal flow rates was also selected based on the Ergun Equation (see Equation 3.89), where the maximal pressure drop in zones was specified according to the case study.

Common disturbances over the SMB unit were considered to evaluate the control performance in separating racemic mixtures. Those disturbances were related to instrument malfunctions, which significantly affect the purity in the extract and raffinate (ANDRADE NETO *et al.*, 2016). When the disturbance is related to a pump malfunction, the flow rate in that pump is fixed, reducing the degree of freedom for independent external and internal flow rates. It is worth mentioning that if an external pump fails, the raffinate port follows the disturbance to satisfy the global mass balance. In the experimental unit of our group (CUNHA *et al.*, 2019), the raffinate port does not have a pump. Hence, it follows all external variations of flow rates.

Depending on the disturbance, some constraints in the flow rates can be changed or added to the optimization problem of the controller. Those constraints are related with the maximal internal flow rate in a zone. When the disturbance is a pump malfunction, the inequality constraint related to that node is changed. For instance, in the case of failure of the feeding pump, the constraint given by Equation 3.84 is changed by the following equation:

$$Q_{III} - Q_{II} = Q_f^* \quad (3.91)$$

where Q_f^* is the flow rate delivered by the defective pump, which will remain fixed in optimization. In the case of the switching valve malfunction, the switching time (t_s) is fixed, and the manipulated variables are only the four external flow rates. The optimization control problem was solved with the interior point algorithm within the *fmincon* function of Matlab. *fmincon* was selected instead of IPOPT because it allowed using a parallel approximation of derivatives that reduces the computational effort. Furthermore, the maximal number of iterations was set to 8, and the relative tolerance for the objective function was set to 10^{-8} .

Chapter 4

Results and discussion

4.1 Simulation and model validation

The SMB process variants and the discretized models for ED and TD were implemented on the SiMoBed, a tool previously developed in our group (LADES) to simulate the SMB process (NETO, 2015). SiMoBed is formed by a graphical interface, and the discretized internal mathematical models based initially on finite differences (FD). SiMoBed was developed on the suite of MATLAB. In this work, the front-end and the back-end of the SiMoBed were improved to include the following SMB variants: ModiCon, VariCol, PowerFeed processes, and combinations among them. Additionally, the discretized mathematical models based on orthogonal collocation on fixed finite elements were included explicitly and implicitly (see Equations 3.71 and 3.72). Models for the TD were provided explicitly and implicitly for all isotherms of Equations 3.32 to 3.36. The analytic and sparse Jacobian was also implemented for all those models except for the implicit approach that includes the isotherm of Equation 3.35. In the case of the ED models, only the explicit form and the isotherms of Equations 3.32, 3.33, 3.34 and 3.35 were considered. The analytical and sparse Jacobian in the ED model was included for the first three isotherms of Equations 3.32 to 3.36. The mathematical models were supplied in such a way that all integration algorithms of Matlab can be used. Especial emphasis was put on the ode15s and the ode15i that uses backward differences formulae to generate a system of equations solved with a Newton-based method. The graphical interface of the new version of the SiMoBed is presented in Figure 4.1.

In the red rectangles of Figure 4.1 is highlighted the panel where the discretization method is chosen and the panel where operation modes of the SMB process can be selected. Different combinations of operation modes to produce hybrid operations

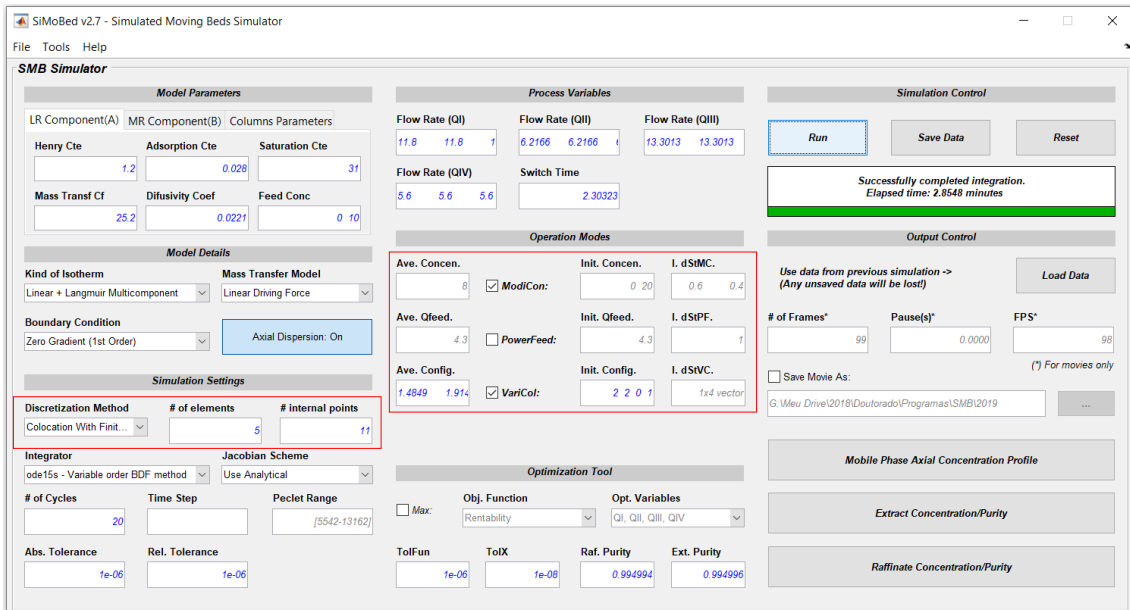


Figure 4.1: Graphical interface of the new version of the SiMoBed tool

can also be selected. In the case of the conventional SMB process, the three operation modes have to be left unchecked. Most of the other functionalities had already been included (NETO, 2015).

Two separations of racemic mixtures were considered as case studies to evaluate and validate the implemented discretization approaches in the SiMoBed. In the first case study, the enantioseparation of praziquantel with an 8-columns SMB process was considered. A linear isotherm describes this mixture, and the equilibrium dispersion model was used to model the process. In the second case study, the enantioseparation of 1,1'-bi-2-naphthol with an 8-columns VariCol process was considered. The bi-Langmuir isotherm type describes the 1,1'-bi-2-naphthol, and the transport dispersion model was used to model this separation.

A new package that simulates individual columns and estimates parameters for the TD and ED models was also developed. That package was called "SimCol" and followed a similar concept of a graphical interface to SiMoBed. The TD and ED models were implemented using orthogonal collocation on fixed finite elements and finite differences. Two case studies were considered to evaluate and validate the SimCol. In the first case, a sensitivity analysis of the parameters of the TD model in terms of total porosity was analyzed. In the second case, the TD model in terms of total porosity was compared with the TD model in terms of bed porosity and the ED model. The details of these studies are presented in Appendix A.

4.1.1 Separation of praziquantel with SMB process

In the separation of PZQ, an 8-columns SMB unit with a configuration of two columns in each section ([2, 2, 2, 2]) was considered. Most model parameters were taken from previous works in the group (ANDRADE NETO *et al.*, 2016; CUNHA *et al.*, 2019). These parameters are presented in Table 4.1.

Table 4.1: Parameters for the separation of a racemic mixture of praziquantel. Index A refers to the less retained enantiomer, and B to one more retained.

Parameter	Value
Number of columns	$n = 8$
Column length and diameter [cm]	$l = 10, d = 1$
Total porosity	$\varepsilon = 0.742$
Dispersion coefficients [$cm^2 \cdot min^{-1}$]	$D_{app,A} = 1.169, D_{app,B} = 1.265$
Feed concentration [$mg \cdot ml^{-1}$]	$c_{f,A} = 1, c_{f,B} = 1$
Switching time [min]	$t_s = 2.36$
Internal flow rate [$cm^3 \cdot min^{-1}$]	$Q_I = 10.71, Q_{II} = 6.51, Q_{III} = 10.49, Q_{IV} = 5.64$

The equilibrium of praziquantel is given by a linear isotherm as follow:

$$q_{e,A} = 4.687c_A \quad (4.1)$$

$$q_{e,B} = 9.417c_B \quad (4.2)$$

where $q_{e,A}$ and $q_{e,B}$ are given in [$mg \cdot ml^{-1}$].

An analysis of convergence was performed for the ED model using finite differences and orthogonal collocation on fixed finite elements. The approximation of the concentration profile with different discretization meshes was evaluated. In the beginning, a coarse mesh was proposed, and then some refinements were made until no important changes were observed in the dynamics of the process. The graphic results of the refinement for the two discretization methods are shown in Figure 4.2. That figure represents the instantaneous internal concentration profiles for the two components over the 8 columns. The profile that appears on the right side corresponds to the less retained component (A), and the profile that appears to the left side to the most retained component (B). That figure was plotted at 50% of the first switching period of 20th cycle. The position of the ports at that instant in the chromatography train, referred as **ext** (extract), **feed** (feed), **raf** (raffinate) and **des** (desorbent), is also shown in Figure 4.2.

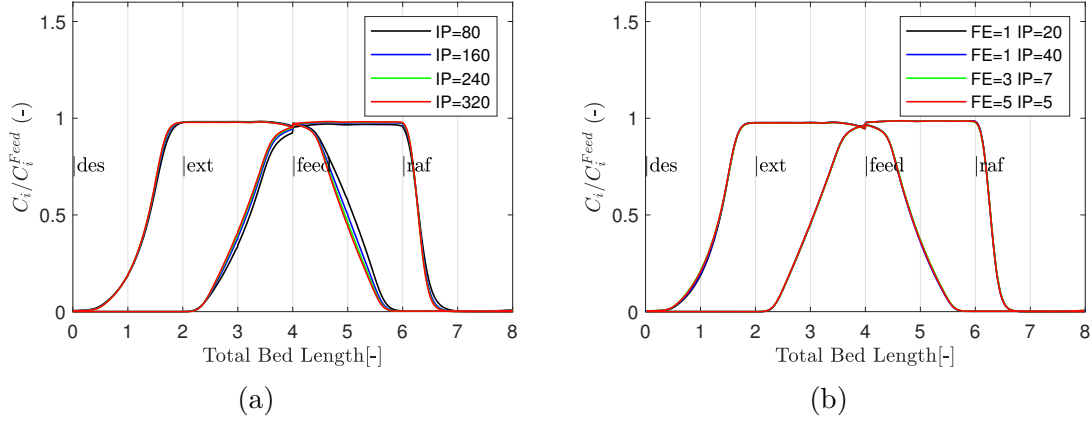


Figure 4.2: Instantaneous internal concentration profiles for components A and B in the separation of praziquantel, considering two spatial discretizations. (a) Finite differences for different internal points (IP) and (b) Polynomial approximation on finite elements for different internal points (IP) and finite elements (FE).

Figure 4.2a shows that for finite differences, a fine discretization mesh is necessary to have a good representation of the concentration profiles. At least 160 internal points (IP) are required to get a good approximation of the system (see Figure 4.2a). Instead, in orthogonal collocation on fixed finite elements (polynomial approximation), a coarse mesh produce good results, as seen in Figure 4.2b. The polynomial approximation allows selecting the appropriate combination between the number of IP and finite elements (FE) to get a good representation of the system. The concentration profiles for the different combinations of IP and FE presented in Figure 4.2b are almost overlaid. In this case, 20 IP and 1 FE or combinations with a total number of IP closer to 20 give a good representation of the system. It is more convenient to use more elements and fewer internal points in the polynomial approximation, especially in regions where the concentration profile presents a flat behavior (KACZMARSKI, 1996). However, increasing the number of elements and reducing internal points will raise the computational effort. Therefore, the appropriate IP and FE can be selected based on a compromise between accuracy and computational effort.

The approximation of internal concentration profile with different meshes of discretization for finite differences and polynomial approximation was compared in the same plot. The results are presented in Figure 4.3. The internal concentration profiles for the two methods are close when a high number of discretization points are used in the FD method (see Figure 4.3). In the case of PA, few discretization points are necessary to get a good approximation. These results are significant because few discretization points in PA produce good results.

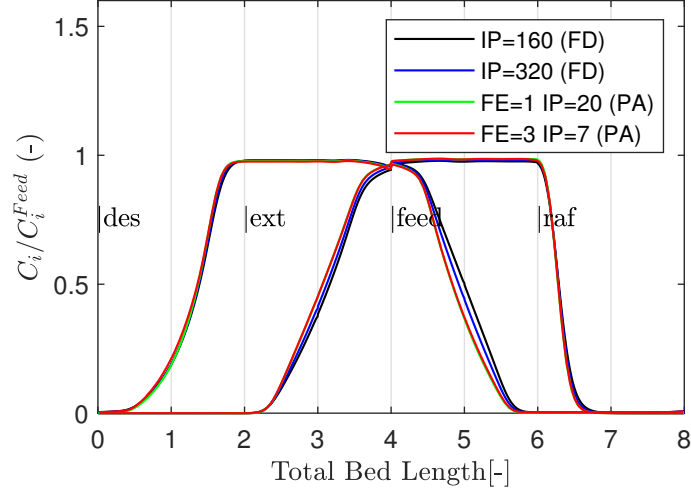


Figure 4.3: Approximation of internal concentration profiles at cyclic steady state, using Finite differences and Polynomial approximation.

4.1.2 Separation of 1,1'-bi-2-naphthol with Varicol process

The two discretization approaches were also evaluated for the TD model based on the bed porosity. In this case, the separation of 1,1'-bi-2-naphthol with 8-columns Varicol process was considered. The initial column configuration of $\mathbf{N}^0 = [1, 2, 2, 2]$ and the average column length of $\bar{\mathbf{N}} = [2.32, 1.63, 2.36, 1.69]$ were used to describe the asynchronous movement of the ports. The model's parameters were obtained from the literature PAIS *et al.* (1997); WONGSO *et al.* (2005); YAO *et al.* (2014) and are presented in Table 4.2.

Table 4.2: Parameters for the enantioseparation of 1,1'-bi-2-naphthol. Index A refers to the less retained enantiomer and index B to the one most retained.

Parameter	Value
Column length and diameter [cm]	$l = 10.5, d = 2.6$
Bed porosity	$\varepsilon_b = 0.4$
Dispersion coefficient [$cm^2 \cdot min^{-1}$]	$D_{ax,A} = 0.0105v, D_{ax,B} = 0.0105v$
Feed concentration [$mg \cdot ml^{-1}$]	$c_{f,A} = 2.9, c_{f,B} = 2.9$
Mass transfer coefficient [min^{-1}]	$k_{eff,A}^* = 6, k_{eff,B}^* = 6$
Switching time [min]	$t_s = 2.81$
Internal flow rate [$cm^3 \cdot min^{-1}$]	$Q_I = 56.83, Q_{II} = 37.80, Q_{III} = 44.82, Q_{IV} = 35.38$

A bi-Langmuir type isotherm describes the adsorption equilibrium for the 1,1'-bi-2-naphthol (PAIS *et al.*, 1997), and it is expressed as follows:

$$q_{e,A} = \frac{80.06 \times 0.0336C_A}{1 + 0.0336C_A + 0.0466C_B} + \frac{0.1 \times 1C_A}{1 + C_A + 3C_B} \quad (4.3)$$

$$q_{e,B} = \frac{80.06 \times 0.0466C_B}{1 + 0.0336C_A + 0.0466C_B} + \frac{0.1 \times 3C_B}{1 + C_A + 3C_B} \quad (4.4)$$

where $q_{e,A}$ and $q_{e,B}$ are given in $[mg \cdot ml^{-1}]$.

The graphical results of the two discretization methods are presented in Figure 4.4. The number of discretization points used in the two methods is the same as the example of praziquantel. Figures 4.4a and 4.4b were plotted at 50% of the first period of the 20th cycle. The positions of ports at that point are also presented in Figure 4.4. Letters A and B refer to the less and the most retained component.

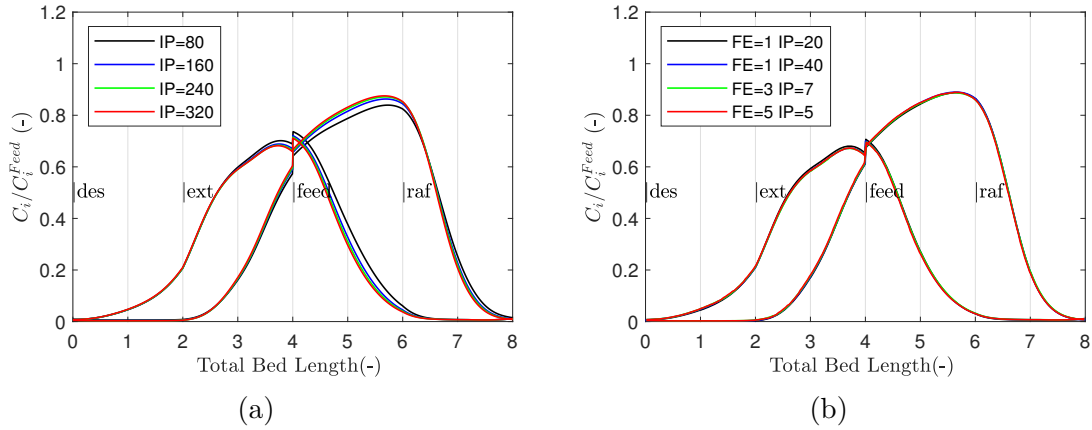


Figure 4.4: Concentration profiles of the components A and B in the separation of 1,1'-bi-2-naphthol, considering two spatial discretization methods. (a) Finite differences for different internal points and (b) Polynomial approximation on finite elements for different internal points and finite elements.

As in the previous example, the polynomial approximation on finite elements had better behavior than finite differences in the approximation of concentration profiles of species A and B (see Figure 4.4). The number of discretization points required to get an accurate approximation of the concentration profiles in the polynomial approximation is much lower than the finite differences. For example, 3 FE and 7 IP describe well the concentrations profiles, whereas at least 320 points are required with finite differences.

The approximation of internal concentration profiles for the two discretization methods were also compared in the same plot for specific grid meshes. The graphical results are presented in Figure 4.5.

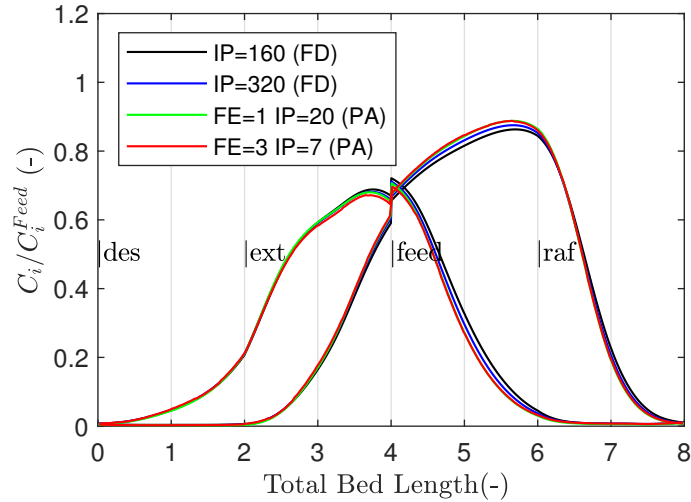


Figure 4.5: Approximation of internal concentration profiles at cyclic steady state, using Finite differences and Polynomial approximation.

Figure 4.5 shows clearly the advantages of polynomial approximation concerning finite differences. A coarse mesh in polynomial approximation gives good results in the prediction of the concentration profiles. Those results are essential because they show that the polynomial approximation with a coarse mesh can predict with accuracy the concentration profiles of systems with more complicated isotherms, as is the case of the bi-Langmuir isotherm.

The computational effort to simulate the enantioseparation of 1,1'-bi-2-naphthol to the cyclic steady state (15 cycles) was determined for the two discretization methods. In the two cases, the discretized models were solved explicitly with the integrator *ode15s*. The analytical and sparse Jacobian was also considered. For the simulations, a PC equipped with an Intel Core i7-8550U 4GHz of processor and 8GB of RAM was used. The results are presented in Table 4.3.

Table 4.3: Computational effort of the two discretization methods using the sparse matrix.

Discretization method	Mesh points	Number of ODEs	CPU time (s)
Finite Differences	320 IP	10240	756.57
Polynomial approximation	3 FE and 7 IP	672	67.35

In Table 4.3, it is observed that the computational effort required to simulate the enantioseparation to the cyclic steady state with the polynomial approximation is lower than with finite differences. This result is expected because the number of equations solved with finite differences was 10240 (4 PDEs/Column, 8 columns, and 320 IP), and the number of equations with polynomial approximation was 672 ((4 PDEs/Column, 8 columns, 3 FE and 7 IP). In general, polynomial approximation

performed better because few discretization points and a low computational effort are required to get accurate results.

4.1.3 Explicit and implicit approaches

The discretized ED and the TD models can be solved explicitly or implicitly as presented in Equations 3.71 and 3.72. The DAEs in the models discretized with FD or PA can be converted in explicit ODEs by solving the algebraic equations inside the differential equation function implemented in Matlab. In the FD, only boundary equations need to be solved, and in PA approximation, boundary and continuity equations between elements need to be solved. In the explicit approach, the ODEs are integrated by applying the algorithm *ode15s* of Matlab, which uses the Jacobian matrix (JM) in the integration process. In the implicit approach, the differential and algebraic equations (DAEs) are solved simultaneously by applying the algorithm *ode15i* that also uses the Jacobian matrix. Those solvers reduce the computational effort to integrate the discretized systems if sparse algebra is used and information about the Jacobian matrix is provided. In this case, the analytical Jacobian in the form of a sparse matrix was considered. The performance in integrating the ODEs and DAEs was evaluated, taking more emphasis on PA.

4.1.3.1 Explicit approach

The dimension of the system of ODEs that need to be solved in the explicit approach depends on the number of components, chromatographic columns, and the number of internal discretization points. The Jacobian matrix for that system is sparse (most elements are zero) since few equations are coupled. The sparsity pattern of the Jacobian matrix depends on the discretization approach. A more sparse pattern is obtained with FD than in PA. However, in the FD, the dimension of the Jacobian Matrix is larger since more discretization points are necessary for each column. The number of Jacobian matrix elements with non-zero values given by the coupling of the ODEs of a column with the other columns is also lower in FD than in PA, as shown later. These positions can be determined based on the inlet concentration of a column ($c_{i,k}^{in}$) that depends on the previous column's outlet concentration ($c_{i,k-1}^{out}$) (see Equations 3.41, 3.42, 3.43 and 3.44). $c_{i,k-1}^{out}$ depends on the internal discretization points, as seen in Equations 3.55 and 3.56 or Equations 3.67 and 3.68. The sparsity pattern of the Jacobian matrix was determined for FD and PA.

The sparse pattern of the Jacobian matrix for the TD model in terms of bed

porosity discretized with FD is calculated for the separation of 1,1'-bi-2-naphthol with 8 columns VariCol process at the beginning of the 10th cycle (in that position, column 1 corresponds to the first column of the zone I). For that purpose, 21 IPs for each column were considered. The graphics results are presented in Figure 4.6. The sparsity pattern for column 3 concerning the discretization points of that column is highlighted in a square, as it is seen in Figure 4.6. It is worth remembering that four groups of ODEs describe each column, where the first two correspond to the fluid and stationary balances of component A and the other two for component B. The points related to the coupling of column 3 with the previous one are highlighted in circles.

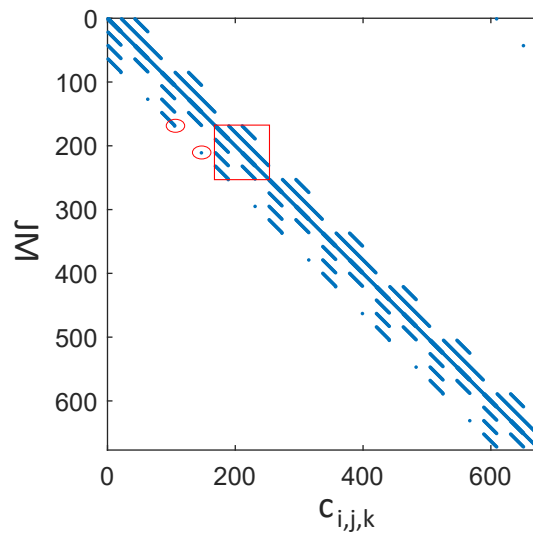


Figure 4.6: Sparse pattern of the Jacobian matrix for finite differences considering 21 IP. The points in the square correspond to the sparsity pattern of column 3. The points in the circle correspond to the coupling of column 3 with the previous column via boundary conditions.

Figure 4.6 shows that the TD model discretized with FD is highly sparse. The non-zero elements were 2,676 out of 456,976. That is, only 0.58% elements are non-zero. That is advantageous because, in the Gaussian elimination operations of the Jacobian matrix, only 0.58% of the Jacobian matrix values have to be considered. The coupling of the ODEs of a column with the previous one is related to only two states (see points in the red circle on Figure 4.6). That was expected since $c_{i,k}^{in}$ depends on the $c_{i,k-1}^{out}$, and this in turn to the last internal discretization point as seen in Equation Equation 3.56.

In the PA, the boundary and node points are solved individually for each column, as was expressed in the last paragraph of Section 3.4.2. The algebraic equation system was solved, starting from the first column of zone I and ending in the last

column of zone IV. In that case, the $c_{i,IV}^{out}$ of Equation 3.41, which is necessary to calculate $c_{i,I}^{in}$, was defined with the assumption of Equation 3.56. As the algebraic equation system for each column is tri-diagonal, the method of Thomas that is efficient for that system was applied (SECCHI and BISCAIA JR, 2020).

The sparse pattern of the Jacobian matrix for PA is also calculated for the separation of 1,1'-bi-2-naphthol with 8-columns VariCol process at the beginning of the 10th cycle, where column 1 corresponds to the first column of zone I. In that calculation, two discretization meshes are examined. In the first case, 1 FE and 21 IP are considered, while in the second 3 FE and 7 IP are used. The graphical results are presented in Figures 4.7a and 4.7b.

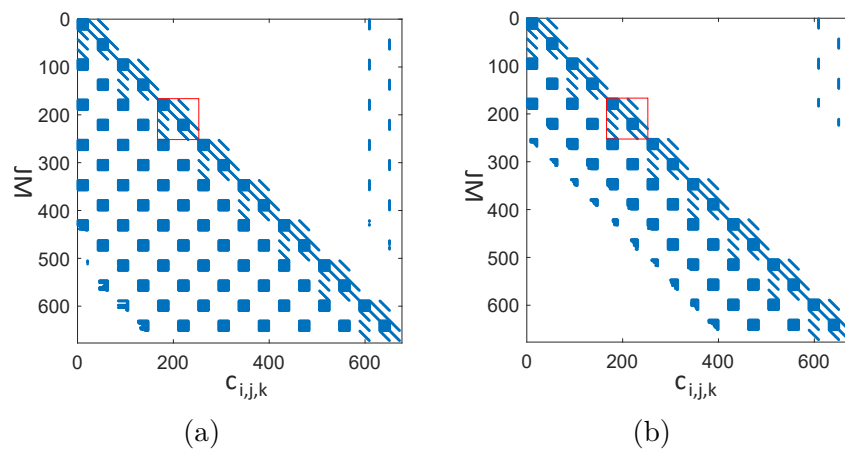


Figure 4.7: Sparse pattern of the Jacobian matrix for polynomial approximation: (a) 1 FE and 21 IP, (b) 3 FE and 7 IP. The points in the square correspond to the sparsity pattern of column 3.

Figure 4.7a and 4.7b show that the Jacobian matrix for the PA has a higher percentage of non-zero elements than FD (see Figure 4.6), as expected. Those percentage of non-zero elements increased in the sparsity pattern of each column with its discretization points and with the discretization point of other columns (coupling with other columns). In the case of the sparsity pattern of a column with its discretization points, as seen in the red square of Figures 4.7a and 4.7b for column 3, the percentage of increment of non-zero elements is related with a higher number of points used to build each polynomial approximation as described by the theory of PA. The non-zero elements of column 3 related to the discretization points with other columns that appear in Figures 4.7a or 4.7b are principally the ones corresponding to columns 1 and 2 (points that are in the left and the same horizontal strip of the red square). The elements of column 3 related to the discretization points of columns 4, 5, 6, 7, and 8 are almost null. That is because the coupling transferred from one column to the other is practically eliminated when it is passed from column 1 (first

of zone I) to 8 (last of zone IV) with the approximation used to estimate the inlet concentration of the first column of zone I. As equivalent characteristics of column 3 apply for other columns, most non-zero elements of the Jacobian matrix appear in the lower triangle region. However, the coupling of each column with columns that are located further away becomes weaker, as seen especially in Figure 4.7b.

The analytical Jacobian used in the integration algorithm in PA does not include all non-zero elements. The ones included were those related to the discretization points of each column as independently. The coupling between columns was neglected. The sparse pattern of simplified analytical Jacobian is presented in Figure 4.8a for 1 FE and 21 IP and in Figure 4.8b for 3 FE and 7 IP.

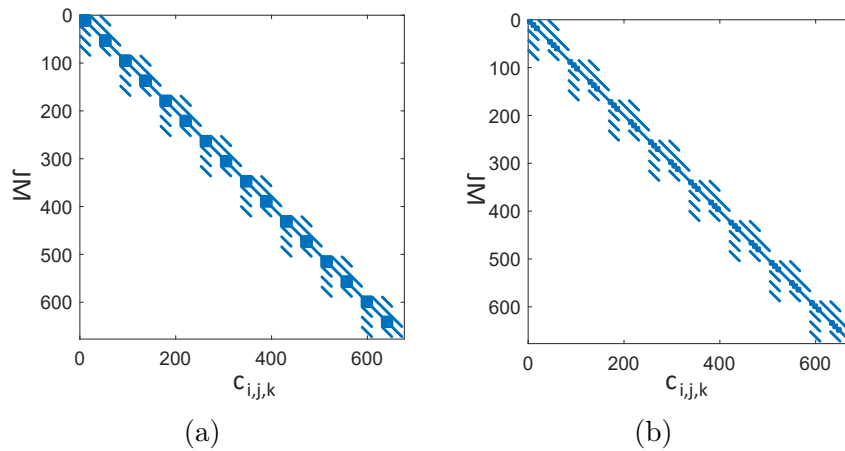


Figure 4.8: Sparse pattern of the Jacobian matrix for polynomial approximation without considering the coupling between columns and between elements. (a) 1 FE and 21 IP, (b) 3 FE and 7 IP.

Figure 4.8 contains the pattern of the main diagonal of Figure 4.7. In the two discretization meshes of Figures 4.8a and 4.8b, the same number of ODEs are solved. The coupling between finite elements presented in Figure 4.7b was also neglected. Therefore, three small squares (related to the 3 FE) instead of one are seen in the main diagonal of Figure 4.8b. The assumption of using a simplified analytical Jacobian can be considered acceptable since the integrator algorithm uses a Newton-based method to solve systems of algebraic equations internally, and an exact Jacobian matrix is not necessarily required. Additionally, the coupling between columns is not the dominant factor in the Jacobian matrix. The coupling between columns located further away from a specific column becomes weaker, as shown in Figures 4.7a and 4.7b. Therefore the proposal used here is valid.

4.1.3.2 Implicit approach

The system of DAEs in PA was also implemented implicitly to evaluate the performance with the explicit approach. In an implicit approach where the DAEs are solved simultaneously, a sparser pattern of the Jacobian matrix than the explicit approach can be obtained. That is because the boundary and node between sub-domains conditions are included as independent states for the integration function. The sparse pattern of Jacobian matrix for the separation of 1,1'-bi-2-naphthol with 8-columns VariCol process is showed in Figure 4.9. The Jacobian was calculated at the beginning of the 10th cycle.

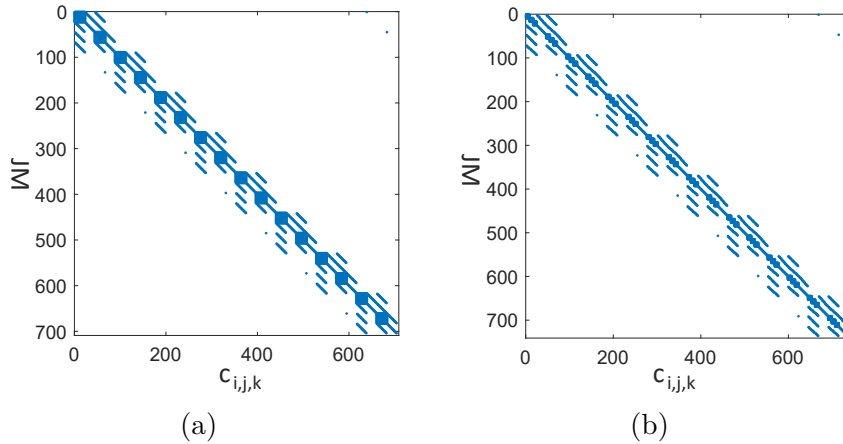


Figure 4.9: Sparse pattern of the Jacobian matrix for polynomial approximation considering an implicit implementation of the DAEs (a) 1 FE and 21 IP, (b) 3 FE and 7 IP.

Figure 4.9 shows that the Jacobian matrix for the implicit approach has fewer non-zero elements than the explicit approximation for PA. However, equations that need to be solved increase since algebraic equations are solved simultaneously with the differential equations. The analytical Jacobian matrix used in the integration algorithm for the implicit approach considers all non-zero elements.

The most convenient approach in terms of computational performance was also evaluated. The explicit and implicit approaches were used to simulate the separation of 1,1'-bi-2-naphthol with the 8-columns Varicol process, and the computation effort was determined. In the implicit and explicit approaches, sparse analytical Jacobian matrices were used in integrators *ode15i* and *ode15s*. In the explicit approach, the simplified Jacobian matrix described in the previous section was used. The computational effort in the two cases to simulate 15 cycles is presented in Table 4.4.

The computational effort in the explicit approach was lower than the implicit approach, as presented in Table 4.4. The simplified analytical Jacobian in the explicit

Table 4.4: Computational effort to solve the DAEs explicitly and implicitly using as integrator *ode15s* and *ode15i*.

Structure DAEs	Mesh points	CPU time (s)	Pur of A in Raf (%)
Explicit approach	3 FE and 7 IP	68.19	97.40
Implicit approach	3 FE and 7 IP	104.90	97.32

approach was effective in reducing the computational effort. In the two approaches, the purity of the products in the last period of the 15th cycle is close, as presented in Table 4.4 for purity of A in the raffinate. As the explicit approach was more efficient than the implicit one, the former will be considered in the following sections.

4.2 Optimization of VariCol process

This section is based on the work of CALDERÓN SUPELANO *et al.* (2020).

A novel approach for the optimization of the VariCol process based on a single NLP formulation was proposed. The new formulation is built based on the average column lengths of three zones, which provide the necessary and sufficient information to describe the VariCol process with minimal movement of the ports. With the average column length, it is possible to deduce the different column configuration sequences in a switching period, and any of them can be used in the optimization problem since they have the same performance in the cyclic steady state (YAO *et al.*, 2014, 2017).

4.2.1 Initial column configurations

The procedure presented in Section 3.2.1.1 to determine the initial column configuration and the column configuration sequence (CCS) is evaluated with three case studies of ACL. These case studies correspond to optimal results for separating 1,1'-bi-2-naphthol with an 8-columns VariCol process that will be presented later. These cases of ACL are $\bar{\mathbf{N}} = [1.76, 2.09, 2.60, 1.55]$, $\bar{\mathbf{N}} = [1.83, 1.98, 2.67, 1.52]$, and $\bar{\mathbf{N}} = [1.85, 2.15, 2.50, 1.50]$. For the first case study, the different CCSs are determined, and their performance at the cyclic steady state is compared.

4.2.1.1 Case 1

In the average column length of $\bar{\mathbf{N}} = [1.76, 2.09, 2.60, 1.55]$, the number of possible combinations, whose sum is equal to the number of columns of the system ($n = 8$), is 6. This number is determined with Equation 3.21, knowing the number of zones with a rational average column number ($nz = 4$) and the number of zones with either the nearest upper or the nearest lower integer values that have to be chosen from the set of nz ($nzc = nz - 2 = 2$). In this case, the relation $nzc = nz - 2$ was used because the difference between n and the sum of all nearest lower integer values (SNLIV) of the average column length (ACL) was 2. Each option of the combinations is formed with two lower integer values and two nearest upper integer values. Those combinations are presented in Table 4.5.

Table 4.5: Combinations of lower and upper integer values of $\bar{\mathbf{N}} = [1.76, 2.09, 2.60, 1.55]$, whose sum is equal to 8

\mathbf{N}^0	\bar{N}_I (1.76)	\bar{N}_{II} (2.09)	\bar{N}_{III} (2.60)	\bar{N}_{IV} (1.55)
\mathbf{N}_1^0	1	3	3	1
\mathbf{N}_2^0	2	2	3	1
\mathbf{N}_3^0	2	3	2	1
\mathbf{N}_4^0	2	2	2	2
\mathbf{N}_5^0	1	3	2	2
\mathbf{N}_6^0	1	2	3	2

The relative switching times for each option of the initial vector in Table 4.5, calculated with Equations 3.17 to 3.19, are presented in Table 4.6. The sum of the relative switching times, according to the constraints of Equations 3.6 to 3.11, is also presented in Table 4.6. Normalized switching time vectors ($\delta\mathbf{t}$) for each initial column configuration option, calculated by displacing $\delta\mathbf{t}_0$ (Equation 3.12), the difference between 1 and the maximum value of $\delta\mathbf{t}_0$, are reported in Table 4.7.

From those results, there are two column configurations that not only do not satisfy the constraints of Equations 3.6 to 3.11 (see the values highlighted in bold in

Table 4.6: Relative switching times for the different possible initial column configurations at the average configuration of $\bar{\mathbf{N}} = [1.76, 2.09, 2.60, 1.55]$

δx	δy	δz	$\delta x + \delta y$	$\delta y + \delta z$	$\delta x + \delta y + \delta z$
-0.76	0.91	0.40	0.15	1.31	0.55
0.24	-0.09	0.40	0.15	0.31	0.55
0.24	0.91	-0.60	1.15	0.31	0.55
0.24	-0.09	-0.60	0.15	-0.69	-0.45
-0.76	0.91	-0.60	0.15	0.31	-0.45
-0.76	-0.09	0.40	-0.85	0.31	-0.45

Table 4.7: Vector of normalized switching times for the initial configuration options

δt_d	δt_e	δt_f	δt_r
0.45	-0.31	0.60	1.00
0.45	0.69	0.60	1.00
-0.15	0.09	1.00	0.40
0.76	1.00	0.91	0.31
0.85	0.09	1.00	0.40
1.00	0.24	0.15	0.55

Table 4.6) but also do not give normalized switching times in the range $(0, 1]$ (see the values highlighted in bold in Table 4.7). Those two-column configurations are also displayed in bold in Table 4.5. Thus, 4 of the 6 options of column configuration can be used as an initial column configuration.

From the results in Table 4.7, it is also possible to see that normalized switching times and, consequently, the sequence of port movements in a switching period is different for each possible initial column configuration. Therefore, the shifting schemes produced from possible initial column configurations and vectors of normalized switching times will have a different sequence of port movements.

4.2.1.2 Case 2

In the average column length of $\bar{\mathbf{N}} = [1.83, 1.98, 2.67, 1.52]$, there are 4 options for possible initial column configurations with a sum of 8 columns since all average values are rational and the difference between n and SNLIV is 3 ($nz = 4$ and $nzc = 3$). In this case, each option of column configuration has 3 nearest upper integer values. The possibilities of column configurations are presented in Table 4.8.

Table 4.8: Options for initial column configuration from the average column length of $\bar{\mathbf{N}} = [1.83, 1.98, 2.67, 1.52]$

\mathbf{N}_0	$\bar{N}_I(1.83)$	$\bar{N}_{II}(1.98)$	$\bar{N}_{III}(2.67)$	$\bar{N}_{IV}(1.52)$
\mathbf{N}_1^0	1	2	3	2
\mathbf{N}_2^0	2	1	3	2
\mathbf{N}_3^0	2	2	2	2
\mathbf{N}_4^0	2	2	3	1

The vectors of normalized switching times were determined for each column configuration option. That allows evaluating which column configuration option can be used as the initial configuration. Those values are presented in Table 4.9.

In this case, all the options for possible initial column configurations generate

Table 4.9: Vector of normalized switching times for the initial configuration options

δt_d	δt_e	δt_f	δt_r
1.00	0.17	0.19	0.52
0.83	1.00	0.02	0.35
0.81	0.98	1.00	0.33
0.48	0.65	0.67	1.00

normalized switching times in the $(0, 1]$ range. For this reason, all of those options can be used as initial column configurations of CCSs.

4.2.1.3 Case 3

In the average column length of $\bar{\mathbf{N}} = [1.85, 2.15, 2.50, 1.50]$, similarly to Case 1, there are 6 options for initial column configuration since the difference between n and SNLIV is 2 ($nz = 4$ and $nzc = 2$). The options were calculated by combining 2 near lower integer values with 2 near upper integer values. The options of column configurations are presented in Table 4.10, and the vectors of normalized switching times are presented in Table 4.11.

Table 4.10: Options for initial column configuration from the average column configuration of $\bar{\mathbf{N}} = [1.85, 2.15, 2.50, 1.50]$

\mathbf{N}^0	$\bar{N}_I(\mathbf{1.85})$	$\bar{N}_{II}(\mathbf{2.15})$	$\bar{N}_{III}(\mathbf{2.50})$	$\bar{N}_{IV}(\mathbf{1.50})$
\mathbf{N}_1^0	1	3	3	1
\mathbf{N}_2^0	2	2	3	1
\mathbf{N}_3^0	2	3	2	1
\mathbf{N}_4^0	2	2	2	2
\mathbf{N}_5^0	1	3	2	2
\mathbf{N}_6^0	1	2	3	2

Table 4.11: Vector of normalized switching times for the initial configuration options

δt_d	δt_e	δt_f	δt_r
0.50	-0.35	0.50	1.00
0.50	0.65	0.50	1.00
0.00	0.15	1.00	0.50
0.85	1.00	0.85	0.35
1.00	0.15	1.00	0.50
1.00	0.15	0.00	0.50

Tables 4.10 and 4.11 show that only three column configurations produce normalized switching times in the range $(0,1]$. In this case, only three options can be used as initial column configurations. The column configuration option with ports

moving at $\delta t_p = 0$ and $\delta t_p = 1$ does not have physical meaning because this initial column configuration of the shifting scheme would disappear in $t_p = 0$.

4.2.1.4 Shifting schemes

From the results of Case 1, it was found that for the average column length of $\bar{\mathbf{N}} = [1.76, 2.09, 2.60, 1.55]$, 4 possible initial column configurations can be used as the starting point of CCS or shifting schemes. For each of the possible initial column configurations and the corresponding normalized shifting time vector, the CCS was calculated. The sequence of column configurations in each case was calculated by adding or subtracting columns in the zones affected by each movement of the ports. For example, in the shifting scheme that starts in the initial column configuration of $\mathbf{N}^0 = [2, 2, 3, 1]$ (see the second option in Table 4.5) and has the normalized switching time vector of $\delta t = [0.45, 0.69, 0.60, 1.00]$ (see Table 4.7), the next column configuration, which is affected by the movement of the dissolvent port, is calculated by adding 1 column to the zone 4 and subtracting a column to zone 1 to get the configuration $[1, 2, 3, 2]$. The other two sequences are calculated based on the movement of the feed and extract ports. The shifting schemes for the four possible initial column configurations in Table 4.5 are presented in Figure 4.10. There, it can be observed that all shifting schemes have the same vectors of column configurations, albeit in different positions. Those vectors are also the same possible initial column configurations in Table 4.5. Additionally, when the shifting schemes are compared to each other, it is found that they follow the same pattern of column configuration sequence but with a shifted starting and ending column configuration. For example, in scheme *b*, the starting point is $\mathbf{N}^0 = [1, 3, 2, 2]$, the second column configuration in scheme *a*, and the ending point is $[1, 2, 3, 2]$, which is the initial column configuration in scheme *a*. Schemes *c* and *d* started from a column configuration shifted from schemes *b* and *c*, respectively.

The purity and recovery in the extract and raffinate for all shifting schemes of Figure 4.10 are presented in Figure 4.11 and Figure 4.12. As can be seen from those figures, both purity and recovery curves in the extract and raffinate ports are the same for the four different shifting schemes after the second cycle and, therefore, at the cyclic steady state. A slight difference between the shifting scheme curves is found only in the first and second cycles due to the shifted initial configuration. According to these results and the ones reported by YAO *et al.* (2014, 2017), in the operation of the VariCol process with the minimal shifting of the ports, any of the shifting schemes can be used to determine the maximal performance of the process since all possible shifting schemes have the same performance in the cyclic steady

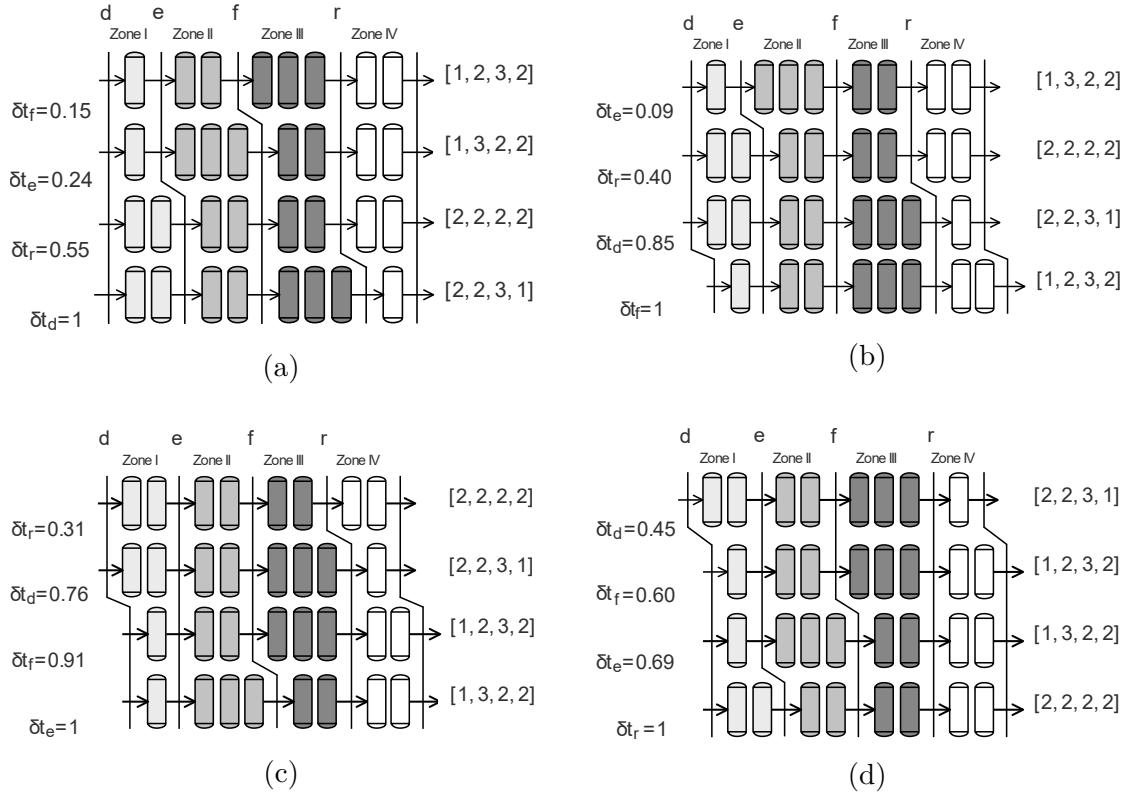


Figure 4.10: Possible shifting schemes with different initial column configurations for the average configuration of $\bar{\mathbf{N}} = [1.76, 2.09, 2.60, 1.55]$

state.

The above results showed that the possible initial column configurations and normalized switching times vectors for feasible shifting schemes could be determined from an average column configuration. The sequence of column configuration of shifting schemes can be determined from those initial column configurations and normalized switching time vectors. Each shifting scheme has the same pattern of column configurations but shifted one column configuration concerning the others. Any of those shifting schemes can simulate the VariCol process since all of them produce the same results in the cyclic steady state. Those characteristics are essential for the optimization problem of a VariCol process based on the average column configuration of three zones because it is unnecessary to define an initial column configuration at the beginning. In each stage of the optimization problem, any possible initial column configuration can be selected. With this approach, it is possible to solve the optimization problem by exploring the entire domain of the VariCol process and not a subdomain, as is the case when using relative switching times as decision variables. That optimization approach was the one presented in Method 2 of Figure 3.2.

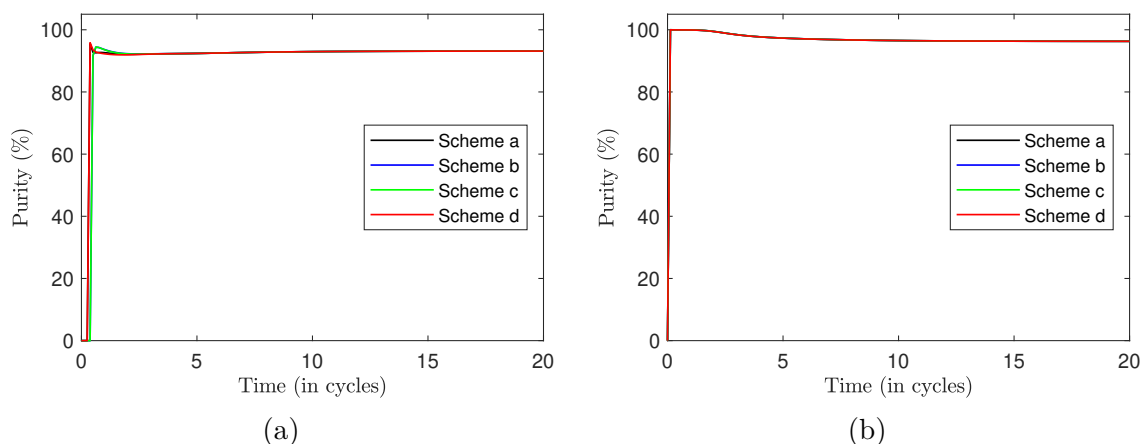


Figure 4.11: Purity for the different shifting schemes in the (a) Extract and (b) Raffinate.

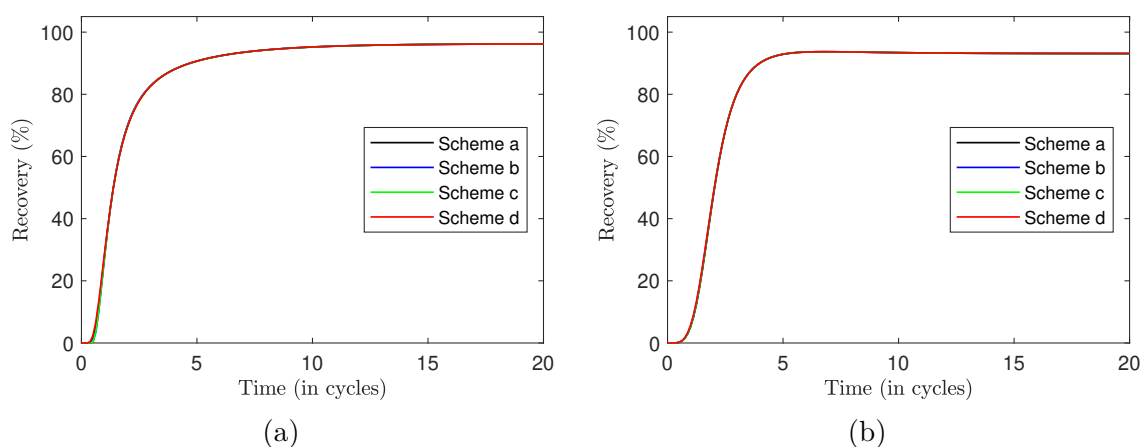


Figure 4.12: Recovery for the different shifting schemes in the (a) Extract and (b) Raffinate.

4.2.2 Optimization examples

Two case studies on enantioseparations were considered to evaluate the performance of the proposed optimization methodology and to study the VariCol process more deeply. In the first case, a separation of 1,1'-bi-2-naphthol with an 8-column VariCol process was considered. In the second case, the separation of Aminoglutethimide (3-(4-aminophenyl)-3-ethyl-2,6-piperidinedio) with a 5-column VariCol process was analyzed. The operating parameters of the two enantioseparations were obtained from the literature and are presented in Table 4.12. The parameters for the enantioseparation of 1,1'-bi-2-naphthol are equivalent to the ones presented in Table 4.2. Those parameters were obtained from the work of YAO *et al.* (2017). In the second case, the parameters were obtained from LIN *et al.* (2016).

The adsorption equilibrium for the separation of 1,1'-bi-2-naphthol is described by the isotherms presented in Equations 4.3 and 4.4. That system has a low selectivity in

Table 4.12: Parameters for the enantioseparation of 1,1'-bi-2-naphthol and aminoglutethimide. Index A refers to the less retained and B to the more retained enantiomers.

Parameter	Case 1	Case 2
Number of columns	$n = 8$	$n = 5$
Column length [cm]	$l = 10.5$	$l = 15$
Column diameter [cm]	$d = 2.6$	$d = 1$
Bed porosity	$\varepsilon_b = 0.4$	$\varepsilon_b = 0.56$
Dispersion coefficient [$cm^2 \cdot min^{-1}$]	$D_{ax,A} = D_{ax,B} = 0.0105 \cdot v$	$D_{ax,A} = D_{ax,B} = 0.0720$
Feed concentration [$mg \cdot ml^{-1}$]	$c_{f,A} = c_{f,B} = 2.9$	$c_{f,A} = c_{f,B} = 2$
Mass transfer coefficient [min^{-1}]	$k_{eff,A}^* = k_{eff,B}^* = 6$	$k_{eff,A}^* = 36, k_{eff,B}^* = 46.8$
Weighting factor	$\lambda_p = 1 \times 10^6$	$\lambda_p = 1 \times 10^6$

the feeding conditions ($\alpha_{A,B} = \frac{q_{e,B}/c_{f,B}}{q_{e,A}/c_{f,A}} = 1, 392$), which is common in enantiomeric separations. For the case of aminoglutethimide racemate, the equilibrium is described by the linear-Langmuir isotherms (LIN *et al.*, 2016). It is described with the following equations:

$$q_{e,A} = 1.614c_A + \frac{16.8 \times 0.045c_A}{1 + 0.045c_A + 0.038c_B} \quad (4.5)$$

$$q_{e,B} = 2.312c_B + \frac{16.8 \times 0.038c_B}{1 + 0.045c_A + 0.038c_B} \quad (4.6)$$

where $q_{e,A}$ and $q_{e,B}$ are given in [$mg \cdot ml^{-1}$].

This system also has a low selectivity in the feed conditions ($\alpha = 1.264$). For the optimization problem of aminoglutethimide with a 5-columns VariCol unit, the possibility of having zones with zero columns in intervals of the switching period was considered. In those cases, the internal flow rates of those zones continued to be considered even though there were no columns. The inlet concentration of columns, $c_{i,k}^{in}$, (see Equation 3.39) that are located after zones without columns is calculated by joining the mass balance equations of the two previous nodes. For example, if zone 1 had zero columns, the inlet concentration would be calculated by joining Equations 3.41 and 3.42.

4.2.2.1 Enantioseparation of 1,1'-bi-2-naphthol

In this case study, several optimization problems were solved both to compare the performance of the 8-columns VariCol process with the conventional 8-columns SMB process and to evaluate the proposed optimization methodology for the VariCol process. The performance of VariCol with SMB was compared, maximizing the

Table 4.13: Optimal operation parameters that maximize the feed flow rate for the enantioseparation of 1,1'-bi-2-naphthol

Optimal operation parameters	SMB 1 (This work)	SMB 2 (This work)	VariCol 1 (Yao et al.)	VariCol 2 (This work)	VariCol 3 (This work)
$Q_I [cm^3min^{-1}]$	58.83	56.83	56.83	56.83	56.83
$Q_d [cm^3min^{-1}]$	21.45	21.45	21.45	21.45	21.45
$Q_e [cm^3min^{-1}]$	20.21	20.57	18.93	19.78	19.98
$Q_f [cm^3min^{-1}]$	7.32	6.77	6.82	7.84	7.24
				(+7.10%)*	(+6.94%)**
$Q_r [cm^3min^{-1}]$	8.56	7.65	9.34	9.50	8.71
$t_s [min]$	2.86	2.89	2.81	2.81	2.85
$\bar{N}_{c,I}$	2	2	2.32	1.76	1.86
$\bar{N}_{c,II}$	2	2	1.63	2.09	1.90
$\bar{N}_{c,III}$	2	2	2.36	2.60	2.65
$\bar{N}_{c,IV}$	2	2	1.69	1.55	1.59
$\langle P_e \rangle [\%]$	93.00	92.21	93.00; 92.21 ⁺	93.00	92.21
$\langle P_r \rangle [\%]$	96.20	97.68	96.20; 97.68 ⁺	96.20	97.68

*Percent values are related to SMB 1. **Percent values are related to SMB 2.

⁺Simulation of Yao et al.'s results with our implemented model.

throughput of the enantioseparation of 1,1'-bi-2-naphthol for the same purities reported by YAO *et al.* (2017). The solvent consumption was also set to the same values used by them. The flow rates of zone I and zone IV were kept constant during the optimization to maintain the solvent consumption constant. The decision variables for the optimization problems of the VariCol process were the average configuration of three zones, the internal flow rates of zones II and III, and the switching period. For the conventional SMB process, the decision variables were the internal flow rates of zones II and III and the switching period. The configuration [2, 2, 2, 2] was set in the conventional SMB as the column arrangement. The results of the optimization problems for the SMB and VariCol processes were listed in Table 4.13 as SMB 1 and VariCol 2, respectively. The results reported by YAO *et al.* (2017), which were obtained using the relative switching times as decision variables, were also included in Table 4.13 as VariCol 1. The purities reported by YAO *et al.* (2017) were slightly different from those obtained by simulating their results with our implemented model, as can be seen in the values of purities that are in bold for VariCol 1 in Table 4.13. New optimization problems were also solved at the updated purities to compare these results with those of YAO *et al.* (2017). The results for these new optimization problems were also presented in Table 4.13 as SMB 2 and VariCol 3.

As Table 4.13 indicates, the optimal point found for the VariCol process with the proposed methodology (VariCol 2) represents a better performance scenario than the conventional SMB process (SMB 1). It was possible to increment the throughput in +7.10% with the same solvent consumption and purity requirement specifications. This result was expected since the asynchronous movement of the ports leads to an improvement in the performance (GONG *et al.*, 2014b; LIN *et al.*, 2016; LUDEMANN-HOMBOURGER *et al.*, 2000; TOUMI *et al.*, 2003, 2002; WONGSO *et al.*, 2005; YANG *et al.*, 2019; YAO *et al.*, 2014, 2017). When comparing the results of the optimized VariCol for the updated purities (92.21% and 97.68% in the extract and raffinate) (VariCol 3) with SMB 2 and with the results reported by YAO *et al.* (2014, 2017) (VariCol 1), VariCol 3 improved the throughput by 6.94% and 6.16%, respectively. The optimal throughput given by VariCol 1 was slightly superior (only 0.74%) to SMB 2. An additional and important aspect of the optimal points found for the VariCol process (VariCol 2 and VariCol 3) with the proposed optimization methodology is that the average configurations of zones II and III were larger than the average configurations of zones I and IV. Those results agreed with the theory because larger zones II and III allow for an increase of the load on the system and, therefore, for an increase in the performance (LUDEMANN-HOMBOURGER *et al.*, 2000; TOUMI *et al.*, 2003).

The differences in optimal throughput reported in Table 4.13 can also be compared in terms of the instantaneous internal concentration profiles. The internal concentration profiles for SMB 1 and VariCol 2 are presented in Figure 4.13a. The profiles for SMB 2, VariCol 1, and VariCol 3 are shown in Figure 4.13b. The shifting schemes used to plot the instantaneous internal concentration profiles of the optimal points of the VariCol process in Figure 4.13a and Figure 4.13b were chosen in such a way that the final column configuration ended in $[2, 2, 2, 2]$, which is the same column configuration of SMB 1 and SMB 2. Additionally, the optimal concentration profiles for SMB 1 and SMB 2 was plotted at the end of the first switching period of the 20th cycle, and the optimal concentration profiles for VariCol 1, VariCol 2, and VariCol 3 were plotted at the end of the last switching period of the 20th cycle. That was made to guarantee that the inlet and outlet ports of the operation modes were in the same position.

Figure 4.13a shows that the instantaneous internal concentration profile of VariCol 2 is larger and higher than SMB 1. This same behavior is seen in Figure 4.13b, where VariCol 3 is also larger and higher than SMB 2 and VariCol 1. An increment in the feed flow rate caused those internal concentration profiles to change, which was possible with the asynchronous shifting of ports and the appropriate ACL.

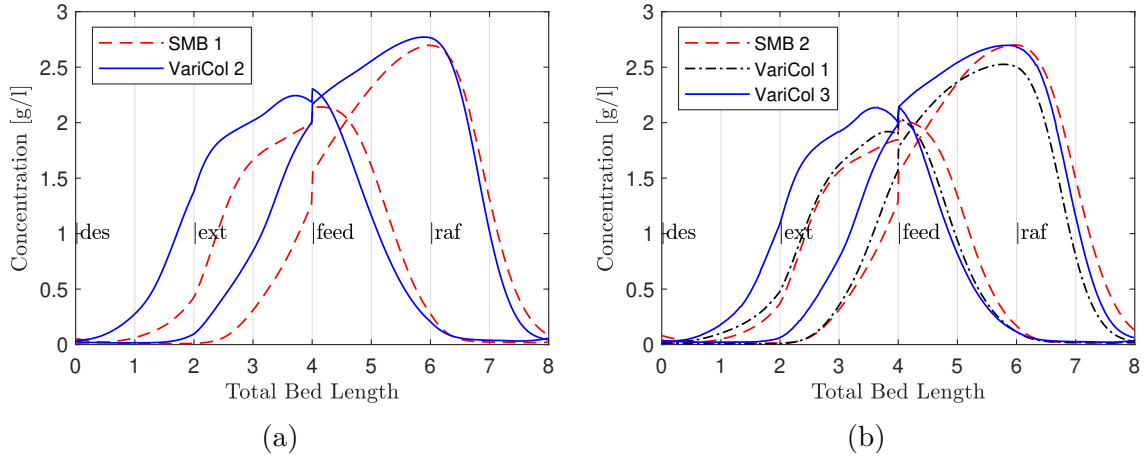


Figure 4.13: Comparison of instantaneous internal concentration profiles for (a) SMB1 with VariCol 2, (b) SMB 2 with VariCol 1 and VariCol 3.

Table 4.14: Separation performance of the VariCol and SMB processes at the cyclic steady state

Index	SMB 1	VariCol 4
$\langle P_e \rangle$ [%]	93.00	93.70 (+0.75%)
$\langle P_r \rangle$ [%]	96.20	96.64 (+0.46%)
$\langle R_e \rangle$ [%]	96.35	96.61 (+0.27%)
$\langle R_r \rangle$ [%]	92.99	93.66 (+0.72%)

A common way to compare the advantage of one operation mode over others employed in literature is to maximize achievable product purity under the same throughput (YANG *et al.*, 2019; YU *et al.*, 2015). A new optimum for the VariCol process (VariCol 4) – one which maximizes the purity in the extract and raffinate for the same feed flow rate – was obtained to compare the performance of conventional SMB and VariCol in terms of purities. In this new optimization problem, the decision variables were only the ACL of three zones. The values used for the internal flow rates and the switching period were the same as SMB 1. The objective function of the optimization problem was the same, but the desired raffinate and extract purities were set to 99.00% and 96.00%, respectively. The optimal vector of the ACL was $\bar{\mathbf{N}} = [1.60, 2.25, 2.37, 1.78]$. The purity of products was incremented by 0.75% and 0.46% and the recovery by 0.27% and 0.72% for the extract and raffinate, as can be seen in Table 4.14. The increment of purity in the products was less pronounced than the increment of the feed flow rate, showing that a small increase of this requirement can significantly increment the throughput. Therefore, a more direct comparison of performance is seen in terms of feed flow rate and not in terms of purity.

In the optimization approach proposed by YAO *et al.* (2014, 2017) (Method 1), the optimal operating point is found to solve a sequence of optimization problems

Table 4.15: Initial options for Method 1 that are equivalent to the initial average column configuration $\bar{\mathbf{N}} = [1.50, 2.62, 2.43, 1.45]$ for Method 2

Option	Initial configuration	Initial relative switching times
1	[1 3 2 2]	$\delta x = -0.50, \delta y = 0.38, \delta z = -0.43$
2	[2 2 3 1]	$\delta x = 0.50, \delta y = -0.62, \delta z = 0.57$
3	[2 3 2 1]	$\delta x = 0.50, \delta y = 0.38, \delta z = -0.43$
4	[1 3 3 1]	$\delta x = -0.50, \delta y = 0.38, \delta z = 0.57$

(see Figure 3.2a). In the method proposed in this work, referred to as Method 2 (see Figure 3.2b), the optimal operating point is found by solving a single NLP that allows for exploring all average column domains. In order to compare Method 1 with Method 2 in terms of computational effort, some additional optimization problems were solved for equivalent initial points. Those optimization problems were solved using as decision variables only the relative switching times for Method 1 and the ACL for Method 2. The internal flow rates and the switching period were set to the same values of VariCol 2. The optimal solutions obtained by the two methods have to lead to the same ACL of VariCol 2. For a given initial point in terms of ACL for Method 2, there are several equivalent initial points for the Method 1 that can be expressed in terms of initial column configurations and relative switching times. For example, in the case of the initial ACL of $\bar{\mathbf{N}} = [1.50, 2.62, 2.43, 1.45]$, there are 4 feasible equivalent initial points for Method 1 that can be determined according to the theory in Section 3.2.1.1. Note that conform to Section 3.2.1.1 for the ACL of $\bar{\mathbf{N}} = [1.50, 2.62, 2.43, 1.45]$, the difference between n and SNLIV is 2 ($n - \text{SNLIV} = 2$). Therefore 6 possible combinations are obtained by setting $nz = 4$ and $nzc = nz - 2 = 2$, where only 4 are feasible initial column configurations (see Section 3.2.1.1 and 4.2.1). Those initial points, which fall in different subdomains or search regions with origin in the initial column configuration, are presented in Table 4.15. The computational effort to find the solution of the NLP problem with the initial average column length of $\bar{\mathbf{N}} = [1.50, 2.62, 2.43, 1.45]$ in Method 2 was compared with the computational effort to find the optimal solution for all equivalent initial points in Method 1. The equivalent initial points for the previous ACL, which are formed by initial column configurations and shifting times (see Table 4.15), were evaluated in Method 1.

The number of necessary sequential optimizations to find the optimal solution in Method 1 was different for each option in Table 4.15. Two of the initial points needed a single optimization problem, and the other two needed two sequential optimization problems. Initial points that needed only one optimization problem were the ones that fell in a subdomain with origin in an initial column configuration that matched with the ones of the optimal solution, which in this case is known in advance because

Table 4.16: Computational effort for the methodology proposed by Yao et al. YAO *et al.* (2014, 2017) – Method 1, and for the one proposed in this work – Method 2

Initial configurations	Methodology	Number of NLPs	CPU time [min]
[1 3 2 2]	Method 1	1	186.25
[2 2 3 1]	Method 1	1	297.75
[2 3 2 1]+ [2 2 2 2]	Method 1	2	151.20+419.02
[1 3 3 1]+ [2 2 3 1]	Method 1	2	122.28+207.49
	Method 2	1	152.11

the solution is the same as the one for VariCol 2 ($\bar{\mathbf{N}} = [1.76, 2.09, 2.60, 1.55]$). The feasible initial column configurations of VariCol 2 are the same four displayed in regular font style in Table 4.5, determined by setting $nz = 4$, $nzc = nz - 2 = 2$ ($n - \text{SNLIV} = 2$) and evaluating which of them is physically feasible (see detailed procedure of Case 1 in Section 4.2.1). The initial options that needed only one optimization problem to find the optimal solution were those with the initial column configuration of $\mathbf{N}^0 = [1, 3, 2, 2]$ and $\mathbf{N}^0 = [2, 2, 3, 1]$. The other options needed two sequential optimization problems because the first optimization problem led to scenarios where all initial column configurations for the second optimization problem coincided with the initial column configurations in the optimal solution. In the case of the initial point $\delta x = 0.50$, $\delta y = 0.38$, $\delta z = -0.43$ with the correspondent column configuration of $[2, 3, 2, 1]$, the solution of the first optimization problem was $\delta x = 0.15$, $\delta y = 0.85$, $\delta z = -0.50$. Those relative switching times and the initial column configuration led to the ACL of $\bar{\mathbf{N}} = [1.85, 2.15, 2.50, 1.50]$. This new ACL has three possible initial column configurations, as shown in the values with regular font style of Table 4.10. As all these initial column configurations coincide with the ones in the optimal solution, any of the options for the starting point of the subsequent optimization problem will lead to the optimal solution. The initial column configuration $\mathbf{N}^0 = [2, 2, 2, 2]$ was selected as the origin of the subdomain of the second optimization problem, where the optimal solution was found. In the last option in Table 4.15, which is the initial point $\delta x = -0.50$, $\delta y = 0.38$, $\delta z = 0.57$ with the initial column configuration of $\mathbf{N}^0 = [1, 3, 3, 1]$, the solution of the first optimization problem led to a solution that corresponds to an ACL of $\bar{\mathbf{N}} = [1.58, 2.20, 2.80, 1.42]$. As all initial column configurations for the next sequential optimization problem matched the optimal solution, one of the initial column configurations was selected as the origin of the next subdomain, which in this case was $[2, 2, 3, 1]$. The computational effort for the optimization problems based on Method 1 and Method 2, measured as CPU time, is presented in Table 4.16.

The computational effort of Method 2 was lower than all cases of Method 1,

even when the optimal solution in Method 1 was found with only one optimization problem, as can be seen in the last row in Table 4.16. In the cases where the number of sequential optimizations was two, in addition to the high computational effort, it is necessary to include the time for deciding a new initial point in the second optimization problem since Method 1 has not been automatized. Besides, the maximum number of sequential optimization problems for Method 1 could be greater than two when the solution of the first optimization problem led to an initial column configuration that did not match the one in the optimal solution. The method proposed in this work (Method 2) was superior to Method 1 because the optimization problem was solved in only one NLP with less computational effort. Therefore, the proposed approach is advantageous for real-time applications of the VariCol process.

4.2.2.2 Enantioseparation of aminoglutethimide

In this example, the performance of the VariCol process with 5 columns was compared with the SMB process with 6 columns through several optimizations. The objective was to maximize the throughput of the enantioseparation of aminoglutethimide. Initial optimization problems were solved by setting the purity in the extract and raffinate to the same values reported by LIN *et al.* (2016). The decision variables for the optimization problem of the VariCol process were the ACL of three zones, the internal flow rates of zones II and III, and the switching period. In the conventional SMB process, the decision variables were the internal flow rates of zones II and III and the switching period. The column configuration used in the SMB process was [1, 2, 2, 1]. The results of the optimization problems for the SMB and the VariCol processes are listed in Table 4.17 as SMB 3 and VariCol 6. The results reported by LIN *et al.* (2016), which were obtained in a gross optimization with a 5-columns VariCol process unit, were also included in Table 4.17 as VariCol 5. The purity in the output ports, especially in the raffinate one, is slightly different from those reported by LIN *et al.* (2016) when VariCol 5 is simulated with our implemented model, as seen in Table 4.17 for the values of VariCol 5 in bold. An additional optimization problem was solved for the updated values of purities to compare the results with the ones reported by LIN *et al.* (2016). The new optimum was also presented in Table 4.17 as VariCol 7.

Table 4.17 indicates that for high purity in the extract and raffinate (99.80%) and the same solvent consumption, the optimum found for the SMB process with 6 columns (SMB 2) had a higher performance (+127.03%) than the optimum of the VariCol process with 5 columns (VariCol 6). The productivity of the SMB process with 6 columns was +90.24% higher than the VariCol process with 5 columns.

Table 4.17: Optimal operation parameters that maximize the feed flow rate for the enantioseparation of aminoglutethimide

Optimal operation parameters	SMB 3 (This Work)	VariCol 5 (Lin et al.)	VariCol 6 (This work)	VariCol 7 (This Work)
$Q_I [cm^3 min^{-1}]$	12.00	12.00	12.00	12.00
$Q_d [cm^3 min^{-1}]$	3.35	3.35	3.35	3.35
$Q_e [cm^3 min^{-1}]$	2.24	1.92	2.11	2.03
$Q_f [cm^3 min^{-1}]$	0.84	0.54	0.37	0.79
	(+127.03%)*			(+46.30%)**
$Q_r [cm^3 min^{-1}]$	1.95	1.97	1.61	2.11
$t_s [min]$	1.98	2.00	2.01	1.96
$\bar{N}_{c,I} [-]$	1	1.0	0.86	0.87
$\bar{N}_{c,II} [-]$	2	1.5	1.60	1.71
$\bar{N}_{c,III} [-]$	2	1.5	1.46	1.44
$\bar{N}_{c,IV} [-]$	1	1.0	1.08	0.98
$\langle P_e \rangle [\%]$	99.80	99.80;	99.80	99.83
		99.83 ⁺		
$\langle P_r \rangle [\%]$	99.80	99.80;	99.80	98.22
		98.22 ⁺		
$\langle Pr_e \rangle$	0.078	0.058;	0.041	0.086
$[g cm^{-3} CSP day^{-1}]$	(+90.24%)*	0.059 ⁺		(+45.76%)**
$\langle Pr_r \rangle$	0.078	0.059;	0.041	0.087
$[g cm^{-3} CSP day^{-1}]$	(+90.24%)*	0.060 ⁺		(+45.00%)**

*Percent values are related to VariCol 6. **Percent values are related to VariCol 5.

⁺Simulation of results of LIN *et al.* (2016) with our implemented model.

In this case, the additional column in the SMB process helped to reach a higher throughput and productivity at the elevated purities of 99.80%, concerning the VariCol process. In the case of comparing the optimal solution that was found for the updated purities (VariCol 7) with the results reported by LIN *et al.* (2016) (VariCol 5), the performance was increased by 46.30% for the same solvent consumption. This increment in the performance shows the potential of the proposed methodology to explore all possible operation domains with a single NLP to find an appropriate operating point in the VariCol process. Similar to the previous example, the optimal solution in VariCol 6 and VariCol 7 presented an average number of columns in zones II and III, which was greater than those in zones I and IV, as expected since the separation occurs in those zones.

In VariCol 6 and VariCol 7, the average length in some zones was less than 1, meaning that the number of columns in those zones was zero during a specific interval of the switching period. VariCol 6 had one zone with an ACL lower than one (zone I), while VariCol 7 had two (zone I and zone IV). The operation of the

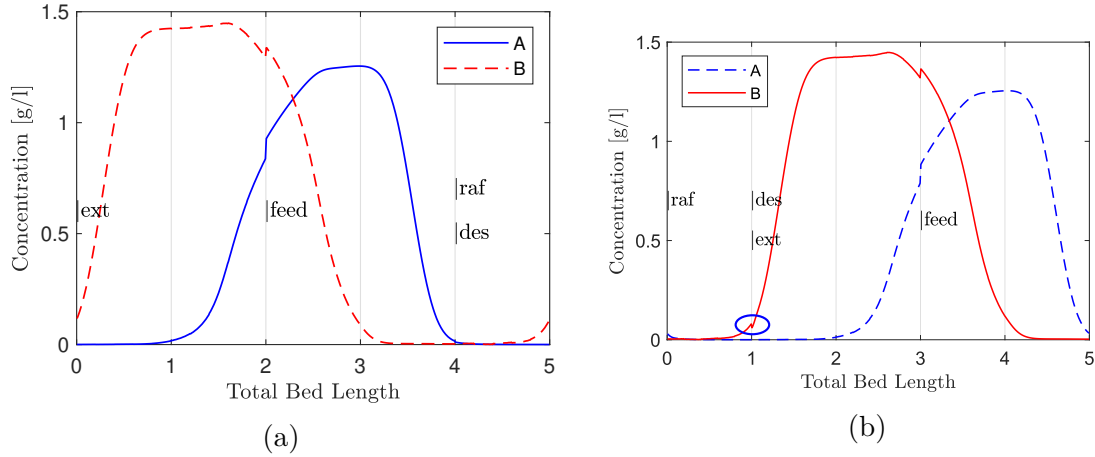


Figure 4.14: Instantaneous internal concentration profiles for the less (A) and the more retained component (B) when (a) zone IV has zero columns and (b) zone I has zero columns.

VariCol unit for this condition was analyzed in terms of the shifting scheme and internal concentration profiles. For example, in VariCol 7, where ACL for zones I and II were less than 1, one of the shifting schemes that can be determined from the ACL is the scheme $\mathbf{N}^0 = [1, 1, 2, 1]$, $\mathbf{N}^1 = [1, 2, 1, 1]$, $\mathbf{N}^2 = [1, 2, 2, 0]$, $\mathbf{N}^3 = [0, 2, 2, 1]$ with the normalized ST vector $\delta\mathbf{t} = [0.87, 1.00, 0.29, 0.85]$. From those sequences of column configurations and the normalized ST vector, the first zone with zero columns was zone IV during the interval $(0.85 - 0.87)t_s$ and then zone I at the interval $(0.87 - 1.00)t_s$. When zone IV has zero columns, the raffinate port and the solvent port are gathered together in the same node. In the case of zone I having zero columns, the desorbent port and the extract port meet in the same node. Instantaneous internal concentration profiles were plotted to verify the effect in the internal concentration when zones IV and zone I have zero columns, as presented in Figure 4.14. Figure 4.14a, which represents zone IV having zero columns, was plotted at 85.01% of the last switching period of the 20th cycle. Figure 4.14b, which represents zone I having zero columns, was plotted at 90.00% of the first switching period of the 20th cycle.

Figure 4.14a demonstrates that when zone IV has zero columns near the node where the raffinate and dissolvent ports meet, the internal concentration was low, and no change was perceived in the profile. Figure 4.14b, which represents when zone I has zero columns, there is a small oscillation in the internal concentration profile near the node where solvent and extract ports gather together, as highlighted with the circle. This oscillation corresponds to a small dilution in the input concentration of the column that follows that node, caused by joining Equations 3.41 and 3.42.

Additional optimizations for other extract and raffinate purities were also solved

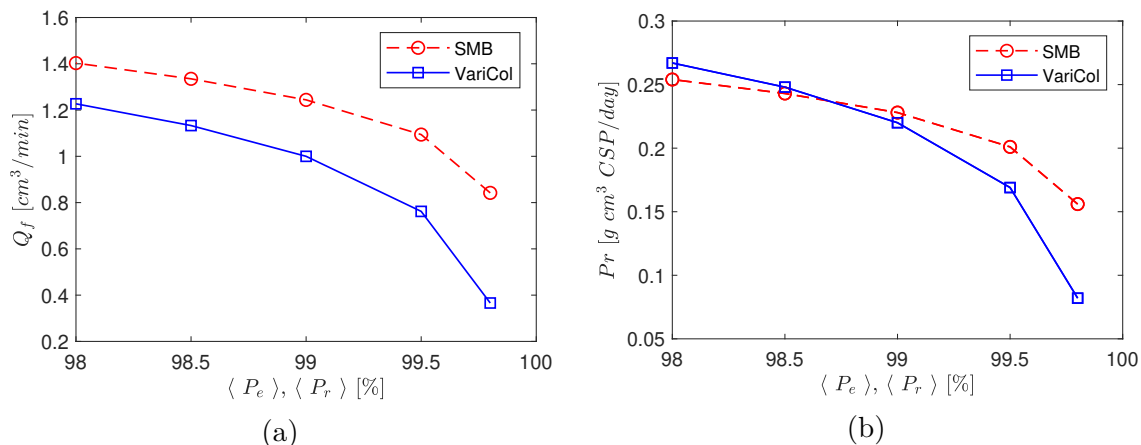


Figure 4.15: Pareto optimal solutions of 5-columns VariCol process and 6-columns SMB for variation of (a) feed flow rate with purities and (b) productivity of raffinate with purities.

to compare the performance of the 5-columns VariCol and the 6-columns SMB processes. The new extract and raffinate purity values used were 99.50%, 99.00%, 98.50%, and 98.00%. Optimal solutions for the 5-columns VariCol and the 6-columns SMB processes, including the point of 99.80%, are shown in Figure 4.15. The feed flow rate and productivity ($Pr_e + Pr_r$) were plotted as a function of the extract and raffinate purity.

Figure 4.15a indicates that when the extract and raffinate purity was decreased, the throughput of the 5-columns VariCol process incremented faster than that of the 6-columns SMB process. The difference in maximum feed flow rates between the two operation modes decreased, and it was smaller at a purity of 98.00%, which was the lowest value evaluated. When the separation performance is compared in terms of productivity (see Figure 4.15b), the 6-columns SMB process behaved better at high purities, but when the purities were decreased below about 98.70%, the 5-columns VariCol process had higher productivity. That higher productivity of the 5-columns VariCol process is caused by the faster increment of throughput using a fewer chiral stationary phase than the 6-columns SMB process. Those results show that when the required extract and raffinate purity is very high, the use of additional columns could be more favorable. However, when the purities are not so high, fewer columns can be used without a significant performance loss if the system is operated at the optimal point.

4.3 Performance comparison of some SMB process variants

This section is based on the a work of CALDERÓN SUPELANO *et al.* (2021).

A detailed study based on the maximal throughput that could reach the ModiCon, the VariCol, the conventional SMB, and the hybrid ModiCon+VariCol is presented. Particular emphasis is placed on the ModiCon process and in its combination with the VariCol processes. That combination is proposed based on the different characteristics of the VariCol process, which are the different column configuration sequences for the same average column length (YAO *et al.*, 2014, 2017). The optimization of the VariCol process and the hybrid ModiCon+VariCol is determined considering the methodology proposed in our previous section for the VariCol process. Different optimization problems were carried out to study some unique characteristics of the ModiCon and the ModiCon+VariCol processes and compare their performance with the VariCol and conventional SMB processes. These problems were based on the enantioseparation of guaifenesin. The throughput was maximized for specific purity values considering SMB process variants with 5 and 6 columns. In all optimization problems, the TD model in terms of total porosity was considered.

The enantioseparation of guaifenesin in systems with columns packed with cellulose tris 3,5-dimethylphenylcarbamate (stationary phase) was considered as a case of study. As the mobile phase, the mixture of n-hexane/ethanol (70/30) was used. The operation parameters for the separation of the guaifenesin racemate were obtained from the literature (GOMES *et al.*, 2010; GONG *et al.*, 2014a; YANG *et al.*, 2019; ZABKOVA *et al.*, 2009). Those parameters are presented in Table 4.18 together with the weighting factor (see Equation 3.74) used in the optimization.

The isotherms that describe the equilibrium between the adsorbed and fluid phases for the guaifenesin are given by the following linear-Langmuir type (GONG *et al.*, 2014a):

$$q_{e,A} = 1.22c_A + \frac{31 \times 0.028c_A}{1 + 0.028c_A + 0.098c_B} \quad (4.7)$$

$$q_{e,B} = 2.2c_B + \frac{31 \times 0.098c_B}{1 + 0.028c_A + 0.098c_B} \quad (4.8)$$

where $q_{e,A}$ and $q_{e,B}$ are given in $[mg \cdot ml^{-1}]$.

Table 4.18: Parameters for the enantioseparation of guaifenesin racemate. Index A refers to the less retained and B to the most retained enantiomers

Parameter	value
Column length [cm]	$l = 15$
Column diameter [cm]	$d = 1$
Particle size [μm]	$d_p = 20$
Total porosity [–]	$\varepsilon = 0.69$
Bed porosity [–]	$\varepsilon_b = 0.44$
Dispersion coefficient [$\text{cm}^2 \cdot \text{min}^{-1}$]	$D_{app,A} = 0.0221, D_{app,B} = 0.0165$
Feed concentration [$\text{mg} \cdot \text{cm}^{-3}$]	$\bar{c}_{f,A} = \bar{c}_{f,B} = 4$
Mass transfer coefficient [min^{-1}]	$k_{eff,A} = 25.2, k_{eff,B} = 45$
Fluid viscosity [cP]	$\mu = 0.512$
Fluid density [g/l]	$\rho = 0.702$
Weighting factor [–]	$\lambda = 1 \times 10^6$

4.3.1 ModiCon

In the ModiCon process design, the values of feed concentration in each subinterval ($\mathbf{c}_{f,i}$) and the times of each one ($\delta\mathbf{t}_{sb}$) need to be defined. As the upper bound of feed concentration can be reached during the optimization for some subintervals, the definition of that value is an important factor in operating the ModiCon process. That upper bound defines how far one can go in each subinterval in the nonlinear region of the adsorption isothermal to improve the separation without having solubility problems. The influence of the upper bound on a feed concentration pattern with modulation of two subintervals was evaluated for the enantioseparation of guaifenesin, performing three optimizations for different upper bounds but keeping the average feed concentration of each component fixed at $4 [\text{mg} \cdot \text{cm}^{-3}]$. The upper bounds were 8, 10, and $12 [\text{mg} \cdot \text{cm}^{-3}]$, which are values where the guaifenesin would not precipitate (GONG *et al.*, 2014a,b; YANG *et al.*, 2019). The purity values for the extract and raffinate were set to 99.5%, and the solvent consumption was set to $Q_d = 6.2 [\text{cm}^3 \cdot \text{min}^{-1}]$. Q_d was obtained by fixing the internal flow rates of zone I and IV ($Q_I = 11.8$ and $Q_{IV} = 5.6 [\text{cm}^3 \cdot \text{min}^{-1}]$). These values were the same ones used by YANG *et al.* (2019). For all cases, the total column number in the system was 6, and the column configuration (number of columns in each zone) was [1, 2, 2, 1]. The optimal results for the three cases of the ModiCon process are presented in Table 4.19 as ModiCon 1, ModiCon 2, and ModiCon 3. The effect of including a third subinterval in the ModiCon process was also evaluated for the upper feed concentration bound of $10 [\text{mg} \cdot \text{cm}^{-3}]$ and is discussed later. The maximal throughput results were also compared with the conventional and VariCol operation modes. Optimization problems were also solved for these other operation modes at the same solvent consumption and purity. These results were also included in Table

4.19 as SMB 1 and VariCol 1, respectively. For optimization of the VariCol process, the methodology proposed for the VariCol process was used.

Table 4.19: Optimal operation parameters for the ModiCon process with two modulations in the feed concentration

Parameters	SMB 1	VariCol 1	ModiCon 1	ModiCon 2	ModiCon 3
$Q_I [cm^3 \cdot min^{-1}]$	11.80	11.80	11.80	11.80	11.80
$Q_{IV} [cm^3 \cdot min^{-1}]$	5.60	5.60	5.60	5.60	5.60
$Q_d [cm^3 \cdot min^{-1}]$	6.20	6.20	6.20	6.20	6.20
$\langle P_e \rangle [\%]$	99.50	99.50	99.50	99.50	99.50
$\langle P_r \rangle [\%]$	99.50	99.50	99.50	99.50	99.50
$\mathbf{c}_{f,i} [mg \cdot cm^{-3}]$	4	4	[0, 8]	[0, 10]	[0, 12]
$\delta t_{sb} [-]$	1	1	[0.5, 1]	[0.6, 1]	[2/3, 1]
$\bar{\mathbf{N}} [-]$	[1, 2, 2, 1]	[1.40, 1.84, 1.86, 0.90]	[1, 2, 2, 1]	[1, 2, 2, 1]	[1, 2, 2, 1]
$t_s [min]$	2.41	2.29	2.43	2.42	2.42
$Q_{II} [cm^3 \cdot min^{-1}]$	6.18	6.52	5.93	5.91	5.86
$Q_{III} [cm^3 \cdot min^{-1}]$	9.85	10.30	11.74	12.69	13.55
$Q_e [cm^3 \cdot min^{-1}]$	5.63	5.28	5.87	5.89	5.94
$Q_f [cm^3 \cdot min^{-1}]$	3.67	3.78	5.81	6.79	7.69
		(+3.00%)	(+58.31%)	(+85.01%)	(+109.54%)
$Q_r [cm^3 \cdot min^{-1}]$	4.25	4.70	6.14	7.09	7.95
$\langle c_e \rangle [mg \cdot cm^{-3}]$	2.56	2.84	3.94	4.58	5.15
$\langle c_r \rangle [mg \cdot cm^{-3}]$	3.45	3.20	3.77	3.80	3.85
$\langle Pr_e \rangle$	0.95	0.99	1.52	1.77	2.01
$[g \cdot cm^{-3} \cdot CSP \cdot day^{-1}]$					
$\langle Pr_r \rangle$	0.96	0.99	1.52	1.77	2.01
$[g \cdot cm^{-3} \cdot CSP \cdot day^{-1}]$					
$\langle SC_e \rangle [cm^{-3} \cdot mg^{-1}]$	0.43	0.41	0.27	0.23	0.20
$\langle SC_r \rangle [cm^{-3} \cdot mg^{-1}]$	0.42	0.41	0.27	0.23	0.20

The optimal feed concentration pattern obtained for the three cases of the ModiCon process is formed by the feed concentration at the lower bound in the first subinterval and the feed concentration at the upper bound in the second subinterval, as shown for $\mathbf{c}_{f,i}$ in Table 4.19. That optimal pattern for the three cases corresponds to the one presented in Figure 2.4. As the three cases were determined based on the same average feed concentration, the second subinterval duration ($\delta t_{sb,2} - \delta t_{sb,1}$) decreased as the upper bound of feed concentration increased. The performance in the separation compared in terms of maximal throughput was much higher than the conventional operation, and increases as the feed concentration upper bound also increases. The throughput of ModiCon 1, ModiCon 2, and ModiCon 3 was 58.04%, 85.01%, and 109.54% higher than the SMB 1. The reduction of the duration and the increase of the feed concentration in the second subinterval raise the ModiCon 3 performance compared with ModiCon 1 and ModiCon 2. The performance of

the ModiCon process was also higher than the VariCol process, which was only 3.00% higher than the SMB 1. The higher performance of the ModiCon process can also be seen in Figure 4.16, where a larger feed flow rate leads to an increment of concentration profile height. That figure is plotted at 50% of the first switching period of the 25th cycle for ModiCon 2 and SMB 1. For the ModiCon process, that point is before the modulation (60% of switching period). For VariCol 1, an equivalent point was defined based on the CCS because the position of ports in columns needs to be the same. That point was the 50% of the last switching period of the 25th cycle. The CCS used was: $\mathbf{N}^0 = [2, 2, 1, 1]$, $\mathbf{N}^1 = [2, 2, 2, 0]$, $\mathbf{N}^3 = [1, 2, 2, 1]$, $\mathbf{N}^4 = [2, 1, 2, 1]$ ($\delta\mathbf{t} = [0.24, 0.84, 1.00, 0.14]$), which has the same column configuration ($\mathbf{N}^3 = [1, 2, 2, 1]$) as the other operation modes at the 50% of the switching period. At those conditions, the cyclic steady state is already reached for all operation modes.

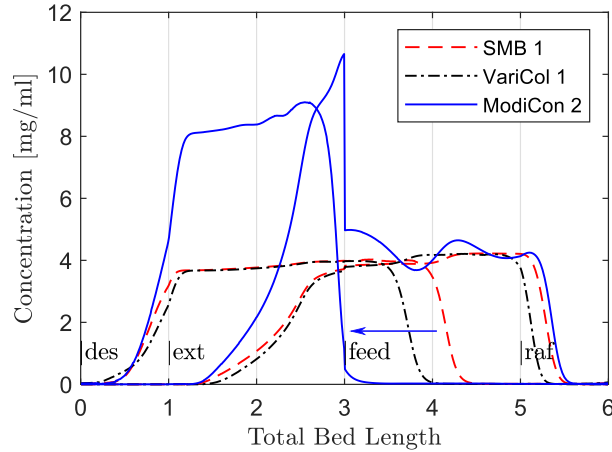


Figure 4.16: Comparison of instantaneous internal concentration profiles for SMB 1, VariCol 1 and ModiCon 2 at the cyclic steady state. The arrow mark shows the displacement to the left of the most retained component of ModiCon 2 compared with the SMB 1. The SMB 1 and ModiCon 2 were plotted at 50% of the first switching period of the 25th cycle. The VariCol 1 was plotted at an equivalent point that was at 50% of the last switching period of the 25th cycle.

In the optimal operating conditions of the ModiCon process, the increment of feed flow rate leads to a different effect on the products compared with the SMB process. In the raffinate, the flow rate rises without significant changes in its average concentration, while in the extract, the average concentration increases without significant variation on its flow rate, as it can be seen in ModiCon 1, ModiCon 2 and ModiCon 3 of Table 4.19. That behavior can also be seen in Figure 4.16. The internal flow rate of Zone III (Q_{III}) for ModiCon 2 and ModiCon 3 was higher than Q_I , different from the SMB process, where it was reported as the highest in zone I (ANICETO *et al.*, 2018; NICOUD, 2015; RODRIGUES, 2015; SÁ GOMES

and RODRIGUES, 2012; SCHMIDT-TRAUB *et al.*, 2012). Although Q_{III} was the highest, it was below the flow rate upper bound that was set to $27 [cm^3 \cdot min^{-1}]$, corresponding to a pressure drop of 6 bar (see Equation 3.89).

The modulation in the feed concentration pattern, given by zero and maximum concentrations in the first and second subintervals, generates a displacement in the front side of the concentrations profile (wave) of the most retained component (B) to the left. That displacement is shown in Figure 4.16 for ModiCon 2 concerning SMB 1 (see the arrow mark). It can also be seen more clearly in an online [video](#) that makes part of the publication of this chapter (CALDERÓN SUPELANO *et al.*, 2021). That video shows the transient concentration profiles for ModiCon 2 and SMB 1 from the start of the operation to the cyclic steady state. Note that the displacement is given even though the throughput of ModiCon 2 is higher than the SMB 1 (see Table 4.19). With the modulation, the front side of B in zone II reaches the feed node (the concentration waves travel in the same direction of the fluid phase flow) almost when the feed concentration changes from zero to the maximal (second subinterval). The front side has less time to travel through zone III than the one of SMB 1 before being transferred again to zone II with the shifting of the feed node. That generates a reduction of the mean propagation velocity in the concentration profile of B in zone III, taking into account the entire switching period. The reduction of the mean propagation velocity of B in zone III leads to an increment in the concentration profile in zones I and II (see the profile of ModiCon 2 in Figure 4.16 and its concentration in the extract in Table 4.19). Additionally, in zone II, the rear side of the less retained component (A) remains almost in the same position. With the increment of B in the zone I without changing the rear side A in zone II, separating B at high purity becomes the limiting factor in improving the throughput. The reduction and increase of feed concentration also produce a deceleration and an acceleration on the propagation velocity of waves when nonlinear equilibrium isotherms are considered (SCHRAMM *et al.*, 2003a,b). The acceleration in the propagation velocity of waves caused by the increment of the feed concentration can be correlated with the fast desorption of component B in zone I, allowing increases the throughput even more. The rear and front sides of the concentration profile of component A are almost at the same positions as the ones of SMB 1. Therefore, the mean propagation velocity of that component was not affected by the modulation and variation of feed concentration. The variation of the propagation velocities of components A and B can be seen in the transient concentration profile of ModiCon 2 in the online [video](#), where a widening and shrinkage of the concentration fronts is presented with the modulation of feed concentration.

The internal concentration profile of the less retained component of the ModiCon

2 at the CSS presents some oscillations and has a peak that exceeds the maximum value of feed concentration (see Figure 4.16). The oscillations are explained with the modulation of feed concentration that produces sudden changes in the internal concentration, as was also reported in the work of YANG *et al.* (2019). In the online [video](#), the behavior of these oscillations can be better seen. The oscillations reduce their amplitude each time they move further away from the feed node due to the different propagation velocities (see online [video](#)). The maximum concentration of component A at each time of the switching period is presented in Figure 4.17. That concentration is higher than the feed concentration of the second subinterval ($10 [mg \cdot cm^{-3}]$) during most of the switching period. In the first subinterval of feed concentration, the maximal concentration of A increased and decreased smoothly, but it oscillates with narrow and sharp peaks at the beginning of the second subinterval. The maximum concentration of A was $10.77 [mg \cdot cm^{-3}]$ and took place at 60.52% of the switching period, just a short time after the modulation of feed concentration. Although the maximum concentration values of A in the entire switching period are inside the solubility limits (GONG *et al.*, 2014a,b; YANG *et al.*, 2019), they need to be taken into account in the design of the VariCol process to avoid the precipitation phenomenon inside the columns.

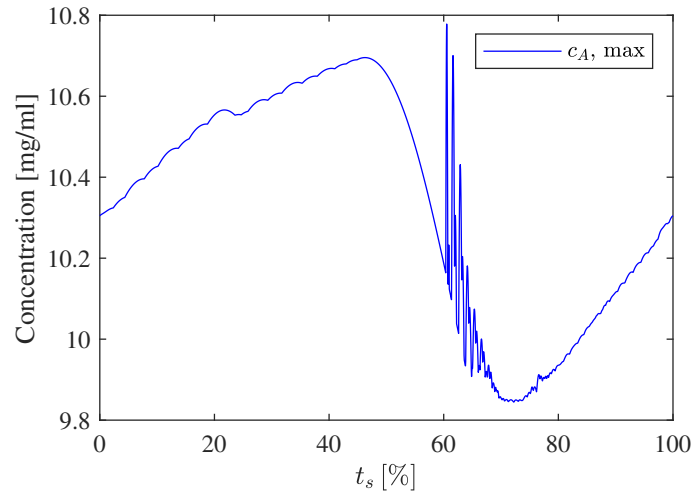


Figure 4.17: Variation of the maximal concentration of the less retained component (A) during a switching period for a feed concentration modulation pattern of: $\mathbf{c}_{f,i} = [0, 10] [mg \cdot cm^{-3}]$ and $\delta \mathbf{t}_{sb} = [0.6, 1]$.

The modulation of three subintervals did not lead to improvements in the maximal throughput. The optimal internal flow rates and switching period were the same as ModiCon 2. The values of feed concentrations and the normalized times of subintervals were $[0, 6.12, 10] [mg \cdot cm^{-3}]$ and $[0.6, 0.6, 1] [-]$, that are also the same as ModiCon 2 since the duration of the second subinterval was zero. That is a significant result because the most straightforward operation (two modulations) can reach the same performance as three or maybe more subintervals. Therefore, the

design of the modulation pattern of the ModiCon process is reduced to select the duration and the limit of feed concentration of the last subinterval that guarantees a desired average feed concentration. The effect of the average feed concentration is not studied here. However, as higher and lower average feed concentration leads to low and high feed flow rates, the definition of average feed concentration could also be constrained with minimum and maximum limits of feed flow rates (SCHRAMM *et al.*, 2003a,b).

4.3.2 Hybrid ModiCon+VariCol operation mode

In this section, the new characteristics obtained in the hybrid operation mode of ModiCon+VariCol, which are the flexibility in the employment of chromatographic columns and modulation of feed concentration, are analyzed. The optimal results of ModiCon 2 (Q_{II} , Q_{III} , t_s , $\mathbf{c}_{f,i}$, $\delta\mathbf{t}_{sb}$) and VariCol 1 ($\bar{\mathbf{N}}$) presented in Table 4.17 were initially considered in the combined mode. The inclusion of the feed concentration modulation pattern of ModiCon 2 on the different CCSs of VariCol 1 was analyzed. The most appropriate CCS to include the modulation of the feed concentration based on the port that moves simultaneously with the switching period was determined through optimization. The optimization of ModiCon+VariCol was based on the strategy proposed previously for the VariCol process.

In the VariCol process, for the same vector of average column lengths, different shifting times associated with a distinct CCS produce the same results in the cyclic steady state (YAO *et al.*, 2014). These CCSs are shifted relative to each other, and in each case, a different port of the chromatographic structure moves at the same time with the switching period. For instance, in the average column lengths of $\bar{\mathbf{N}} = [1.40, 1.84, 1.86, 0.90]$, that is the optimal VariCol 1 presented in Table 4.17, the CCS where the feed port (t_f) moves at the same time of the switching period (t_s) is the same one used to plot Figure 4.13 ($\mathbf{N}^0 = [2, 2, 1, 1]$, $\mathbf{N}^1 = [2, 2, 2, 0]$, $\mathbf{N}^2 = [1, 2, 2, 1]$, and $\mathbf{N}^3 = [2, 1, 2, 1]$). The normalized switching time vector that produces that sequence as also previously described is $\delta\mathbf{t} = [0.24, 0.84, 1.00, 0.14]$ (see Equation 3.1), where the order of movement of the ports is: t_r , t_d , t_e and t_f . All possible CCSs and the order movement of the ports for that average column lengths are presented on the diagrams of Figure 4.18. Each case of Figure 4.18 is referenced as a scheme.

In the combination of ModiCon and VariCol processes, the feed concentration pattern needs to be included in the shifting times of the CCSs. When it is made in the shifting times of specific CCS, the feed concentration pattern can also be

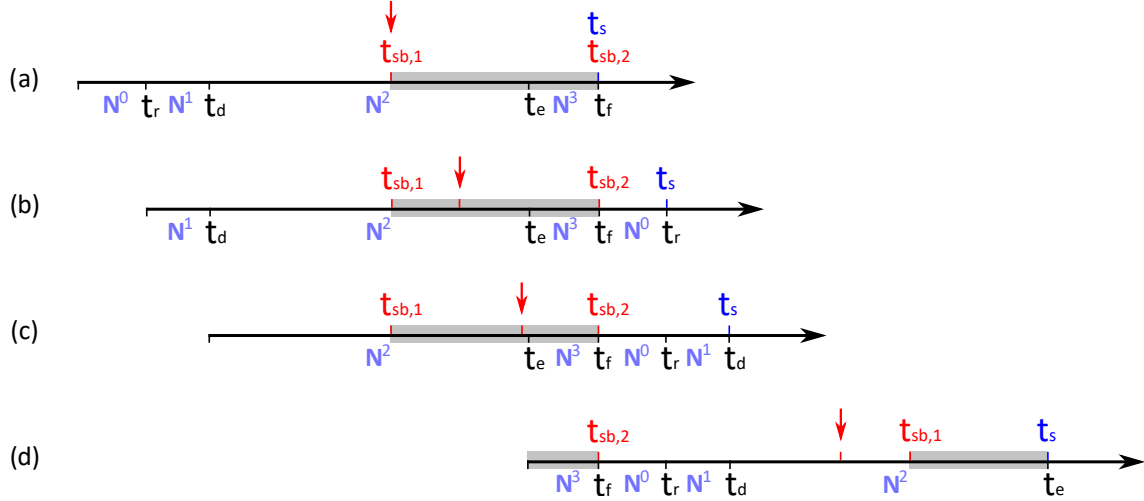


Figure 4.18: Possibilities to incorporate the modulation pattern of ModiCon process formed by $\mathbf{c}_{f,i} = [0, 10] [mg \cdot cm^{-3}]$ and $\delta \mathbf{t}_{sb} = [0.6, 1]$ in the shifting schemes of VariCol process obtained from the average column lengths of $\bar{\mathbf{N}} = [1.40, 1.84, 1.86, 0.90]$. $t_{sb,1}$ and $t_{sb,2}$ could be positioned at the actual position presented in the figure or at the arrow signal for $t_{sb,1}$ and the switching period (t_s) for $t_{sb,2}$.

displaced in the others to get the same results in the cyclic steady state. That characteristic is evaluated considering as an example the inclusion of the optimal pattern of feed concentration of ModiCon 2 (see Table 4.17) in the first case of CCS of Figure 4.18 (scheme (a)) that is the one where t_f moves at the same time of t_s . The position of normalized times of subintervals $\delta \mathbf{t}_{sb} = [t_{sb,1}, t_{sb,2}] = [0.6, 1]$ in the scheme (a) can also be seen in Figure 4.18, where $t_{sb,2}$ coincide with t_f and t_s . The same results in the cyclic steady state are obtained for the other CCSs (scheme (b), (c) and (d)), displacing $\delta \mathbf{t}_{sb}$ the same proportion that these CCSs are displaced concerning the scheme (a). When that displacement is applied for $\delta \mathbf{t}_{sb}$, the $t_{sb,2}$ continue to coincide with the position of t_f that does not match more with t_s (see Figure 4.18 for scheme (b), (c) and (d)). The duration of the second subinterval, which is the one with the maximal concentration, was also highlighted in gray in Figure 4.18 for all schemes of CCSs to see better the difference of the displacement in the modulation of feed concentration pattern. However, for these other schemes, it is necessary to consider three subintervals for feed concentration pattern to get the same results in the cyclic steady of the ModiCon+VariCol process, which are more complex scenarios than the one used in the scheme (a). The obtained values of feed concentration patterns are presented in Table 4.20 for the different schemes. The purity in the extract and raffinate is also calculated for these CCSs after reaching the cyclic steady state. These values are also presented in Table 4.20. The purity in all cases was the same, as expected, since these schemes in the combination of ModiCon 2 and VariCol 1 represent the same condition in the cyclic steady state.

Table 4.20: The new configuration in the modulation pattern of feed concentration after displacement, which keeps the feed port as the reference

Schemes	$\mathbf{c}_{f,i} [mg \cdot cm^{-3}]$	$\delta\mathbf{t}_{sb} [-]$	$\langle P_e \rangle [\%]$	$\langle P_r \rangle [\%]$
Scheme (a)	[0, 10]	[0.60, 1]	99.23	99.75
Scheme (b)	[0, 10, 0]	[0.46, 0.86, 1]	99.23	99.75
Scheme (c)	[0, 10, 0]	[0.36, 0.76, 1]	99.23	99.75
Scheme (d)	[10, 0, 10]	[0.16, 0.76, 1]	99.23	99.75

The feed concentration pattern might also be included in any of the schemes of Figure 4.18 without considering any displacement. In those cases, the positions of the normalized times of subintervals ($\delta\mathbf{t}_{sb} = [t_{sb,1}, t_{sb,2}] = [0.6, 1]$) in the schemes (a), (b), (c), and (d)) are represented by the arrow signal in Figure 4.18 for $t_{sb,1}$ and the switching period (t_s) for $t_{sb,2}$. The inclusion of the feed concentration pattern without displacements produces different results in the cyclic steady state in terms of purity in the extract and raffinate, as presented in Table 4.21. From that results, the one with higher values of purity for the products was the scheme (a) where t_f moves simultaneously as t_s . As those results could be different for other scenarios, it is necessary to define which of the CCS should be used as a reference in modeling the hybrid operation.

Table 4.21: Purity in the extract and the raffinate for the hybrid ModiCon+VariCol considering a displacement in the modulation pattern of feed concentration for the different CCSs

Schemes	$\mathbf{c}_{f,i} [mg \cdot cm^{-3}]$	$\delta\mathbf{t}_{sb} [-]$	$\langle P_e \rangle [\%]$	$\langle P_r \rangle [\%]$
Scheme (a)	[0, 10]	[0.60, 1]	99.23	99.75
Scheme (b)	[0, 10]	[0.60, 1]	96.02	73.88
Scheme (c)	[0, 10]	[0.60, 1]	89.11	62.21
Scheme (d)	[0, 10]	[0.60, 1]	99.57	76.40

The appropriate CCS that should be used to combine ModiCon and VariCol processes, which is defined based on a specific port that moves at the same time of switching period, was evaluated through optimization. For this task, four optimizations were carried out, considering in each case a different reference port (t_d , t_e , t_f and t_r). The objective of the optimizations was to maximize the throughput, keeping the purity of extract and raffinate fixed. The optimizations parameters were the same as in Table 4.18, and the feed concentration pattern was fixed the same as ModiCon 2 of Table 4.17. The optimization procedure was based on the methodology proposed for the VariCol process. As the CCS needs to be selected in each optimization stage, the one based on the desired reference port was always selected for each studied case. The results of the optimizations are presented in Table 4.22.

Table 4.22: Optimal results for the hybrid ModiCon+VariCol that were obtained using different reference ports

Parameters	MC+VC 1 (t_d)	MC+VC 2 (t_e)	MC+VC 3 (t_f)	MC+VC 4 (t_r)
$Q_I [cm^3 \cdot min^{-1}]$	11.80	11.80	11.80	11.80
$Q_{IV} [cm^3 \cdot min^{-1}]$	5.60	5.60	5.60	5.60
$Q_d [cm^3 \cdot min^{-1}]$	6.20	6.20	6.20	6.20
$\langle P_e \rangle [\%]$	99.50	99.50	99.50	99.50
$\langle P_r \rangle [\%]$	99.50	99.50	99.50	99.50
$\mathbf{c}_{f,i} [mg \cdot cm^{-3}]$	[0, 10]	[0, 10]	[0, 10]	[0, 10]
$\delta \mathbf{t}_{sb} [-]$	[0.6, 1]	[0.6, 1]	[0.6, 1]	[0.6, 1]
$\bar{\mathbf{N}} [-]$	[1.99, 2.01, 1.04, 0.96]	[2.10, 2, 0.99, 0.91]	[1.94, 2.38, 0.78, 0.90]	[1.96, 2.17, 1.00, 0.87]
$t_s [min]$	2.26	2.26	2.28	2.26
$Q_{II} [cm^3 \cdot min^{-1}]$	6.32	6.33	6.24	6.30
$Q_{III} [cm^3 \cdot min^{-1}]$	13.51	13.53	13.50	13.51
$Q_e [cm^3 \cdot min^{-1}]$	5.48	5.47	5.56	5.50
$Q_f [cm^3 \cdot min^{-1}]$	7.18	7.20	7.26	7.21
$Q_r [cm^3 \cdot min^{-1}]$	7.91	7.93	7.90	7.91
$\delta \mathbf{t}$	[1.00, 0.01, 1.00, 0.96]	[0.10, 1.00, 1.00, 0.01]	[0.32, 0.38, 1.00, 0.22]	[0.13, 0.17, 1.00, 1.00]
$\mathbf{N}^0 [-]$	[1, 3, 1, 1]	[3, 2, 0, 1]	[2, 3, 0, 1]	[2, 3, 1, 0]
$\langle c_e \rangle [mg \cdot cm^{-3}]$	5.22	5.24	5.20	5.22
$\langle c_r \rangle [mg \cdot cm^{-3}]$	3.61	3.62	3.65	3.63
$\langle Pr_e \rangle [g cm^{-3} CSP day^{-1}]$	1.88	1.88	1.90	1.89
$\langle Pr_r \rangle [g cm^{-3} CSP day^{-1}]$	1.88	1.88	1.90	1.89
$\langle SC_e \rangle [cm^{-3} \cdot mg^{-1}]$	0.22	0.22	0.21	0.22
$\langle SC_r \rangle [cm^{-3} \cdot mg^{-1}]$	0.22	0.22	0.21	0.22

From the results of Table 4.22, the reference port that improved the throughput the most in the combination ModiCon+VariCol was the feed port, as can be seen in the optimal MC+VC 3. The optimal throughput for the other reference ports was close to the t_f , but inferior, as seen in the values of feed flow rate in Table 4.22. The results of MC+VC 1, MC+VC 2, and MC+VC 4 were close to MC+VC 3, because in all cases t_f moves simultaneously as the respective reference port, as it can be seen in the switching times ($\delta \mathbf{t}$) in Table 4.22, which according to Equation 3.1, the normalized t_f is in the third position of this vector. These results indicate that the feed port has the most significant influence in the separation when modulation of feed concentration is included. This result was expected since this port has a higher control in reducing the mean propagation velocity of the concentration profile of zone III, as described in Section 4.3.1. The use of t_f as the only reference port simplifies the design of the hybrid ModiCon+VariCol because there is only one option of shifting scheme to get the best results in the separation.

Another significant result of Table 4.22 is the average column length of zones. In this case, the lengths of zones I and II are higher than zones III and IV, different from VariCol and SMB processes where the lengths of zones II and III were the largest (LUDEMANN-HOMBOURGER *et al.*, 2000; TOUMI *et al.*, 2003). For example, for the optimal VariCol of the previous section (see VariCol 1 in Table 4.17), a larger length of separation zones (zones II and III) was obtained. With the modulation of feed concentration, a larger zone III is not required anymore to adsorb the more retained component since the front side of the concentration profile is shifted to the left (see the arrow mark on Figure 4.13). However, instead, larger zones I and II promote the regeneration of the adsorbent and desorb the less retained component, increasing the separation of the most retained component in the extract. These characteristics allow enhancing the throughput of VC+MC 3 in 97.82% and 6.92% concerning the SMB 1 and ModiCon 2 of Table 4.17. The average length of some zones in the optimal results of Table 4.22 was lower than 1 column, meaning that in some intervals of the switching period, those zones will have zero columns. For optimal average lengths of Table 4.22, zone IV was lower than 1 column in all cases. An interesting result was obtained for MC+VC 2 and MC+VC 3, where zone III was also lower than 1 column. That indicates that the feed and raffinate ports meet at the same node in a subinterval of the switching period. It happens at the beginning of the switching period when the feed concentration is zero, as shown in the \mathbf{N}^0 and $\delta\mathbf{t}$ of Table 4.22. For instance, the CCS of MC+VC 3, where t_f moves at t_s , is $\mathbf{N}^0 = [2, 3, 0, 1]$, $\mathbf{N}^1 = [2, 3, 1, 0]$, $\mathbf{N}^2 = [1, 3, 1, 1]$ and $\mathbf{N}^3 = [2, 2, 1, 1]$, and the shifting times are $\delta\mathbf{t} = [0.39, 0.43, 1.00, 0.27]$. Zone III has zero columns in the initial column configuration (\mathbf{N}^0). That is from 0 to the time when the raffinate port moves ($\delta t_r = 0, 27$), which is lower than the time when the first subinterval of the feed concentration ends ($t_{sb,1} = 0.6$).

4.3.3 Performance comparison of 5- and 6-columns operation modes

The ModiCon process was studied for other column configurations, based on the optimal result of the hybrid operation, where zone I and II were larger than zones III and IV. The performance of SMB, ModiCon, VariCol, and ModiCon+VariCol processes was also compared for different purity values in the extract and raffinate. Systems with 6 columns were considered for the SMB and VariCol processes. 5 and 6 columns were considered for the ModiCon and the ModiCon+VariCol processes.

As the average column length of zones for the optimal MC+VC 3 of the previous section (see Table 4.22) was far from the column configuration $[1, 2, 2, 1]$ used in

ModiCon 2 (see Table 4.17), better results could also be expected in the ModiCon process for column configurations where zone I and II were larger. That issue was evaluated with an optimization problem for the ModiCon process considering the column configuration of [2, 2, 1, 1] that is closer to the optimal average column lengths of the hybrid operation. The optimization result refereed as ModiCon 4 is presented in Table 4.23, together with the optimal MC+VC 3. The operation of the ModiCon and the hybrid processes with 5 columns is also evaluated. In this case, for the ModiCon process, two optimization problems were solved for the columns configurations [2, 1, 1, 1] and [1, 2, 1, 1]. Only one problem was solved for the hybrid operation to find the appropriate average column length of zones. Those results are also included in Table 4.23 as ModiCon 5, ModiCon 6, and MC+VC 5.

Table 4.23: Optimal operating parameters for the ModiCon process and the hybrid operation mode ModiCon+VariCol considering systems with 5 and 6 columns

Parameters	ModiCon	MC+VC	ModiCon	ModiCon	MC+VC
	4	3	5	6	5
$Q_I [cm^3 \cdot min^{-1}]$	11.80	11.80	11.80	11.80	11.80
$Q_{IV} [cm^3 \cdot min^{-1}]$	5.60	5.60	5.60	5.60	5.60
$Q_d [cm^3 \cdot min^{-1}]$	6.20	6.20	6.20	6.20	6.20
$\langle P_e \rangle [\%]$	99.50	99.50	99.50	99.50	99.50
$\langle P_r \rangle [\%]$	99.50	99.50	99.50	99.50	99.50
$n [-]$	6	6	5	5	5
$\mathbf{c}_{f,i} [mg \cdot cm^{-3}]$	[0, 10]	[0, 10]	[0, 10]	[0, 10]	[0, 10]
$\delta \mathbf{t}_{sb} [-]$	[0.6, 1]	[0.6, 1]	[0.6, 1]	[0.6, 1]	[0.6, 1]
$\bar{\mathbf{N}} [-]$	[2, 2, 1, 1]	[1.94, 2.38, 0.78, 0.90]	[2, 1, 1, 1]	[1, 2, 1, 1]	[1.48, 1.92, 0.70, 0.90]
$t_s [min]$	2.28	2.28	2.27	2.41	2.30
$Q_{II} [cm^3 \cdot min^{-1}]$	6.27	6.24	7.32	5.92	6.22
$Q_{III} [cm^3 \cdot min^{-1}]$	13.48	13.50	12.49	12.70	13.30
$Q_e [cm^3 \cdot min^{-1}]$	5.53	5.56	4.48	5.88	5.58
$Q_f [cm^3 \cdot min^{-1}]$	7.21	7.26	5.17	6.78	7.08
	(+96.46%)*	(+97.82%)*	(+40.87%)*	(+84.74%)*	(+92.92%)*
$Q_r [cm^3 \cdot min^{-1}]$	7.88	7.90	6.89	7.10	7.70
$\langle c_e \rangle [mg \cdot cm^{-3}]$	5.19	5.20	4.59	4.59	5.05
$\langle c_r \rangle [mg \cdot cm^{-3}]$	3.64	3.65	2.99	3.80	3.66
$\delta \mathbf{t} [-]$	[1, 1, 1, 1]	[0.32, 0.38, 1.00, 0.22]	[1, 1, 1, 1]	[1, 1, 1, 1]	[0.40, 0.92, 1.00, 0.30]
$\mathbf{N}^0 [-]$	[2, 2, 1, 1]	[2, 3, 0, 1]	[2, 1, 1, 1]	[1, 2, 1, 1]	[2, 2, 0, 1]
$\langle Pr_e \rangle$	1.88	1.90	1.62	2.13	2.22
$[g \cdot cm^{-3} \cdot CSP \cdot day^{-1}]$					
$\langle Pr_r \rangle$	1.88	1.90	1.62	2.13	2.22
$[g \cdot cm^{-3} \cdot CSP \cdot day^{-1}]$					
$\langle SC_e \rangle [cm^{-3} \cdot mg^{-1}]$	0.22	0.21	0.30	0.23	0.22
$\langle SC_r \rangle [cm^{-3} \cdot mg^{-1}]$	0.22	0.21	0.30	0.23	0.22

*Percent values are related to SMB 1 of Table 4.17.

Table 4.23 shows that the performance of ModiCon 4 that has the column configuration of [2, 2, 1, 1] was higher than ModiCon 2 (see Table 4.17) and lower, but closer, than the hybrid operation MC+VC 3. The increment of length of zones I and II improved the separation of the most retained component as expected since it facilitates the regeneration of the adsorbent. The performance of ModiCon 4 and MC+VC 3 was very high compared with SMB 1, with throughput 96.46% and 97.82% higher, respectively. Although there were no great benefits in terms of throughput of MC+VC 3 compared with the ModiCon 4, the hybrid operation was a guideline to define the appropriate column configuration of the ModiCon process. In the case of 5 columns, the ModiCon operation that had the highest performance was the one with a column configuration ([1, 2, 1, 1]) closer to the optimal result of the average column length of the hybrid operation mode (MC+VC 5). The throughput of ModiCon 6 and MC+VC 5 based on 5 columns was 84.74% and 92.92% higher than SMB 1. Unlike the case of 6 columns for the ModiCon and the ModiCon+VariCol processes, the hybrid operation with 5 columns (MC+VC 5) had a slightly higher throughput than the ModiCon operation (ModiCon 6). As the ModiCon+VariCol process takes the synergy effect of each operation individually, this hybrid operation could be more attractive in systems with a low number of columns, where the column utilization flexibility in zones given by the VariCol process is necessary. Additionally, the practicability of the ModiCon+VariCol process will be relatively easy if the extensions of the ModiCon and VariCol processes are already included in an SMB unit. Another significant result of Table 4.23 is that the operation modes with 5 columns (ModiCon 6, MC+VC 5) had higher productivity than 6 columns. In the case of 5 columns, the stationary phase is better used than in the case of 6 columns.

The internal concentration profiles of the optimal results for the ModiCon and ModiCon+VariCol processes were presented in Figure 4.19 for 6 (ModiCon 4 and MC+VC 3) and 5 (ModiCon 5 and MC+VC 6) columns. For ModiCon 4 and ModiCon 6, Figure 4.19 was plotted at 50% of the first switching period of the 25th cycle. MC+VC 3 and MC+VC 5 were plotted at 50% of the last switching period of the 25th cycle. Note that at those points, the column configuration of the ModiCon process matches with the ModiCon+VariCol process. In both Figure 4.19a and Figure 4.19b, a displacement between ModiCon and ModiCon+VariCol is seen. That displacement is associated with the modulation of the length of zones in the ModiCon+VariCol process. The maximal concentrations of the less retained component were 10.76, 10.85, 10.79, 10.74 [$mg \cdot cm^{-3}$] for ModiCon 4, MC+VC 3, ModiCon 6, MC+VC 4, respectively, and took place at a short time after modulation of feed concentration as presented in Figure 4.17. All maximal concentrations are inside the solubility limit (GONG *et al.*, 2014a,b; YANG *et al.*, 2019).

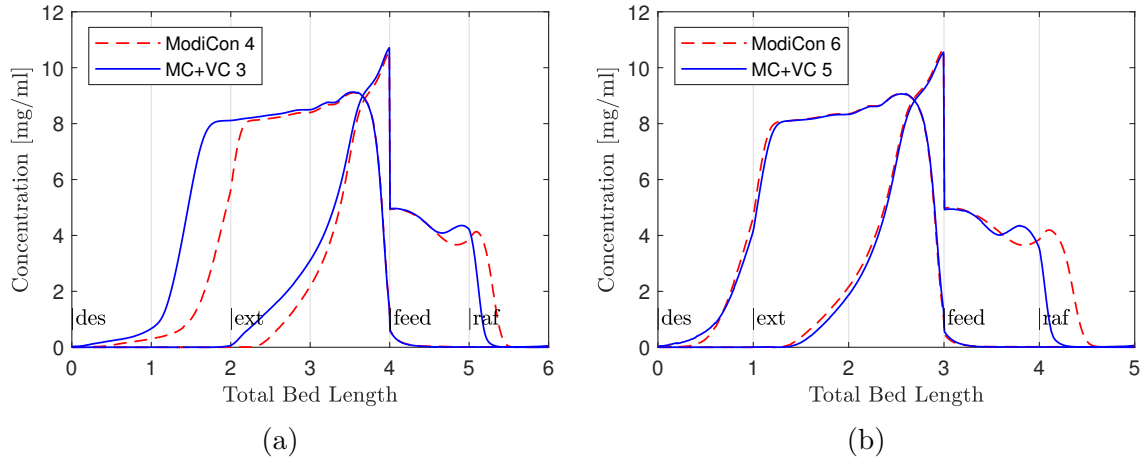


Figure 4.19: Comparison of instantaneous internal concentration profiles of the ModiCon and ModiCon+VariCol processes for system with 6 and 5 columns. (a) ModiCon 4 and MC+VC 3, (b) ModiCon 6 and MC+VC 5. ModiCon 4 and ModiCon 6 were plotted at 50% of the first switching period of the 25th cycle. MC+VC3 and MC+VC5 were plotted at 50% of the last switching period of the same 25th cycle.

The performance for 6 and 5 columns was also compared for some operation modes for different product purity values. For this task, new optimization problems were solved for purity values in the extract and raffinate of 98.5%, 97.5%, 96.5%, and 95%. In the case of 6 columns, the operation modes of SMB (SMB_6col), VariCol (VC_6col), ModiCon (MC_6col), and the hybrid ModiCon+VariCol (VC+MC_6col) were considered. In the case of 5 columns, the last two were evaluated (MC_5col, MC+VC_5col). In the ModiCon process, the column configurations of [2, 2, 1, 1] and [1, 2, 1, 1] were considered for 6 and 5 columns. Those column configurations were the ones with higher performance for the purity of 99.5 % (see Table 4.23). The results are presented in Figure 4.20 for maximal throughput and productivity ($Pr_e + Pr_r$).

Figure 4.20 shows that the throughput and productivity of the ModiCon and the hybrid ModiCon+VariCol processes for 6 and 5 columns are relatively higher compared with the SMB and the VariCol processes with 6 columns for all purity values in the extract and raffinate. These performance parameters for the different operation modes increased proportionally as the purity was decreasing. The throughput of hybrid operation with 5 columns was very close with the ModiCon and the ModiCon+VariCol processes with 6 columns. It was higher in terms of productivity (see Figure 4.20b) because a less stationary phase is required.

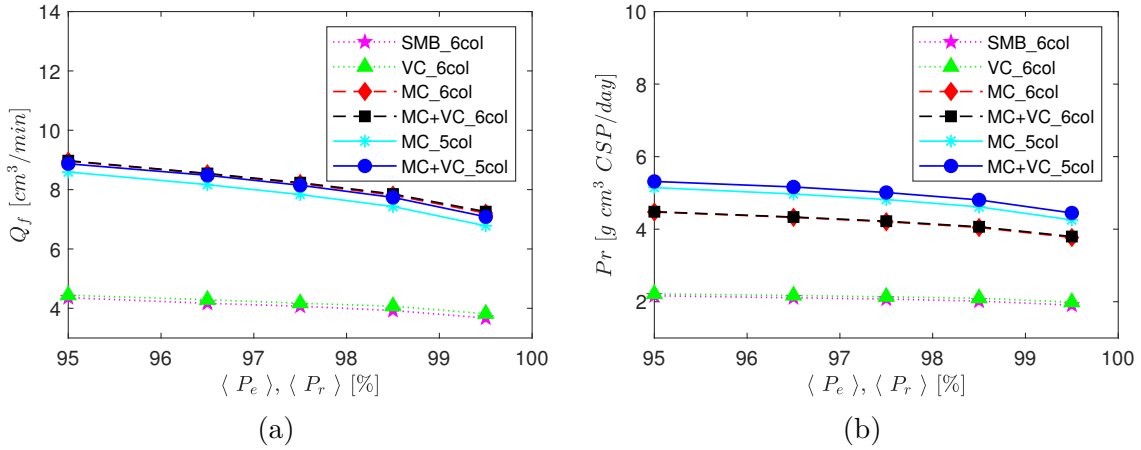


Figure 4.20: Maximal throughput and productivity concerning extract and raffinate purity values for 5- and 6-columns SMB, VariCol, ModiCon, and the hybrid ModiCon+VariCol processes. (a) throughput vs. purity. (b) Productivity vs. purity.

4.3.4 Performance comparison of 6-columns SMB with 3-columns ModiCon+VariCol processes at unequal product purities

In the enantioseparations, the interest can be related to obtaining only one of the enantiomers at high purity (HARRIEHAUSEN *et al.*, 2020; LORENZ and SEIDEL-MORGENSTERN, 2014). In those cases, the number of columns in the SMB process variants can be reduced. The hybrid ModiCon+VariCol process might be essential in those situations since it has the flexibility to operate with a small number of columns. The potential of the ModiCon+VariCol process with 3 columns was evaluated and compared with the SMB process with 6 columns for unequal purity in products. Two scenarios at different purity values in the products were evaluated. In the first scenario (scenario 1), the purity in the extract was set at 99.5% and the purity of raffinate at 90%. In the second scenario (scenario 2), the purity of raffinate was set at 99.5% and the purity of extract purity at 90%. In each scenario, the throughput at desired purities was maximized for the SMB and the ModiCon+VariCol processes. The optimal results are presented in Table 4.24 as SMB 2 and MC+VC 6 for Scenario 1 and SMB 3 and MC+VC 7 for scenario 2. An additional optimization was conducted at a purity of 99.5% for extract and raffinate, and it was also included in Table 4.24 as MC+VC 8.

Table 4.24 shows that the throughput and productivity of 3-columns ModiCon+VariCol are higher than the 6-columns SMB process independently of the product of interest. The highest throughput in the ModiCon+VariCol process occurred when the desired product was the raffinate and not the extract. That agrees with the previous results. The ModiCon+VariCol process with feed concentration

Table 4.24: Optimal operation parameters for the 6-columns SMB and the 3-columns ModiCon+VariCol processes at unequal purity in the products

Parameters	SMB 2	SMB 3	MC+VC 6	MC+VC 7	MC+VC 8
$Q_I [cm^3 \cdot min^{-1}]$	11.80	11.80	11.80	11.80	11.80
$Q_{IV} [cm^3 \cdot min^{-1}]$	5.60	5.60	5.60	5.60	5.60
$Q_d [cm^3 \cdot min^{-1}]$	6.20	6.20	6.20	6.20	6.20
$\langle P_e \rangle [\%]$	99.50	90	99.50	90	99.50
$\langle P_r \rangle [\%]$	90	99.50	90	99.50	99.50
$n [-]$	6	6	3	3	3
$\mathbf{c}_{f,i} [mg \cdot cm^{-3}]$	4	4	[0, 10]	[0, 10]	[0, 10]
$\delta \mathbf{t}_{sb} [-]$	1	1	[0.6, 1]	[0.6, 1]	[0.6, 1]
$\bar{\mathbf{N}} [-]$	[1, 2, 2, 1]	[1, 2, 2, 1]	[0.51, 1.11, 0.50, 0.88]	[1.04, 0.95, 0.52, 0.49]	[0.74, 0.85, 0.46, 0.95]
$t_s [min]$	2.03	2.41	2.35	2.39	2.55
$Q_{II} [cm^3 \cdot min^{-1}]$	7.35	5.60	6.73	6.12	8.47
$Q_{III} [cm^3 \cdot min^{-1}]$	11.53	9.80	12.55	12.49	9.58
$Q_e [cm^3 \cdot min^{-1}]$	4.45	6.20	5.06	55.68	3.33
$Q_f [cm^3 \cdot min^{-1}]$	4.18	4.20	5.81	6.38	1.11
$Q_r [cm^3 \cdot min^{-1}]$	5.93	4.20	6.95	6.89	3.98
$\langle c_e \rangle [mg \cdot cm^{-3}]$	3.32	2.67	4.65	4.47	1.34
$\langle c_r \rangle [mg \cdot cm^{-3}]$	2.81	3.56	3.33	3.30	1.11
$\delta \mathbf{t} [-]$	[1, 1, 1, 1]	[1, 1, 1, 1]	[0.62, 0.11, 1.00, 0.50]	[0.99, 0.95, 1.00, 0.48]	[0.59, 0.85, 1.00, 0.54]
$\mathbf{N}^0 [-]$	[1, 2, 2, 1]	[1, 2, 2, 1]	[0, 2, 0, 1]	[1, 1, 0, 1]	[1, 1, 0, 1]
$\langle Pr_e \rangle$ [$g \cdot cm^{-3} \cdot CSP \cdot day^{-1}$]	0.97	1.09	3.09	3.34	0.58
$\langle Pr_r \rangle$ [$g \cdot cm^{-3} \cdot CSP \cdot day^{-1}$]	1.10	0.98	3.05	2.99	0.58
$\langle SC_e \rangle [cm^{-3} \cdot mg^{-1}]$	0.42	0.37	0.26	0.24	1.39
$\langle SC_r \rangle [cm^{-3} \cdot mg^{-1}]$	0.37	0.41	0.27	0.27	1.40

*Percent values are related to SMB 1 of Table 4.17.

pattern based on zero feed concentration in the first subinterval and the maximum in the second turns the separation of extract at high purity the limiting factor to improve even more the separation. Although separating raffinate with high purity produced the highest throughput, the performance when separating the extract with high purity was also close. Those results are significant because the ModiCon+VariCol process with the half of columns increases the throughput concerning the SMB process. That improvement leads to a reduction in capital cost because the number of columns is lowered. The efficiency and recovery of the desired product could be increased even more in the ModiCon+VariCol process when the non-desired enantiomer (distomer) can be converted into a racemic mixture. Recent works have shown the potential of including a racemization reactor for the distomer product (BREVEGLIERI *et al.*, 2021a,b; HARRIEHAUSEN *et al.*, 2020; VALENTI *et al.*,

2021). On the other hand, when high purity in the two outlet streams is required, the productivity drops a lot, as can be seen in MC+VC 8 of Table 4.24. Therefore reducing the number of columns too much is not convenient when high purities in the extract and raffinate are required.

In the 3-columns ModiCon+VariCol process, one or more than one zones disappear during a switching period. The zones that disappear are those with an average length lower than 1. MC+VC 6 and MC+VC 7 had 3 zones lower than 1, while MC+VC 8 had the four zones lower than 1, as seen in Table 4.24. Although the ModiCon+VariCol process operated with 3 columns, the concept of four zones is kept since the zones that disappear in the different subintervals change. These zones can be determined from elements in the different vectors of the CCS that have zero values. The CCS where t_f moves simultaneously with t_s for MC+VC 6 is: $\mathbf{N}^0 = [0, 2, 0, 1]$, $\mathbf{N}^1 = [1, 1, 0, 1]$, $\mathbf{N}^3 = [1, 1, 1, 0]$, $\mathbf{N}^4 = [0, 1, 1, 1]$ ($\delta\mathbf{t} = [0.62, 0.11, 1.00, 0.50]$). In that example, MC+VC 6 operates with two zones from the beginning of the switching period to the switching time of t_e . In the other subintervals, it operates with three zones.

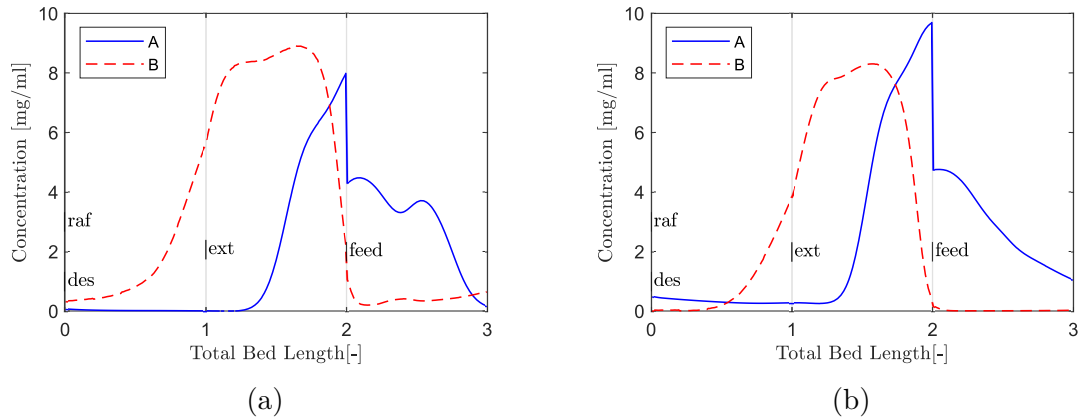


Figure 4.21: Internal concentration profiles for (a) MC+VC 6 and (b) MC+VC 7. The profiles were plotted at the 50% of first switching period of 25th cycle.

The internal concentration profiles for MC+VC 6 and MC+VC 7 of Table 4.24 are presented in Figures 4.21a and 4.21b. Those profiles were plotted at 50% of the first period of the 25th cycle. Different behaviors are seen in these figures. In Figure 4.21a, where the desired product is the extract, it is seen that the less retained component does not contaminate the extract, but the most retained component contaminates the raffinate. That behavior can also be deduced from the optimal average column length of zones for MC+VC 6. A relatively larger average zone IV was required to regenerate the fluid phase and avoid contaminating the extract with A. In Figure 4.21b an opposite behavior is seen. In that case, the MC+VC 7 had a relatively larger average zone I to desorb the most retained component and avoid

contamination in the raffinate.

4.4 Control

The performance of nonlinear model predictive control (NMPC) was evaluated for the VariCol and the ModiCon process. The controller aims to demonstrate its efficiency in meeting the product's specifications and operating in an optimal condition. For the control, a tool called SiMoCon that was generated in the suite of Matlab was used. This tool was developed previously in our group (NETO, 2015) and followed the same philosophy of SiMoBed. The SiMoCon is formed by a digital twin of the SMB process and the NMPC control strategy. For its application in this work, the back-end of the SiMoCon was updated. The variants of the SMB process and the TD and ED models discretized with orthogonal collocation on fixed finite elements were included. Some additional changes were also introduced mainly in the manipulated flow rates to have a closer representation of the experimental unit in our group. The models for the digital twin and the controller were based on the transport dispersion model discretized with orthogonal collocation on fixed finite elements. Two enantioseparations were considered case studies, one for the VariCol process and the other for the ModiCon process. The performance of the NMPC was evaluated with some measured disturbances related to instrumentation malfunction. In those disturbances, it was considered that the model used in the controller represents the VariCol and ModiCon process without error, *i.e.*, the model is perfect. Before applying the disturbances, it was considered that the plant was operating at an optimal point, and it had already reached the cyclic steady state. The disturbances were applied in the first cycle.

4.4.1 Separation of 1,1'-bi-2-naphthol with the VariCol process

The purity in the extract and raffinate in the separation of 1,1'-bi-2-naphthol with an 8-columns VariCol process was controlled with the NMPC. The control architecture presented in Figure 3.3 was applied. The initial status of the VariCol unit was the cyclic steady state, and the operating condition corresponds to an optimal point. Some disturbances in the switching period and the switching times of ports were considered as case study to evaluate the controller performance. The disturbances were applied after the first cycle. The optimal operating point for the separation of 1,1'-bi-2-naphthol was determined through offline optimization. The objective

function of the optimization problem was the same used for the controller, which is based on the maximization of the throughput and minimization of desorbent consumption for purities in the extract and raffinate of 93% and 96%, respectively. The parameters of the TD model and the isotherms are the same as Table 4.12 and Equations 4.3 and 4.3. In the optimization, all internal flow rates, the switching period, and the average column length were considered decision variables. The upper bound for the internal flow rates was set in $66 [cm^3 \cdot min^{-1}]$, corresponding to a maximal pressure drop of 3 bar in zones (see Equation 3.89). The optimal results are presented in Table 4.25, together with other important parameters used in the VariCol process.

Table 4.25: Optimal operation parameters for the enantioseparation of 1,1'-bi-2-naphthol with a 8-columns VariCol process and a maximal pressure drop of 3 bar for each zone

Parameter	Value	Parameter	Value
$\langle P_e \rangle$ [%]	93.00	Q_{II} [$cm^3 \cdot min^{-1}$]	35.03
$\langle P_r \rangle$ [%]	96.00	Q_{III} [$cm^3 \cdot min^{-1}$]	43.56
\bar{N} [-]	[1.71, 2.41, 2.58, 1.30]	Q_{IV} [$cm^3 \cdot min^{-1}$]	33.04
δt [-]	[0.12, 0.41, 1.00, 0.42]	Q_d [$cm^3 \cdot min^{-1}$]	22.94
\mathbf{N}^0 [-]	[2, 3, 2, 1]	Q_e [$cm^3 \cdot min^{-1}$]	20.95
t_s [min]	2.88	Q_f [$cm^3 \cdot min^{-1}$]	8.53
Q_I [$cm^3 \cdot min^{-1}$]	55.98	Q_r [$cm^3 \cdot min^{-1}$]	10.52

Table 4.25 shows that the optimal internal flow rate of zone I was the highest, but it was below the upper bound defined by the maximal pressure drop. The maximal performance of the VariCol process was not limited by the upper bound defined in the pressure drop. The optimal average column length was based on larger zones II and III as expected for the VariCol process. The normalized switching times of the ports (δt) and the initial column configuration (\mathbf{N}^0) correspond to the CCS where the feed port moves simultaneously to the switching period.

The tuning parameters of the controller were selected by trial and error. Those parameters are based on a compromise between computational effort and the robustness of the controller. The sampling time, the prediction horizon (H_p), and the control horizon (H_c) were set to $1t_s$, $H_p = 8t_s$ (1 cycle), and $H_c = 1t_s$, respectively. The weighting factors for the setpoint term and desorbent term were $\lambda_1 = 10^6$ and $\lambda_2 = 0.1$ (see Equation 3.90). Those values were the same used to calculate the optimal initial operation point. Disturbances in the switching period and the switching time of outlet ports were considered. The second disturbance is more associated with the VariCol process operation.

4.4.1.1 Disturbance on the switching period

The first disturbance applied in the VariCol process was a reduction and increment of -25% and +25% concerning the initial value of the switching period (t_s). These disturbances were applied at the end of the first cycle. The response of the system on open-loop (without the controller actions) for the positive and negative disturbances is presented in Figure 4.22a. The system's response on closed loop (the controller is activated) is analyzed for the disturbance with the highest effect on the purity of products. Those results are shown in Figure 4.22b and correspond for the disturbance of -25% in the switching period.

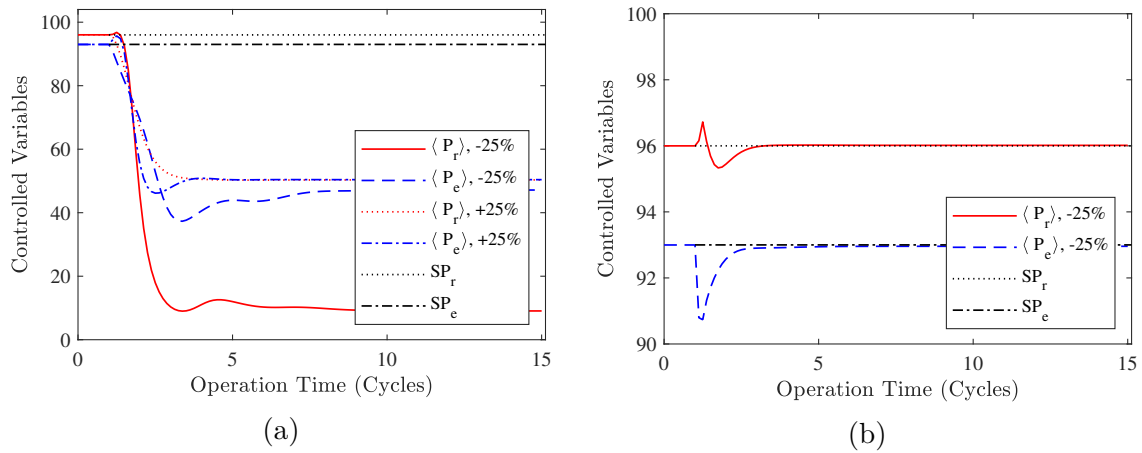


Figure 4.22: Response of the VariCol process to a disturbance on the switching period. (a) Uncontrolled system for disturbances of +25% and -25%; (b) controlled system for disturbance of -25%.

Figure 4.22a shows that the positive and negative disturbances in the switching period had a significant effect on the purity of the extract and the raffinate. In the two cases, the purity of extract and raffinate fell below 50%. That shows that disturbances in the switching period had relevant effects on the system, making even the less and the most retained components appear in a higher proportion in the inverted ports. When the controller was activated for the negative disturbance, it responded satisfactorily, bringing back the purities to the desired values, as observed in Figure 4.22b. The purities were returned to the desired values in about two cycles. Those results show the potential of the NMPC controller to reject disturbances that could bring deleterious effects on the quality of the products. The control actions applied to reject the disturbance were determined using the four internal flow rates as decision variables. The manipulated variables were Q_d , Q_e , Q_f , and Q_{II} . The variations of the manipulated and the internal flow rates are presented in Figures 4.23a and 4.23b.

Figure 4.23a shows that the first control action was slightly aggressive to correct

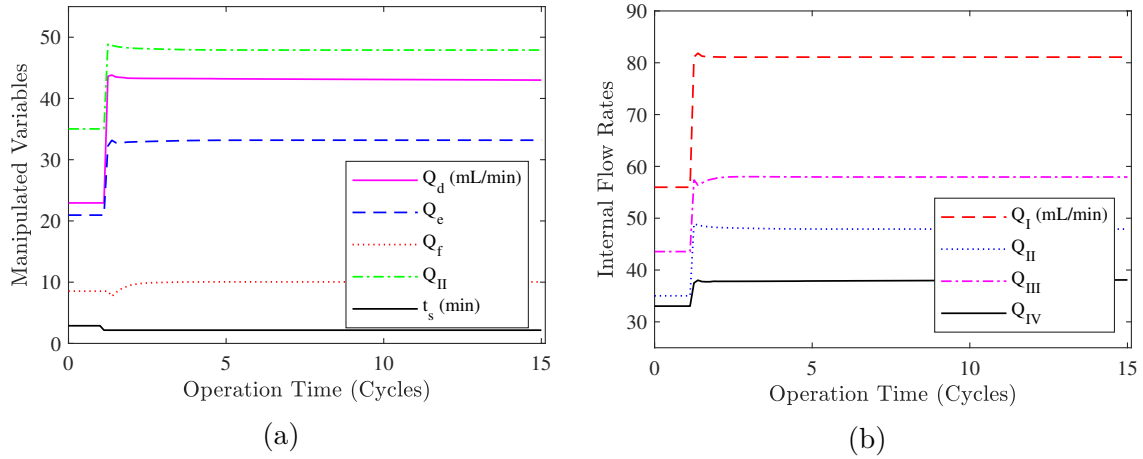


Figure 4.23: Manipulated variables and internal flow rates for the disturbance of -25% on the on the flow rate of desorbent pump. (a) Disturbance and manipulated; (b) Internal flow rates.

the effect of the disturbance. That response of the controller is due to the magnitude of the disturbance and the lower control horizon ($H_c = 1$). However, the control actions were adequate, and the controller stabilized in a short time. The reduction in the switching period was counteracted with an increase in the internal flow rates as seen in Figure 4.23b. It was necessary to increase the upper bound of the internal flow rate of zone I above de value defined for the pressure drop of 3 bar ($66 [cm^3 \cdot min^{-1}]$) to make the system's control possible. The new point had an elevated increment in the solvent with a small increment in the throughput, as seen in Figures 4.23a and 4.23b. The difference between the computational effort to calculate the control actions and the sampling time (the same switching period) is presented in Figure 4.24.

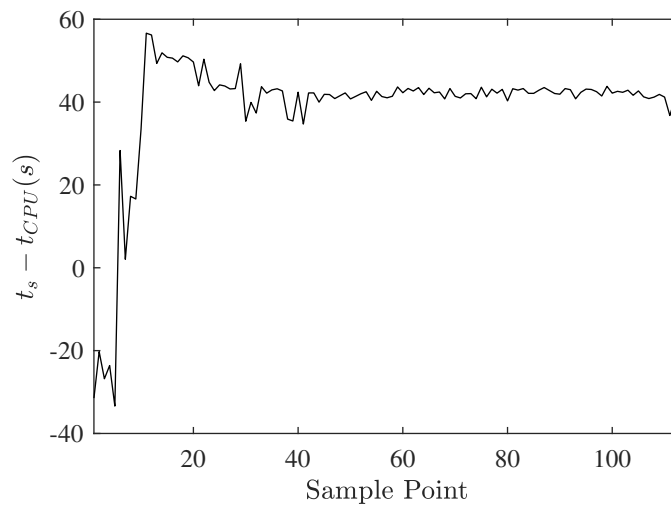


Figure 4.24: Difference between the sampling time and the computational effort required to solve the control optimization problem.

Figure 4.24 shows that the difference between the computational effort and the

sampling time was negative at the beginning of the disturbance. For most of the points, it was positive. That shows the potential of the NMPC to be used in real-time applications. The computational effort could be improved with a more efficient computer or other tuning parameters. For instance, the sampling time could be increased to more than one switching period. However, in those cases, a longer time interval might be necessary to control the system. Additionally, the disturbance could have a more significant effect on the quality of the products before returning the purity to the desired values.

4.4.1.2 Disturbance on the switching time of extract and raffinate and ports

Common disturbances that can take place in the VariCol process are the variation of the switching time of some of the ports. In this case, a reduction of 25% in the switching time of the extract port (t_e) and an increment of 25% in the switching time of the raffinate port (t_r) were considered. The disturbances were applied for the CCS, where t_f moves simultaneously with t_s . The disturbances only affected switching times of extract and raffinate ports and not the switching period. The vector of normalized switching time of ports ($\delta\mathbf{t}$) before the disturbances is presented in Table 4.25, where t_e and t_r are in the second and last positions, according to Equation 3.1. The CCS continues to be the same after the disturbances since the order of movements of ports does not change. The values that $\delta\mathbf{t}$ takes after the disturbances of t_e and t_r are [0.12, 0.31, 1.00, 0.42] and [0.12, 0.41, 1.00, 0.52]. As the average column lengths also changes with the disturbances, the new values are [1.81, 2.31, 2.58, 1.30] (disturbance in t_e) and [1.71, 2.41, 2.48, 1.40] (disturbance in t_r). The response of the system for the disturbances without the control actions is presented in Figure 4.25a. The system's response with the controller activated is analyzed for the disturbance with the highest effect on the purity of products. Those results are shown in Figure 4.25b and correspond for the negative disturbance of disturbance t_e .

Figure 4.25a shows that the disturbance of t_e affects more the purity in the extract, and the disturbance of t_r affects the purity of the raffinate principally. The maximal variation of purity in each case was around 1%. Although the disturbances had minor effects on the system, a control strategy is necessary to guarantee the quality of products. When the controller is activated for the negative disturbance of t_e , the purity of the extract and raffinate was brought back to the desired value. After the disturbance, less than three cycles were necessary to fulfill the product's quality requirements. The optimization-based control problem was determined using

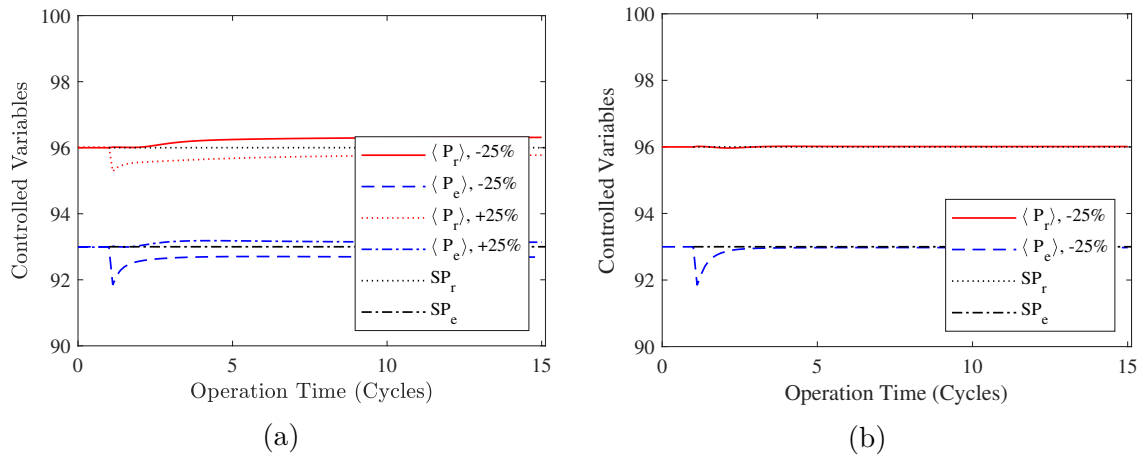


Figure 4.25: Response of the VariCol process to a disturbance on the switching time of extract and raffinate ports. (a) Uncontrolled system for disturbances of -25% and +25%; (b) controlled system for disturbance of -25% in t_e .

the four internal flow rates as decision variables. The manipulated variables were Q_d , Q_e , Q_f , and Q_{II} . The manipulated variables and the internal flow rates are presented in Figures 4.26a and 4.26b.

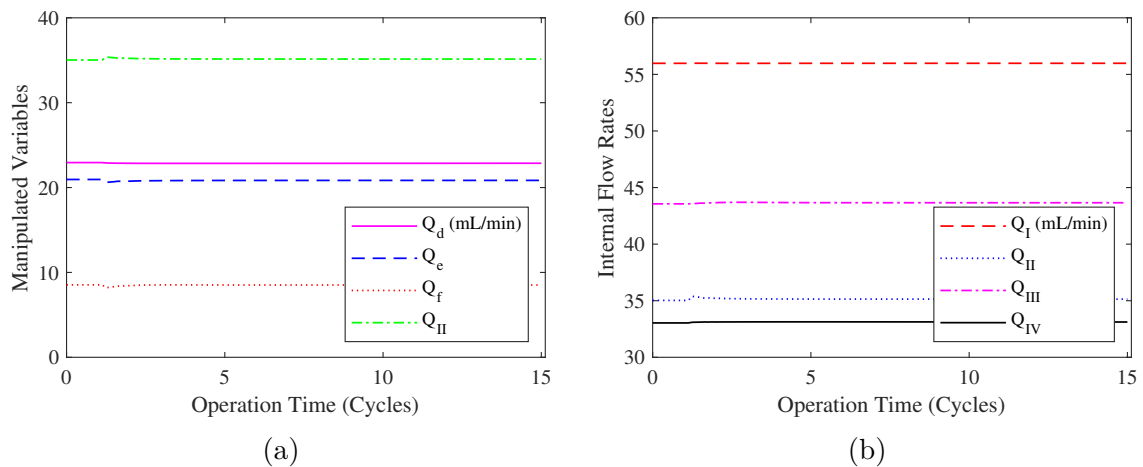


Figure 4.26: Manipulated variables and internal flow rates for the disturbance of -25% on the extract port's switching time. (a) Manipulated variables; (b) Internal flow rates.

Figure 4.26a shows that a slight reduction in feed flow rate was necessary to reject the disturbance. The control actions were smooth, although the controller had a small horizon, $H_c = 1$. The manipulated variables stabilized in a short time, as seen in Figure 4.26a. The reduction in solvent consumption for the new optimal point calculated with the controller was less noticeable than the throughput decrease (see Figure 4.26a and 4.26b). The difference between the computational effort to calculate the control actions and the sampling time is presented in Figure 4.27.

Figure 4.27 shows that the difference between the computational effort and the

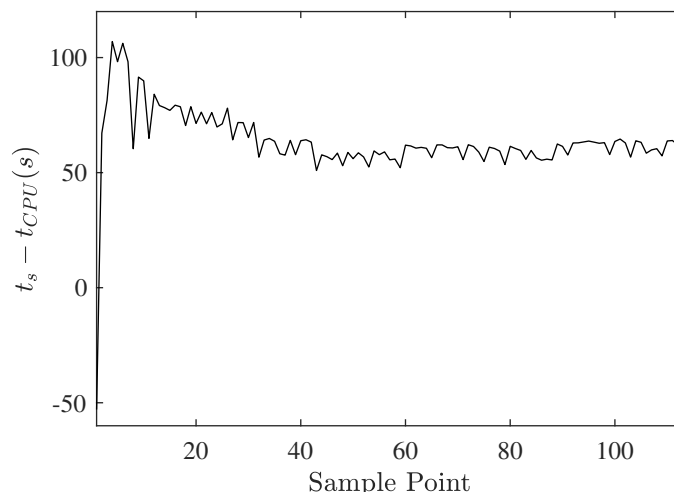


Figure 4.27: Difference between the sampling time and the computational effort required to solve the control optimization problem.

sampling time was negative only in the first sampling point. On the other points, it was positive. That shows the potential of the NMPC for real-time applications of disturbances associated with the VariCol process. The computational effort in the first point could be reduced with a more appropriate initial optimization point, a more efficient computer, and other tuning parameters.

4.4.2 Separation of guaifenesin with the ModiCon process

The extract and raffinate purity was controlled with the NMPC for the enantioseparation of guaifenesin with a 6-columns ModiCon process. The control architecture presented in Figure 3.3 was applied. The ModiCon process considered is based on large zones I and II and a feed concentration pattern of zero in the first subinterval and the maximal in the second, which are the characteristics that most improve the separation, as presented in Section 4.3. The column configuration used for the 6-columns ModiCon process was [2, 2, 1, 1], and the pattern of feed concentration was 0 mg/ml in the first 60% of t_s and 10 mg/ml in the remaining 40%, as ModiCon 4 of Table 4.23. The optimal operating point for the enantioseparation of guaifenesin with the ModiCon process was determined through offline optimization. The objective function was the same as the controller, based on maximizing the throughput and minimizing the solvent consumption for the desired purity of 99% in the products (see Equation 3.90). The parameters and isotherms of the TD model were the same as in Table 4.18 and Equations 4.7 and 4.8. In the optimization, all internal flow rates and the switching period were considered as decision variables. The upper bound for the internal flow rates was set to $27\text{ [cm}^3 \cdot \text{min}^{-1}\text{]}$, corresponding to a maximal pressure drop of 6 bar in the zones (see Equation 3.89). The optimal result for the

switching period and the internal flow rates are presented in Table 4.26, together with main characteristics of the ModiCon process used.

Table 4.26: Optimal operation parameters for the enantioseparation of guaifenesin with a 6-columns ModiCon process and a maximal pressure drop of 6 bar for each zone

Parameter	Value	Parameter	Value	Parameter	Value
$\langle P_e \rangle$ [%]	99.00	t_s [min]	1.09	Q_d [$cm^3 \cdot min^{-1}$]	11.92
$\langle P_r \rangle$ [%]	99.00	Q_I [$cm^3 \cdot min^{-1}$]	24.56	Q_e [$cm^3 \cdot min^{-1}$]	11.27
$\mathbf{c}_{f,i}$ [$mg \cdot cm^{-3}$]	[0, 10]	Q_{II} [$cm^3 \cdot min^{-1}$]	13.28	Q_f [$cm^3 \cdot min^{-1}$]	13.72
$\delta \mathbf{t}_{sb}$ [-]	[0.6, 1]	Q_{III} [$cm^3 \cdot min^{-1}$]	27.00	Q_r [$cm^3 \cdot min^{-1}$]	14.37
$\bar{\mathbf{N}}$ [-]	[2, 2, 1, 1]	Q_{IV} [$cm^3 \cdot min^{-1}$]	12.63		

Table 4.26 shows that in the optimal operating condition for the 6-columns ModiCon process, the flow rate of zone III was the largest and also reached the upper bound defined by the maximal pressure drop. Therefore, the maximal throughput in this system is limited by the highest allowable pressure drop in zones. Table 4.26 also shows that the optimal switching period decreased significantly, more than half that ModiCon 4 of Table 4.23. In the control of the SMB process, the sampling time is usually defined as the switching period since the average purity is known in each period (ANDRADE NETO *et al.*, 2016; SONG *et al.*, 2006a; TOUMI and ENGELL, 2004). This example is challenging since calculating the control actions in a shorter time than the sampling time is one of the difficulties in applying the NMPC. Additionally, in the operating conditions, the enantioseparation of the guaifenesin with the ModiCon process occurs in a region with nonlinear equilibrium, which is a more complex scenario than in the case of operating in a region with linear equilibrium.

The tuning parameters of the controller were selected by trial and error and are the same used in the previous case study. In this case study, disturbances in the desorbent pump, feed pump, and solenoid valve malfunctions were considered. The last disturbance is most related to the ModiCon process operation.

4.4.2.1 Desorbent pump malfunction

A common disturbance that could take place in an SMB unit is the desorbent pump malfunction. In this case, positive and negative variations of 25% in the flow rate of desorbent were considered. A change in the flow rate of the raffinate stream follows that disturbance to guarantee the mass balance. That stream is the one that does not have a pump and follows all the other external disturbances. The response of the system without the control actions for the positive and negative disturbances is

presented in Figure 4.28a. The system's response with the controller activated is analyzed for the disturbance with the highest effect on the purity of products. Those results are shown in Figure 4.28b and correspond for the disturbance of -25% in the flow rate of desorbent.

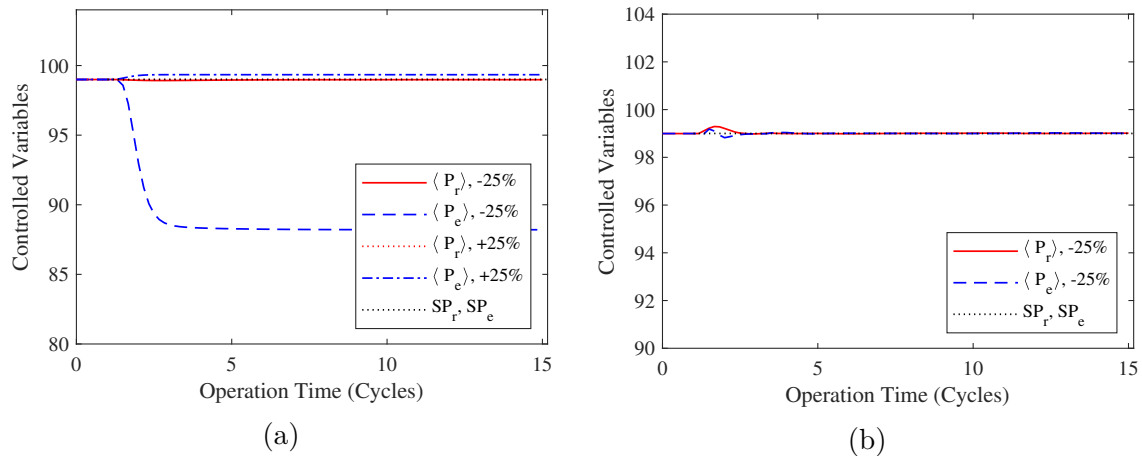


Figure 4.28: Response of the ModiCon process to a disturbance on the flow rate of desorbent pump. (a) Uncontrolled system for disturbances of -25% and +25%; (b) controlled system for disturbance of -25%.

Figure 4.28a shows that the disturbances affected specially the extract purity. No variations in the the raffinate purity were seen. The negative disturbance was the one that produced the most variation in the extract purity. It fell from 99% to almost 88%. That result was expected since the system was operating in an optimal point that uses the minimal solvent consumption to reach the desired purity. The positive disturbance improved the purity of the extract, which was also expected. When the NMPC was activated to respond to the negative disturbance (see Figure 4.28), the controller rejected it and brought back the purity of the extract at the value of 99%. The control took about 2 cycles to fulfill the requirements of purity in the extract after the disturbance was applied. That is an important result since the controller was able to respond satisfactorily to a disturbance of a high magnitude. The manipulated and decision variables to reject de disturbance were Q_e , Q_f , Q_{II} and t_s . The flow rate of the desorbent was fixed after the disturbance was applied. The manipulated variables and the internal flow rates are presented in Figures 4.29a and 4.29b.

Figure 4.29a shows that the control actions were slightly aggressive when the disturbance took place. That is mainly because the disturbance has a significant magnitude, and the control horizon was low ($H_c = 1$). However, those control actions were effective in response to the disturbance. The new operation point calculated with the control shows that the performance of the system decreased. As the desorbent decreased, the throughput also decreased. The switching period needed to return

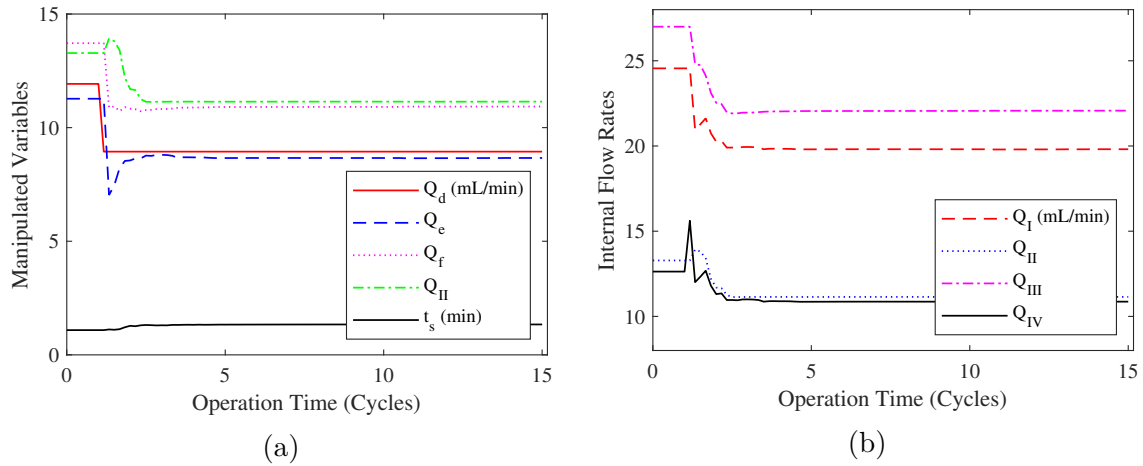


Figure 4.29: Manipulated variables and internal flow rates for the disturbance of -25% on the flow rate of desorbent pump. (a) Disturbance and manipulated variables; (b) Internal flow rates.

the purity of the extract in the desired value increased, as seen in Figure 4.29a. That allowed to increase the time window to calculate the control actions since the switching period is the same sampling time. The difference in the sampling time and the computational effort to solve the nonlinear control optimization problem is showed in Figure 4.30.

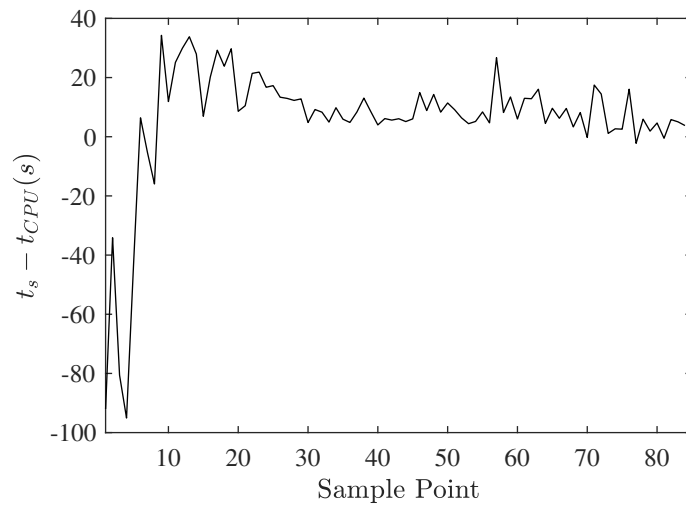


Figure 4.30: Difference between the sampling time and the computational effort required to solve the control optimization problem.

The difference between the sampling time and computational burden was positive in most of the cycles. However, at the beginning of the disturbance, it was negative. A reduction of computational effort can be obtained with a more efficient computer (more cores and a faster processor). Additionally, larger sampling times can be selected, for example, two or three switching periods. However, in those cases, controlling the system will take more time, and the quality of products could be

affected for a longer time interval. Although the computational exceeded the limits of the sampling time at the beginning of the disturbance, the results are significant since the controller shows the potential to be used in future real-time applications.

4.4.2.2 Feeding pump malfunction

Another common disturbance that can take place in the SMB unit is the feeding pump malfunction. In this case, positive and negative disturbances of 25% in the feed flow rate were considered. The disturbances were applied at the end of the first cycle. The response of the system in an open loop for the negative and positive disturbances is presented in 4.31a. The system's response with the controller activated is analyzed for the disturbance with the highest effect on the purity of products. Those results are shown in Figure 4.31b and correspond to the positive disturbance in the feeding pump.

The system's response to the positive disturbance when the controller is activated is presented in Figure 4.31b.

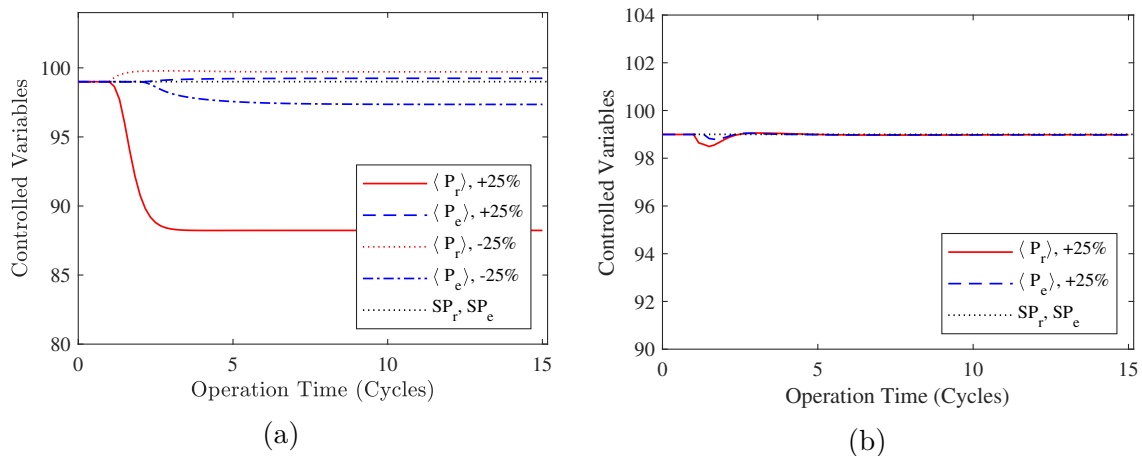


Figure 4.31: Response of the ModiCon process to a disturbance on the flow rate of feed pump. (a) Uncontrolled system for disturbances of +25% and -25%; (b) controlled system for disturbance of +25%.

Figure 4.31a shows that the positive disturbance had a more significant effect on the purity of products. The purity of raffinate was the most affected, and it fell from 99% to about 88%. An increment in the feed flow rate also needs an increment in desorbent consumption to keep the quality of products. The negative disturbance had a minor effect on the purity of products, as seen in Figure 4.31a. Note that the effects of the disturbance on the feed flow rate were opposite to those of the desorbent flow rate. When the control is activated for the disturbance of +25% in the feed flow rate, the purity values were brought back to the desired value in an interval fewer

than two cycles, as seen in Figure 4.31b. The controller's response was adequate for this disturbance, showing the potential of the NMPC controller for challenging disturbances. The manipulate and decision variables to reject the disturbance were Q_e , Q_d , Q_{II} , and t_s . The feed flow rate was fixed after the disturbance was applied. The control actions applied in the system to reject the disturbance and the internal flow rates are presented in Figures 4.32a and 4.32b.

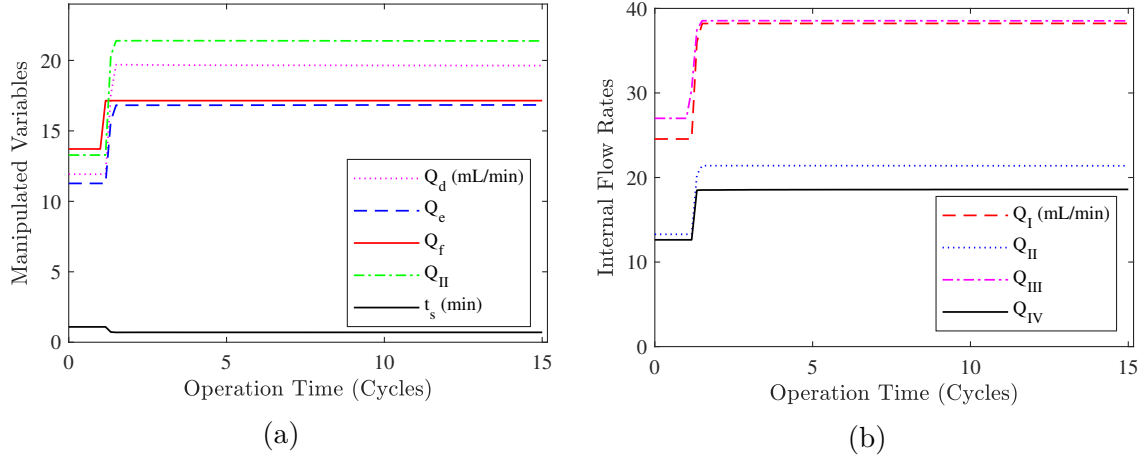


Figure 4.32: Manipulated variables and internal flow rates for the disturbance of +25% on the on the flow rate of feed pump. (a) Disturbance and manipulated variables; (b) Internal flow rates.

Figure 4.32a shows that the most decisive action of the controller was at the beginning of the disturbance, which was expected due to the high magnitude of the disturbance and the control horizon of 1. Although the control horizon was low, it was effective since no oscillations were seen in the manipulated variables, common in controllers with aggressive responses. The controller's actions led to an increase in all the external flow rates and a decrease in the switching period. The desorbent flow rate presented a high increase to compensate for the rise of the feed flow rate and keep the quality in the products. The internal flow rates also increased, as seen in Figure 4.32b. The values of internal flow rates of zones I and III were higher than $27 [cm^3 \cdot min^{-1}]$ that was the initial upper bound defined for a pressure drop of 6 bar. In this case, it was necessary to disregard the upper bound of maximal pressure drop in the optimal control problem to bring back the purity of products in the desired value. Attempts to control the system with upper bounds in the pressure drop that lead to a maximal internal flow rate of zone III below that one of Figure 4.32b were also made. In those cases, the controller could not bring back the purities to the desired value, leaving an offset error. Therefore, in the design of the SMB process variants, flexibility for additional increments in the pressure drop needs to be considered. The difference between the computational effort to calculate the control actions and the sampling times was also calculated for all sampling points. The

results are presented in Figure 4.33.

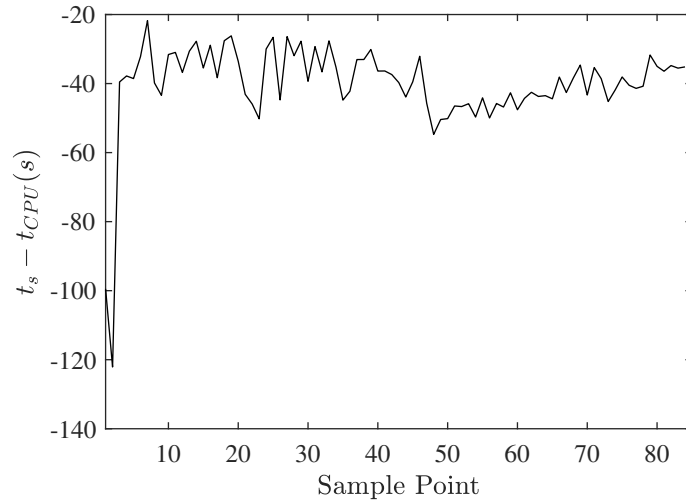


Figure 4.33: Difference between the sampling time and the computational effort required to solve the control optimization problem.

Figure 4.33 shows that the difference between the computational effort and the sampling time was negative in all sampling points. The reduction of the switching period to $t_s = 0.70 [min]$ (the same sampling time) after the disturbance, as seen in Figure 4.32a, affected those results. Larger sampling times and a most efficient computer can be used to reduce the computational effort. The positive feed flow rate disturbance was a complex and challenging scenario. The controller responded satisfactorily, fulfilling the purity requirements and bringing the system to a new optimal operating point.

4.4.2.3 Solenoid valve malfunction

An SMB unit can be adapted into two modulation subintervals ModiCon process using a solenoid valve with two inputs. One of the malfunctions that could occur in this valve is the duration of feed concentration subintervals. Two disturbances in the times of subintervals (δt_{sb}) in a switching period were considered. Those disturbances were the variations of -25% and +25% concerning the duration of the first subinterval, getting the times of $\delta t_{sb} = [0.45, 1]$ and $\delta t_{sb} = [0.75, 1]$. The feed concentration in the subintervals was kept in $\mathbf{c}_{f,i} = [0, 10] [mg \cdot cm^{-3}]$. The response of the system to those two disturbances without any control actions is presented in Figure 4.34a. The system's response with the controller activated is presented for the disturbance with the highest effect on the purity of products. Those results are shown in Figure 4.34b and correspond to the negative disturbance of the first subinterval.

The response of the system to the negative disturbance when the controller is activated is presented in Figure 4.34b.

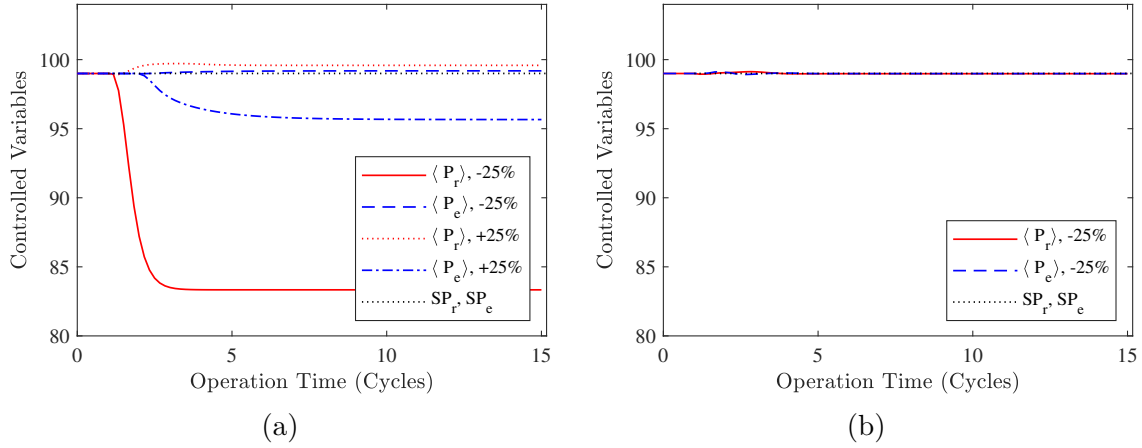


Figure 4.34: Response of the ModiCon process to a disturbance on the times of subintervals (δt_{sb}). (a) Uncontrolled system for disturbances of -25% and +25% concerning the first subinterval; (b) Controlled system for disturbance of -25%.

Figure 4.34a shows that the negative disturbance in $t_{sb,1}$ has a more significant effect on the purity of products than the positive disturbance. The purity of the raffinate was the most affected by the negative disturbance. It fell from 99% to almost 84%. The positive disturbance in $t_{sb,1}$ produced a slight variation in the purities. When the controller was activated for the disturbance of -25%, the purity values were brought back to the desired values, as seen in Figure 4.34b. The controller was able to keep the purity of the two products above 99% all the time. Those results are significant because it shows the potential of using the NMPC to control the most diverse disturbances for the conventional SMB process and its variants. The control actions applied to reject the disturbance were determined using the four internal flow rates as decision variables. The manipulated variables were Q_d , Q_e , Q_f , and Q_{II} . The variation of the manipulated and the internal flow rates are presented in Figures 4.35a and 4.35b.

Figure 4.35a shows that the first control actions after the disturbance were decisive to fulfill the purity requirements. Although the controller was aggressive, it performed well to control the system. The new optimal operation point calculated with the controller's action decreased the external flow rates and, therefore, the throughput. That can be associated with the increment of the average concentration in the system from $\bar{c}_{f,i} = 4$ to $\bar{c}_{f,i} = 5.5$, caused by the rise in the duration of the second subinterval with the disturbance. Increments in the average feed concentration could lead to a reduction of the external flow rates (SCHRAMM *et al.*, 2003a,b). However, the internal flow rates of zone I and II in the new optimal operating point were below the upper bound of the optimization control problem ($27 [cm^3 \cdot min^{-1}]$), as seen in

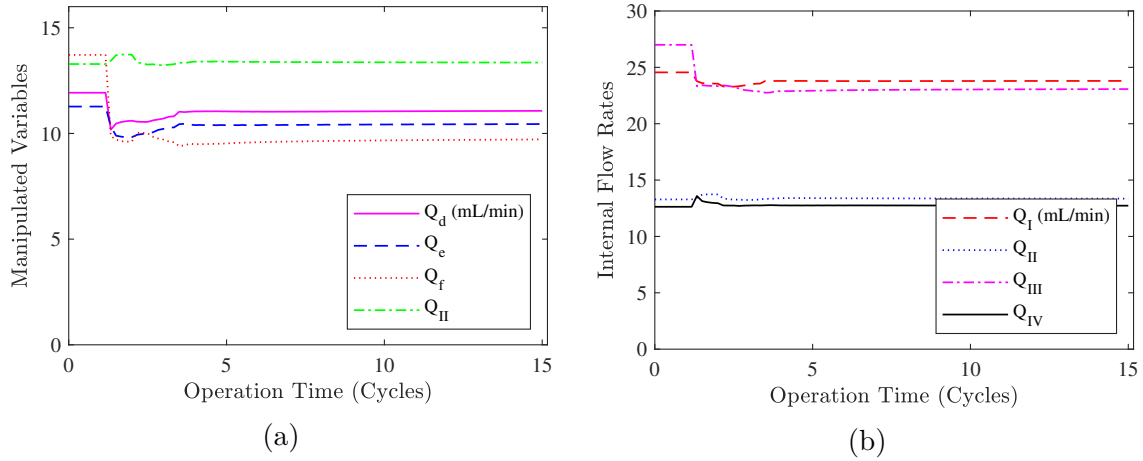


Figure 4.35: Manipulated variables and internal flow rates for the disturbance of -25% on the $t_{sb,1}$. (a) manipulated variables; (b) Internal flow rates.

Figure 4.35b. That result is explained because the switching period was not used as a decision variable in the optimization control problem. The difference between the computational effort and the sampling time to calculate the control actions is presented in Figure 4.36.

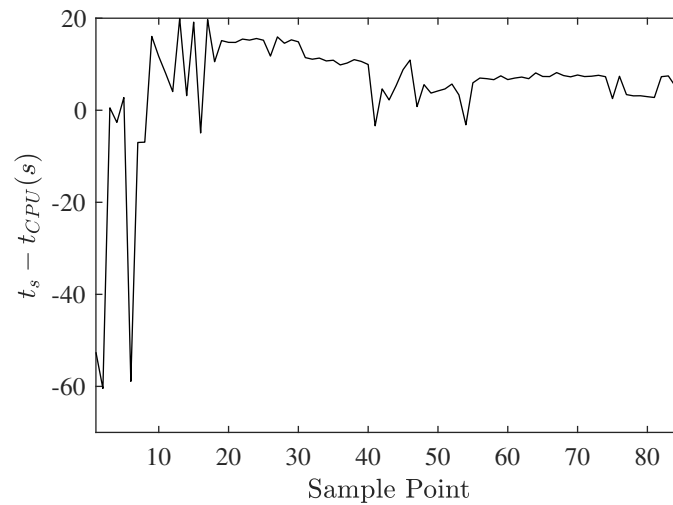


Figure 4.36: Difference between the sampling time and the computational effort required to solve the control optimization problem.

At the beginning of disturbance and in few other points, the difference between computational effort and sampling time was negative, as seen in Figure 4.36. However, in most of the points, it was positive. As described in the previous case studies, the computational effort could be improved with a more efficient computer and other tuning parameters. For example, the sampling time could be increased.

Chapter 5

Conclusions and future works

5.1 Conclusions

Simulation and model Validation

The front-end and the back-end of the package called SiMoBed were improved to include different SMB process variants. Those variants were ModiCon, VariCol, PowerFeed, and combinations among them. In the back-end of SiMoBed, the equilibrium dispersion and the transport dispersion mathematical models for chromatographic columns were discretized and implemented explicitly and implicitly for different types of isotherms. The orthogonal collocation on fixed finite elements was used as the discretization method. The performance of explicit and implicit approaches was evaluated and compared with some case studies. The explicit approach was also compared with an equivalent explicit approach for the mathematical models discretized with finite differences.

The explicit and implicit approaches of the mathematical models discretized with orthogonal collocation on fixed finite elements had some advantages and disadvantages compared to each other. The sparsity of the implicit approach was more convenient than the one of the explicit approach. However, the number of equations solved simultaneously in each integration stage increased for the implicit approach. When the two approaches were compared for the enantioseparation of 1,1'-bi-2-naphthol with the VariCol process, the explicit approach's computational effort was inferior to the implicit one. For optimizing and controlling the SMB process variants, the explicit approach was adopted. When comparing the explicit approach for orthogonal collocation on fixed finite elements with the equivalent explicit one for finite differences, the former was much more efficient, approximating the solution

and reducing the computational effort. In orthogonal collocation, much smaller discretization points were required to get a good approximation. About 20 internal points (taking into account internal points of all elements) were required, while in finite differences at least 320 internal points were needed. That produces a significant difference in the number of differential equations that need to be solved and, therefore, computational effort.

Optimization of VariCol process

A new approach to solve the design optimization problem for the VariCol process, with minimal port-shifting, was proposed. In this approach, the optimization problem for all possible operation regions was solved with only one NLP that includes the average column length of three zones in the decision variables. The advantage of using average column lengths is because all possible CCSs for the VariCol process can be determined. These CCSs can be used in the optimization stage since they give the same results in the cyclic steady state. Therefore, the optimization problem of the VariCol process with the average column length as decision variables covers the entire search region.

Various optimization problems were carried out to evaluate the proposed optimization strategy and deeply study the VariCol process. Two enantioseparations with different types of isotherms and model parameters were considered as examples. In the first case, different optimizations that maximize the throughput for the enantioseparation of 1,1'-bi-2-naphthol, described by a bi-Langmuir isotherm, were solved for both 8-columns VariCol and 8-columns SMB units. From those optimizations, the asynchronous movement of the ports of the VariCol process allowed for an increment of the throughput in 7.10% at the same purities as the SMB. Additionally, it was shown that the performance in terms of the computational effort of the proposed optimization methodology was superior to the one based on the relative switching times. In the second case study, the optimization of the aminoglutethimide enantioseparation, labeled with a linear-Langmuir isotherm, was accomplished with the 5-columns VariCol and 6-columns SMB units. These optimizations showed that the productivity of the 5-columns VariCol process was inferior to the 6-columns SMB process for purities higher than 98.70%. However, when the desired purities decreased, the performance incremented faster than the 6-columns SMB process. The proposed methodology that reduces the MINLP formulation to an NLP formulation presented an excellent performance in the two case studies. That is advantageous for real-time applications and hybrid operation modes that include the asynchronous movement of the ports.

Performance comparison of some SMB process variants

The operation modes based on the modulation of feed concentration, the length of zones, and the combination of these two, were studied and compared with the conventional operation. The enantioseparation of guaifenesin was considered as a case study. A detailed analysis was presented for the ModiCon process. The combination of the ModiCon and the VariCol processes was described in detail. The performance of different operation modes with 5 and 6 columns was compared.

In the ModiCon process study, the optimal modulation pattern of feed concentration is formed by two subintervals. More than two subintervals do not improve the optimal solution. In these two subintervals, the first one is based on null feed concentration, and the second one in the maximal concentration defined by the solubility limit. The intermittence in the feed concentration leads to a shifting of the front side of the concentration profile of the most retained component to the left in zone III and the variation of the wave propagation velocity. That allows an increment in the throughput compared to the SMB process based on a constant feed. That is a significant result for the ModiCon process since there is a slight increase in complexity concerning the SMB. Adapting a real SMB plant to operate in those conditions would be simple.

In the hybrid ModiCon+VariCol, although the VariCol process has different column configuration sequences with the same results in the cyclic steady state, the appropriate column configuration sequence to make the integration was the one where the feed port moves simultaneously as the switching period. In the optimizations of the hybrid ModiCon+VariCol, larger zones I and II were found, different of the VariCol and the SMB processes where the larger zones are II and III. From those results, it was found that the ModiCon process with larger zones I and II also produce the best results. The modulation of feed concentration caused that behavior. It is worth noting that the throughput of the ModiCon and the hybrid ModiCon+VariCol processes with larger zones I and II almost doubled compared with the conventional operation.

In systems with 6 columns, additional benefits were not seen with the hybrid operation than the ModiCon process. In the 5 columns, the combination of ModiCon+VariCol had a more pronounced throughput than the ModiCon process alone. Using a rational length of zones takes more relevance in systems with a low number of columns than a system with a higher column number. Therefore the application of hybrid operation could be more interesting for systems with a low number of columns. In systems with many columns, the ModiCon+VariCol process could be used as

a reference guide to define the appropriate column configuration in the ModiCon process.

Control

The efficiency of nonlinear model predictive control was evaluated for the VariCol and the ModiCon process. The transport dispersion model discretized with orthogonal collocation on fixed finite elements was used as the controller and the digital twin model. Positive and negative disturbances of 25% related, especially with instrumentation malfunction, were applied in the digital twin. Some of these disturbances can only occur in the VariCol or ModiCon processes. The enantioseparations of 1,1'-bi-2-naphthol and guaifenesin were considered as examples to apply the different disturbances. In the first enantioseparation, disturbances in the switching period and the switching time of outlet ports were applied. In the second enantioseparation, disturbances in the desorbent flow rate, feed flow rate, and the duration of the first subinterval of feed concentration were applied. In the two enantioseparations, the initial operating point was determined through offline optimization.

The controller responded satisfactorily to all disturbances. In all cases, it fulfilled the purity of raffinate and extract and optimized the process's economics. For some sampling points in some disturbances, the computational effort was higher than the sampling time. In those cases, The computational effort could be reduced using more efficient computers and other tuning parameters. For example, in the last case, two or more switching periods could be used as sampling time. Although the computational effort of the controller exceeded the sampling time in some cases, it has a high potential to be used in future real-time applications. The high advantage of the NMPC is that it could reject the most disturbances for any SMB process variant.

5.2 Future works

Different theoretical and experimental works can be performed with the contributions of this work. Some examples are presented as follow:

- The performance of the different SMB process variants can be evaluated and compared experimentally, emphasizing the theoretical results obtained in this thesis for the ModiCon and ModiCon+VariCol processes.

- The NMPC can be implemented and evaluated experimentally for the SMB process and its different variants.
- Evaluate which of the transport dispersion model can be more appropriate to better represent experimental data, if the transport dispersion in terms of total or bed porosity.
- Evaluate the wave propagation theory for optimization and control of the SMB process and its variants.
- Study the separation of ternary or more component mixtures theoretically, with two or more units in a cascade of variants of the SMB process.
- Controlling and optimizing the SMB unit using artificial intelligence techniques.
- Integrate the SMB process with other units, such as racemization and crystallization.

References

- ABEL, S., ERDEM, G., AMANULLAH, M., et al., 2005, “Optimizing control of simulated moving beds—experimental implementation”, *Journal of Chromatography A*, v. 1092, n. 1, pp. 2–16.
- ANDRADE NETO, A., SECCHI, A., SOUZA JR, M., et al., 2016, “Nonlinear model predictive control applied to the separation of praziquantel in simulated moving bed chromatography”, *Journal of Chromatography A*, v. 1470, pp. 42–49.
- ANICETO, J. P., SILVA, C. M., 2015a, “Preparative chromatography: batch and continuous”, *Analytical separation science*, pp. 1207–1313.
- ANICETO, J. P., SILVA, C. M., 2015b, “Simulated moving bed strategies and designs: from established systems to the latest developments”, *Separation & Purification Reviews*, v. 44, n. 1, pp. 41–73.
- ANICETO, J. P., CARDOSO, S. P., SILVA, C. M., 2016, “General optimization strategy of simulated moving bed units through design of experiments and response surface methodologies”, *Computers & Chemical Engineering*, v. 90, pp. 161–170.
- ANICETO, J., AZENHA, I., DOMINGUES, F., et al., 2018, “Design and optimization of a simulated moving bed unit for the separation of betulinic, oleanolic and ursolic acids mixtures: Experimental and modeling studies”, *Separation and Purification Technology*, v. 192, pp. 401–411. ISSN: 1383-5866. doi: <https://doi.org/10.1016/j.seppur.2017.10.016>. Available in: <https://www.sciencedirect.com/science/article/pii/S1383586617314193>.
- AZEVEDO, D. C., RODRIGUES, A. E., 1999, “Design of a simulated moving bed in the presence of mass-transfer resistances”, *AIChE journal*, v. 45, n. 5, pp. 956–966.

- AZEVEDO, D. C., RODRIGUES, A. E., 2001, “Fructose–glucose separation in a SMB pilot unit: modeling, simulation, design, and operation”, *AIChE journal*, v. 47, n. 9, pp. 2042–2051.
- BAGCHUS, W. M., BEZUIDENHOUT, D., HARRISON-MOENCH, E., et al., 2019, “Relative Bioavailability of Orally Dispersible Tablet Formulations of Levo- and Racemic Praziquantel: Two Phase I Studies”, *Clinical and Translational Science*, v. 12, n. 1, pp. 66–76. doi: <https://doi.org/10.1111/cts.12601>. Available in: <<https://ascpt.onlinelibrary.wiley.com/doi/abs/10.1111/cts.12601>>.
- BENTLEY, J., KAWAJIRI, Y., 2013, “Prediction-correction method for optimization of simulated moving bed chromatography”, *AIChE Journal*, v. 59, n. 3, pp. 736–746.
- BONILLA-PETRICIOLET, A., MENDOZA-CASTILLO, D. I., REYNEL-ÁVILA, H. E., 2017, *Adsorption processes for water treatment and purification*. Springer.
- BORGES DA SILVA, E., ULSON DE SOUZA, A., GUELLI U. SOUZA, S., 2002, “The use of simulated moving bed in chromatographic separation: study of the SMB configuration”, *Separation science and technology*, v. 37, n. 7, pp. 1489–1504.
- BREVEGLIERI, F., OTGONBAYAR, T., MAZZOTTI, M., 2021a, “Optimizing the Yield of a Pure Enantiomer by Integrating Chiral Simulated Moving Bed Chromatography and Racemization. Part 1: Experiments”, *Industrial & Engineering Chemistry Research*.
- BREVEGLIERI, F., OTGONBAYAR, T., MAZZOTTI, M., 2021b, “Optimizing the Yield of a Pure Enantiomer by Integrating Chiral SMB Chromatography and Racemization. Part 2: Theory”, *Industrial & Engineering Chemistry Research*.
- BROUGHTON, D. B., GERHOLD, C. G., 1961. “Continuous sorption process employing fixed bed of sorbent and moving inlets and outlets”. maio 23. US Patent 2,985,589.
- CALCATERRA, A., D’ACQUARICA, I., 2018, “The market of chiral drugs: Chiral switches versus de novo enantiomerically pure compounds”, *Journal of Pharmaceutical and Biomedical Analysis*, v. 147, pp. 323 – 340. ISSN: 0731-7085. doi: <https://doi.org/10.1016/j.jpba.2017.07.008>. Available in:

<<http://www.sciencedirect.com/science/article/pii/S0731708517314838>>. Review issue 2017.

CALDERÓN SUPELANO, R., BARRETO JR, A. G., ANDRADE NETO, A. S., et al., 2020, “One-step optimization strategy in the simulated moving bed process with asynchronous movement of ports: A VariCol case study”, *Journal of Chromatography A*, v. 1634, pp. 461672. ISSN: 0021-9673. doi: <https://doi.org/10.1016/j.chroma.2020.461672>. Available in: <<https://www.sciencedirect.com/science/article/pii/S0021967320309468>>.

CALDERÓN SUPELANO, R., BARRETO, A. G., SECCHI, A. R., 2021, “Optimal performance comparison of the simulated moving bed process variants based on the modulation of the length of zones and the feed concentration”, *Journal of Chromatography A*, v. 1651, pp. 462280. ISSN: 0021-9673. doi: <https://doi.org/10.1016/j.chroma.2021.462280>. Available in: <<https://www.sciencedirect.com/science/article/pii/S0021967321004040>>.

CHANKVETADZE, B., 2001, “Enantioseparation of chiral drugs and current status of electromigration techniques in this field”, *Journal of Separation Science*, v. 24, n. 9, pp. 691–705. doi: [https://doi.org/10.1002/1615-9314\(20010901\)24:9<691::AID-JSSC691>3.0.CO;2-E](https://doi.org/10.1002/1615-9314(20010901)24:9<691::AID-JSSC691>3.0.CO;2-E). Available in: <<https://onlinelibrary.wiley.com/doi/abs/10.1002/1615-9314%2820010901%2924%3A9%3C691%3A%3AAID-JSSC691%3E3.0.CO%3B2-E>>.

CHING, C., LIM, B., LEE, E., et al., 1993, “Preparative resolution of praziquantel enantiomers by simulated counter-current chromatography”, *Journal of Chromatography A*, v. 634, n. 2, pp. 215–219.

CHITSULO, L., ENGELS, D., MONTRESOR, A., et al., 2000, “The global status of schistosomiasis and its control”, *Acta tropica*, v. 77, n. 1, pp. 41–51.

CIOLI, D., PICA-MATTOCCIA, L., 2003, “Praziquantel”, *Parasitology Research*, v. 90, n. 1, pp. S3–S9.

COLLINS, A. N., SHELDRAKE, G., CROSBY, J., 1997, *Chirality in industry II: Developments in the commercial manufacture and applications of optically active compounds*, v. 2. John Wiley & Sons.

CUNHA, F. C., SECCHI, A. R., DE SOUZA JR, M. B., et al., 2019, “Separation of praziquantel enantiomers using simulated moving bed chromatographic unit with performance designed for semipreparative applications”, *Chirality*, v. 31, n. 8, pp. 583–591. doi: <https://doi.org/10.1002/chir.23084>. Available

in: <<https://onlinelibrary.wiley.com/doi/abs/10.1002/chir.23084>>.

- D'ACQUARICA, I., AGRANAT, I., 2020, "Chiral switches of chloroquine and hydroxychloroquine: potential drugs to treat COVID-19", *Drug Discovery Today*, v. 25, n. 7, pp. 1121–1123. ISSN: 1359-6446. doi: <https://doi.org/10.1016/j.drudis.2020.04.021>. Available in: <<https://www.sciencedirect.com/science/article/pii/S1359644620301677>>.
- DICPINIGAITIS, P. V., GAYLE, Y. E., 2003, "Effect of Guaifenesin on Cough Reflex Sensitivity", *Chest*, v. 124, n. 6, pp. 2178 – 2181. ISSN: 0012-3692. doi: <https://doi.org/10.1378/chest.124.6.2178>. Available in: <<http://www.sciencedirect.com/science/article/pii/S0012369215316767>>.
- ERDEM, G., ABEL, S., MORARI, M., et al., 2004a, "Automatic control of simulated moving beds", *Industrial & engineering chemistry research*, v. 43, n. 2, pp. 405–421.
- ERDEM, G., ABEL, S., MORARI, M., et al., 2004b, "Automatic control of simulated moving beds II: Nonlinear isotherm", *Industrial & engineering chemistry research*, v. 43, n. 14, pp. 3895–3907.
- FENWICK, A., SAVIOLI, L., ENGELS, D., et al., 2003, "Drugs for the control of parasitic diseases: current status and development in schistosomiasis", *Trends in parasitology*, v. 19, n. 11, pp. 509–515.
- FRANCOTTE, E. R., 2001, "Enantioselective chromatography as a powerful alternative for the preparation of drug enantiomers", *Journal of Chromatography A*, v. 906, n. 1-2, pp. 379–397.
- FRANCOTTE, E. R., RICHERT, P., 1997, "Applications of simulated moving-bed chromatography to the separation of the enantiomers of chiral drugs", *Journal of Chromatography A*, v. 769, n. 1, pp. 101–107.
- GANETSOS, G., BARKER, P. E., 1992, *Preparative and production scale chromatography*, v. 61. CRC Press.
- GARCIA, M.-S. G., BALSACANTO, E., BANGA, J. R., et al., 2006, "Dynamic optimization of a simulated moving bed (SMB) chromatographic separation process", *Industrial & engineering chemistry research*, v. 45, n. 26, pp. 9033–9041.

- GARDINI, L., SERVIDA, A., MORBIDELLI, M., et al., 1985, “Use of orthogonal collocation on finite elements with moving boundaries for fixed bed catalytic reactor simulation”, *Computers & chemical engineering*, v. 9, n. 1, pp. 1–17.
- GASMI, A., PEANA, M., NOOR, S., et al., 2021, “Chloroquine and hydroxychloroquine in the treatment of COVID-19: the never-ending story”, *Applied microbiology and biotechnology*, pp. 1–11.
- GIRI, B. K., HAKANEN, J., MIETTINEN, K., et al., 2013, “Genetic programming through bi-objective genetic algorithms with a study of a simulated moving bed process involving multiple objectives”, *Applied Soft Computing*, v. 13, n. 5, pp. 2613–2623.
- GOMES, P. S., ZABKOVA, M., ZABKA, M., et al., 2010, “Separation of chiral mixtures in real SMB units: The FlexSMB-LSRE”, *AIChE Journal*, v. 56, n. 1, pp. 125–142. doi: <https://doi.org/10.1002/aic.11962>. Available in: <<https://aiche.onlinelibrary.wiley.com/doi/abs/10.1002/aic.11962>>.
- GONG, R., LIN, X., LI, P., et al., 2014a, “Adsorption equilibrium and kinetic study of guaifenesin enantiomers on cellulose tris 3,5-dimethylphenylcarbamate packed column”, *Chemical Engineering Journal*, v. 244, pp. 128 – 136. ISSN: 1385-8947. doi: <https://doi.org/10.1016/j.cej.2014.01.050>. Available in: <<http://www.sciencedirect.com/science/article/pii/S1385894714000758>>.
- GONG, R., LIN, X., LI, P., et al., 2014b, “Experiment and modeling for the separation of guaifenesin enantiomers using simulated moving bed and Varicol units”, *Journal of Chromatography A*, v. 1363, pp. 242–249. ISSN: 0021-9673. doi: <https://doi.org/10.1016/j.chroma.2014.06.098>. Available in: <<https://www.sciencedirect.com/science/article/pii/S0021967314010437>>. Enantioseparations - 2014.
- GROSSMANN, C., AMANULLAH, M., ERDEM, G., et al., 2008, “‘Cycle to cycle’optimizing control of simulated moving beds”, *AIChE journal*, v. 54, n. 1, pp. 194–208.
- GUIOCHON, G., 2002, “Preparative liquid chromatography”, *Journal of Chromatography A*, v. 965, n. 1-2, pp. 129–161.
- GUIOCHON, G., FELINGER, A., SHIRAZI, D. G., 2006, *Fundamentals of preparative and nonlinear chromatography*. Elsevier.

- HARRIEHAUSEN, I., WRZOSEK, K., LORENZ, H., et al., 2020, "Assessment of process configurations to combine enantioselective chromatography with enzymatic racemization", *Adsorption*, v. 26, pp. 1199–1213.
- HASAN, M. F., FIRST, E. L., FLOUDAS, C. A., 2017, "Discovery of novel zeolites and multi-zeolite processes for p-xylene separation using simulated moving bed (SMB) chromatography", *Chemical Engineering Science*, v. 159, pp. 3–17.
- JENCK, J. F., AGTERBERG, F., DROESCHER, M. J., 2004, "Products and processes for a sustainable chemical industry: a review of achievements and prospects", *Green Chemistry*, v. 6, n. 11, pp. 544–556.
- JUPKE, A., EPPING, A., SCHMIDT-TRAUB, H., 2002, "Optimal design of batch and simulated moving bed chromatographic separation processes", *Journal of Chromatography A*, v. 944, n. 1-2, pp. 93–117.
- JUZA, M., MAZZOTTI, M., MORBIDELLI, M., 2000, "Simulated moving-bed chromatography and its application to chirotechnology", *Trends in biotechnology*, v. 18, n. 3, pp. 108–118.
- KACZMARSKI, K., 1996, "Use of orthogonal collocation on finite elements with moving boundaries in the simulation of non-linear multicomponent chromatography. Influence of fluid velocity variation on retention time in LC and HPLC", *Computers & chemical engineering*, v. 20, n. 1, pp. 49–64.
- KACZMARSKI, K., MAZZOTTI, M., STORTI, G., et al., 1997, "Modeling fixed-bed adsorption columns through orthogonal collocations on moving finite elements", *Computers & chemical engineering*, v. 21, n. 6, pp. 641–660.
- KAGAN, L., LAVY, E., HOFFMAN, A., 2009, "Effect of mode of administration on guaifenesin pharmacokinetics and expectorant action in the rat model", *Pulmonary Pharmacology & Therapeutics*, v. 22, n. 3, pp. 260 – 265. ISSN: 1094-5539. doi: <https://doi.org/10.1016/j.pupt.2008.12.020>. Available in: <<http://www.sciencedirect.com/science/article/pii/S109455398001521>>.
- KASPEREIT, M., JANDERA, P., ŠKAVRADA, M., et al., 2002, "Impact of adsorption isotherm parameters on the performance of enantioseparation using simulated moving bed chromatography", *Journal of Chromatography A*, v. 944, n. 1-2, pp. 249–262.

- KAWAJIRI, Y., BIEGLER, L. T., 2006, "Optimization strategies for simulated moving bed and PowerFeed processes", *AIChE Journal*, v. 52, n. 4, pp. 1343–1350.
- KAWAJIRI, Y., BIEGLER, L. T., 2008, "Large scale optimization strategies for zone configuration of simulated moving beds", *Computers & Chemical Engineering*, v. 32, n. 1-2, pp. 135–144.
- KLATT, K.-U., HANISCH, F., DÜNNEBIER, G., 2002, "Model-based control of a simulated moving bed chromatographic process for the separation of fructose and glucose", *Journal of Process Control*, v. 12, n. 2, pp. 203–219. ISSN: 0959-1524. doi: [https://doi.org/10.1016/S0959-1524\(01\)00005-1](https://doi.org/10.1016/S0959-1524(01)00005-1). Available in: <<https://www.sciencedirect.com/science/article/pii/S0959152401000051>>.
- KLOPPENBURG, E., GILLES, E. D., 1999a, "Automatic control of the simulated moving bed process for C8 aromatics separation using asymptotically exact input/output-linearization", *Journal of Process Control*, v. 9, n. 1, pp. 41–50.
- KLOPPENBURG, E., GILLES, E. D., 1999b, "A new concept for operating simulated moving-bed processes", *Chemical Engineering & Technology: Industrial Chemistry-Plant Equipment-Process Engineering-Biotechnology*, v. 22, n. 10, pp. 813–817.
- LEE, K. B., KASAT, R. B., COX, G. B., et al., 2008, "Simulated moving bed multi-objective optimization using standing wave design and genetic algorithm", *AIChE journal*, v. 54, n. 11, pp. 2852–2871.
- LENTINI, G., CAVALLUZZI, M. M., HABTEMARIAM, S., 2020, "COVID-19, Chloroquine Repurposing, and Cardiac Safety Concern: Chirality Might Help", *Molecules*, v. 25, n. 8. ISSN: 1420-3049. doi: 10.3390/molecules25081834. Available in: <<https://www.mdpi.com/1420-3049/25/8/1834>>.
- LI, S., FENG, L., BENNER, P., et al., 2014, "Using surrogate models for efficient optimization of simulated moving bed chromatography", *Computers & Chemical Engineering*, v. 67, pp. 121–132.
- LIN, G., YOU, Q., CHENG, J., 2011, "Chiral Drugs", *Chemistry and Biological Action*. Wiley, ed, v. 1.
- LIN, X., GONG, R., LI, J., et al., 2016, "Enantioseparation of racemic aminoglutethimide using asynchronous simulated moving bed chromatography", *Journal of Chromatography A*, v. 1467, pp. 347–355.

- LIU, J., CAO, R., XU, M., et al., 2020, “Hydroxychloroquine, a less toxic derivative of chloroquine, is effective in inhibiting SARS-CoV-2 infection in vitro”, *Cell discovery*, v. 6, n. 1, pp. 1–4.
- LIU, Y., QIAN, M., WANG, X., et al., 1993, “Levo-praziquantel versus praziquantel in experimental and clinical treatment of schistosomiasis japonica.” *Chinese medical journal*, v. 106, n. 8, pp. 593–596.
- LIU, Y., WANG, X., WANG, J.-K., et al., 2004, “Structural characterization and enantioseparation of the chiral compound praziquantel”, *Journal of pharmaceutical sciences*, v. 93, n. 12, pp. 3039–3046.
- LORENZ, H., SEIDEL-MORGENSTERN, A., 2014, “Processes to separate enantiomers”, *Angewandte Chemie International Edition*, v. 53, n. 5, pp. 1218–1250.
- LUDEMANN-HOMBOURGER, O., NICOUD, R., BAILLY, M., 2000, “The “VARI-COL” process: a new multicolumn continuous chromatographic process”, *Separation Science and Technology*, v. 35, n. 12, pp. 1829–1862.
- MA, Z., GUIOCHON, G., 1991, “Application of orthogonal collocation on finite elements in the simulation of non-linear chromatography”, *Computers & chemical engineering*, v. 15, n. 6, pp. 415–426.
- MA, Z., WANG, N.-H., 1997, “Standing wave analysis of SMB chromatography: linear systems”, *AIChE Journal*, v. 43, n. 10, pp. 2488–2508.
- MAIER, N. M., FRANCO, P., LINDNER, W., 2001, “Separation of enantiomers: needs, challenges, perspectives”, *Journal of Chromatography A*, v. 906, n. 1-2, pp. 3–33.
- MARKETWATCH, 2021. “Global Chiral Chemicals Market: Facts & Figures by Region and Country Wise Analysis in a Latest 2020 Research Report”. <https://www.marketwatch.com/press-release/chiral-chemicals-market-2021-top-countries-data-with-global-industry-analysis-opportunities-market-size-trends-growth-and-forecast-2026-2021-07-11>, jul. Online; accessed 10 august 2021.
- MAZZOTTI, M., STORTI, G., MORBIDELLI, M., 1997, “Optimal operation of simulated moving bed units for nonlinear chromatographic separations”, *Journal of Chromatography A*, v. 769, n. 1, pp. 3–24.

- MEIER, H., BLASCHKE, G., 2001, “Investigation of praziquantel metabolism in isolated rat hepatocytes”, *Journal of pharmaceutical and biomedical analysis*, v. 26, n. 3, pp. 409–415.
- MILLER, L., GRILL, C., YAN, T., et al., 2003, “Batch and simulated moving bed chromatographic resolution of a pharmaceutical racemate”, *Journal of Chromatography A*, v. 1006, n. 1-2, pp. 267–280.
- MINCEVA, M., RODRIGUES, A. E., 2005, “Two-level optimization of an existing SMB for p-xylene separation”, *Computers & Chemical Engineering*, v. 29, n. 10, pp. 2215–2228. ISSN: 0098-1354. doi: <https://doi.org/10.1016/j.compchemeng.2005.08.001>. Available in: <<https://www.sciencedirect.com/science/article/pii/S0098135405001857>>.
- MURAKAMI, H., 2006, “From racemates to single enantiomers—chiral synthetic drugs over the last 20 years”. In: *Novel optical resolution technologies*, Springer, pp. 273–299.
- NEGAWA, M., SHOJI, F., 1992, “Optical resolution by simulated moving-bed adsorption technology”, *Journal of Chromatography A*, v. 590, n. 1, pp. 113–117.
- NETO, A. S. A., 2015, *MODELING, CONTROL AND OPTIMIZATION OF THE ENANTIOMERIC SEPARATION OF PRAZIQUANTEL IN SIMULATED MOVING BED*. Tese de Mestrado, Universidade Federal do Rio de Janeiro.
- NGUYEN, L. A., HE, H., PHAM-HUY, C., 2006, “Chiral drugs: an overview”, *International journal of biomedical science: IJBS*, v. 2, n. 2, pp. 85.
- NICOUD, R.-M., 2015, *Chromatographic Processes*. Cambridge University Press.
- NICOUD, R.-M., FUCHS, G., ADAM, P., et al., 1993, “Preparative scale enantioseparation of a chiral epoxide: comparison of liquid chromatography and simulated moving bed adsorption technology”, *Chirality*, v. 5, n. 4, pp. 267–271.
- NOGUEIRA, I. B. R., MARTINS, M. A. F., RODRIGUES, A. E., et al., 2020, “Novel Switch Stabilizing Model Predictive Control Strategy Applied in the Control of a Simulated Moving Bed for the Separation of Bi-Naphthol Enantiomers”, *Industrial & Engineering Chemistry Research*, v. 59, n. 5, pp. 1979–1988. doi: 10.1021/acs.iecr.9b05238. Available in: <<https://doi.org/10.1021/acs.iecr.9b05238>>.

- NOGUEIRA, I. B., RIBEIRO, A. M., MARTINS, M. A., et al., 2017, “Dynamics of a True Moving Bed separation process: Linear model identification and advanced process control”, *Journal of Chromatography A*, v. 1504, pp. 112–123.
- PAIS, L. S., LOUREIRO, J. M., RODRIGUES, A. E., 1997, “Modeling, simulation and operation of a simulated moving bed for continuous chromatographic separation of 1, 1'-bi-2-naphthol enantiomers”, *Journal of Chromatography A*, v. 769, n. 1, pp. 25–35.
- PAIS, L. S., LOUREIRO, J. M., RODRIGUES, A. E., 1998, “Modeling strategies for enantiomers separation by SMB chromatography”, *AIChE Journal*, v. 44, n. 3, pp. 561–569.
- PAIS, L. S., RODRIGUES, A. E., 2003, “Design of simulated moving bed and Varicol processes for preparative separations with a low number of columns”, *Journal of Chromatography A*, v. 1006, n. 1, pp. 33–44. ISSN: 0021-9673. doi: [https://doi.org/10.1016/S0021-9673\(03\)00557-0](https://doi.org/10.1016/S0021-9673(03)00557-0). Available in: <<https://www.sciencedirect.com/science/article/pii/S0021967303005570>>. International Symposium on Preparative and Industrial Chromatography and Allied Techniques.
- RAJENDRAN, A., PAREDES, G., MAZZOTTI, M., 2009, “Simulated moving bed chromatography for the separation of enantiomers”, *Journal of Chromatography A*, v. 1216, n. 4, pp. 709–738.
- REPORTLINKER, 2021. “Chiral Chemicals Market Research Report by Product, by Technology, by Application, by State - United States Forecast to 2026 - Cumulative Impact of COVID-19”. <https://www.reportlinker.com/p06082610/Chiral-Chemicals-Market-Research-Report-by-Product-by-Technology-by-Application-by-State-United-States-Forecast-to-Cumulative-Impact-of-COVID-19.html>, jun. Online; accessed 10 august 2021.
- RODRIGUES, A., 2015, *Simulated moving bed technology: principles, design and process applications*. Butterworth-Heinemann.
- RODRIGUES, A. E., TONDEUR, D., 1981, *Percolation processes: theory and applications*. N. 33. Springer.
- RODRIGUES, A. E., LEVAN, M. D., TONDEUR, D., 2012, *Adsorption: Science and technology*, v. 158. Springer Science & Business Media.

- RUTHVEN, D. M., CHING, C., 1989, “Counter-current and simulated counter-current adsorption separation processes”, *Chemical Engineering Science*, v. 44, n. 5, pp. 1011–1038.
- SÁ GOMES, P., RODRIGUES, A. E., 2012, “Simulated moving bed chromatography: from concept to proof-of-concept”, *Chemical Engineering & Technology*, v. 35, n. 1, pp. 17–34.
- SCHMIDT-TRAUB, H., SCHULTE, M., SEIDEL-MORGENSTERN, A., 2012, *Preparative chromatography*, v. 130. Wiley Online Library.
- SCHRAMM, H., KASPEREIT, M., KIENLE, A., et al., 2002, “Improving Simulated Moving Bed Processes by Cyclic Modulation of the Feed Concentration”, *Chemical Engineering & Technology*, v. 25, n. 12, pp. 1151–1155. doi: [https://doi.org/10.1002/1521-4125\(20021210\)25:12<1151::AID-CEAT1151>3.0.CO;2-Y](https://doi.org/10.1002/1521-4125(20021210)25:12<1151::AID-CEAT1151>3.0.CO;2-Y). Available in: <<https://onlinelibrary.wiley.com/doi/abs/10.1002/1521-4125%2820021210%2925%3A12%3C1151%3A%3AAID-CEAT1151%3E3.0.CO%3B2-Y>>.
- SCHRAMM, H., KIENLE, A., KASPEREIT, M., et al., 2003a, “Improved operation of simulated moving bed processes through cyclic modulation of feed flow and feed concentration”, *Chemical Engineering Science*, v. 58, n. 23-24, pp. 5217–5227.
- SCHRAMM, H., KASPEREIT, M., KIENLE, A., et al., 2003b, “Simulated moving bed process with cyclic modulation of the feed concentration”, *Journal of Chromatography A*, v. 1006, n. 1-2, pp. 77–86.
- SCHULTE, M., STRUBE, J., 2001, “Preparative enantioseparation by simulated moving bed chromatography”, *Journal of Chromatography A*, v. 906, n. 1-2, pp. 399–416.
- SECCHI, A., BISCAIA JR, E., 2020, *Métodos Numéricos para Engenheiros Químicos Algoritmos e Aplicações*.
- SEIDEL-MORGENSTERN, A., KESSLER, L. C., KASPEREIT, M., 2008, “New developments in simulated moving bed chromatography”, *Chemical Engineering & Technology: Industrial Chemistry-Plant Equipment-Process Engineering-Biotechnology*, v. 31, n. 6, pp. 826–837.
- SHAMPINE, L. F., REICHEL, M. W., 1997, “The matlab ode suite”, *SIAM journal on scientific computing*, v. 18, n. 1, pp. 1–22.

- SILVA, V. M., MINCEVA, M., RODRIGUES, A. E., 2004, “Novel analytical solution for a simulated moving bed in the presence of mass-transfer resistance”, *Industrial & engineering chemistry research*, v. 43, n. 16, pp. 4494–4502.
- SONG, I.-H., LEE, S.-B., RHEE, H.-K., et al., 2006a, “Identification and predictive control of a simulated moving bed process: Purity control”, *Chemical engineering science*, v. 61, n. 6, pp. 1973–1986.
- SONG, I.-H., LEE, S.-B., RHEE, H.-K., et al., 2006b, “Optimization-based predictive control of a simulated moving bed process using an identified model”, *Chemical Engineering Science*, v. 61, n. 18, pp. 6165–6179.
- SONG, I.-H., AMANULLAH, M., ERDEM, G., et al., 2006c, “Experimental implementation of identification-based optimizing control of a simulated moving bed process”, *Journal of Chromatography A*, v. 1113, n. 1-2, pp. 60–73.
- SONG, J.-Y., KIM, K.-M., LEE, C.-H., 2016, “High-performance strategy of a simulated moving bed chromatography by simultaneous control of product and feed streams under maximum allowable pressure drop”, *Journal of Chromatography A*, v. 1471, pp. 102–117. ISSN: 0021-9673. doi: <https://doi.org/10.1016/j.chroma.2016.10.015>. Available in: <<https://www.sciencedirect.com/science/article/pii/S0021967316313474>>.
- SUBRAMANI, H., HIDAJAT, K., RAY, A., 2003, “Optimization of simulated moving bed and Varicol processes for glucose–fructose separation”, *Chemical Engineering Research and Design*, v. 81, n. 5, pp. 549–567.
- SUVAROV, P., KIENLE, A., NOBRE, C., et al., 2014, “Cycle to cycle adaptive control of simulated moving bed chromatographic separation processes”, *Journal of Process Control*, v. 24, n. 2, pp. 357–367.
- SWARTZ, C. L., KAWAJIRI, Y., 2019, “Design for dynamic operation - A review and new perspectives for an increasingly dynamic plant operating environment”, *Computers & Chemical Engineering*, v. 128, pp. 329 – 339. ISSN: 0098-1354. doi: <https://doi.org/10.1016/j.compchemeng.2019.06.002>. Available in: <<http://www.sciencedirect.com/science/article/pii/S0098135419300705>>.
- TOUMI, A., ENGELL, S., LUDEMANN-HOMBOURGER, O., et al., 2003, “Optimization of simulated moving bed and Varicol processes”, *Journal of Chromatography A*, v. 1006, n. 1-2, pp. 15–31.

- TOUMI, A., ENGELL, S., DIEHL, M., et al., 2007, “Efficient optimization of simulated moving bed processes”, *Chemical Engineering and Processing: Process Intensification*, v. 46, n. 11, pp. 1067–1084.
- TOUMI, A., ENGELL, S., 2004, “Optimization-based control of a reactive simulated moving bed process for glucose isomerization”, *Chemical Engineering Science*, v. 59, n. 18, pp. 3777–3792. ISSN: 0009-2509. doi: <https://doi.org/10.1016/j.ces.2004.04.009>. Available in: <<https://www.sciencedirect.com/science/article/pii/S0009250904002118>>.
- TOUMI, A., HANISCH, F., ENGELL, S., 2002, “Optimal operation of continuous chromatographic processes: mathematical optimization of the VARICOL process”, *Industrial & engineering chemistry research*, v. 41, n. 17, pp. 4328–4337.
- VALENTI, G., TINNEMANS, P., BAGLAI, I., et al., 2021, “Combining incompatible processes for deracemization of a Praziquantel derivative under flow conditions”, *Angewandte Chemie International Edition*, v. 60, n. 10, pp. 5279–5282.
- VALERY, E., MOREY, C., 2012. “Process and device for separating fractions of a mixture”. jul. 10. US Patent 8,216,475.
- VAZ, A. I. F., VICENTE, L. N., 2009, “PSwarm: a hybrid solver for linearly constrained global derivative-free optimization”, *Optimization Methods & Software*, v. 24, n. 4-5, pp. 669–685.
- VILLADSEN, J., MICHELSEN, M. L., 1978, *Solution of differential equation models by polynomial approximation*. Prentice-Hall.
- WÄCHTER, A., BIEGLER, L. T., 2006, “On the implementation of an interior-point filter line-search algorithm for large-scale nonlinear programming”, *Mathematical programming*, v. 106, n. 1, pp. 25–57.
- WANNER, G., HAIRER, E., 1996, *Solving ordinary differential equations II*. Springer Berlin Heidelberg.
- WONGSO, F., HIDAJAT, K., RAY, A. K., 2005, “Improved performance for continuous separation of 1, 1'-bi-2-naphthol racemate based on simulated moving bed technology”, *Separation and purification technology*, v. 46, n. 3, pp. 168–191.
- WORLD HEALTH ORGANIZATION, 2020. “Solidarity” clinical trial for COVID-19 treatments. UPDATE: solidarity trial reports interim results”. <https://www.who.int/news-room/press-releases/2020/07/20-sol-trial-reports-interim-results>.

[//www.who.int/emergencies/diseases/novel-coronavirus-2019/global-research-on-novel-coronavirus-2019-ncov/solidarity-clinical-trial-for-covid-19-treatments](http://www.who.int/emergencies/diseases/novel-coronavirus-2019/global-research-on-novel-coronavirus-2019-ncov/solidarity-clinical-trial-for-covid-19-treatments). Online; accessed 10 August 2021.

- WORLD HEALTH ORGANIZATION, 2006. “Preventive chemotherapy in human helminthiasis. Coordinated use of anthelmintic drugs in control interventions: a manual for health professionals and programme managers.” http://apps.who.int/iris/bitstream/handle/10665/43545/9241547103_eng.pdf?sequence=1.
- XIE, Y., WU, D., MA, Z., et al., 2000, “Extended standing wave design method for simulated moving bed chromatography: linear systems”, *Industrial & Engineering Chemistry Research*, v. 39, n. 6, pp. 1993–2005.
- XIE, Y., KOO, Y.-M., WANG, N.-H. L., 2001, “Preparative chromatographic separation: simulated moving bed and modified chromatography methods”, *Biotechnology and Bioprocess Engineering*, v. 6, n. 6, pp. 363.
- XIONG, X., WANG, K., TANG, T., et al., 2021, “Development of a chiral HPLC method for the separation and quantification of hydroxychloroquine enantiomers”, *Scientific reports*, v. 11, n. 1, pp. 1–7.
- YANG, Y., LU, K., GONG, R., et al., 2019, “Separation of guaifenesin enantiomers by simulated moving bed process with four operation modes”, *Adsorption*, v. 25, n. 6, pp. 1227–1240.
- YAO, C., TANG, S., YAO, H.-M., et al., 2014, “Study on the number of decision variables in design and optimization of Varicol process”, *Computers & Chemical Engineering*, v. 68, pp. 114–122.
- YAO, C., JING, K., LING, X., et al., 2017, “Application of dodecahedron to describe the switching strategies of asynchronous simulated-moving-bed”, *Computers & Chemical Engineering*, v. 96, pp. 69–74.
- YU, Q., WANG, N.-H., 1989, “Computer simulations of the dynamics of multi-component ion exchange and adsorption in fixed beds—gradient-directed moving finite element method”, *Computers & chemical engineering*, v. 13, n. 8, pp. 915–926.
- YU, Y., WOOD, K. R., LIU, Y., 2015, “Simulation and comparison of operational modes in simulated moving bed chromatography”, *Industrial & Engineering Chemistry Research*, v. 54, n. 46, pp. 11576–11591.

- ZABKOVA, M., ZABKA, M., RODRIGUES, A. E., 2009, "Separation of Racemic Chiral Drugs Using Immobilized CHIRALPAK IA: Methodology for Preparative Scale Development", *Separation Science and Technology*, v. 44, n. 2, pp. 275–303. doi: 10.1080/01496390802590079. Available in: <<https://doi.org/10.1080/01496390802590079>>.
- ZANG, Y., WANKAT, P. C., 2002, "SMB operation strategy- partial feed", *Industrial & engineering chemistry research*, v. 41, n. 10, pp. 2504–2511.
- ZHANG, Y., HIDAJAT, K., RAY, A. K., 2007, "Enantio-separation of racemic pindolol on α -acid glycoprotein chiral stationary phase by SMB and Varicol", *Chemical Engineering Science*, v. 62, n. 5, pp. 1364–1375. ISSN: 0009-2509. doi: <https://doi.org/10.1016/j.ces.2006.11.028>. Available in: <<https://www.sciencedirect.com/science/article/pii/S000925090600738X>>.
- ZHANG, Z., HIDAJAT, K., RAY, A. K., et al., 2002, "Multiobjective optimization of SMB and varicol process for chiral separation", *AIChE Journal*, v. 48, n. 12, pp. 2800–2816.
- ZHANG, Z., MAZZOTTI, M., MORBIDELLI, M., 2003, "PowerFeed operation of simulated moving bed units: changing flow-rates during the switching interval", *Journal of Chromatography A*, v. 1006, n. 1-2, pp. 87–99.
- ZHANG, Z., MAZZOTTI, M., MORBIDELLI, M., 2004a, "Continuous chromatographic processes with a small number of columns: comparison of simulated moving bed with Varicol, PowerFeed, and ModiCon", *Korean Journal of Chemical Engineering*, v. 21, n. 2, pp. 454–464.
- ZHANG, Z., MORBIDELLI, M., MAZZOTTI, M., 2004b, "Experimental assessment of powerfeed chromatography", *AIChE Journal*, v. 50, n. 3, pp. 625–632. doi: <https://doi.org/10.1002/aic.10056>. Available in: <<https://aiche.onlinelibrary.wiley.com/doi/abs/10.1002/aic.10056>>.
- ZHONG, G., GUIOCHON, G., 1996, "Analytical solution for the linear ideal model of simulated moving bed chromatography", *Chemical Engineering Science*, v. 51, n. 18, pp. 4307–4319.
- ZÚÑIGA, I. T., WOUWER, A. V., 2014, "Optimization of VARICOL SMB processes using hybrid modeling and nonlinear programming", *Computers & Chemical Engineering*, v. 71, pp. 1–10.

ZWANG, J., OLLIARO, P. L., 2014, “Clinical Efficacy and Tolerability of Praziquantel for Intestinal and Urinary Schistosomiasis—A Meta-analysis of Comparative and Non-comparative Clinical Trials”, *PLOS Neglected Tropical Diseases*, v. 8, n. 11 (11), pp. 1–15. doi: 10.1371/journal.pntd.0003286. Available in: <<https://doi.org/10.1371/journal.pntd.0003286>>.

Appendix A

Chromatographic column simulator

A new package that simulates individual columns and carries out parameter estimations for the TD and ED models was developed. That package was called "SimCol" and is formed by a graphical interface and the discretized mathematical models for the TD and ED. The two discretization methods, finite differences and orthogonal collocation on fixed finite elements, were included. The analytical Jacobian was also included for the different models. The graphical interface of SimCol is presented in Figure A.1.

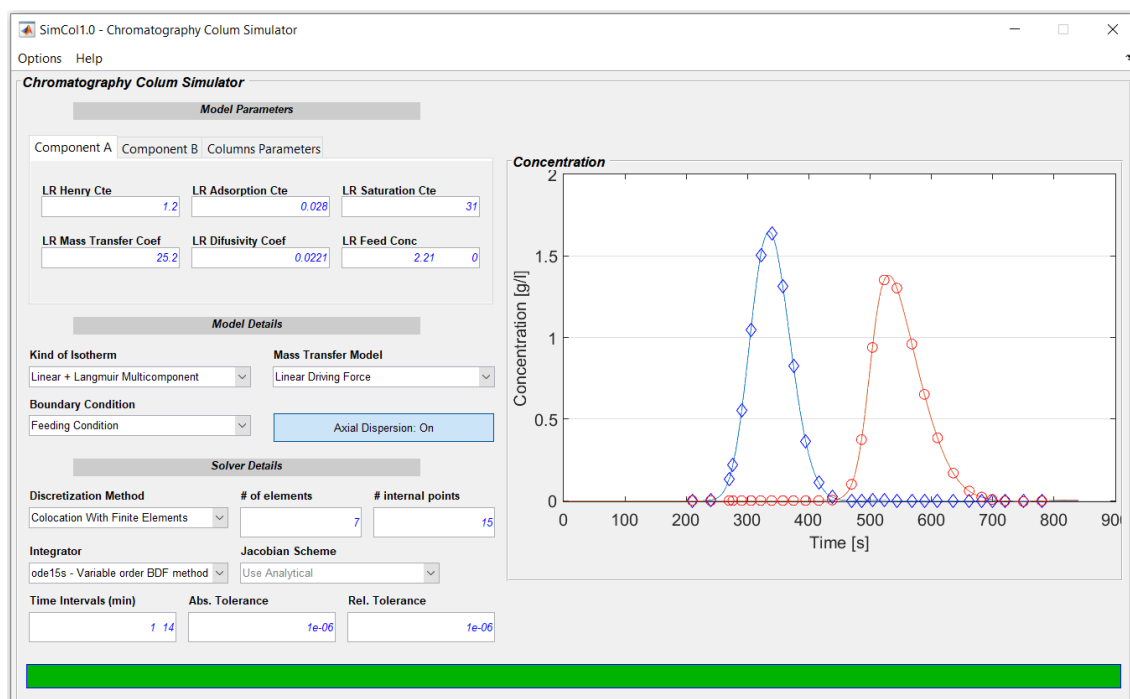


Figure A.1: Graphical interface of the SimCol tool, a package to simulate and estimate parameters in individuals columns.

The elution curves obtained from pulse experiments can be used in the SimCol

tool to estimate some TD and ED model parameters. These parameters can be adsorption isotherm parameters, dispersion coefficients, mass transfer coefficients, and porosity. The use of SimCol tool is evaluated in two case studies based on the TD model. In the first case, sensitive analysis of the parameters of the TD model for the racemic mixture of guaifenesin was considered. In the second case, the TD model in terms of total porosity was compared with the one in terms of bed porosity. The parameters of the second model were estimated from the first. Additionally, the TD and ED models were also compared.

A.1 Sensitivity analysis for the parameters of the transport dispersion model

In the sensitivity analysis, the change of the chromatography elution curves is evaluated with the variation of some critical mathematical model parameters. The elution curves represent the separation peaks of less and the most retained components of the racemic mixture of guaifenesin. The model used to predict these elution curves is the TD model in terms of total porosity. The initial parameters of the model are the same as in Table 4.18, and the adsorption isotherms are the same as presented in Equations 4.7 and 4.7. The time, the feed concentration, and the feed flow rate of the pulse used were the same applied by GONG *et al.* (2014a) in a theoretical and experimental study for guaifenesin. These parameters were 1 *min*, 2.21 *mg/ml*, and 3 *ml/min*.

In the sensitivity analysis, positive and negative variations of 50% concerning nominal values are applied for some critical parameters of the TD model. These parameters are the apparent dispersion coefficients, the effective mass transfer coefficients, the total porosity, and the Henry constant of the isotherm. In the case of total porosity, only a negative variation of 50% is applied, taking the porosity value from the range of total porosity to that of the bed porosity (ANICETO and SILVA, 2015a). The positive or negative variations for dispersion coefficients, mass transfer coefficients, and Henry constant are applied simultaneously for the less and the most retained enantiomers. The graphical results are presented in Figure A.2.

Figure A.2 shows different effects in the elution profiles for each one of the parameters. The parameter that produced a minor variation of the concentration profiles was the apparent dispersion coefficient. The positive and negative variation of this parameter produced only slight changes in the peak heights, as seen in Figures A.2a and A.2b. The variation in the effective mass transfer coefficient was more

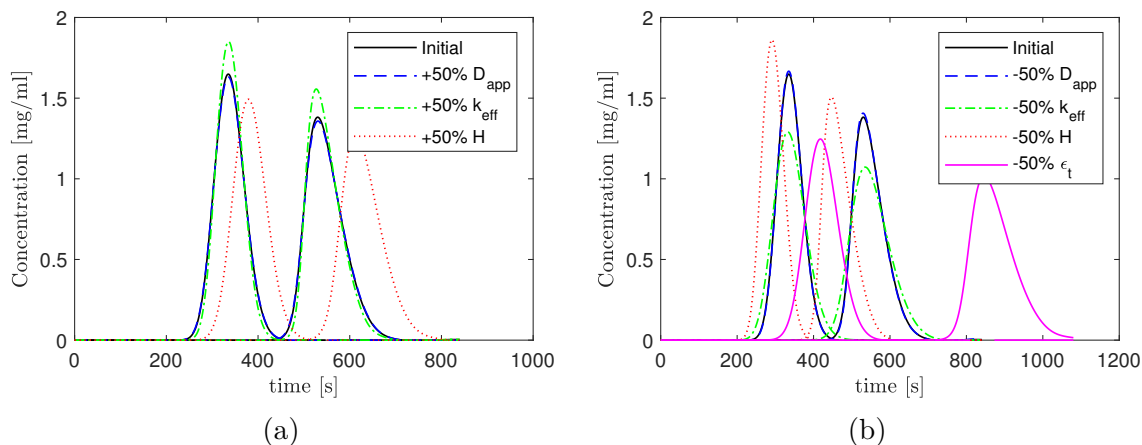


Figure A.2: Sensitivity analysis for critical parameters of the transport dispersion model. (a) Positive variations; (b) Negative variations

pronounced than the dispersion coefficient. In this case, changes in the height and the broadening of the peaks are seen (see Figures A.2a and A.2b). The parameters that produce the highest variations in the elution peaks are the Henry constant of the isotherm and the total porosity. Those variations are related to the height and width of the peaks, the displacement of the elution times concerning the nominal values, and the distance between peaks. Those results are significant for applications such as model-based control, where the parameters of the theoretical model need to be adjusted with the experimental results because it gives an idea of which parameters could produce a better fitting.

A.2 Comparison between different models

The transport dispersion models in terms of total and bed porosity are obtained with different assumptions in the adsorbent particles. Although the two models are used in the literature to describe enantioseparations, it is common to find confusion in the employment of each one of them. The relation between these two models was evaluated and compared by simulating a pulse of a racemic mixture in a chromatographic column and simulating the enantioseparation of the same racemic mixture with 3-columns ModiCon+VariCol process. The relation between the TD model in terms of total porosity and the ED model was also compared for these two simulations.

In the first comparison the mixture considered was the enantioseparation of guaifenesin described with the TD model in terms of total porosity (Model 1) (GONG *et al.*, 2014a). The parameters for the TD model in terms of bed porosity (Model 2) were calculated or estimated from the definition of some parameters and

the elution curves determined with Model 1. For parameter estimation, the SimCol tool and the Particle Swarm Optimization (PSwarm) algorithm were used. The PSwarm algorithm was used from the Matlab suite (VAZ and VICENTE, 2009). The parameters and isotherms used in Model 1 were the same as in Table 4.18 and Equations 4.7 and 4.8. The parameters of the pulse were set in 1 *min*, 10 *mg/ml*, and 3 *ml/min*.

The equivalence between the TD models was initially evaluated considering the same isotherm parameters in Model 2 as in Model 1 but estimating the dispersion coefficients, the mass transfer coefficients, and the bed porosity. However, it was impossible to find a good fit in the elution curve of Model 2 with the one of Model 1 for a bed porosity in the 0.26-0.48 range (ANICETO and SILVA, 2015a), which is the expected range of this parameter. The solution always led to the same value of total porosity. That was expected because the variation of dispersion and mass transfer coefficients do not produce changes in the elution times that counteract the effects produced with the variation of porosity, as seen in Figure A.2 of the previous section.

An equivalence between TD models can be found adjusting the isotherm parameters for Model 2 since it also changes the elution times of the components in the chromatographic columns (see Figure A.2). Although the new isotherms parameters may not represent the real equilibrium, they were estimated together with mass transfer coefficients. For the bed porosity, the same value reported in Table 4.18 was used, which was determined by GONG *et al.* (2014a) with an empirical correlation. The axial dispersion coefficients ($D_{ax,i}$) were determined with Equation 3.30. The calculated and estimated parameters for Model 2 are presented in Table A.1 and Equations A.1 and A.2. The graphical results of the two models are presented in Figure A.3a for the simulation of the elution curves. The estimated parameters were also used to simulate the case MC+VC 6 of Table 4.24, and the results are presented in Figure A.3b.

$$q_{e,A} = 0.956c_A + \frac{31.616 \times 0.0203c_A}{1 + 0.0203c_A + 0.0646c_B} \quad (\text{A.1})$$

$$q_{e,B} = 1.261c_B + \frac{31.616 \times 0.0646c_B}{1 + 0.0203c_A + 0.0646c_B} \quad (\text{A.2})$$

where $q_{e,A}$ and $q_{e,B}$ are given in [*mg · ml*⁻¹].

The result of Figure A.3a shows that with the estimation of the isotherms parameters and mass transfer coefficients, Model 2 got a good approximation of the elution curves. Perhaps an even better approximation could have been achieved

Table A.1: Parameters for the the racemic mixture of guaifenesin used in the transport dispersion model in terms of bed porosity. Index A refers to the less retained and B to the most retained enantiomers

Parameter	value
Column length [cm]	$l = 15$
Column diameter [cm]	$d = 1$
Particle size [μm]	$d_p = 20$
Bed porosity [-]	$\varepsilon_b = 0.44$
Dispersion coefficient [$\text{cm}^2 \cdot \text{min}^{-1}$]	$D_{ax,A} = 0.0347, D_{ax,B} = 0.0259$
Mass transfer coefficient [min^{-1}]	$k_{eff,A}^* = 35.84, k_{eff,B}^* = 57.59$
Pulse time [min]	$t = 1$
Pulse Feed concentration [$\text{mg} \cdot \text{ml}^{-1}$]	$c_{f,A} = c_{f,B} = 10$
Feed flow rate [$\text{cm}^3 \cdot \text{min}^{-1}$]	$Q_f = 3$

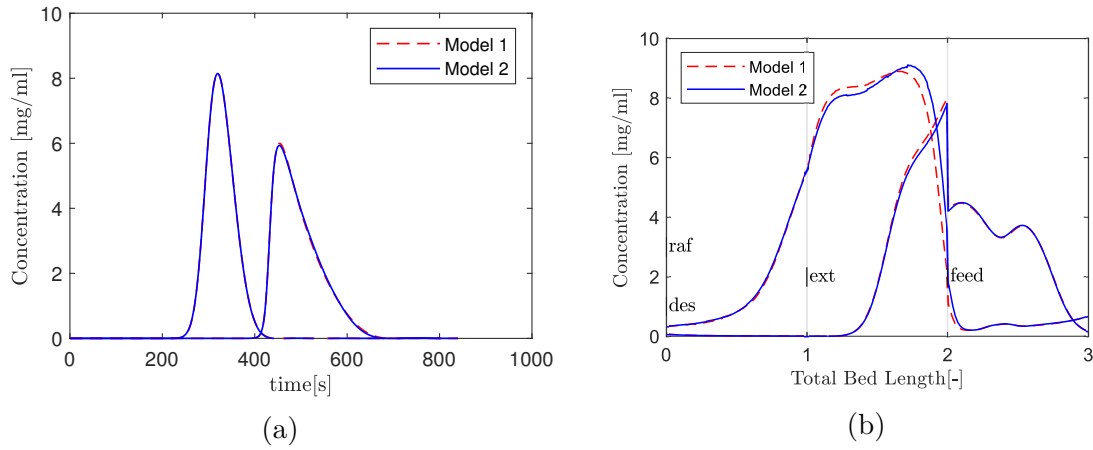


Figure A.3: Comparison of two dispersion models for simulating (a) the elution curves, (b) and the internal concentration profiles of the enantioseparation of ModiCon+VariCol with 3 columns at the 50% of first switching period of 25th cycle.

using the bed porosity as an adjustment parameter. When the estimated parameters are used to simulate the MC+VC 6 of Table 4.24, the slight difference between the results of the models becomes more critical, as seen in Figure A.3b. Although the results between Model 1 and Model 2 are not entirely overlapping for MC+VC 6, Model 2 represented well the dynamics of the process. Those results show that Model 1 and Model 2 could be used to represent the same elution, but in one of the cases, a hypothetical equilibrium needs to be used.

A common approach of the literature is using the equilibrium dispersion model instead of the TD model. In the ED model, the mass transfer effects are neglected, and the dispersion coefficient lumps different effects. The TD model in terms of total porosity (Model 1) was compared with the ED model (Model 3) with adjusted dispersion coefficients. The parameter for Model 1 where the same used in Figure A.3a. The parameters for Model 3 are the same as Model 1 except for the dispersion

coefficients. The lumped dispersion coefficients were estimated from the elution profiles of Model 1. The obtained values were: $D_{lum,A} = 0.3293 [cm^2 \cdot min^{-1}]$ and $D_{lum,B} = 0.1765 [cm^2 \cdot min^{-1}]$. The graphical results for the two models are presented in Figure A.4.

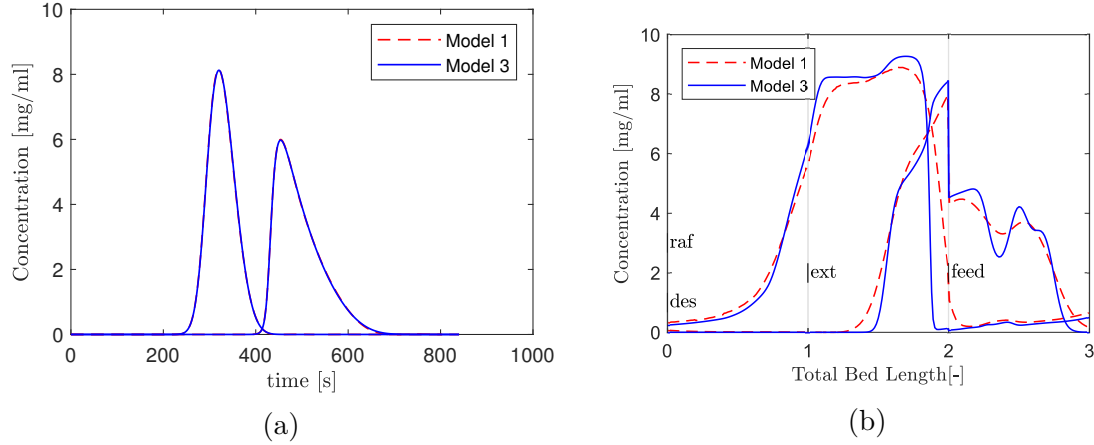


Figure A.4: Comparison of TD model and ED model for (a) the elution curves, (b) the internal concentration profiles of the enantioseparation of ModiCon+VariCol with 3 columns at the 50% of first switching period of 25th cycle.

Figure A.4a shows that for the case of the chromatography elution pulse, a good agreement between the TD model and the ED model is seen. However, when the ED model is used to simulate the MC+VC6 process, a variation in the internal concentration profiles with the TD model is seen (see Figure A.4b). That indicates that although the results of the models agree well on the pulse, when more complex operations are simulated, a discrepancy between the models can be found. Those deviations could be reduced by adjusting the models directly over the curves of these more complex operations. Adapting simplified models but preserving the phenomenological part at the operating points in the process, such as the SMB and its variants, can be interesting in applications such as non-linear model predictive control.

A.3 Conclusion

A package that simulates individual columns and carries out parameter estimation for the transport dispersion and equilibrium dispersion models was implemented. That package was called SimCol and is formed by a graphical interface and the models for individual chromatographic columns. The models were implemented using orthogonal collocation on fixed finite elements and finite differences. The application of SimCol was evaluated with two case studies based on the racemic mixture of

guaifenesin. In the first case, a sensitivity analysis for parameters of the TD model in terms of total porosity was considered. In the second case, the TD model in terms of total porosity was compared with the TD model in terms of bed porosity and the ED model. The parameters for the last two models were estimated from the elution curves of the first model.

In the TD model's sensitivity analyses, the parameters that produced the slightest variation in the elution peaks were the dispersion and mass transfer coefficients. The variations of these parameters were related to the height and width of elution peaks. On the other side, the highest variation was produced with the isotherm parameters and porosity. The variations were related to the height and width of elution peaks, the elution times, and the distance between peaks. Comparing TD in terms of total and bed porosity, quite close results were found in the last model when at least the mass transfer coefficients and isotherms parameter were estimated from the former model. Comparing the TD model in terms of total porosity with the ED model, a good approximation was obtained by adjusting only the lumped dispersion coefficient in the ED.